1-1-1982

Multi-frequency radio observations of compact extragalactic sources : time variability and correlation with optical variations.

Thomas Joseph Balonek
University of Massachusetts Amherst

Follow this and additional works at: https://scholarworks.umass.edu/dissertations_1

MULTI-FREQUENCY RADIO OBSERVATIONS

OF COMPACT EXTRAGALACTIC SOURCES:

TIME VARIABILITY

AND

CORRELATION WITH OPTICAL VARIATIONS

A Dissertation Presented

By

THOMAS JOSEPH BALONEK

Submitted to the Graduate School of the
University of Massachusetts in partial fulfillment
of the requirements for the degree of

DOCTOR OF PHILOSOPHY

September   1982

Astronomy

MULTI-FREQUENCY RADIO OBSERVATIONS

OF COMPACT EXTRAGALACTIC SOURCES:

TIME VARIABILITY

AND

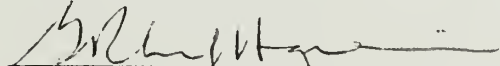CORRELATION WITH OPTICAL VARIATIONS

A Dissertation Presented

By

THOMAS JOSEPH BALONEK

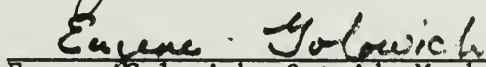Approved as to style and content by:
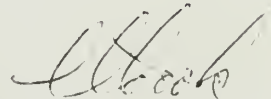
_____
William A. Dent, Chairman of Committee

_____
G. Richard Huguenin, Member

_____
Eugene Tademaru, Member

_____
Eugene Golowich, Outside Member

_____
Leroy F. Cook, Department Head
Physics and Astronomy

ACKNOWLEDGEMENTS

This dissertation is the culmination of my academic and personal career as a graduate student. It is as much a reflection of my interactions with many individuals as it is a record of the research conducted during the past years. The dissertation would not have reached its completion were it not for these people. It is not possible to acknowledge all the individuals whose advice, concern, encouragement, and friendship I have received. However, several people deserve special thanks.

A multitude of individuals have assisted in the acquisition of the observations reported within. The telescope operators, engineers, and administrative staffs at Haystack Observatory, NRAO Green Bank, and NRAO at Kitt Peak have been instrumental in obtaining the high quality observations reported here and in making the frequent observing runs enjoyable. In particularly I'd like to thank Steve Sanders who has been conducting "Dent-1" observations for as long a period as I (and with as much concern), and Beasley for being responsive to my requests for additional observing time and for assistance in understanding the Haystack system. I have benefited much from discussions with the "friends of the telescopes" at these institutions - Aubrey Haschick, Pat Crane, and Rick Howard.

The optical observations have been kindly provided in computer readable format by Joseph Pollack and Andy Pica, without whose assistance Chapter VI would not have been possible. Their efforts

represent the years of diligent observing and hard work of the entire quasar monitoring group at the University of Florida, led by Alex Smith.

The FCRAO continuum observations likewise were possible only because of the efforts of many individuals at the University of Massachusetts. In particular, Pete Schloerb who spent many nights with me at Quabbin during the initial stages in the development of the continuum system, and who, along with John Kapitzky, developed many of the observing procedures now in use at the observatory; to all those who have spent countless hours helping me perform the observations (especially Pete Schloerb and Read Predmore); the engineering staff for their work in the development of the receivers and backends; the members of the 1980 panel setting crew whose efforts led to the increased accuracy of the antenna surface (Al Rodman, Paul Mackinen, Gordon McIntosh, all the panel setters who risked their lives and sanity, and Pete Schloerb who helped direct the effort); John Kapitzky, Nick Scoville, and the others who developed the software necessary to the observations and data reduction; Ron Snell and Pete Schloerb for S_{cal}; the scheduling committee for granting me observing time; and G. Richard Huguenin for his personal encouragement and directorship of the FCRAO project.

ABSTRACT

MULTI-FREQUENCY RADIO OBSERVATIONS

OF COMPACT EXTRAGALACTIC SOURCES:

TIME VARIABILITY AND

CORRELATION WITH OPTICAL VARIATIONS

(September 1982)

Thomas J. Balonek, B.A., Cornell University

M.S., PhD., University of Massachusetts

Directed by: William A. Dent

In order to investigate the evolution of compact extragalactic radio
sources, three observing programs were undertaken. These programs were:
single epoch spectra for 113 sources were compiled from near-
simultaneous observations at seven frequencies (between 1.4 and 90 GHz);
monthly observations were conducted at $\lambda 3$ mm to search for short
timescale variations; radio (15.5 GHz) and optical variations in 45
sources were searched for correlated activity.

The observed radio spectra are the first compilation of near-
simultaneous observations of this sample of regularly monitored variable
sources. These sources exhibit a wide range of variability and spectral
characteristics, thus constituting a useful sample for comparison with
theoretical models for radio emission mechanisms.

The high frequency radio observations of variable extragalactic
radio sources are important for studying the evolution of flux density

outbursts, which are affected at lower frequencies by opacity effects and expansion processes. The observations at millimeter wavelengths provide a probe of the physical conditions in the energetic radio core. The monthly observations reported here reveal several instances of rapid variations with timescales comparable to those observed at optical wavelengths. The dimensions of the emitting region inferred from the radio variations is one light month, assuming non-relativistic motion. Several outbursts observed at millimeter wavelengths were undetectable at longer wavelengths. The outburst spectra typically exhibit a maximum at 30 GHz, with the high frequency (>30 GHz) spectral index often remaining constant during the outburst decay.

The radio and optical variations revealed many instances of correlated activity. Characteristic timescales of correlated activity ranged from rapid (monthly) outbursts to long timescale (decade) trends. These events displayed a range of optical-radio time delays, from simultaneous events to delays of several years. The results of the correlation search indicate that in many sources the optical and radio emission mechanisms are related, with the radiation being emitted from a common volume.

TABLE OF CONTENTS

LIST OF TABLES

LIST OF ILLUSTRATIONS

C H A P T E R   I

INTRODUCTION

"Variability of evidence is not
evidence of variability."

S. Spangler

Compact extragalactic sources in quasi-stellar objects (QSOs) and galactic nuclei have been studied intensely at frequencies throughout the electromagnetic spectrum (from radio to x-ray) during the past two decades. The compact sources are presumably associated with the intense central energy producing regions in these objects. Luminosities as large as $\sim 10^{46}$ ergs/sec, from regions typically light years in size, have been observed in the most luminous quasars. The compact sources exhibit luminosity and structural changes on timescales of days to decades. These active compact core sources are probably the energy source for the large extended radio emission associated with some elliptical galaxies and quasars (cf. review by Miley 1980).

In order to understand the physical conditions within the compact components and the emission mechanisms operative in these luminous objects, it has become clear that coordinated observations over a broad frequency range are required. Knowledge of the evolution of the total flux density, polarization, and structural properties is necessary to differentiate between possible emission mechanisms.

1

A general review of the physical models which have been proposed to account for the observed emission in compact sources is given in §1. The observational programs which were undertaken for this dissertation are discussed in §2.

§1. Physical Models

Spectral shape. The emission mechanism responsible for the radio emission from compact sources is assumed to be synchrotron radiation from relativistic electrons. This mechanism may also be the source of the infrared and optical radiation. The radio spectrum of a compact source is generally flat ($-0.5< \alpha <+0.5$, where the flux density S is a function of frequency, $S \propto \nu^\alpha$) throughout the frequency range ~1 to 100 GHz. The spectrum will peak at the frequency where the source becomes opaque to its own synchrotron radiation. For a homogeneous source with a power-law particle energy distribution, $N(E) \, dE \propto E^{-\gamma} \, dE$, this frequency is given by

$$\nu_m \propto S^{2/5} \; \theta^{-4/5} \; B^{1/5} \; (1+z) \qquad\qquad (I-1)$$

where B is the magnetic field, θ is the angular size, z is the redshift, and S is the flux density. At frequencies above ν_m where the opacity, τ, is $\ll 1$, the spectral index $\alpha = (1-\gamma)/2$. At frequencies where the source is opaque ($\tau \gg 1$), the spectral index is $\alpha = 5/2$.

This standard synchrotron model (Kellermann and Pauliny-Toth 1969) can account for the general radio characteristics of compact sources,

but investigation of a large sample of source spectra reveal inadequacies in this simple model. In compact sources, typical values of the high and low frequency spectral indices lie in the range 0 to -0.8 and +1.5 to +0.5, respectively. Several models have been proposed to explain the deviation of the observed spectral indices from the theoretical values.

In a multiple outburst model, several distinct components at differing stages of evolution combine to produce a spectrum which is flat over several decades of frequency. This model predicts slight "dips" in the spectrum at frequencies between the maxima of the individual components. The spectra observed are smoother than could be expected by the superposition of several components (Cook and Spangler 1980).

In inhomogeneous source models the magnetic fields and particle densities are a function of radius ($B \propto B_0/r^2$, $\rho \propto \rho_0/r^2$) (Condon and Dressel 1973; deBruyn 1976; Marscher 1977a). At high frequencies the spectral index is the same as predicted by the simple homogeneous model, but at lower frequencies the spectral index is flatter, in closer agreement with the observations. Marscher (1977b) has investigated the flat radio spectrum of 0735+178 in terms of this model.

A flat spectrum can also be produced by an electron distribution having $\gamma \sim 1$ with high and low energy cutoffs (Moffett 1974). A low energy cutoff in the electron distribution results in a spectral index of 1/3 at frequencies below the flux density maximum. A high energy

cutoff in N(E) results in a spectral index steeper than ~2, since the synchrotron spectrum falls exponentially with frequency. Several flat spectrum radio sources exhibit this type of spectrum at infrared and optical wavelengths (Bregman et al 1981; Rieke, Lebofsky, and Wisniewski 1982). These sources are faint or not detectable at optical wavelengths due to the steep spectrum.

A relativistic Maxwellian distribution of particle energy, $N(E) = N_0 E^\gamma \exp^{-E^2/\sigma^2}$ with $E=\gamma m_0 c^2$, $\gamma \gg 1$, produces a low and high frequency spectrum similar to that of the power law distribution with low and high energy cutoffs (Wardle 1977; Jones and Hardee 1979).

Spectral evolution. The physical conditions which result in the observed time variations in compact sources have not been adequately explained. Models in which a cloud of relativistic particles expands adiabatically (van der Laan 1966; Kellermann and Pauliny-Toth 1968) do not predict (except in a few instances) the observed evolution of variable sources. The predictions for the time dependence of the frequency at which the spectrum peaks and the peak flux density of an outburst do not match the observed variations (Andrew et al 1978; Altschuler and Wardle 1977). Models invoking continual injection of particles (Peterson and Dent 1973) can explain the variations in several sources (Aller, Aller, and Hodge 1981). Models in which relativistic jets of particles are ejected nearly along the line of sight can account for some of the observed variability characteristics (Blandford and Konigl 1979).

Structural evolution. Very long baseline interferometry observations of compact sources reveal changes in source structure (see Preuss 1981 for review). The milli-arcsecond (~light year) structure changes on timescales of months to years. A large number of sources display "superluminal" expansion, in which components are separating at angular rates corresponding to velocities greater than the speed of light ($v > 10c$), if a cosmological redshift is assumed (Cohen et al 1977). Theoretical models to explain this super-light motion are reviewed by Blandford, McKee, and Rees (1977). The most popular interpretation explains the phenomena by bulk relativistic motion of the radiating particles directed close to the line of sight to the observer.

In addition to the detection of superluminal motion, VLBI observations set limits to the size of the compact cores of order light years. This size is comparable to the size inferred from radio variations at centimeter wavelengths.

Radio-infrared-optical spectra. The observed broad band radio-infrared-optical spectra (O'Dell et al 1978) are consistent with a synchrotron origin to the emission, radiating from a volume with radially decreasing magnetic field and relativistic particle distributions. The optical radiation (with the short timescale of variations implying a small volume) originates in the central region, while the radio radiation is produced in a surrounding or adjacent larger region. Correlated optical and infrared variations (Rieke and Kinman 1974), and polarization obser-

vations which reveal nearly constant position angle and high percent linear polarization at optical, infrared, and millimeter wavelengths (Rudnick et al 1978) suggest a common emission mechanism and volume of emission. Correlated variations in total flux and polarization between radio and infrared-optical frequencies would support this view.

§2. Observational Programs

Several observational programs can provide information on the emission processes at radio and infrared-optical wavelengths: single epoch radio-infrared-optical spectra; monitoring of frequency dependent flux density variations; frequency and time dependent linear polarization measurements; and frequency and time dependent small scale structure.

Single epoch multi-frequency observations of a large sample of sources are useful in determining the distribution of spectral shapes that must be accounted for by the emission mechanism models. Studies of the spectral evolution can place additional constraints on possible models. The timescale of variation can set limits to the size of the emitting region.

The study of correlated activity at radio and optical wavelengths is important for investigating the emission mechanisms in compact sources. Though synchrotron radiation is accepted as the mechanism producing the observed radio emission, it is not yet clear that this process is the

major contributing mechanism to the observed infrared-optical emission. Other mechanisms, such as synchrotron self-Compton, have been invoked to explain the radiation at these wavelengths. Correlated radio-optical behavior in several sources would argue in favor of a single emission mechanism, within a common volume, throughout this frequency range.

In this dissertation, three observational programs were undertaken to investigate evolution of compact extragalactic sources. Single epoch spectra were compiled from near-simultaneous observations at seven radio frequencies; monthly observations were conducted at 3 mm in a search for short timescale variations; and a search was made for correlated radio and optical variations.

The observations which were conducted to determine the single epoch spectra are described in Chapter II, and the spectra presented in Chapter V. The 3 mm radio observations are described in Chapter III. The observed rapid variations at 3 mm are presented and discussed in Chapter IV. The search for correlated radio and optical variability is discussed in Chapter VI. The radio and optical variations which were used in the correlation study are presented in Appendix A. The results of the numerical cross-correlation study are graphically presented in Appendix B.

C H A P T E R   II

DATA ACQUISITION AND REDUCTION

§1. The Source Sample

The results presented in this dissertation are based upon synoptic radio measurements made at frequencies between 2.7 and 90 GHz, and photographic B and PG optical observations. The radio data were obtained as part of an extensive study of radio variations in extragalactic sources which has been undertaken during the past 13 years by several individuals at the University of Massachusetts. The author has been involved in this program during the past six years. The optical observations were obtained as part of an eleven year program at the University of Florida, and have been kindly provided by participants in that program. These programs constitute the largest collection of data on the spectral evolution at radio and optical wavelengths of a substantial number of sources. The long time base and uniform time sampling of these two data sets lend themselves readily to investigation of correlated activity between the radio and optical variations.

The objects observed in these studies are primarily quasars (quasi-stellar objects, QSOs), but include several BL Lacertae type quasi-stellar objects (BL Lac objects), and compact galaxies such as Seyfert, N, or elliptical galaxies. The term "extragalactic variable source" will be employed throughout this thesis when referring to these objects as a class. The term "quasar" will also be used when discussing the

class of objects, and should be understood as comprising all the above
mentioned subclasses of extragalactic sources.

The forty five objects which are common to both the radio and opti-
cal studies are listed in Table 1. The sixty eight extragalactic and
galactic objects which were observed at radio wavelengths but which are
not included in the radio-optical study are listed in Table 2. These
two sets of sources will be referred to as the "variability sample".
Given are the IAU (International Astronomical Union) source designation
(based upon the source's celestial coordinates: right ascension and
declination), other common names for the object, the radio source posi-
tion (with reference), and the corresponding optical identification and
redshift (z). The radio positional accuracy varies, depending upon the
reference, but is typically <0.1 arc seconds. The coordinates listed
are the most accurate published positions and may differ by a few
arcseconds from the earlier published positions used during the radio
observations. The redshifts have been determined either from emission
or absorption lines in the optical spectrum of the compact source, or
from emission lines in the galaxy or "nebulosity" surrounding the com-
pact source. The BL Lac objects which do not have measured redshifts
due to the lack of observed emission or absorption lines are indicated
by dashes in the redshift column. The distinction between QSOs and BL
Lac objects is not clearly defined (see, for example, Stein, O'Dell, and
Strittmatter (1976)). Some objects have been classified in the litera-
ture as both QSOs and BL Lac objects. The identifications given in

TABLE 1

POSITIONS AND REDSHIFTS
FOR SOURCES IN OPTICAL-RADIO CORRELATION ANALYSIS

| OBJECT | OTHER NAME | RADIO POSITION | | | | | OPTICAL IDENTIFICATION | | |
		RA (1950) h m s	DEC (1950) ° ' "		REF[1]	TYPE[2]	REDSHIFT[3]		REF[4]
0007+106	IIIZw2	00 07 56.8	10 41 48.		K	Seyfert	0.089	(em)	A
0048-097		00 48 09.5	-09 45 45.		J	BL Lac	-----		A
0133+476		01 33 55.1	47 36 13.0		G	QSO	0.860	(em)	A
0219+428	3C 66A	02 19 29.7	42 48 31.		J	BL Lac	(0.444)	(em)	A
0229+131		02 29 02.5	13 09 40.4		G	QSO	2.065	(em)	A
0235+164		02 35 52.6	16 24 03.9		H	BL Lac	0.852	(ab)	A
"							0.524	(ab)	A
0306+102	OE 110	03 06 21.0	10 17 52.		J	BL Lac	-----		A
0333+321	NRAO 140	03 33 22.4	32 08 36.6		F	QSO	1.258	(em)	A
0336-019	CTA 26	03 36 59.0	-01 56 17.0		F	QSO	0.852	(em)	A
0420-014		04 20 43.5	-01 27 28.7		G	QSO	0.915	(em)	A
"							0.633	(ab)	A
0430+052	3C 120	04 30 31.6	05 14 59.5		F	Seyfert	0.0334	(gal)	B
0440-003		04 40 05.3	-00 23 20.5		H	QSO	0.850	(em)	A
0735+178		07 35 14.1	17 49 09.3		G	BL Lac	0.424	(ab)	A
0736+017		07 36 42.5	01 44 00.1		G	QSO	0.191	(em)	A
0851+202	OJ 287	08 51 57.3	20 17 58.4		F	BL Lac	(0.306)	(em)	A
0906+015		09 06 35.2	01 33 47.3		H	QSO	1.018	(em)	A
0953+254		09 53 59.7	25 29 33.5		F	QSO	0.712	(em)	A
1101+384	MKN 421	11 01 40.6	38 28 43.		J	BL Lac	0.0308	(gal)	A
1116+128		11 16 20.8	12 51 06.5		I	QSO	2.118	(em)	A
"							1.949	(ab)	A
1127-145		11 27 35.7	-14 32 54.8		G	QSO	1.187	(em)	A
1156+295		11 56 57.8	29 31 26.0		I	QSO	0.729	(em)	A
1219+285	W Coma	12 19 01.1	28 30 36.5		G	BL Lac	-----		A
1226+023	3C 273	12 26 33.2	02 19 43.3		F	QSO	0.158	(em)	A
1253-055	3C 279	12 53 35.8	-05 31 08.0		F	QSO	0.538	(em)	A
1308+326		13 08 07.6	32 36 40.2		H	BL Lac	0.996	(em)	A
"							0.879	(ab)	A

TABLE 1 (continued)

1510−089		15 10 08.9	−08 54 48.0	G	QSO	0.361	(em)	A
1514−241	Ap Libra	15 14 45.3	−24 11 22.6	H	BL Lac	0.049	(gal)	A
1638+398	NRAO 512	16 38 48.2	39 52 30.1	F	QSO	(1.67)	(em)	L
1641+399	3C 345	16 41 17.6	39 54 10.8	F	QSO	0.595	(em)	A
1652+398	MKN 501	16 52 11.7	39 50 25.0	H	BL Lac	0.034	(gal)	A
1730−130	NRAO 530	17 30 13.5	−13 02 45.9	F	QSO	0.901	(em)	E
1749+701		17 49 03.4	70 06 39.5	G	BL Lac	(0.76)	(em)	A
1749+096	OT 081	17 49 10.4	09 39 42.7	G	BL Lac	-----		A
1807+698	3C 371	18 07 18.5	69 48 57.0	F	N	0.0500	(gal)	B
1845+797	3C 390.3	18 45 37.8	79 43 03.4	B	N	0.0568	(gal)	B
1921−293		19 21 42.2	−29 20 24.9	G	QSO−BL	0.3525	(em)	C,D
2131−021		21 31 35.2	−02 06 40.0	H	BL Lac	0.557	(em)	A
2134+004		21 34 05.2	00 28 25.7	F	QSO	1.936	(em)	A
2145+067		21 45 36.1	06 43 40.9	H	QSO	0.990	(em)	A
2200+420	BL Lac	22 00 39.4	42 02 08.6	F	BL Lac	0.0688	(gal)	A
2216−038		22 16 16.4	−03 50 40.7	H	QSO	1.404	(em)	A
2223−052	3C446	22 23 11.1	−05 12 17.8	G	QSO	1.404	(em)	A
"						0.8472	(ab)	A
2230+114	CTA 102	22 30 07.8	11 28 22.7	F	QSO	1.037	(em)	A
2251+158	3C 454.3	22 51 29.5	15 52 54.3	F	QSO	0.859	(em)	A
2345−167		23 45 27.7	−16 47 52.8	F	QSO	0.600	(em)	A

Notes to Table 1

(1) Reference for radio position. Error typically <1.0". Optical positions can be found in references A and B.
(2) Identifications: QSO= quasi-stellar object, BL Lac= BL Lacertae type quasi-stellar object, N= N galaxy, Seyfert= Seyfert galaxy.
(3) em= emission line redshift, ab= absorption line redshift, gal= redshift of associated galaxy.
(4) Reference for optical identification and redshift.

References for Table 1

A. Hewitt and Burbidge (1980).
B. Burbidge and Crowne (1979).
C. Wills and Wills (1981).
D. Wright (1980).
E. Marscher and Broderick (1981).
F. Wade and Johnston (1977).
G. Draft of "Report of working group on the identification of radio/ optical sources", 24 April 1979.
H. Ulvestad et al (1981).
I. "JPL Catalog of VLBI Sources", December 1975.
J. Weiler and Johnston (1980).
K. Schnopper et al (1978).
L. Shapiro et al (1979).

TABLE 2

POSITIONS AND REDSHIFTS
FOR SOURCES NOT IN OPTICAL-RADIO CORRELATION ANALYSIS

		RADIO POSITION				OPTICAL	IDENTIFICATION	
OBJECT	OTHER NAME	RA (1950)	DEC (1950)	REF[1]	TYPE[2]	REDSHIFT[3]		REF[4]
		h m s	° ' "					
0106+013		01 06 04.5	01 19 01.1	F	QSO	2.107	(em)	A
0234+285	CTD 20	02 34 55.6	28 35 11.9	I	QSO	1.213	(em)	A
0237-027		02 37 13.7	-02 47 32.5	G				
0238-084	NGC 1052	02 38 37.4	-08 28 08.3	Q	E3	0.0047	(gal)	T
0240-002	NGC 1068	02 40 06.5	-00 13 31.3	S	Seyfert	0.0037	(gal)	Z
0300+470	4C 47.08	03 00 10.1	47 04 33.7	G	BL Lac	-----		A
0316+161	CTA 21	03 16 09.1	16 17 40.4	H	EF			O
0316+413	3C 84	03 16 29.6	41 19 51.9	F	Seyfert	0.0177	(em)	B
0355+508	NRAO 150	03 55 45.3	50 49 20.3	F	U			U
0404+767	4C 76.03	04 04 00.1	76 48 52.5	V	GAL			V
0405-123		04 05 27.4	-12 19 30.3	a	QSO	0.574	(em)	A
0415+379	3C 111	04 15 00.6	37 54 19.3	R	N	0.0485	(gal)	B
0433+295[5]	3C 123	04 33 55.4	29 34 14.0	a	E/CD	0.2177	(gal)	B
0454-234	OF-292	04 54 57.3	-23 29 29.1	H	U			U
0458-020		04 58 41.3	-02 03 33.4	H	QSO	2.286	(em)	A
0528-250		05 28 05.2	-25 05 44.5	H	QSO	2.765	(em)	A
··						2.8120	(ab)	A
0528+134		05 28 06.7	13 29 42.2	H	QSS			V
0552+398	DA 193	05 52 01.4	39 48 21.9	F	QSO	(2.365)	(em)	A
0605-085		06 05 36.0	-08 34 19.3	F	U			U
0607-157		06 07 26.0	-15 42 03.4	G	QSO	0.324	(em)	A
0723-008		07 23 17.8	-00 48 55.4	H	N	0.1280	(gal)	B
0727-115		07 27 58.1	-11 34 52.6	H				
0748+126		07 48 05.1	12 38 45.3	H	QSO	0.889	(em)	A
0754+100	OI 090.4	07 54 22.6	10 04 39.		BL Lac	-----		A
0814+425	OJ 425	08 14 51.7	42 32 07.7	F	QSS			V
0829+046	OJ 049	08 29 10.9	04 39 50.9	I	BL Lac	-----		A
0831+557	4C 55.16	08 31 04.4	55 44 41.4	F	GAL	0.2420	(gal)	B
0834-201		08 34 24.6	-20 06 30.4	H	QSS			U
0836+710	4C 71.07	08 36 21.5	71 04 22.4	H				
0859-140		08 59 54.9	-14 03 38.8	H	QSO	1.327	(em)	A

TABLE 2 (continued)

0923+392	4C 39.25	09 23 55.3	39 15 23.6	F	QSO	0.699	(em)	A
0951+699	M 82	09 51 42.0	69 54 57.6	S	IRR	0.0009	(gal)	B
1055+018		10 55 55.3	01 50 03.7	G	QSO	0.890	(em)	A
1215+303	ON 325	12 15 21.1	30 23 39.9	G	BL Lac	-----		A
1228+126[5]	3C 274	12 28 17.6	12 40 01.6	I	E2	0.0043	(gal)	B
1322-427	NGC 5128	13 22 31.5	-42 45 31.		E	0.0016	(gal)	B
1328+307[6]	3C 286	13 28 49.7	30 45 58.6	H	QSO	0.849	(em)	A
"						0.6920	(ab)	A
1334-127	1335-12	13 34 59.9	-12 42 00.0		GAL			U
1345+125	4C 12.50	13 45 06.2	12 32 20.3	H	S0	0.1218	(gal)	B
1354-152	OP-192	13 54 28.6	-15 12 51.8	H	QSS			U
1404+286	OQ 208	14 04 45.6	28 41 29.2	F	Seyfert	0.0768	(gal)	B
1413+135		14 13 33.9	13 34 17.4	H	QSO	0.26	(gal)	P
1418+546	OQ 530	14 18 06.2	54 36 57.9	H	BL Lac	-----		A
1458+718	3C 309.1	14 58 56.6	71 52 10.8	M	QSO	0.905	(em)	A
"						0.8890	(ab)	A
1502+106	OR 103	15 02 00.2	10 41 17.7	F	QSO	1.833	(em)	A
1548+056		15 48 06.9	05 36 12.4	N	QSS			U
1555+001	DA 393	15 55 17.7	00 06 43.5	F	QSO	1.770	(em)	A
1607+268		16 07 09.3	26 49 18.6	H				
1611+343		16 11 47.9	34 20 19.8	F	QSO	1.401	(em)	A
1622-253		16 22 42.0	-25 20 44.0					
1633+382	4C 38.41	16 33 30.6	38 14 10.0	H	QSO	1.814	(em)	A
1642+690		16 42 18.0	69 02 13.2	G				
1656+053		16 56 05.6	05 19 47.0	I	QSO	0.879	(em)	A
1739+522	4C 51.37	17 39 29.0	52 13 10.4	G	QSO	1.375	(em)	A
1741-038		17 41 20.6	-03 48 49.0	F	QSS			U
1828+487	3C 380	18 28 13.5	48 42 41.0	M	QSO	0.692	(em)	A
1909+048	SS 433	19 09 21.3	04 53 53.1	Y	G0			Y
1958-179	OV-198	19 58 04.6	-17 57 16.9	H	QSO	0.650	(em)	A
2005+403		20 05 59.6	40 21 02.8	G	QSO	1.736	(em)	A
2021+614	OW 637	20 21 13.3	61 27 18.1	F				
2037+511	3C 418	20 37 07.5	51 08 35.7	F	QSO	1.686	(em)	A
2037+421[5]	DR 21	20 37 14.3	42 08 55.	c	HII			b
2048+312	CL 4	20 48 47.4	31 16 11.	X	G0/QSO			X
2105+420[6]	NGC 7027	21 05 09.4	42 02 03.	W	PN			
2121+053	OX 036	21 21 14.8	05 22 27.3	I	QSO	1.878	(em)	A

TABLE 2 (continued)

2155-152	OX-192	21 55 23.6	-15 15 34.	I	BL Lac	-----		A
2201+315	4C 31.63	22 01 01.4	31 31 05.9	G	QSO	0.297	(em)	A
2243-123	OY-172.6	22 43 39.8	-12 22 40.2	H	QSO	0.630	(em)	A

Notes to Table 2

(1) Reference for radio position. Error typically <1.0". Optical positions can be found in references A and B. Blanks indicate uncertainty in the reference for the radio position.

(2) Identifications: QSO= quasi-stellar object, BL Lac= BL Lacertae type quasi-stellar object, QSS= quasi-stellar source with no measured redshift, N= N galaxy, Seyfert= Seyfert galaxy, E=Elliptical galaxy, SO= SO galaxy, CD= CD galaxy, GAL= galaxy of unspecified type, EF= empty field, U= unidentified, HII= galactic HI region, PN= planetary nebula, GO= galactic object, blank= no reference for identification found.

(3) em= emission line redshift, ab= absorption line redshift, gal= redshift of associated galaxy.

(4) Reference for optical identification and redshift. Blanks indicate no reference found for optical identification.

(5) Primary calibration source for frequencies > 7.9 GHz.

(6) Secondary calibration source for frequencies > 7.9 GHz.

References for Table 2

A. Hewitt and Burbidge (1980).
B. Burbidge and Crowne (1979).
F. Wade and Johnston (1977).
G. Draft of "Report of working group on the identification of radio/ optical sources", 24 April 1979.
H. Ulvestad et al (1981).
I. "JPL Catalog of VLBI Sources", December 1975.
M. Wade (1970).
N. Brosche, Wade, and Hjellming (1973).
O. Kristian and Sandage (1970).
P. Bregman et al (1981).
Q. Condon and Dressel (1978).
R. Brosche and Campbell (1979).
S. Condon et al (1981).
T. Humason, Mayall, and Sandage (1956).
U. Altschuler and Wardle (1976) and references within.
V. Peacock et al (1981).
W. Baars et al (1977).
X. Webster and Ryle (1976).
Y. Geldzahler, Pauls, and Salter (1980).
Z. Walker (1968).
a. Andrew et al (1978) and references within.
b. Dent (1972).
c. Wynn-Williams (1971).

Tables 1 and 2, used throughout this dissertation, correspond to the
most common identification in the current literature.

§2. Radio Observations

Introduction. Currently, about 100 sources are regularly observed at
five radio frequencies between 2.7 and 90 GHz at time intervals ranging
from one to four months. Measurements made at λ3mm are discussed
separately in Chapter III. In addition, two epoch measurements were
obtained for a subset of sources at 1.4 and 5.0 GHz in order to better
define the centimeter radio spectra. The spacings of the observations
are determined by scheduling constraints at the observatories and by
source activity. The 7.9 and 15.5 GHz observations, performed at
Haystack Observatory[1], constitute the primary observational work of this
dissertation. The acquisition and reduction of this data has been the
responsibility of the author during the last six years. The uniform,
closely spaced observations at these frequencies are used in the search
for correlations between the radio and optical variations. The lower
(2.7 GHz) and higher (31.4 and 89.6 GHz) observations do not have ade-
quate temporal sampling to permit a detailed investigation of the radio-
optical correlations. The radio outbursts are usually initially opaque
at 2.7 GHz and maxima would be delayed relative to the optical events.
The data at all seven frequencies are used in the study of the radio
spectral evolution of outbursts which appear to have correlated optical
activity.

In the following sections, a brief review is given of the observing procedures and data reduction techniques at each of the seven radio frequencies. The techniques employed in reduction of the 7.9 and 15.5 GHz observations are discussed in more detail since these measurements constitute the major data used in the subsequent analysis. The observing and reduction procedures at 1.4 and 5.0 GHz are fully discussed since the methods employed have not been previously published. Relevent parameters of the receivers and telescopes used at each frequency, compiled from appropriate observatory literature, are given in Table 3.

1.4 GHz (21 cm). Observations were conducted at two epochs (5-6 September 1978 and 4-6 December 1978) at 1.4 GHz (λ 21.4 cm) using the National Radio Astronomy Observatory (NRAO)[2] 300-foot antenna, located in Green Bank, West Virginia. The purpose of these sets of observations was to extend to lower frequencies the radio spectra of the approximately one hundred sources in the sample whose radio variations have been observed at higher frequencies.

The basic parameters of the receiver and telescope are given in Table 3. The observing procedures and system performance descriptions are covered in detail in the NRAO internal report "300-foot Telescope Observer's Manual, 1975". A review of the important observing techniques and reduction procedures follows.

The 300' antenna, being a transit telescope, is limited to a single drift scan observation of a source each sidereal day. Due to several

TABLE 3

RADIO TELESCOPE AND RECEIVER PARAMETERS[1]

Frequency, Wavelength (GHz, cm)	Telescope size	Beamwidth (' arc)	System Temperature (K)	Receiver Bandwidth (MHz)	Receiver Type	Feed Horns, Polarization	Peak Aperture Efficiency (%)
1.4 21.4	NRAO 300'	9.7	60	40	cooled upconverter	two, total power orthogonal linear	54
2.695 11.1	NRAO 300'	5.2	120	100	degenerate paramp	3 horn, pol. switched linear	52
4.995 6.0	NRAO 300'	2.7	70	580	cooled paramp	two – beam switched circular	40
7.875 3.8	Haystack 120'	4.6	150	20	cooled paramp	one, load switch circular	40
15.5 1.9	Haystack 120'	2.2	2000	1200	two channel tunnel diode	two – beam switched orthogonal linear	30
31.4 0.96	NRAO 36'	3.7	500 (each channel)	1000	mixer	two – beam switched orthogonal linear	51
89.6 0.33	NRAO 36'	1.3	280 (each beam)	500	cooled mixer	two – beam switched orthogonal linear	30

Notes to Table 3

(1) Compiled from literature provided by the observatories.

sources having nearby right ascensions[3], some sources were not observed at 1.4 GHz. Additionally, the two observing sessions did not have uniform coverage in right ascension, resulting in many sources not being observed in one or both observing sessions. The 300' telescope cannot observe sources below -20° declination.

A source was observed by positioning the telescope at the current source declination, allowing the source to drift through the antenna beam as the earth rotates beneath the celestial object. The observed power output from the receiver was integrated every 2 seconds, with this ensemble of points constituting a scan. The power output was converted to an antenna temperature by comparison with the receiver response to a known temperature calibration tube. Scans were at least three (times secant declination) minutes in duration, sufficiently long that empty (blank) sky was observed several beamwidths prior to and following the source transit.

The scans were reduced using the standard NRAO program "Condare". To measure the source strength, a linear baseline was fit to the data obtained when the source was not in the main beam of the telescope. The convolution of the antenna beam pattern with a small diameter source can be approximated by a Gaussian. A Gaussian profile was least-squares fit to the scan, with the free parameters being the peak antenna temperature, central position, and half power width (HPW) of the Gaussian.

For non-point (extended) sources the peak antenna temperature must be corrected by a source size correction factor (CS) in order to obtain

the integrated antenna temperature. For a source which is small com-
pared to the antenna beam size, the convolution of the telescope beam
profile with the source brightness distribution is approximately a
Gaussian but with a larger HPW. The source size correction factor can
be determined from the HPW of the fitted Gaussian. No observed program
sources possessed fitted HPW's that would require source size correction
factors to the peak antenna temperature. Candidate calibration sources
which were found to be extended were excluded from the final calibration
list.

The pointing characteristics of the telescope are regularly
assessed by the staff at NRAO. No effort was made to correct for
pointing errors in declination (these errors would result in decreased
apparent source strength since the antenna beam would not be pointed
directly at the source). The pointing accuracy of the 300' antenna is
generally better than $\frac{1}{2}$', which for the 10' half power beamwidth at
1.4 GHz corresponds to an error in the flux density determination of
less than $\frac{1}{2}$%. Additionally, such pointing errors, if constant in time,
would be removed in later stages of calibration, since all sources would
require the same multiplicative pointing correction factor. Diurnal or
day-to-day variations in telescope pointing would be reflected in a time
dependent system efficiency.

The aperture efficiency of the 300' antenna is a function of the
declination (or zenith angle) at which the telescope is pointed, due to

changing gravitational forces which produce deformations in the dish and support structure. The aperture efficiency of a telescope is given by

$$\varepsilon_A = \frac{2 k T_A}{S A_g} \qquad \text{(II-1)}$$

where T_A is the observed antenna temperature corrected by the source size correction factor, k is Boltzmann's constant (1.38×10^{-23} J/K), A_g is the geometrical cross-sectional area of the telescope, and S is the flux density of the source. For the 300', $A_g = 6567$ m^2. When S is expressed in units of Jansky's[4] (Jy) and T_A in degrees Kelvin, equation II-1 reduces to

$$\frac{S}{T_A} = \frac{0.420}{\varepsilon_A} \qquad . \qquad \text{(II-2)}$$

The quantity S/T_A is called the calibration constant, $CC(\delta)$, and is a function of declination, δ.

To determine the calibration constant (or the aperture efficiency), sources of known flux density were observed throughout the observing session, interspersed amongst the variable source sample. The standard, or calibration, sources were selected from a list of source positions and flux densities compiled by Crane (1978). The gain calibration was calculated with the program "Find300" written by P. Crane at NRAO. A fourth order polynomial was fit to the observed calibration constant as a function of declination. Candidate calibration sources were deleted as standards if their measured calibration constant differed appreciably

from those of other sources at nearby declinations. These deleted stan-
dards may have had poorly determined flux densities in the earlier sur-
veys, or they may be variable sources. A typical declination dependent
calibration constant curve is shown in figure 1.

The 1.4 GHz system consists of two feeds whose beams are separated
in the sky by ~1 minute of arc. Thus two measurements of the source
antenna temperature are obtained from each scan. The feeds are sen-
sitive to orthogonal linear polarizations. The strength of a linearly
polarized source, as observed by each feed, would depend on the source
polarization position angle and the feed orientation. Few compact
extragalactic sources exhibit linear polarizations as great as 4% at
1.4 GHz. Thus, typical source linear polarizations (less than 4%) would
not readily be detectable in these sets of observations since the com-
bined measurement and calibration error is of comparable magnitude. The
output from both feeds were calibrated separately, and the appropriate
declination dependent calibration constants were applied to the observed
antenna temperatures to obtain the source flux density. The measure-
ments from the orthogonal feeds were then added to obtain the total
source flux density. No sources exhibited obvious polarization.

The error in each flux density determination is the quadratic sum
of the error from the Gaussian fitting procedure and the error in the
calibration constant. This latter error reflects errors in the assumed
standard source flux densities, measurement errors in the Gaussian

Figure 1.   The declination dependent aperture efficiency at 1.4 GHz for the NRAO 300' antenna derived from measurements obtained 4-6 December 1978.   The calibration sources (assumed non-variable sources of known flux density) used in defining the gain curve are from a compilation by Crane (1978).   A fourth order polynomial was fit to the observed calibration constant as a function of declination.   The calibration constant is defined in equation II-2.

Declination Dependent
Aperture Efficiency
300 – foot antenna
1.4 GHz   feed 1
4 – 6   Dec. 1978
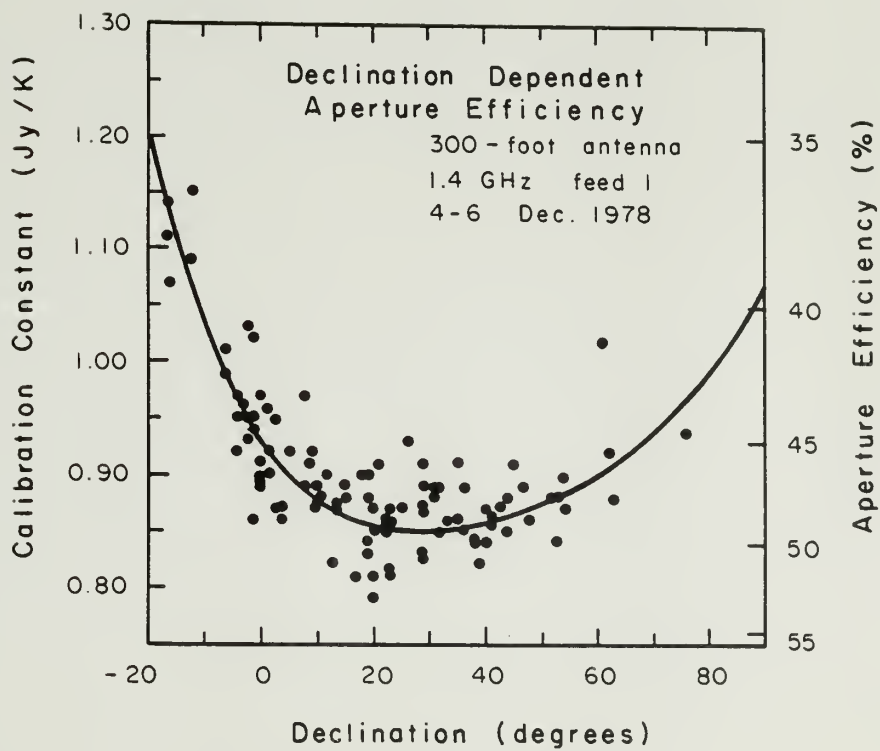
fitting, and any temporal changes in gain due to pointing or receiver/antenna stability. The error in determining the calibration constant is typically <5%, due primarily to uncertainties in the flux densities of the calibration sources. This calibration error is a systematic error, and should be similar for all observing sessions if the same family of calibration sources are used.

A statistical error (termed "confusion") due to the contribution of background, unrelated sources to the observed source strength produces an additional statistical error in the calculated source flux density. This error results from emission in the beam pattern either at the source position (making the source appear stronger than it actually is) or in the neighboring "off source" position (making the source appear weaker). The magnitude of this statistical error can be calculated from the number/flux density relationship for extragalactic sources (the log N / log S relationship; von Hoerner, 1975). For the 300' beam at 1.4 GHz, the confusion level is less than 0.03 Jy (e.g. a source of strength less than 0.03 Jy has a probability of 1 of appearing within three beamwidths of the source position). The affect of confusion is lower at the higher frequencies.

The individual flux density measurements (weighted by their errors) were then averaged. The quoted flux density error was taken to be the larger of two error calculations - the standard deviation of the individual measurements (external error) or the representative error in an

individual measurement (internal error). The flux densities and errors for both the calibration sources and the variability sample sources are presented in Tables 4 and 5, respectively, for the two epochs of observations.

Absolute flux density measurements for sources at declinations less than $-10°$ or greater than $+60°$ may be in error by a multiplicative factor. The lack of calibrators at high and low declinations results in some uncertainty in the absolute gain calibration in these ranges. The calibration constant gain curves for each observing session were compared. No systemmatic difference existed between the shapes of the individual gain curves except for a few per cent difference at the extreme declinations. These variations are reflected in larger calibration constant errors at these declinations.

Different calibration sources were used during the two observing sessions due to differences in the sidereal time coverage and duration of the two sessions. To test for different gain calibration between the two sessions, the ratio

$$R = \frac{S_D}{S_S} \tag{II-3}$$

was calculated for each source, where S_S and S_D are the average measured flux densities for the September and December observing sessions. For the 48 calibration sources common to both sessions, $R = 1.010 \pm 0.004$, with a median value of 1.011. Restricting the calculation to sources

TABLE 4

1.4 GHz FLUX DENSITY MEASUREMENTS
FOR CALIBRATION SOURCES AND SOURCES NOT IN VARAIBILITY SAMPLE

		Flux Density (Jy)							
	Other	5-6 Sept 1978			4-6 Dec 1978			Assumed[2]	
Object	Names	Flux	Error	N[1]	Flux	Error	N[1]	Flux	Error
0003-003	3C 2	3.64 ±	0.13	(2)	3.76 ±	0.10	(4)	3.54 ±	0.12
0019-000		2.82	0.06	(2)	2.85	0.08	(4)	2.73	0.07
0030+196	3C 12	1.88	0.04	(2) NC	1.84	0.05	(4)	1.72	0.06
0035-024	3C 17	6.14	0.14	(2)	6.36	0.16	(2)	6.25	0.17
0038+328	3C 19	-			3.11	0.09	(2)	3.12	0.08
0051-038	3C 26	2.12	0.05	(2)	2.16	0.06	(4)	2.11	0.09
0056-001		2.42	0.08	(2) NC	2.46	0.09	(4) NC	2.16	0.07
0117-155	3C 38	5.05	0.16	(2)	5.11	0.13	(4)	4.95	0.13
0112-017		0.90	0.02	(2) NC	0.84	0.03	(4) NC	1.20	0.11
0125+287	3C 42	2.75	0.06	(2)	2.74	0.08	(4)	2.64	0.18
0145+532	3C 52	3.67	0.11	(2)	3.80	0.13	(4)	3.72	0.10
0159-117	3C 57	2.94	0.09	(2)	3.07	0.09	(4)	3.24	0.14
0206+355		2.03	0.07	(2)	2.03	0.07	(4)	2.15	0.06
0218-021	3C 63	-			3.41	0.09	(2)	3.32	0.08
0255+574		-			0.12	0.02	(4) NC	-	
0307+169	3C 79	-			4.64	0.29	(2)	4.59	0.40
0309+390		1.82	0.05	(2)	1.83	0.05	(2)	1.73	0.05
0331-013	3C 89	2.69	0.06	(2)	2.72	0.07	(2)	2.72	0.07
0428+205		-			3.56	0.10	(2)	3.81	0.09
0450+314	3C 131	2.74	0.07	(2)	2.77	0.08	(4)	2.90	0.15
0507+290		1.89	0.07	(2)	1.90	0.06	(4)	1.90	0.06
0515+508	3C 137	1.85	0.06	(2) NC	1.95	0.06	(4) NC	2.22	0.14
0531+194		6.58	0.12	(2)	6.50	0.19	(4)	6.73	0.14
0540+187		2.20	0.06	(2)	2.23	0.09	(4)	2.24	0.06
0624-058	3C 161	-			18.76	0.47	(4)	19.03	0.13
0640+233	3C 165	-			2.38	0.07	(4)	2.40	0.20
0651+542	3C 171	-			3.64	0.12	(4)	3.66	0.14
0659+445		-			2.34	0.07	(2)	2.47	0.07
0711+146	3C 175.1	-			1.98	0.06	(2)	2.04	0.06
0743-006		-			0.87	0.02	(2)	0.80	0.08

TABLE 4 (continued)

0758+143	3C 190	–				2.45	0.07	(4)		2.47	0.07
0806+426	3C 194	–				2.03	0.06	(2)		2.05	0.06
0809+483	3C 196	–				13.99	0.40	(2)		13.85	0.28
0824+294	3C 200	–				1.92	0.06	(4)		2.00	0.11
0941+100	3C 226	–				2.32	0.07	(4)		2.25	0.06
0947+145	3C 228	–				3.39	0.10	(2)		3.47	0.08
1003+351	3C 236	–				3.21	0.10	(2)		3.24	0.08
1005+077	3C 237	–				6.24	0.17	(2)		6.25	0.15
1039+029		–				2.73	0.07	(2)		2.84	0.07
1040+123	3C 245	–				3.09	0.16	(2)		3.06	0.08
1059−010	3C 249	–				2.64	0.12	(2)		2.56	0.07
1111+408	3C 254	2.89	0.16	(1)		–				3.05	0.13
1138+015		2.61	0.10	(1)		2.51	0.07	(2)		2.47	0.07
1140+223	3C 263.1	–				2.90	0.08	(2)		2.96	0.07
1147+130	3C 267	2.18	0.11	(1)		2.28	0.06	(2)		2.16	0.07
1148−001		–				2.89	0.09	(2)		3.06	0.08
1153+317		–				2.81	0.08	(2)		2.77	0.07
1201−041		–				2.19	0.05	(2)		2.10	0.06
1206+439	3C 268.4	1.82	0.08	(1)	NC	1.97	0.06	(2)		2.04	0.09
1229−021		–				1.63	0.04	(2)		1.76	0.05
1237−101		1.67	0.08	(1)	NC	1.58	0.05	(4) NC	1.93	0.11
1318+113		2.21	0.07	(2)		2.22	0.07	(2)		2.18	0.06
1323+321		4.17	0.11	(2)	NC	4.33	0.06	(2)		4.56	0.10
1328+254	3C 287	6.74	0.14	(2)		6.54	0.19	(2)		6.72	0.14
1340+053		1.70	0.06	(1)		1.62	0.08	(2) NC	1.73	0.11
1413+349		1.91	0.05	(2)	NC	1.95	0.06	(2)		2.09	0.09
1420+198	3C 300	3.39	0.08	(2)		3.43	0.10	(2)		3.44	0.08
1425−011	3C 300.1	2.87	0.07	(2)	NC	2.87	0.08	(2) NC	3.30	0.17
1441+522	3C 303	2.47	0.12	(2)		2.51	0.08	(2)		2.46	0.07
1448+634	3C 305	2.93	0.10	(2)		3.01	0.11	(2)		2.94	0.09
1517+204	3C 318	2.47	0.05	(2)		2.52	0.07	(2)		2.50	0.07
1523+033		1.87	0.04	(2)		1.94	0.05	(2)		1.86	0.06
1543+005		1.48	0.04	(2)	NC	1.56	0.05	(2) NC	1.71	0.05
1615+324	3C 332	2.40	0.06	(2)		–				2.40	0.06
1618+177	3C 334	–				1.98	0.08	(2)		2.12	0.13
1626+396	3C 338	–				3.59	0.10	(2)		3.53	0.09
1658+471	3C 349	–				3.19	0.12	(2)		3.18	0.08
1704+608	3C 351	–				3.12	0.11	(2)		3.52	0.10
1716+006		2.10	0.05	(2)		2.12	0.06	(2)		2.18	0.06
1819+396		3.26	0.09	(2)		3.32	0.10	(2)		3.39	0.08

TABLE 4 (continued)

Source	3C	Flux	Err	(N)	Flux	Err	(N)	Flux	Err
1938-155		–			7.20	0.16	(2)	7.17	0.15
1939+605	3C 401	4.92	0.14	(2)	–			4.75	0.14
2003-025		–			2.05	0.06	(2)	2.01	0.06
2012+234	3C 409	13.36	0.27	(2)	13.49	0.39	(2)	13.04	0.27
2018+231		–			1.84	0.05	(2)	1.75	0.05
2019+098	3C 411	3.22	0.05	(2)	3.18	0.09	(2)	3.18	0.08
2030+257	3C 414	–			1.71	0.08	(2)	1.81	0.06
2104+763	3C 427.1	3.74	0.02	(2)	3.78	0.16	(2)	3.70	0.18
2111+620	3C 429	2.42	0.07	(2)	2.54	0.09	(2)	2.53	0.08
2126+073	3C 435	1.98	0.04	(2)	–			2.01	0.06
2128+048		–			3.92	0.11	(2)	3.98	0.09
2153+377	3C 438	6.78	0.19	(2)	6.83	0.19	(4)	6.70	0.14
2209+081		–			1.68	0.05	(2)	1.80	0.06
2210+016		2.60	0.05	(2)	2.67	0.07	(2)	2.60	0.07
2309+090	3C 456	2.42	0.05	(2)	2.42	0.07	(4)	2.51	0.08
2314+038	3C 459	4.23	0.08	(2)	4.35	0.12	(4)	4.17	0.10
2324+405	3C 462	2.49	0.08	(2)	2.41	0.07	(4)	2.38	0.12
2337+220	3C 466	2.12	0.04	(2)	2.12	0.06	(4)	2.13	0.07
2349-014		–			1.55	0.05	(2)	1.63	0.12
2356+437	3C 470	2.03	0.06	(2) NC	1.96	0.06	(2)	1.88	0.06

Notes to Table 4

(1) Number of measurements included in average. Two measurements are obtained each day (2 feeds). An "NC" following the number of observations indicates that the source was not used as a calibration source, due either to suspected source variability or a poorly determined assumed flux density.

(2) Assumed flux density for calibration sources. Values are from list provided by Crane (1978). These values were used in determining the declination dependent antenna aperture efficiency.

TABLE 5

1.4 GHz FLUX DENSITY MEASUREMENTS
FOR SOURCES IN VARIABILITY SAMPLE

| Object | Other Names | Flux Density (Jy) | | | | | | Variability Index $(V)^2$ |
| | | 5-6 Sept 1978 | | | 4-6 Dec 1978 | | | |
		Flux	Error	N^1	Flux	Error	N^1	
0007+106	IIIZw2	0.13 ±	0.02	(1)	0.14 ±	0.02	(4)	0.3
0048-097		0.88	0.03	(2)	1.19	0.06	(4)	4.3
0106+013		2.86	0.07	(2)	2.75	0.08	(4)	-1.0
0133+476		1.61	0.05	(2)	1.63	0.05	(4)	0.3
0229+131		1.16	0.02	(2)	1.25	0.04	(4)	2.0
0235+164		1.71	0.03	(2)	1.39	0.04	(2)	-6.8
0238-084	NGC 1052	-			0.67	0.02	(2)	-
0300+470		1.80	0.05	(2)	1.72	0.05	(4)	-1.2
0316+161	CTA 21	-			7.53	0.21	(2)	-
0316+413	3C 84	16.07	0.46	(2)	16.75	0.47	(2)	1.0
0333+321	NRAO 140	-			3.15	0.10	(2)	-
0336-019	CTA 26	2.39	0.05	(2)	2.19	0.06	(2)	-2.7
0355+508	NRAO 150	5.05	0.15	(2)	5.22	0.16	(4)	0.8
0405-123		3.17	0.12	(2)	3.24	0.08	(4)	0.5
0415+379	3C 111	-			14.62	0.42	(2)	-
0420-014		0.89	0.02	(2)	1.07	0.05	(2)	3.2
0430+052	3C 120	6.22	0.11	(2)	5.99	0.16	(2)	-1.2
0440-003		2.16	0.05	(2)	2.39	0.06	(4)	2.8
0458-020		1.67	0.04	(2)	1.65	0.04	(4)	-0.4
0528+134		1.08	0.02	(2)	1.38	0.04	(4)	6.4
0552+398	DA 193	-			1.45	0.04	(4)	-
0605-085		-			3.06	0.07	(2)	-
0607-157		-			1.75	0.04	(2)	-
0723-008		-			2.47	0.07	(4)	-
0727-115		-			2.17	0.05	(4)	-
0735+178		-			1.79	0.05	(2)	-
0736+017		-			2.35	0.06	(2)	-
0748+126		-			1.47	0.04	(4)	-
0754+100	OI 090.4	-			0.63	0.02	(4)	-
0814+425	OJ 425	-			1.49	0.04	(4)	-

TABLE 5 (continued)

0831+557	4C 55.16	–			7.97	0.26	(4)	–
0836+710	4C 71.07	–			4.12	0.17	(3)	–
0851+202	OJ 287	–			1.83	0.13	(4)	–
0859–140		–			3.21	0.10	(4)	–
0923+392	4C 39.25	–			2.48	0.08	(4)	–
0953+254		–			0.84	0.03	(4)	–
1055+018		–			2.90	0.14	(4)	–
1101+384	MKN 421	0.92	0.16	(1)	0.75	0.03	(2)	–1.3
1116+128		–			2.09	0.06	(4)	
1127–145		6.23	0.37	(1)	6.47	0.33	(4)	0.5
1215+303	ON 325	0.59	0.02	(1)	0.58	0.02	(4)	–0.4
1219+285	W Coma	1.69	0.05	(2)	1.84	0.07	(2)	1.7
1226+023	3C 273	–			44.79	1.16	(2)	–
1253–055	3C 279	10.91	0.37	(2)	10.77	0.36	(2)	–0.3
1308+326		1.08	0.07	(2)	1.46	0.05	(2)	3.6
1334–127	1335–12	1.72	0.05	(2)	1.74	0.04	(2)	0.3
1345+125	4C 12.50	5.01	0.08	(2)	5.03	0.14	(2)	0.1
1354–152	OP–192	1.30	0.04	(2)	1.09	0.02	(2)	–5.4
1404+286	OQ 208	0.72	0.02	(2)	0.68	0.02	(2)	–1.5
1502+106	OR 103	1.53	0.03	(2)	1.69	0.05	(2)	2.7
1510–089		1.44	0.04	(2)	1.45	0.04	(2)	0.2
1548+056		2.00	0.04	(2)	–			–
1555+001	DA 393	1.53	0.04	(2)	1.36	0.04	(2)	–3.2
1607+268		4.43	0.10	(2)	4.51	0.13	(2)	0.5
1611+343		2.61	0.07	(2)	2.68	0.08	(2)	0.7
1633+382	4C 38.41	1.99	0.06	(2)	1.88	0.08	(2)	–1.1
1638+398	NRAO 512	0.44	0.02	(2)	–			–
1641+399	3C 345	6.91	0.29	(2)	7.75	0.22	(2)	2.1
1656+053		1.62	0.06	(1)	–			–
1730–130	NRAO 530	5.13	0.21	(2)	–			–
1739+522	4C 51.37	–			0.75	0.02	(2)	–
1741–038		1.67	0.04	(2)	–			–
1749+701		–			1.52	0.06	(2)	–
1807+698	3C 371	2.31	0.06	(2)	2.39	0.09	(2)	0.7
1828+487	3C 380	–			13.55	0.39	(2)	–
1845+797	3C 390.3	12.54	0.80	(1)	10.14	0.45	(2)	–3.0
1909+048	SS 433	0.73	0.02	(2)	0.81	0.05	(2)	1.5
1958–179	OV–198	–			0.56	0.03	(2)	–
2005+403		3.11	0.09	(2)	–			–
2037+511	3C 418	5.66	0.25	(2)	5.75	0.17	(2)	0.3

TABLE 5 (continued)

2048+312 CL 4	0.71	0.02 (2)	0.75	0.06 (4)	0.6
2121+053 OX 036	1.88	0.04 (2)	1.74	0.05 (4)	−2.2
2131−021	1.99	0.08 (1)	1.91	0.06 (4)	−0.8
2134+004	3.08	0.07 (2)	2.91	0.08 (4)	−1.6
2145+067	3.06	0.05 (2)	3.03	0.08 (4)	−0.3
2200+420 BL LAC	2.97	0.10 (2)	2.20	0.07 (2)	−7.6
2201+315 4C 31.63	−		2.05	0.06 (2)	−
2216−038	0.98	0.03 (2)	1.02	0.03 (4)	0.9
2223−052 3C446	5.80	0.25 (2)	5.93	0.22 (4)	0.4
2230+114 CTA 102	5.79	0.35 (2)	6.08	0.18 (4)	0.7
2243−123 OY−172.6	2.42	0.07 (2)	2.39	0.06 (4)	−0.3
2251+158 3C 454.3	10.10	0.44 (2)	10.47	0.51 (4)	0.5
2345−167	3.27	0.11 (2)	3.44	0.08 (4)	1.2

Notes to Table 5

(1) Number of measurements included in average. Two measurements are obtained each day (2 feeds).
(2) The variability index, V (defined in equation II-5), is a measure of the source variability between Sept. and Dec. 1978.

stronger than 2 Jy gives R = 1.011 ± 0.004 (37 sources). There is no declination or time dependence in the quantity R. The use of different calibrator sources for the two sessions thus introduces a 1% offset in the calculated flux densities. No adjustment was made to the flux densities to compensate for this effect since it is much smaller than the errors quoted for the gain curve fitting procedure, and it is not known which of the two gain curves correspond more closely to an absolute flux density scale.

The calibration and variability sample ("program") sources were checked for evidence of variability in the three months between the observing sessions. The quantity R was calculated for each source. To determine the uncertainty in the quantity R, the variance σ_R^2 was calculated from the errors (σ_S and σ_D) to the flux densities (S_S and S_D) for the September and December sessions. The variance in R is given by

$$\frac{\sigma_R^2}{R^2} = \frac{\sigma_S^2}{S_S^2} + \frac{\sigma_D^2}{S_D^2} \tag{II-4}$$

The quantity σ_R is the standard deviation in the measurement of the ratio R. A variability index, V, can be defined

$$V = \frac{R - 1}{\sigma_R} \tag{II-5}$$

which is a measure of the variability of a source between the two sessions (the number of standard deviations which the quantity R is from unity).

The quantity V is given for the variability sample sources in Table 5. This quantity is plotted in figure 2 for both the calibration and variability sample sources. The median of both distributions is 0.3; the offset from zero is due to the 1% difference in calibration scales for the two sessions. There is no strong dependence of V on source flux density or declination. The scatter in V for the calibration sources is smaller than would be expected for a Gaussian distribution with $\sigma = \sigma_R$. Except for the weak source 0112-017 (V = -1.7), all 47 calibrators are within 1.3 σ_R of the average V of 0.3. This distribution of V indicates that the quoted flux density errors may be overestimated as a result of an overestimation of the errors attributable to the calibration fitting procedure. This would occur if the assumed calibration source flux densities were not well determined from the original surveys. This is feasible since the calibration source flux densities were compiled from several references. Better determination of the calibration source flux densities would result in smaller calibration errors and resultant smaller flux density errors.

The distribution of the variability index for the variability sample differs markedly from that for the calibration sources. Based only upon measurements at these two epochs, we define sources with 1.5 < V-0.3 as "possible" variables, sources with 2 < V-0.3 < 3 as "probable" variables, and those with V-0.3 > 3 as "variable". The narrower observed distribution of V for the calibration sources than expected for a Gaussian distribution makes the exact values of V

Figure 2. Degree of variability at 1.4 GHz for 97 sources during the three month interval 5 Septemeber to 5 December 1978. The variability index, V (defined in equations II-3 thru 5), is a measure of the variability of a source (relative to the errors in the two measurements) between the two observing sessions. The offset from zero of both distributions (median V=0.3) is due to a 1% difference in calibration scales between the two sessions. No adjustment has been made to the flux density scales to compensate for this offset since it is not known which of the calibration scales corresponds more closely to an absolute flux density scale. The distribution of variability index for sources used to derive the declination dependent calibration constant can be represented by a Gaussian noise distribution. The distribution for sources in the variability sample indicates that 26% of the sources are "probably" variable ($|V-0.3| > 2.0$) over the three month interval, with an additional 12% being "possibly" variable ($|V-0.3| > 1.5$).

Degree Of Variability At 1.4 GHz
(Between 5 Sept. And 5 Dec. 1978)
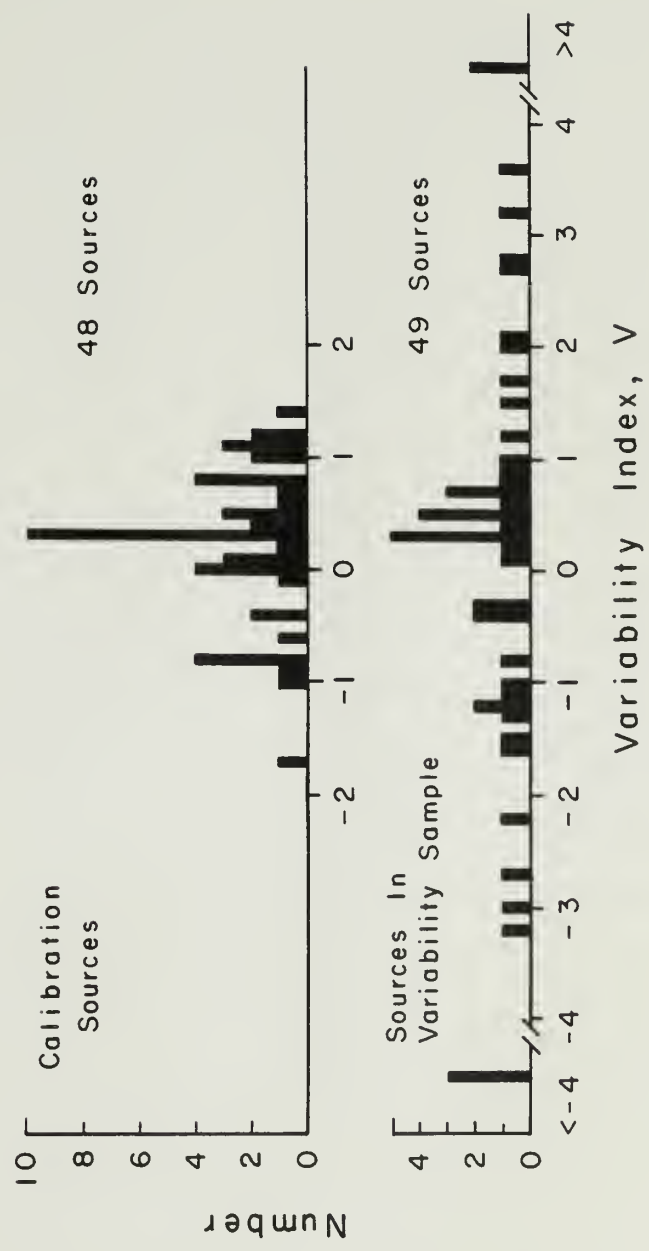
defining these "variability classes" somewhat arbitrary. The spectra of these sources are discussed further in Chapter V.

2.7 GHz (11 cm). Systematic observations of source flux density and linear polarization have been conducted at 2.695 GHz (λ 11.1 cm) using the NRAO 300-foot antenna. Approximately two hundred variable and calibration sources have been observed during twenty eight week-long sessions between 1972.67 and 1981.10. The purpose of this set of observations is to study the polarization and flux density variations in a large sample of extragalactic sources at long centimeter wavelengths, where opacity effects will be important to the observed outburst profiles. These observations constitute the lowest frequency sample of regular polarization and flux density variations in extragalactic sources.

The basic receiver and telescope parameters are given in Table 3. The observing procedures and reduction routines are described in detail by Kapitzky (1976). The observations have been obtained and reduced by several individuals throughout the $8\frac{1}{2}$ years that this program has been conducted (J.E. Kapitzky, M.F. Hartman, C.P. O'Dea, W.A. Dent, and the author).

The same observing procedures are employed for the 2.7 GHz observations as at 1.4 GHz, with one major difference. Since polarization as well as flux density is being measured, three linearly polarized feeds are used. Each feed is calibrated separately, using calibration sources with known flux density and polarization parameters. The polarized com-

ponent of the flux density in compact variable extragalactic sources is typically very weak (a few per cent of the total flux density), requiring the average of several daily scans in order to obtain sufficient signal-to-noise measurements. The data was reduced and calibrated by procedures similar to those previously discussed for the 1.4 GHz data. A full description of these procedures is given by Kapitzky (1976).

The flux density measurements obtained from this program are used in subsequent chapters in discussions of source variability and radio spectral evolution of outbursts.

5.0 GHz (6 cm). Observations were conducted at two epochs (2-5 September 1978 and 3-4 December 1978) at 4.995 GHz (λ 6.0 cm) using the NRAO 300-foot antenna. These observations were obtained at nearly the same epochs as the previously described 1.4 GHz observations. The calibration and variability sample sources were similar.

The receiver and telescope parameters are given in Table 3. As for the 1.4 GHz observations, reduction of scans was accomplished using the "Condare" routine, and "Find 300" was used to calibrate the declination dependent telescope gain.

Source observations were similar to those made at 1.4 GHz except that the 5.0 GHz system is a two feed, beam switched system. The power output from two circularly polarized feeds are differenced, fed into two

separate receivers, and integrated every second. The rapid switching between the feeds decreases the observed effects of sky background and receiver gain fluctuations. The power output is converted to antenna temperature by comparison with the receiver response to a known temperature calibration tube. The two beams are separated in the sky by three half power beamwidths (HPBW). The orientation of the two beams in right ascension and declination is adjustable. As a result of the differencing of the output from the two feeds, a scan contains two approximate gaussian profiles, one with a positive deflection and a second with a negative deflection (with their peaks separated by three HPBWs). The combination of two feeds and two receivers provides four measurements of the source strength during each source transit. Baselines were fit to the portion of the scans containing blank sky. Gaussian profiles were fit independently to the positive and negative profiles.

For the September observations, only the output from one receiver was analyzed. The relative gain of the two beams (the positive and negative profiles) was determined from observations of a few sources with the feeds positioned at the same declination. The remaining observations were conducted with the feed box rotated such that the two beams were offset by a half power beamwidth in declination. This orientation provided information on the telescope declination pointing. The small beamwidth of the 5.0 GHz system causes observations at this frequency to be very sensitive to pointing inaccuracies. Pointing errors of $1/2'$ correspond to a flux density error of 10% for the 2.7' beam at this fre-

quency, indicating that declination position errors can result in large uncertainties in source flux densities. A source will appear stronger in one of the two beams if the telescope is not positioned accurately at the source declination. By measuring the strength of the positive and negative responses in each scan, the pointing error can be determined and applied to the data to obtain a corrected (for pointing) antenna temperature. During the September session, the pointing was sufficiently in error that the signal in one beam was often less than half that of the other beam. The declination dependent gain curve determined using the pointing corrections exhibited more scatter than the gain curve calculated using only the single feed with the larger observed antenna temperatures. The increased scatter was a result of the pointing errors being so large that pointing correction factors were poorly determined (the pointing correction method is beneficial only when the pointing is in error by less than $\sim\frac{1}{2}$ HPBW). The gain curve for the feed with the lesser antenna temperatures was also found to be poorly determined. Using the results from both feeds appeared to degrade the quality of the derived flux densities, so only the single feed was used in flux density calculations for the September session. The pointing errors are reflected as a scale factor in the calibration constant gain curve. A sixth order polynomial was used in the determination of the declination dependent gain curve (lower order polynomials did not produce as good a fit at the extreme elevations for this observing session), and the error in the calibration constant was assumed to be 5% at all declinations.

For the December observations, the feeds were oriented east-west, so no declination pointing information was obtained. Errors in the flux density scale resulting from declination dependent pointing errors (if constant in time) would be removed by the calibration constant fitting procedure. This feed orientation provided four measurements of the source strength during each source transit. Fourth order polynomials were used to fit for the declination dependent calibration constant. A typical set of data and fitted gain curve are shown in figure 3. The four sets of data were calibrated separately, with the results averaged (as was done with the 1.4 GHz data) to obtain the quoted flux densities.

The derived flux densities for calibration and variability sample sources for the two epochs of observations at 5.0 GHz are given in Tables 6 and 7, respectively. The quoted errors are the larger of the external and internal errors. The gain curves were not well determined for low ($<-10°$) or high ($>+60°$) declinations, due to a lack of many calibration sources at these declinations and the rapid declination dependent change in telescope efficiency. Flux densities of sources in these declination ranges may be systematically in error in either observing session.

A test was done to determine the consistency of the calibration factors between the two sessions. For the 64 calibration sources common to both sessions, the flux ratio defined in equation II-3 is R = 0.986 ±.009, with a median value of 0.988. For sources stronger than 1 Jy,

Figure 3. The declination dependent aperture efficiency at 5.0 GHz for the NRAO 300' antenna derived from measurements obtained 3-4 December 1978. The calibration sources (assumed non-variable sources of known flux density) used in defining the gain curve are from a compilation by Crane (1978). A fourth order polynomial was fit to the observed calibration constant as a function of declination. The calibration constant is defined in equation II-2.

Declination Dependent
Aperture Efficiency
300-foot antenna
5.0 GHz   feed 2
3-4 Dec. 1978

TABLE 6

5.0 GHz FLUX DENSITY MEASUREMENTS
FOR CALIBRATION SOURCES AND SOURCES NOT IN VARIABILITY SAMPLE

		Flux Density (Jy)							
Object	Other Names	2-5 Sept 1978			3-4 Dec 1978			Assumed[2]	
		Flux	Error	N[1]	Flux	Error	N[1]	Flux	Error
0003-003	3C 2	1.47 ±	0.08	(3)	1.47 ±	0.06	(4)	1.41 ±	0.04
0019-000		1.16	0.06	(3)	1.13	0.05	(4)	1.05	0.04
0030+196	3C 12	0.80	0.04	(3)	0.78	0.04	(4)	0.82	0.03
0035-024	3C 17	2.52	0.13	(2)	2.62	0.11	(4)	2.72	0.07
0038+328	3C 19	1.07	0.07	(1)	–			1.26	0.09
0051-038	3C 26	0.60	0.03	(1)	0.64	0.03	(4)	0.61	0.04
0056-001		1.39	0.07	(2)	1.30	0.06	(4)	1.46	0.05
0117-155	3C 38	1.51	0.08	(2)	1.42	0.05	(4)	1.42	0.07
0112-017		0.92	0.05	(3) NC	0.89	0.04	(4) NC	1.16	0.04
0116+082		1.08	0.06	(1)	–			1.18	0.04
0125+287	3C 42	0.83	0.05	(1)	0.88	0.04	(4)	0.84	0.04
0145+532	3C 52	1.45	0.08	(3)	1.49	0.04	(4)	1.48	0.06
0154+286	3C 55	0.55	0.04	(1) NC	–			0.88	0.10
0159-117	3C 57	1.36	0.07	(1)	1.39	0.05	(4)	1.25	0.04
0206+355		0.92	0.05	(3)	0.87	0.04	(4)	0.87	0.03
0223+341		1.30	0.07	(1)	–			1.20	0.04
0255+574		–			0.13	0.01	(4) NC	–	
0307+169	3C 79	1.20	0.06	(2)	1.23	0.07	(4)	1.31	0.04
0309+390		0.72	0.05	(1)	–			0.73	0.01
0319+121		1.00	0.07	(1)	–			1.10	0.04
0331-013	3C 89	–			0.69	0.03	(4) NC	0.81	0.06
0411+141		0.78	0.05	(1)	0.74	0.04	(4)	0.89	0.03
0428+205		2.22	0.14	(1)	–			2.31	0.06
0450+314	3C 131	0.82	0.04	(3)	0.79	0.04	(4)	0.86	0.04
0507+290		0.61	0.03	(3)	0.58	0.03	(4)	0.65	0.06
0515+508	3C 137	0.60	0.03	(3)	0.61	0.02	(4)	0.57	0.04
0531+194		2.37	0.12	(3)	2.23	0.12	(4)	2.53	0.05
0540+187		0.76	0.04	(3)	0.70	0.04	(4)	0.63	0.05
0621+400	3C 159	0.71	0.06	(1)	–			0.70	0.01
0624-058	3C 161	6.68	0.34	(2)	6.56	0.28	(4)	6.73	0.09

TABLE 6 (continued)

0640+233	3C 165	0.70	0.04	(2)		0.69	0.04	(4)	0.77	0.03
0651+542	3C 171	1.22	0.06	(2)		1.21	0.03	(4)	1.22	0.04
0655+699		–				0.69	0.02	(4)	0.69	0.01
0659+445		0.57	0.04	(1)		–			0.54	0.01
0702+749	3C 173.1	0.86	0.05	(1)		0.81	0.02	(4)	0.77	0.06
0711+146	3C 175.1	0.60	0.05	(1)		–			0.56	0.05
0742+103		3.85	0.20	(2)	NC	3.30	0.17	(4) NC	3.84	0.07
0758+143	3C 190	0.85	0.06	(1)		0.76	0.04	(4)	0.82	0.06
0809+483	3C 196	4.38	0.23	(2)		4.39	0.14	(4)	4.36	0.06
0820+225		1.62	0.12	(1)		–			1.61	0.04
0824+294	3C 200	0.65	0.04	(2)		0.66	0.03	(4)	0.66	0.03
0915–118		12.53	0.67	(1)	NC	–			–	–
0941+100	3C 226	0.56	0.03	(2)	NC	0.54	0.03	(4) NC	0.64	0.05
0947+145	3C 228	1.16	0.10	(1)		1.12	0.06	(4)	1.14	0.06
1003+351	3C 236	1.45	0.11	(1)		1.41	0.06	(4)	1.34	0.08
1005+077	3C 237	2.12	0.15	(1)		–			2.01	0.06
1040+123	3C 245	–				1.46	0.07	(4)	1.39	0.04
1140+223	3C 263.1	0.84	0.06	(2)		0.79	0.04	(4)	0.78	0.03
1148–001		1.86	0.11	(1)		–			1.97	0.04
1153+317		1.16	0.08	(1)		–			0.95	0.04
1157+732	3C 268.1	2.66	0.16	(1)		2.71	0.07	(4)	2.62	0.06
1206+439	3C 268.4	0.65	0.05	(2)		0.58	0.02	(4)	0.60	0.03
1237–101		1.01	0.06	(2)	NC	1.02	0.04	(4) NC	1.53	0.05
1318+113		0.83	0.04	(2)		0.87	0.05	(4)	0.77	0.03
1323+321		2.42	0.16	(2)		2.26	0.11	(4)	2.31	0.06
1328+254	3C 287	3.31	0.20	(2)		3.24	0.17	(4)	3.26	0.06
1340+053		0.75	0.04	(2)		0.71	0.04	(4)	0.79	0.05
1409+524	3C 295	6.85	0.40	(1)		6.92	0.18	(4)	6.53	0.08
1413+349		1.02	0.07	(1)	NC	1.04	0.05	(4) NC	1.35	0.14
1419+419	3C 299	0.96	0.05	(2)		0.92	0.03	(8)	0.90	0.05
1425–011	3C 300.1	0.94	0.05	(2)		0.91	0.03	(8)	0.94	0.06
1434+036		1.22	0.07	(1)		1.24	0.06	(4)	1.28	0.02
1441+522	3C 303	1.01	0.07	(1)		1.00	0.03	(4)	0.94	0.06
1448+634	3C 305	0.92	0.05	(2)		0.96	0.02	(4)	0.92	0.04
1453–109		–				1.56	0.06	(4)	1.57	0.05
1514+072	3C 317	0.88	0.06	(1)		0.90	0.05	(4)	0.87	0.04
1517+204	3C 318	0.76	0.05	(1)		0.76	0.04	(4)	0.75	0.03
1518+046		1.08	0.06	(2)		1.11	0.06	(4)	0.99	0.03
1523+033		0.66	0.03	(3)		0.66	0.03	(8)	0.68	0.04
1543+005		0.81	0.04	(3)		0.79	0.03	(8)	0.88	0.05

TABLE 6 (continued)

1553+202	3C 326.1	0.74	0.05	(1)	–			0.86	0.06
1615+324	3C 332	–			0.84	0.03	(8)	0.83	0.03
1618+177	3C 334	0.61	0.03	(3)	–			0.57	0.03
1622+238	3C 336	–			0.79	0.04	(8)	0.69	0.06
1624+416		1.09	0.06	(2)	–			1.31	0.02
1626+396	3C 338	0.43	0.03	(1)	–			0.49	0.03
1627+234	3C 340	–			0.77	0.04	(8)	0.69	0.03
1648+050		9.36	0.61	(1) NC	–			–	
1658+471	3C 349	–			1.10	0.04	(4)	1.14	0.04
1704+608	3C 351	1.04	0.07	(1)	1.17	0.03	(4)	1.21	0.05
1716+006		0.75	0.04	(3)	0.75	0.03	(8)	0.77	0.05
1819+396		0.81	0.04	(3)	0.83	0.03	(4)	0.97	0.01
1833+653	3C 383	–			0.78	0.02	(2)	0.80	0.01
1938–155		2.35	0.13	(3)	2.21	0.08	(4)	2.31	0.06
2003–025		0.93	0.06	(2)	–			0.93	0.05
2012+234	3C 409	–			3.10	0.17	(4)	3.12	0.05
2018+231		1.02	0.05	(2)	–			1.20	0.06
2019+098	3C 411	0.87	0.07	(1)	0.91	0.05	(4)	0.87	0.06
2104+763	3C 427.1	0.94	0.05	(3)	0.88	0.02	(4)	0.96	0.06
2111+620	3C 429	–			0.72	0.02	(4)	0.79	0.08
2126+073	3C 435	0.60	0.04	(1)	–			0.56	0.03
2128+048		1.95	0.10	(2)	1.99	0.10	(4)	1.97	0.05
2153+377	3C 438	1.55	0.11	(1)	1.51	0.06	(4)	1.54	0.06
2203–188		4.13	0.22	(1)	–			4.62	0.12
2209+081		0.75	0.04	(2) NC	–			1.09	0.04
2210+016		1.06	0.07	(1)	1.05	0.05	(4)	1.02	0.04
2309+090	3C 456	0.77	0.04	(3)	0.78	0.04	(4)	0.67	0.03
2314+038	3C 459	1.28	0.06	(3)	1.23	0.06	(4)	1.36	0.04
2324+405	3C 462	0.95	0.06	(3)	0.94	0.04	(4)	1.12	0.10
2337+220	3C 466	0.71	0.04	(2)	0.74	0.04	(4)	0.75	0.05
2349–014		0.64	0.04	(1)	–			0.70	0.03
2356+437	3C 470	0.40	0.04	(1) NC	0.37	0.02	(4) NC	0.55	0.03

Notes to Table 6

(1) Number of measurements included in average. In September, only one flux density measurement was obtained each day (N = number of days source observed). In December, four measurements were obtained each day (2 feeds - beam switched, two receivers; N/4 = number of days source observed). An "NC" following the number of observations indicates that the source was not used as a calibration source, due either to suspected source variability or a poorly determined assumed flux density.

(2) Assumed flux density for calibration sources. Values are from list provided by Crane (1978). These values were used in determining the declination dependent antenna aperture efficiency.

TABLE 7

5.0 GHz FLUX DENSITY MEASUREMENTS
FOR SOURCES IN VARIABILITY SAMPLE

		Flux Density (Jy)						
Object	Other Names	2-5 Sept 1978			3-4 Dec 1978			Variability
		Flux	Error	N[1]	Flux	Error	N[1]	Index (V)[2]
0007+106	IIIZw2	0.52 ±	0.03	(3)	0.64 ±	0.03	(4)	2.5
0048−097		1.29	0.07	(3)	1.47	0.06	(4)	1.8
0106+013		3.31	0.17	(3)	3.27	0.14	(4)	−0.2
0133+476		1.85	0.10	(3)	1.93	0.06	(4)	0.7
0229+131		1.81	0.09	(3)	1.94	0.10	(4)	0.9
0235+164		1.63	0.09	(2)	1.83	0.09	(4)	1.5
0238−084	NGC 1052	1.37	0.08	(1)	−			−
0300+470		2.26	0.11	(3)	2.25	0.07	(4)	−0.1
0316+161	CTA 21	2.85	0.22	(1)	−			−
0316+413	3C 84	49.86	3.56	(1)	−			−
0333+321	NRAO 140	2.48	0.16	(1)	−			−
0336−019	CTA 26	2.78	0.16	(1)	2.73	0.11	(4)	−0.3
0355+508	NRAO 150	9.65	0.48	(2)	10.22	0.29	(4)	1.0
0404+767	4C 76.03	2.95	0.16	(1)	−			−
0405−123		1.96	0.11	(2)	1.77	0.06	(4)	−1.6
0415+379	3C 111	4.99	0.40	(1)	−			−
0420−014		2.82	0.14	(2)	3.06	0.12	(4)	1.2
0430+052	3C 120	4.82	0.25	(2)	4.27	0.21	(4)	−1.8
0433+295	3C 123	16.17	1.06	(1)	−			−
0440−003		1.61	0.08	(3)	1.54	0.07	(4)	−0.7
0458−020		1.79	0.06	(3)	1.89	0.08	(4)	1.0
0528+134		1.91	0.10	(3)	2.42	0.12	(4)	2.9
0552+398	DA 193	4.61	0.24	(3)	4.44	0.18	(4)	−0.6
0605−085		2.82	0.15	(2)	−			−
0607−157		2.53	0.14	(1)	1.79	0.07	(4)	−6.1
0723−008		2.18	0.11	(2)	2.05	0.09	(4)	−0.9
0727−115		3.85	0.20	(2)	3.68	0.13	(4)	−0.7
0735+178		2.19	0.14	(1)	−			−
0736+017		2.01	0.12	(1)	1.82	0.09	(4)	−1.3
0748+126		1.94	0.10	(2)	1.50	0.08	(4)	−4.0

TABLE 7 (continued)

0754+100 OI 090.4	0.87	0.05	(2)	0.63	0.03	(4)	−5.1
0814+425 OJ 425	1.60	0.08	(2)	1.59	0.06	(4)	−0.1
0831+557 4C 55.16	6.06	0.32	(2)	5.50	0.15	(4)	−1.7
0836+710 4C 71.07	1.97	0.14	(1)	2.40	0.06	(4)	2.4
0851+202 OJ 287	2.71	0.14	(2)	2.78	0.15	(4)	0.3
0859−140	2.45	0.13	(2)	2.14	0.09	(4)	−2.1
0923+392 4C 39.25	7.47	0.38	(2)	7.09	0.27	(4)	−0.8
0951+699 M 82	3.64	0.23	(1)	−			−
0953+254	1.18	0.07	(1)	1.17	0.06	(4)	−0.1
1055+018	−			2.84	0.13	(4)	−
1101+384 MKN 421	0.69	0.04	(2)	0.61	0.03	(4)	−1.7
1116+128	1.17	0.06	(2)	1.28	0.07	(4)	1.1
1127−145	4.87	0.27	(2)	4.54	0.17	(4)	−1.1
1215+303 ON 325	0.49	0.03	(2)	0.48	0.02	(4)	−0.3
1219+285 W Coma	1.87	0.09	(2)	2.03	0.10	(4)	1.1
1226+023 3C 273	40.54	2.34	(1)	−			−
1253−055 3C 279	11.34	0.61	(2)	11.35	0.47	(4)	0.0
1308+326	2.67	0.13	(2)	2.57	0.11	(4)	−0.6
1334−127 1335−12	2.85	0.16	(2)	2.82	0.12	(4)	−0.2
1345+125 4C 12.50	2.92	0.16	(2)	2.72	0.14	(4)	−1.0
1354−152 OP−192	1.81	0.09	(2)	1.47	0.05	(4)	−3.8
1404+286 OQ 208	2.70	0.19	(1)	2.85	0.14	(4)	0.6
1458+718 3C 309.1	3.36	0.20	(1)	−			−
1502+106 OR 103	1.71	0.09	(2)	1.75	0.09	(8)	0.3
1510−089	1.57	0.09	(3)	1.32	0.04	(8)	−2.9
1548+056	1.89	0.10	(3)	1.86	0.09	(8)	−0.2
1555+001 DA 393	1.52	0.08	(2)	1.40	0.05	(8)	−1.3
1607+268	1.61	0.09	(3)	1.65	0.07	(8)	0.3
1611+343	2.08	0.11	(3)	2.12	0.08	(8)	0.3
1633+382 4C 38.41	1.59	0.09	(3)	1.66	0.06	(8)	0.7
1638+398 NRAO 512	0.41	0.02	(2)	0.42	0.02	(4)	0.3
1641+399 3C 345	7.34	0.40	(2)	7.75	0.33	(2)	0.8
1642+690	2.29	0.15	(1)	2.82	0.07	(4)	2.7
1656+053	1.82	0.10	(2)	1.80	0.09	(4)	−0.1
1730−130 NRAO 530	5.30	0.39	(2)	5.16	0.18	(4)	−0.3
1739+522 4C 51.37	0.56	0.04	(1)	1.08	0.03	(4)	6.3
1741−038	2.26	0.14	(2)	−			−
1749+701	1.21	0.08	(1)	1.16	0.03	(4)	−0.6
1749+096	1.22	0.08	(1)	−			−
1807+698 3C 371	1.77	0.10	(3)	1.91	0.05	(4)	1.2

TABLE 7 (continued)

1828+487	3C 380	5.54	0.28 (3)	5.55	0.17 (4)	0.0
1845+797	3C 390.3	3.55	0.19 (2)	2.93	0.07 (4)	-3.6
1909+048	SS 433	0.40	0.02 (2)	0.54	0.03 (4)	3.5
1958-179	OV-198	0.79	0.07 (2)	-		-
2005+403		4.65	0.32 (1)	4.41	0.16 (4)	-0.7
2037+511	3C 418	4.51	0.23 (2)	4.34	0.12 (4)	-0.7
2037+421	DR 21	18.21	1.16 (1)[3]	-		-
2048+312	CL 4	0.43	0.02 (3)	0.36	0.02 (4)	-2.7
2121+053	OX 036	3.01	0.15 (3)	2.67	0.13 (4)	-1.8
2131-021		2.30	0.18 (1)	2.22	0.10 (4)	-0.4
2134+004		9.78	0.52 (2)	9.70	0.45 (4)	-0.1
2145+067		2.54	0.13 (3)	2.44	0.13 (4)	-0.6
2155-152	OX-192	1.59	0.09 (1)	-		-
2200+420	BL LAC	2.68	0.19 (1)	2.32	0.09 (4)	-1.9
2201+315	4C 31.63	1.82	0.15 (1)	-		-
2216-038		3.44	0.17 (2)	3.36	0.14 (4)	-0.4
2223-052	3C 446	3.54	0.19 (3)	3.67	0.16 (4)	0.5
2230+114	CTA 102	3.09	0.16 (3)	2.98	0.15 (4)	-0.5
2243-123	OY-172.6	2.63	0.13 (3)	2.39	0.09 (4)	-1.6
2251+158	3C 454.3	8.02	0.43 (3)	7.91	0.39 (4)	-0.2
2345-167		2.52	0.14 (3)	2.71	0.11 (4)	1.0

Notes to Table 7

(1) Number of measurements included in average. In September, only one flux density measurement was obtained each day (N = number of days source observed). In December, four measurements were obtained each day (2 feeds - beam switched, two receivers; N/4 = number of days source observed).
(2) The variability index, V, is a measure of the variability between Sept. and Dec. 1978. V is defined in equation II-5.
(3) Flux density corrected for extended structure (Peak flux density 17.89 Jy). Source size correction factor from Dent (1972).

R = 0.990 ±.009. The 1% difference in calibration is smaller than the calibration constant errors used in the flux density calculations. No systemmatic dependence of R on declination or time was found.

The calibration and variability sample sources were checked for evidence of variability in the three months between the observing sessions. The variability index, V, given in equation II-5, was calculated for each source. The value of V is listed in Table 7 for variability sample sources. The distribution of V for all sources is shown in figure 4. The median V is -0.15 for the calibration sources and -0.2 for the variability sample sources. The offset of V from zero is consistent with the 1% difference in calibration scales. The distribution of V for the calibration sources is narrower than anticipated for a Gaussian distribution, indicating that the errors in the flux densities are overestimated. The assumed errors in the calibration constant are most likely due to initial inaccuracies in the assumed flux densities of the calibration sources which were compiled from several references. Better determination of the calibration source flux densities would result in smaller calibration errors and smaller resultant flux density errors.

Of the two extreme values of V for sources not in the variability sample, one source is a known variable source. The flat spectrum (Crane, 1978) source 0742+103 (V = -2.3) exhibits variations in the 2.7 GHz data, and is variable at 6.6 and 10.6 GHz (Andrew et al, 1978). The

53

Figure 4. Degree of variability at 5.0 GHz for 136 sources during
the three month interval 4 September to 4 December 1978. The
variability index, V (defined in equations II-3 thru 5), is a measure of
the variability of a source (relative to the errors in the two
measurements) between the two observing sessions. The offset from zero
of both distributions (median V=-0.2) is due to a 1% difference in
calibration scales between the two sessions. No adjustment has been
made to the flux density scales to compensate for this offset since it
is not known which of the calibration scales corresponds more closely to
an absolute flux density scale. The distribution of variability index
for sources used to derive the declination dependent calibration
constant can be represent by a Gaussian noise distribution. The
distribution for sources in the variability sample indicates that 19% of
the sources are "probably" variable ($|V+0.2| > 2.0$) over the three month
interval, with an additional 10% being "possibly" variable
($|V+0.2| > 1.5$). Systemmatic errors in the calibration at 5.0 GHz result
in larger errors in the flux density measurements, resulting in lower
values of V at 5.0 GHz (than at 1.4 GHz) for the same percentage change
in observed flux density.

Degree Of Variability At 5.0 GHz
(Between 4 Sept. And 4 Dec. 1978)
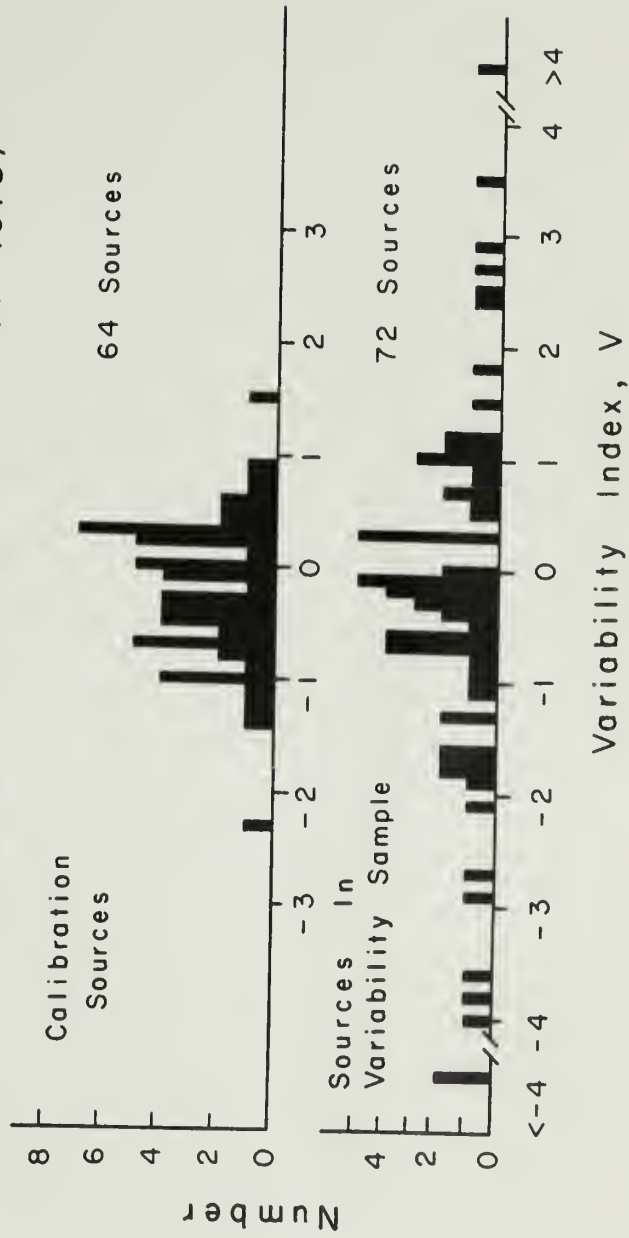
other extreme value (V = 1.5) for 1704+608 (3C 351) may be due to calibration uncertainties at the high declinations for either of the two observing sessions. The large value of V for the high declination variability sample source 1845+797 (3C 390.3) supports this possibility.

The distribution of V for the variability sample differs markedly from that for the calibration sources, but surprisingly the distribution appears qualitatively similar to that of the variability sample sources at 1.4 GHz. (Both frequencies display similar V distributions for the calibration sources and for variability sample sources). According to canonical theories of radio variability, it would be expected that variations would be larger at the shorter wavelengths. The quoted errors for the 5.0 GHz measurements are larger than those at 1.4 GHz (due to the systemmatic errors in the calibration procedure), resulting in lower V values for similar variability ratios, R. This effect narrows the V distribution at 5.0 GHz. The spectra of these sources are discussed further in Chapter V.

7.9 GHz (4 cm) and 15.5 GHz (2 cm). A program to study the radio variations at 7.875 GHz (λ 3.8 cm) and 15.5 GHz (λ 1.9 cm) in extragalactic sources has been conducted since 1969 using the Haystack Observatory 120-foot antenna, located in Westford, Massachusetts. Initially, about 25 sources were regularly observed at these two frequencies. Currently over one hundred extragalactic and galactic variable sources are regularly observed in the program (see Tables 1 and

2 for the current source list). Observations are conducted roughly once per month at each frequency, with sources which have not exhibited rapid variations being observed less frequently. The observations at these two frequencies have the best time coverage of the five regularly observed frequencies.

The basic receiver and telescope parameters are given in Table 3. A review of the Haystack antenna and radome characteristics is given in Meeks and Ruze (1971). The observing procedures and reduction techniques are described by Dent and Kojoian (1972), Dent, Kapitzky, and Kojoian (1974), and Dent and Kapitzky (1976). The observations have been obtained and reduced by the above mentioned individuals and the author. The observing and data reduction techniques are summarized below. Since the procedures are similar for observations at 7.9 and 15.5 GHz, they are discussed concurrently. The observing procedures differ from those used for observations with the NRAO 300-foot antenna since the Haystack antenna can be positioned in both azimuth and elevation over the entire sky.

The 7.9 GHz system consists of a single circularly polarized feed horn, whose output is Dicke-switched against either a cold load or a sky horn directed 45° in elevation above the main antenna beam. Comparison of the two possible switching modes revealed that the noise level was generally lower when observations were made in the load switched mode. This was especially true during fluctuating weather conditions, when the

atmospheric stability differed between the two beams. Most observations were conducted in the load switched mode. In 1972.21, the observing frequency was changed from 7.780 GHz to 7.875 GHz to avoid interference (Dent and Kapitzky, 1976).

The 15.5 GHz system is a dual-feed, beam switched system. The reference beam is displaced by -0.196° in azimuth from the main beam. The two beams are sensitive to orthogonal linear polarization, so the total flux density of a source is the sum of the output from the two beams. The beam switching observing mode reduces the observed effect of atmospheric fluctuations. As a result, the 15.5 GHz system is less sensitive than the 7.9 GHz system to rapidly changing sky conditions.

The pointing characteristics of the Haystack antenna are regularly checked, and pointing tables updated, by the observatory staff. The pointing was checked during all observing sessions by observing strong, small angular size sources using a procedure referred to as a "Discrete Source Scan" (DSS). In a DSS, the telescope is scanned sequentially in azimuth and elevation around the nominal sources position. A linear baseline is fit to each scan, and a Gaussian profile is fit to the antenna response to the source. Pointing corrections are derived for both azimuth and elevation and are subsequently applied to the source position. No DSS observation was made for sources which are too weak to obtain adequate pointing information (sources with flux densities less than a few Jy). Rather, the pointing corrections that were determined from strong sources at a nearby azimuth and elevation are used.

The pointing corrections were not the same for all observing sessions, so they had to be determined during each session. Generally, it was found that both the elevation and azimuth pointing corrections were a function of the telescope azimuth. After removing this effect, no systemmatic dependence on telescope position was found. The telescope pointing was occasionally time dependent, and appears to be dependent upon the ambient radome and telescope temperatures (Haschick, 1981). During the observing sessions, any time dependent pointing corrections were updated as required. A typical set of pointing data for one observing session is shown in Figure 5. After removal of systemmatic pointing errors, the rms pointing accuracy was typically 0.002° in both azimuth and elevation (Haschick, 1981, finds similar rms's based upon observations at 22 GHz). This pointing scatter corresponds to errors in the flux density calibration of ~0.4% at 7.9 GHz and ~1.6% at 15.5 GHz. Scatter in the measured source strengths due to pointing errors is reflected in a scatter in the calibration constant measurements.

After application of the pointing corrections, the source antenna temperature is measured by an "on-off" procedure. In this procedure the main telescope beam is sequentially pointed "off" source (for 8 seconds), "on" source (16 seconds), and "off" source (8 seconds). This sequence constitutes one "on-off" measurement and requires about fifty seconds of real time (no data is taken during telescope movement between the "on " and "off "source positions). At 7.9 GHz, the "off" source

Figure 5. Typical azimuth and elevation pointing errors at 15.5 GHz for the Haystack 120' antenna. The errors are residual errors to the adopted pointing coefficients for the telescope. In this instance the azimuth offset varies nearly linearly as a function of the telescope azimuth. The elevation offset exhibits a stronger dependence on azimuth, differing by as much as 0.015° from the east to the west sky. For comparison, the half-power beamwidth at 15.5 GHz is 0.037°. No systemmatic dependence on elevation was found. The sources 3C274 and DR21 are extended sources, and their pointing offsets should be used with caution for other sources. There is an apparent offset in the elevation pointing for the source DR21, which may be due to the source being extended. The telescope pointing is not well determined for azimuths between 315° and 50° due to a lack of strong sources in that part of the sky.

Measured Pointing Corrections

1-2 March 1980, Haystack 120', 15.5 GHz
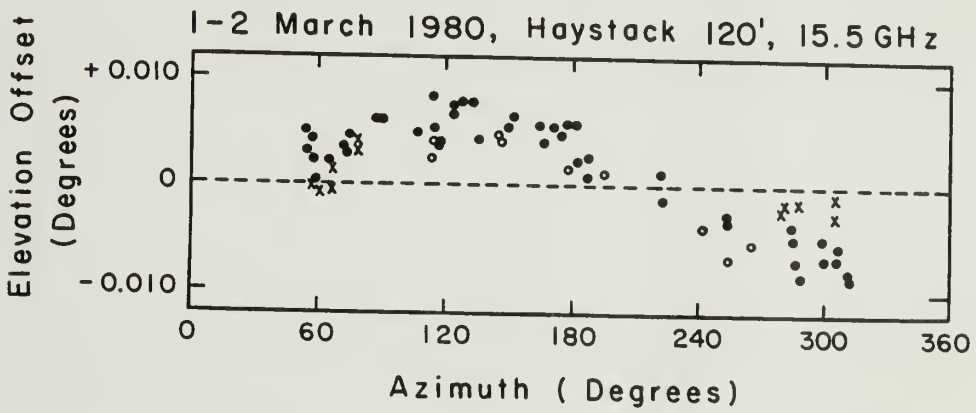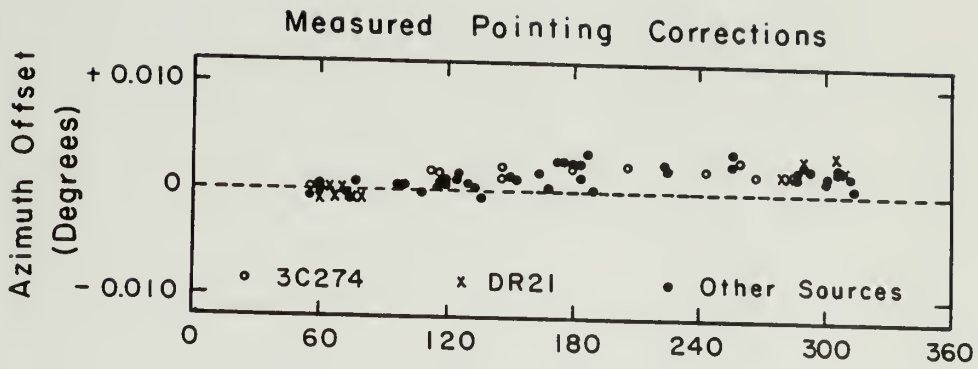
position is offset 0.150°/cosine(elevation) in azimuth from the "on" source position, with the "offs" being alternately displaced on each side of the "on" source position. The average of the "off" measurements is subtracted from the "on" value to obtain the "on-off" temperature. The alternate "offs" remove first order time and position dependent changes in the background sky temperature.

At 15.5 GHz, the "off" position is at the position of the reference (second) beam, which is displaced from the main beam by -0.196°/cosine(elevation) in azimuth. Temporal and positional atmospheric effects are reduced both by the beam switching and position switching procedures. Linear sky background antenna temperature dependence is removed since the "off source beam" is alternately displaced to each side of the source in azimuth. During the transition from the UNIVAC 490 to the present HP-1000 computer to control the telescope pointing, an error was introduced into the pointing software such that at 15.5 GHz the reference beam was not accurately positioned on the source. This error, which existed from 1978.28 to 1979.22, was due to an error in the conversion from degrees to radians used in determining the reference beam offset from the main beam. The error was elevation dependent, being larger at the higher elevations (the offset being proportional to 1/elevation). Corrections were made to the observed "on-off" measurements to compensate for this pointing error.

The number of "on-off" measurements made for a source ranged from

six for strong sources, to up to twenty for weak sources. The error for
an "on-off" sequence, x, is the standard deviation of the sample, given
by

$$error = \frac{\sqrt{\{\sum x^2 - ((\sum x)^2/n)\} / (n-1)}}{\sqrt{n}} \qquad (II-6)$$

where n is the number of "on-off" measurements in the sample of measure-
ments (the summations are from 1 to n). The error in the "on-off"
measurement is due primarly to random fluctuations in the sky background
emission. The "on-off" measurment value is converted to an antenna tem-
perature by comparison to a known temperature calibration tube. Time
dependent receiver gain fluctuations are removed by calibration prior to
each "on-off" sequence at 7.9 GHz, and about once per hour at 15.5 GHz
where the percentage change in the receiver gain is less.

The theoretical rms noise for a radiometer system is given by

$$\Delta T_{rms} = \frac{\alpha \, T_{sys}}{\sqrt{B \, \tau}} \qquad (II-7)$$

where T_{sys} is the system temperature (K), B is the receiver bandwidth
(Hz), τ is the "on" source observing time (seconds), and α is a constant
which depends upon the observing mode. For load switched and position
switched observing (7.9 GHz), $\alpha = 2\sqrt{2}$; for beam and position switched
(15.5 GHz), $\alpha = 2$. For the receiver parameters in Table 3, theoretical
values for ΔT_{rms} for a single "on-off" measurement ($\tau = 16$ seconds) are
0.024 K at 7.9 GHz and 0.029 K at 15.5 GHz. The observed antenna tem-

perature distribution for a series of "on-off" measurements of blank sky (no known source at that position) during clear weather conditions is shown in Figure 6 for observations at 8.4 and 15.5 GHz. Observations were conducted at 8.4 GHz rather than at the normal operating frequency of 7.9 GHz during this system performance test. The observed rms's are about 25% higher than the theoretical values. During a typical observing session the observed rms's range from the theoretical value to several times theoretical, dependent upon the atmospheric stability.

Editting of the "on-off" scans for each source in an observing session is accomplished both by visual inspection of the chart record and numerical analysis of the "on-off" measurements. The chart record displays both the total (unswitched) power of the system and the beam or load switched output from the receiver. Changes in system temperature (due to receiver or telescope gain changes) are monitored on the total power channel. Scans with total power fluctuations greater than a few degrees K were normally deleted from further analysis. Smooth, slowly varying total power changes are usually the result of changes in the atmospheric opacity or radome transmission (from changes in the atmospheric water content or precipitated water on the radome). The gain variations can be calibrated out during later stages in the reduction procedure.

Visual inspection of the chart record can reveal periods of interference from nearby radar facilities, short term atmospheric fluc-

Figure 6. The observed antenna temperature distribution for a series of "on-off" measurements of "blank" sky at 8.4 and 15.5 GHz. The observations were made by tracking positions in the sky with no known radio sources, within the elevation range 30° to 65° (the normal observing range at Haystack Observatory). The distributions can be represented by Gaussian noise distributions with rms's of 0.034 K (8.4 GHz) and 0.030 K (15.5 GHz). For these sets of observations, the calibration constant was 9.4 Jy/K at 8.4 GHz and 4.7 Jy/K (sum of two beams) at 15.5 GHz.

Observed Antenna Temperature For "Blank" Sky
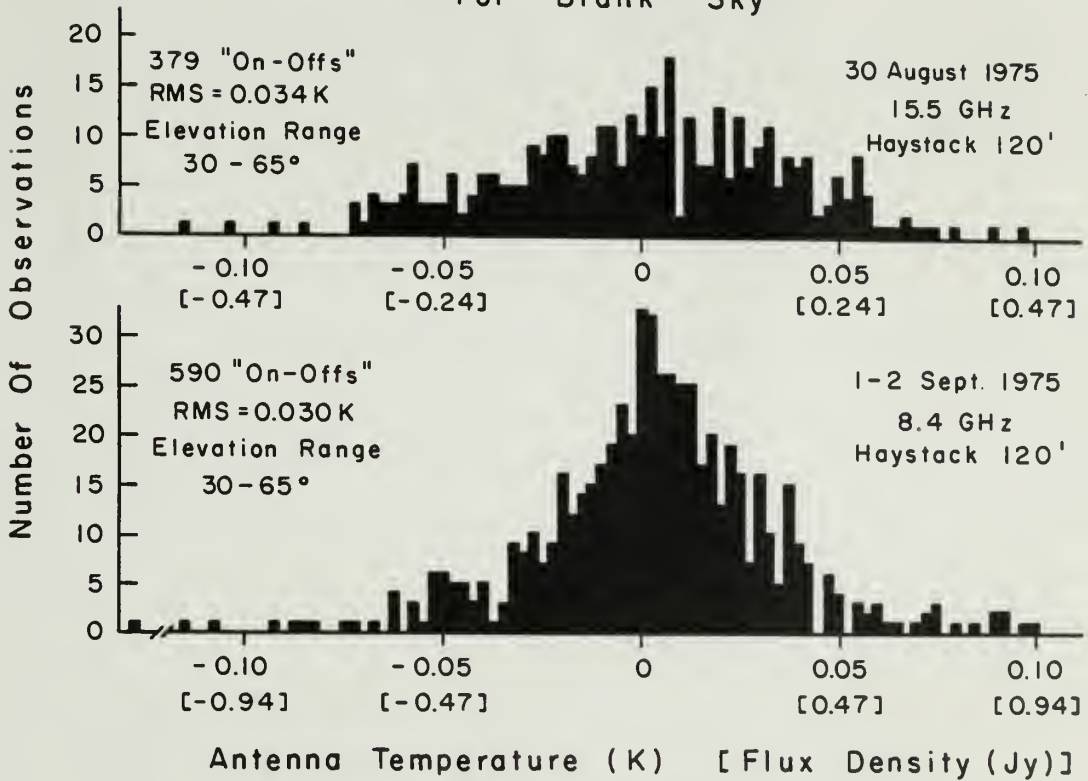
tuations (e.g. clouds), or the presence of the sun or other strong continuum sources in the antenna sidelobe pattern. The sidelobe pattern of the radome enclosed antenna extends out to about 30° from the main beam (Meeks and Ruze, 1971). The presence of the sun in the sidelobe pattern was readily observable out as far as 20° from the main beam. The signature of this effect is markedly different total power levels at the alternate "off" positions (the antenna sidelobe pattern at the sun is stronger for one of the "off" source positions), or time dependent changes in the "on" or "off" source total power (due to changing orientation of the sun with respect to the sidelobe pattern). The entire "on-off" measurement is not reliable due to a possible non-linear or time dependent sky background. In cases where it was clear that the sun was in the sidelobe pattern of the antenna, the entire scan was deleted from further analysis. Sources within 20° of the sun which did not exhibit sky background fluctuations were included in further analysis.

Individual "on-offs" which were beset with interference or atmospheric fluctuations were deleted prior to calculation of the "on-off" average and standard deviation. Additionally, any "on-off" measurements which were greater than 2.3 standard deviations from the average "on-off" value were deleted. The remaining measurements were used to calculate the final observed antenna temperature and error.

The computed average antenna temperatures from the "on-off" measurements were corrected for source resolution, atmospheric extinc-

tion, antenna elevation gain (efficiency) dependence, time dependent antenna efficiency, and radome transmission. Each of these correction factors are discussed below.

The correction for source resolution (CS) depends upon the source angular size and the telescope beam size. The observed peak antenna temperature must be corrected for source resolution to derive the integrated antenna temperature. Sources in the observing program which require this correction are the two primary calibration sources (DR21 and 3C274) and the planets. The source size correction factor for a Gaussian beam and a disk source is given by (Predmore, 1978; Ulich and Haas, 1976)

$$CS = \frac{x^2}{1 - e^{-x^2}} \qquad (II\text{-}8a)$$

where

$$x = \frac{(A + B)/2}{0.60056 \; BW} \qquad (II\text{-}8b)$$

where BW is the telescope beamwidth (arc seconds), and A and B are the source semi-diameters (arc seconds). The size correction factor for a planet depends upon its angular size. The size corrections for DR21 and 3C274 at 7.9 and 15.5 GHz, respectively, are 1.003 and 1.032 (DR21) and 1.027 and 1.052 (3C274).

The atmospheric extinction correction (CA) is given by
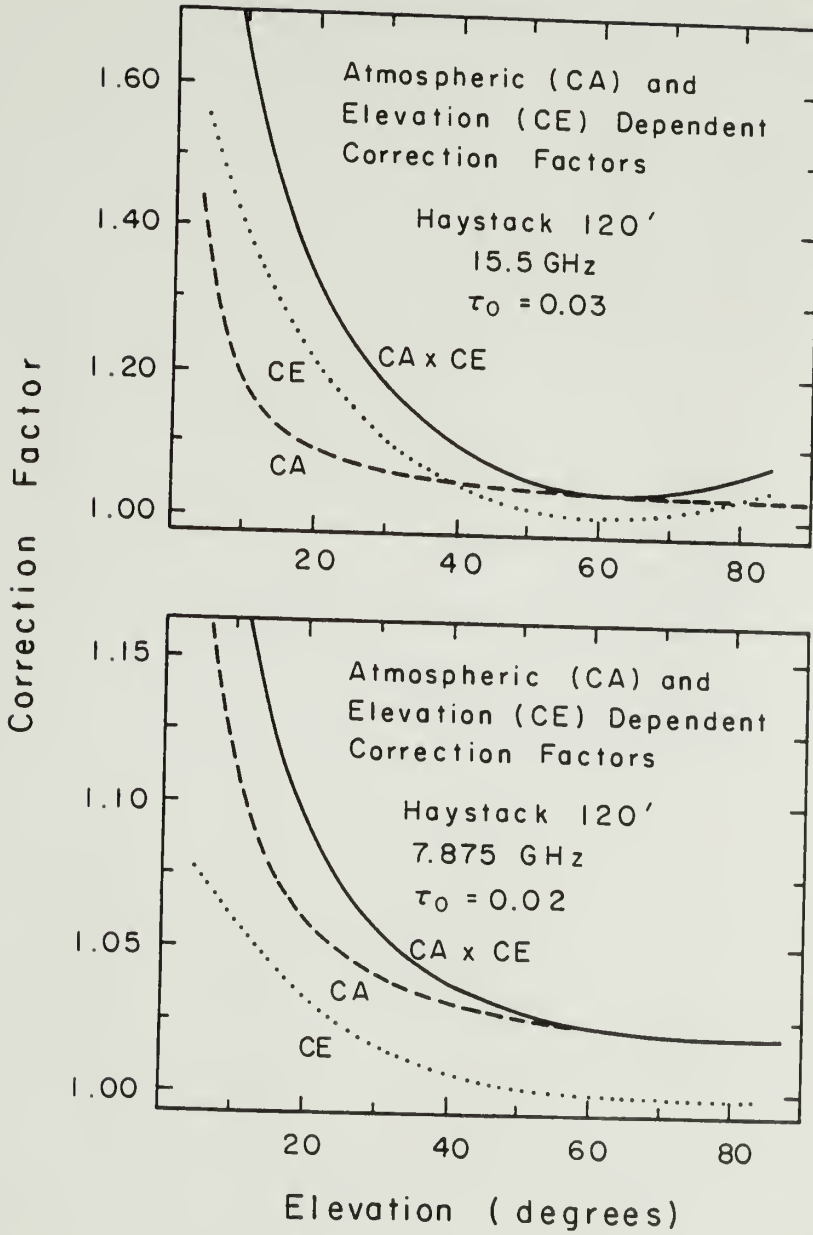
$$CA = e^{(\tau_0/\sin E)} \qquad (II\text{-}9)$$

where E is the source elevation, and τ_0 is the atmospheric opacity at one air mass (at zenith). The atmospheric absorption is due to both a constant contribution from oxygen and a variable contribution from atmospheric water (Waters, 1976). The atmospheric opacity τ_0 can be measured by scanning the antenna in elevation (a "sky dip") and measuring the elevation dependent atmospheric emission. The value of τ_0 has been measured by Dent and Kojoian (1972) and Dent, Kapitzky, and Kojoian (1974). Average values of τ_0 are 0.02 (7.9 GHz) and 0.03 (15.5 GHz). The dominant contribution to the opacity at these frequencies at the elevation of Haystack Observatory is from atmospheric oxygen, with the variable water opacity being at most $1/2$ that of oxygen during acceptable observing conditions. Techniques to accurately measure the atmospheric opacity do not exist for the Haystack antenna, so atmospheric modeling (based upon the ambient temperature and partial pressure of water) must be employed to determine the opacity. An average value (from the full range of expected τ_0) has thus been assumed for all observing sessions. Time dependent atmospheric opacity will be reflected in a time dependent calibration constant, being more pronounced in the source measurements at low elevations (large air mass).

The elevation dependent gain correction (CE) is due to antenna gravitational deformation. The elevation gain correction is determined by measuring the antenna temperature of a strong source at several elevations, correcting the observed temperatures by the atmospheric correction, and fitting a least-squares polynomial to the corrected values.

The elevation gain corrections were determined by Dent and Kojoian (1972) and Dent, Kapitzky, and Kojoian (1974), and have been checked regularly during subsequent observing sessions. Minor differences between the adopted gain curves and the measured values during any single observing session may in part be attributed to atmospheric changes or temperature dependent antenna deformations. No major discrepancies have been found with the adopted gain curves during the decade since they were determined. The adopted elevation gain curves are shown in Figure 7.

It was occasionally necessary to make time dependent gain corrections to the data, which appeared to correlate with changes in the ambient radome or telescope dish temperatures. These gain changes are apparently due to differential deformation of the antenna surface and support structure as a result of temperature gradients across the surface and backstructure. The temperature at several points on the antenna structure was routinely monitored during the observing sessions. When time dependent gain changes were detected, a correlation was searched for between the gain and several telescope temperature parameters. No clearcut relationship, which applies in all cases, has been found between the gain changes and any specific temperature. The telescope efficiency appears to be a function of a combination of the average temperature of the antenna, the temperature differential between the upper and lower portions of the dish, the differential between the dish surface and the support structure, and the time rate of change of these parameters.

Figure 7. Elevation gain (CE) and atmospheric (CA) correction factors for the Haystack 120' antenna at 15.5 and 7.875 GHz. The assumed atmospheric opacity is $\tau_0 = 0.03$ at 15.5 GHz and 0.02 at 7.875 GHz. The elevation gain curves are not well-defined at elevations above ~70°. The observed antenna temperature for a source is multiplied by these two factors (CE and CA) to derive a corrected antenna temperature.

71

Atmospheric (CA) and
Elevation (CE) Dependent
Correction Factors

Haystack 120'
15.5 GHz
$\tau_0 = 0.03$

CE

CA x CE

CA

Atmospheric (CA) and
Elevation (CE) Dependent
Correction Factors

Haystack 120'
7.875 GHz
$\tau_0 = 0.02$

CA x CE

CA

CE

Correction Factor

Elevation (degrees)

In October, 1976, a vent was installed at the top of the radome (commonly referred to as the "Dent vent"), allowing warm air to escape from the radome, being replaced by cooler air drawn in from outside the radome. Circulating fans to mix the air within the radome are run during times of the year when large day to night temperature fluctuations would result in temperature gradients in the radome and on the antenna surface. Since the installation of the vent, the number of observing sessions which exhibited large gain fluctuations has sharply decreased. Evidence of telescope efficiency changes with temperature changes at frequencies above 20 GHz has been documented by Haschick (1981).

Variations have been observed in the radome transmission during periods of fog or dew. These variations are due to changes in the moisture content on the radome surface (Dent and Kojoian, 1972). The radome reflectivity can be determined by measuring the total power output (total system temperature) from the receiver. The difference between the observed total power and the expected total power at that elevation during dry weather conditions provides an estimate of the radome reflectivity. The reflectivity changes result in changes in the telescope effective area (efficiency).

Corrections for gain changes (CG) due to telescope efficiency or radome transmission have been applied to the observed antenna temperatures when required. Multiplication of the observed antenna tem-

perature by all of the above mentioned corrections gives the resultant corrected antenna temperature.

The corrected antenna temperatures were converted to flux densities by comparing them to sources of known flux density (calibration, or standard, sources). For observations made at frequencies of 7.9 and 15.5 GHz, the primary standard source is the compact HII region DR21. The thermal spectrum of DR21 has been measured by Dent (1972), and for frequencies above ~7 GHz is given by the equation

$$S_\nu = 26.78 - 5.63 \log \nu \text{ (GHz)} \qquad (II-10)$$

with an uncertainty of about 3% in the absolute flux density level. The flux density of DR21 was determined relative to the flux density scale of Kellermann, Pauliny-Toth, and Williams (1969) (the KPW scale) at frequencies below 15 GHz, and relative to the planets Jupiter and Saturn at higher frequencies. Two other primary calibration sources (3C274 and 3C123) were used in calibrating the 7.9 and 15.5 GHz results. The flux densities, measured relative to DR21 by Dent and Kojoian (1972) and Dent, Kapitzky, and Kojoian (1974) at 7.9 and 15.5 GHz, respectively, are 48.37 and 28.30 Jy (3C274) and 10.76 and 4.97 Jy (3C123).

The three primary calibration sources were observed every few hours (more often during changing weather conditions) throughout the observing period to check the system gain stability. The factor by which the corrected antenna temperature of a source must be multiplied to derive the flux density is called the calibration constant. Typical measured

calibration constants for the Haystack antenna are in the range 6.5-7.0 Jy/K (7.9 GHz) and 8.0-9.0 Jy/K (15.5 GHz). For the Haystack 120' antenna (A_g = 1050 m^2) the relationship between the telescope efficiency and the calibration constant (equation II-1) reduces to

$$CC = \frac{2.63}{\varepsilon_A} \, .$$ (II-11)

The measured efficiency during optimum observing conditions was ~40% at 7.9 GHz and ~30% at 15.5 GHz. The error in the averaged calibration constant was taken to be the standard deviation of an individual measurement of calibration constant. This error ranged from one to four percent, depending upon the atmospheric and telescope temperature stability during the observing session. During those observing sessions when the gain correction (CG) did not remove all time dependent system gain changes, either a linear or parabolic time dependence was fit to the individual calibration constant values.

The flux density of each source was calculated by multiplying the corrected antenna temperatures by the appropriate calibration constant. The error in a flux density measurement is a combination of the error in the "on-off" measurement, the errors in the correction factors (CA, CE, and CG) which were applied to the observed antenna temperature, and the error in the adopted calibration constant. The flux density measurements are discussed in subsequent chapters.

31.4 GHz (1 cm) and 90 GHz (3 mm). A program to study the radio

variations at 31.4 GHz (λ 0.96 cm) and 89.6 GHz (λ 0.33 cm) in extragalactic sources has been conducted since 1970 using the NRAO 36' antenna, located at Kitt Peak, Arizona. The number of sources observed at each frequency has increased since the inception of the program, as the sensitivity of the millimeter receivers has increased. Currently, all sources listed in Tables 1 and 2 are regularly observed at 31.4 GHz, with only a few of the weaker sources omitted at 89.6 GHz. Observations are conducted once every three months at both frequencies. The time coverage at these two frequencies is not as good (due to scheduling constraints) as the monthly coverage of the 7.9 and 15.5 GHz observations. Additional measurements made at λ ~3 mm have been obtained since 1979 with the 45-foot millimeter antenna of the Five College Radio Astronomy Observatory (FCRAO). The observing procedures and results are discussed in detail in Chapters III and IV.

The basic receiver and telescope parameters for the NRAO 36' observations are given in Table 3. The observing procedures and reduction techniques at 31.4 and 90 GHz are described by Dent and Hobbs (1973) and Hobbs and Dent (1977). The observing frequency was changed from 85.2 GHz to 89.6 GHz in 1974. The observing procedures are similar to those described for the Haystack Observatory observations. The observations have been obtained primarily by Dent and Hobbs, with the author assisting in the observations and data reduction during the past four years.

Accurate flux density measurements at millimeter wavelengths at Kitt Peak are more difficult to obtain than the Haystack measurements, because the atmospheric opacity at millimeter wavelengths is more sensitive to the atmospheric water content (Waters, 1976) and the Kitt Peak telescope is not enclosed within a radome (thus coupling the telescope temperature to the ambient temperature changes). Consequently, frequent calibration is more important (and challenging) at millimeter wavelengths than at longer wavelengths. Beam switched observing is required to remove rapid atmospheric fluctuations. Beam switching at 90 GHz is accomplished by "nodding" the subreflector between the source position and neighboring "blank" sky. At 31.4 GHz, beam switching is achieved by comparison of the output from two feed horns (as in the 15.5 GHz observations).

Pointing checks were made by use of a procedure referred to as a "Five Point" observation. In the five point observations, the telescope is pointed at the nominal source position, and at points displaced $1/2$ half power beamwidth above and below (in elevation) and to the "left" and "right" (in azimuth) of the source position. A two dimensional Gaussian profile is fit to the observed source strength at these five points. The pointing corrections thus derived are applied to the source position. The pointing errors were found to be a function of both the azimuth and elevation of the telescope. For weak sources, pointing corrections that had been determined from strong sources at nearby azimuths and elevations were used.

The source strength was measured by the "on-off" procedure described for the 7.9 and 15.5 GHz observations. The on source observing time was typically 20 seconds (shorter for strong sources), with up to 20 "on-off" measurements being made for most sources. The source antenna temperature was determined by comparison of the source strength with the receiver response to a known temperature noise tube.

The atmospheric opacity was determined by measuring the relative atmospheric temperature ($T_{atm}(el)$) at several elevations (a "sky dip"). A least squares fit was made to the equation

$$T_{atm}(el) = A \, \tau_o \, csc(el) + constant \qquad \text{(II-12)}$$

where A was typically ~280° at 31.4 GHz and 260° at 90 GHz. Values of τ_o during optimum weather conditions were 0.02 (31.4 GHz) and 0.07 (90 GHz), but occasionally were as high as 0.05 and 0.20, respectively, during less favorable observing conditions.

No elevation gain corrections are required at 31.4 or 90 GHz for the 36' antenna as a result of the backstructure rigidity. However, temperature changes of the antenna structure result in deformation of the dish surface, producing focus and gain changes. The focus is constantly updated automatically, based upon reading from temperature sensors at several points on the antenna. Time dependent gain changes were monitored by measuring calibration sources every few hours. The primary calibration sources used were DR21 (18.35 and 16.9 Jy at 31.4 and 90 GHz, respectively) and 3C274 (17.0 and 8.64 GHz). The source

size correction factor (CS) for these two sources at 31.4 and 90 GHz are 1.012 and 1.084 (DR21) and 1.022 and 1.080 (3C274). At 90 GHz, the total flux density of DR21 is a combination of the flux density of the thermal HII region measured by Dent (1972) and a contribution from an infrared dust component associated with DR21 (Ulich, 1981). The planets were used as secondary standards when insufficient measurements existed of the primary calibration sources. There is some evidence that Jupiter and Saturn are variable at millimtere wavelengths.

For the 36' antenna, the relationship between the telescope efficiency and the calibration constant (equation II-1) is given by

$$CC = \frac{29.2}{\varepsilon_A} \ . \qquad (II-13)$$

The measured efficiency during optimum observing conditions was typically 50% at 31.4 GHz and 25% at 90 GHz.

The flux density of a source was calculated by multiplying the observed antenna temperature by the derived calibration constant. The error in the flux density is a combination of the error in the "on-off" measurement and the error in the average calibration constant. The flux density measurements are discussed in subsequent chapters.

6.6 GHz (5cm) and 10.6 GHz (3cm) (and miscellaneous radio measurements).
Measurements from systemmatic studies of variations in extragalactic sources which have been conducted by other investigators are used in the

analysis of radio source evolution in the following chapters. Particularly, the sample of measurements at 6.6 GHz (λ 4.5 cm) and 10.6 GHz (λ 2.8 cm) obtained with the Algonquin Radio Observatory is used because of its extensive long-term data base for about 50 sources. Descriptions of the observing procedures and results are given by Medd et al (1972) and Andrew et al (1978). This program began in 1966 at both frequencies. The 6.6 GHz measurements were discontinued in mid-1973, while the published 10.6 GHz measurements extend through 1976. The results from this study will be used as published. Andrew et al (1978) find that their flux density scale may be 3.1% ±0.5% higher at 10.6 GHz and 3.7 ±0.7% lower at 6.6 GHz than the flux density scale of Dent (1972) used for observations presented in this dissertation.

Flux density measurements at millimeter and centimeter wavelengths, taken from the literature, will be used in discussions of individual sources. These measurements will be referenced when used.

§3. Optical Observations

The optical measurements used in this dissertation in the search for correlations between the radio and optical variability in a sample a extragalactic sources (Chapter VI) have been obtained at Rosemary Hill Observatory[6] as part of a program at the University of Florida to photographically monitor optical variations in more than 200 objects. The program (begun in 1968) and the results have been discussed by Scott et

al (1976), Pollock et al (1979), and Pica et al (1980). The measure-
ments used in this dissertaion include observations reported in the
above references as well as recently obtained, unpublished observations
(Pollock, 1981; Pica, 1981). The results have kindly been provided in
computer card format by Pollock and Pica. The forty five sources which
are common to the University of Florida optical study and the University
of Massachusetts radio program (discussed in section 2) are given in
Table 1.

In the correlation analysis, the optical observations are converted
from magnitudes into units of flux density. The original observations
were reported in either photographic (m_{pg}) or B (m_B) magnitudes. For
three sources measurements were obtained in both the m_{pg} and
m_B magnitude systems. The photographic magnitudes were converted to the
photometric B magnitude scale by using empirically determined
m_B-m_{pg} corrections as given by Pollock et al (1979). The three sources
(0735+178, 0851+202, and 1641+399) were corrected by m_B-m_{pg} = -0.20,
+0.50, and +0.60, respectively.

The conversion from magnitude to flux density is given by

$$S_\nu = S_{o\nu} \ 10^{-0.4 \ (m_\nu - A_\nu)} \qquad \text{(II-14)}$$

where m_ν is the apparent magnitude at frequency ν, A_ν is the
interstellar extinction in the direction of the source at that frequency
$S_{o\nu}$ is a multiplicative constant, and S_ν is the flux density in units of
Janskies. Using the flux conversion scale of Schild, Peterson, and Oke

(1971), this equation can be rewritten

$$S_B \text{ (mJy)} = 3.90 \ C_B \ 10^{-0.4 \ (m_B - 15.0)}$$

$$\text{(II-15a)}$$

$$S_{pg} \text{ (mJy)} = 3.65 \ C_{pg} \ 10^{-0.4 \ (m_{pg} - 15.0)}$$

where

$$\text{(II-15b)}$$

$$C_\nu = 10^{-0.4 \ A_\nu}$$

$$\text{(II-15c)}$$

and the 1σ flux density error is

$$\Delta S_\nu \text{ (mJy)} = 0.5 \ (\ S_\nu \ 10^{0.4 \ \Delta m_\nu} - S_\nu \ 10^{-0.4 \ \Delta m_\nu} \ )$$

$$\text{(II-15d)}$$

Here, the flux densities are in units of milli-Janskies, and C_B and C_{pg} are correction factors for interstellar extinction. The interstellar extinction correction is dependent upon the model used for the galactic interstellar dust content. In the variability correlation analysis this correction would appear as a constant multiplicative factor for each source. For this reason, no correction has been made to the optical flux densities to account for interstellar extinction. The figures presented in Chapter VI have had the magnitude values of Pollock (1981) and Pica (1981) converted to flux density by equation II-15, with no correction applied for interstellar extinction (e.g. $C_\nu = 1.0$).

The errors in the optical flux density are larger for high flux density values than for lower flux density values. This is due to the optical magnitude measurements from the Florida study having about the same quoted error, regardless of magnitude. When the source is bright, this magnitude error corresponds to a larger flux density error than when the source is faint.

Care must be taken when visually inspecting the optical variations presented in the figures in Chapter VI, since isolated high flux density measurements with correspondingly high errors may not represent as significant a variation as imagined from a casual inspection of the light curve. Converting the optical magnitudes to flux density accentuates the short-term behavior of the outbursts. The optical outbursts presented in Chapter VI appear more "spiked" than the logarithmic magnitude scale normally used when optical observations are presented. The flux density scale does give a better indication of the rapid fluctuations of the outbursts, and provides a better impression of the total energy contained within an outburst.

The measurements from the University of Florida optical study will be used in the statistical analysis of radio-optical correlations in Chapter VI. No effort has been made to do a comprehensive literature search to supplement the Florida optical measurements. (Pollock (1982) is compiling a thorough list of variations in a sample of optically violent variables (OVV's). Optical and infrared measurements from other references which are relevent to the analysis of individual sources will be presented in the discussions of the individual sources.

C H A P T E R   III

CONTINUUM MEASUREMENTS WITH THE FCRAO MILLIMETER ANTENNA

§1. Introduction

In 1979 a program was initiated at the Five College Radio Astronomy Observatory[5] (FCRAO) to study the short timescale variations in extragalactic sources at millimeter wavelengths. Observations are being conducted at frequencies between 85 and 115 GHz with the 45-foot FCRAO antenna, located in New Salem, Massachusetts. This program complements the program conducted with the NRAO[2] 36-foot antenna in which quarterly observations are obtained at 89.6 GHz (Hobbs and Dent, 1977). A few sources were also observed at FCRAO at frequencies between 41 and 48 GHz during 1979 and 1980. These programs are coordinated with similar observing programs at frequencies between 31.4 and 2.7 GHz (Dent and Hobbs, 1973; Dent and Kapitzky, 1976; Dent and Kojoian, 1972; Kapitzky, 1976). The present high sensitivity of the FCRAO and NRAO systems provides an unprecedented opportunity to study the short term, low amplitude variability at short wavelengths in a large sample of extragalactic sources.

The amplitude and timescale of variability differ significantly between millimeter and centimeter wavelengths. Typically, outbursts are first observed at millimeter wavelengths where the emission of the outburst is not self absorbed, with the onset and peak of an outburst being

delayed at lower frequencies where the contiunuum spectrum is opaque. In most (though not all) sources the outbursts are stronger at millimeter wavelengths than at the longer wavelengths, consistent with models in which expanding regions of relativistic particles are responsible for the radio radiation. The timescale of the rise and decay of outbursts is typically shorter at the higher frequencies, making it possible to separate outbursts that overlap at the lower frequencies.

Studying the variations at millimeter wavelengths provides information on the physical conditions within the source which is not available from the longer wavelength observations. The observed variations at millimeter wavelengths delineate the acceleration and energy loss mechanisms of the relativistic particles, whereas at longer wavelengths these processes are masked by the effects of higher opacity and the subsequent expansion processes. By observing at millimeter wavelengths it is possible to observe deeper into the core of the emitting region responsible for the radio, and presumably the infrared and optical, radiation. The study of the evolution of outbursts in extragalactic radio sources has been hindered by the lack of well-sampled observations at millimeter wavelengths.

The flux density measurements reported here represent the initial results from our study of the short term variations in a small sample of extragalactic sources. The measurements were obtained during the developmental stages of the FCRAO continuum system. Knowledge of the system

characteristics and optimal observing techniques for the FCRAO system was gained during the observing sessions reported here. Many of the observing sessions were devoted primarily to testing the antenna performance (such as antenna pointing, beam pattern, and efficiency) and to developing continuum observing procedures, with flux density measurements comprising a minor fraction of the observing time. As with any new system, the ability of the system (and observers) to obtain high quality data is an evolutionary process. The FCRAO continuum system has been improved such that today it is among the most sensitive continuum systems at millimeter wavelengths.

Observations were restricted to the stronger sources at millimeter wavelengths for which high signal to noise measurements could be obtained, and to sources that were suspected of undergoing rapid outbursts which would require frequent observations in order to define the variations. Despite the limited observations obtained, the results of this preliminary study reveal the importance of studying the short term millimeter variations in extragalactic radio sources. The observations reported here reveal short term variations at millimeter wavelengths which were previously undetected and variations at $\lambda 3mm$ which do not appear at the longer wavelengths. The present capabilities of the FCRAO system permit the extension of this study to a larger sample of sources.

The observing techniques and data reduction procedures are discussed in this chapter. The analysis of the spectral evolution of outbursts in several sources is presented in Chapter IV.

§2.   Observations at λ3 mm

<u>Telescope</u> <u>and</u> <u>receiver</u> <u>description.</u>   The receiver sensitivity and antenna surface accuracy of the FCRAO telescope have steadily been improved since continuum observations began in January 1979. Changes in the receiver and surface configurations and observing procedures during the past three years have given rise to four distinct stages of development of the FCRAO 3 mm continuum system.   These stages and the corresponding data reduction procedures will be discussed separately below.

The receivers used at FCRAO are mounted at the Cassegrain focus of the antenna and are single horn systems (sensitive to linear polarization).   From January 1979 to January 1980, the 3 millimeter receiver in use at FCRAO was a room temperature mixer with a double sideband noise temperature ($T_{receiver}$) of about 800K.   Continuum measurements were obtained by integrating the individual channels of a 256 channel, 1 MHz filter bank. The utilized bandwidth was 256 MHz, and the IF was 1.4 GHz. After February 1980, the receiver consisted of a cooled Schottky barrier diode mixer with a 4.75 GHz parametric amplifier IF (Raisanen et al, 1980; Raisanen, 1980).   A quasi-optical system is located in front of this receiver, which contains components used for system calibration, beam chopping, sideband rejection, and continuum and spectral line linear polarization measurements (Goldsmith, 1981; Raisanen, 1980).   The quasi-optical system permits observing in either

double ($T_{receiver} \simeq 250°$) or single sideband ($T_{receiver} \simeq 500°$) mode. In March, 1980, the bandwidth of the continuum backend was increased to ~375 MHz by feeding the IF signal into a single V-to-F converter. Improvements to the receiver were made during the summer, 1981. The development of new cooled mixers and FET amplifiers (IF frequency 1.4 GHz) have resulted in receiver temperatures (double sideband) of ~65-120K throughout the frequency range 80-115 GHz.

Most measurements have been sensitive to linear polarization. Measurements obtained 21-23 March 1981 were obtained with a quarter wave plate installed in the quasi-optical system to provide circular polarization observations. (Source circular polarization is less than 0.1%, so corrections to the total flux density are not important.) On 5 December 1981, each source was observed at two orthogonal linear polarizations, with the results summed to give the total flux density. The early flux density measurements obtained in the single linear polarization mode will have additional uncertainties in total flux density due to the unknown source polarization at millimeter wavelengths. Barvainis (1981) reports detection (using the FCRAO antenna) of linear polarization at 86 GHz of as high as 10% in a few extragalactic sources. For most measurements reported here, the uncertainty due to source polarization is expected to be less than the measurement and calibration uncertainties, and will thus be ignored. Future observations with the more sensitive receiver and antenna will be conducted in either circular polarization or at orthogonal linear polarizations in order to remove

any errors in flux density determination due to source linear polarization.

The surface panels of the antenna have been set three times since construction of the FCRAO telescope. Prior to summer 1979, the surface had been set with the telescope pointed at zenith, such that the peak telescope efficiency was obtained at elevations close to the zenith. During the summer 1979, the surface was reset, again with the telescope pointed at zenith, but with a deformation model applied to the individual panel settings such that maximum efficiency would be obtained near 45° elevation. Observations during the 1979-80 observing season indicated that the efficiency was indeed maximized in the vicinity of 45° elevation, but the beam pattern had not been optimized. Using a different type of theodolite, the surface was again reset during summer 1980, with the telescope pointed at 45° elevation. The resulting surface accuracy was increased such that the efficiency and beam pattern were improved over those of previous years (Schloerb and Snell, 1980). No further resettings of the antenna surface are anticipated, since it is unlikely that any major improvement can be made to the antenna surface. Adjustments in the quasi-optical system prior to the 1981-2 observing have also resulted in an improvement in the overall antenna efficiency.

During the spring 1979 and 1979-80 observing seasons, the continuum system temperature scale was set by comparison of the system response to

known differential temperatures (ambient and cold loads) several times during an observing session. Fluctuations in receiver gain between the calibrations were not determinable. Since summer, 1980, observations have been calibrated using the chopper wheel calibration method (Penzias and Burrus, 1973; Schloerb and Snell, 1980) in which the temperature scale is set before each observation by comparing the response to an ambient load with the sky emission. In this method, the observed antenna temperature of a source is automatically corrected for atmospheric opacity and changes in receiver gain.

In summary, the data reported in this chapter were taken during four distinct periods of receiver/telescope parameters which required different reduction procedures. During the spring 1979 observing season the room temperature mixer was used, temperature scale calibration was accomplished by occasional comparison of source response to ambient and cold loads, and the maximum telescope efficiency was at an elevation near the zenith. During the 1979–1980 season, the room temperature mixer was employed prior to February 1980 (the cooled mixer thereafter), the temperature calibration was accomplished as in 1979 but with the peak antenna efficiency near 45° elevation. In the 1980–81 season, the cooled mixer was used with an IF frequency of 4.75 GHz, temperature and atmospheric opacity were calibrated using the chopper wheel calibration, and the antenna efficiency was optimized for elevations near 45° (with little elevation dependent efficiency). During the fall 1981, season the changes to the system were made such that the cooled mixer was used

with an IF of 1.4 GHz, and calibration was accomplished by an improved chopper wheel calibration method which better modeled the atmospheric contribution to the total system temperature.

Observing procedure. The observing procedure has remained fundamentally the same since continuum observations were begun in January 1979. To remove fluctuations in the sky background and receiver gain fluctuations, it is necessary to rapidly switch between the source position and an adjacent position in the sky in which no source is present ("beam switching"). This is accomplished at FCRAO by use of a standard "beam switching chopper", which consists of a rotating chopper blade. When the chopper blade is in the "open" position the beam from the feed horn is aligned directly with the telescope subreflector. When the blade is in the "closed" position the beam is reflected off the chopper blade onto a parallel mirror and then to the subreflector. The displacement of this "reference" beam from the "main" beam in the sky is determined by the offset of the reflecting mirror from the axis of the telescope. The beam displacement for the FCRAO system has been between ~0.08 and 0.10° (~5 to 6$\frac{1}{2}$ half power beamwidths) in azimuth. The rate of the chopper wheel rotation (the beam switching rate) is adjustable, and was generally between 6 and 12 Hz. No data is taken during the time interval while the chopper blade is partially in front of the feed horn.

Antenna pointing is checked by performing a "five-point" scan on strong sources. In a "five-point", a source is observed at the nomial

source position, and at positions displaced (by about 1/2 half-power beamwidth) symmetrically both in azimuth and elevation (figure 8). A two dimensional gaussian is fit to the measured source strength at the five positions to derive a pointing error relative to the nominal source position.

It was possible to make "five-point" measurements only for the planets and the extragalactic source 3C84, since the other continuum sources in the program were too weak to obtain useful pointing information within a reasonable amount of observing time. The recent improvements to the continuum system and receiver make it feasible to use a larger sample of sources for pointing measurements. The antenna pointing has historically not been well determined at elevations above 70° elevation. The planets do not reach these elevations at FCRAO, and observations of 3C84 have not been extensive in this elevation range.

The pointing characteristics of the antenna are determined prior to each observing season by observing strong continuum and spectral line sources using the "five-point" procedure. These measurements were used to determine the coefficients of a pointing model for the antenna. The pointing model coefficients are revised if subsequent pointing measurements provide better determinations of the coefficients. The rms scatter of the "five-point" measurements which are used to derive the pointing model coefficients has been typically ~5" (0.0015°) in both azimuth and elevation (Schloerb, 1981). This is comparable to the estimated error in the five point position determination from a single scan.

Figure 8a. Five point mapping procedure used to determine antenna pointing offsets. The main antenna beam is pointed alternately at positions displaced from the nominal main beam ("on") source position and a reference ("off") source position offset several beamwidths from the nominal position. The displacement from the central main (MC) and reference (RC) positions is typically at the beam halfpower points (HP) in azimuth (left≡"East"=E; right≡"West"=W) and elevation (up≡"North"=N; down≡"South"=S). The antenna is sequentially pointed at the five pairs of positions: MN-RN, MS-RS, MC-RC, ME-RE, and MW-RW. The difference between the antenna temperature for each pair is calculated, with a two dimensional least-squares gaussian fit to the five differences. The pointing offset is the difference between the calculated source position and the nominal position (MC).

Figure 8b. A representative five-point observation. The planet Venus (flux density ~1900 Jy at this epoch) was observed using the procedure described in figure 8a. The "off" (reference) measurements were made at the position of the beam chopper reference beam, providing pointing offset information for both beams. Visual inspection of the results indicate that the source is located below (S) in elevation (since MS > MN) and to the left (E) in azimuth (since ME > MW) of the nominal main beam center. The pointing offset for the reference beam is minimal. A least-squares gaussian fit to the measurements indicates pointing offsets of 0.0008° (3") in azimuth and −0.0002° (<1") in elevation.

FIVE POINT
MAPPING PROCEDURE

REFERENCE BEAM OFFSET

• MN

• RN

• ME

HP

• MC

• RE

• RC

• MW

• RW

• MS

• RS

MAIN ("ON") BEAM

REFERENCE ("OFF") BEAM

Figure showing Antenna Temperature vs Integration Number for Venus, 5 Dec. 1981, 87.3 GHz, 5-point sequence.
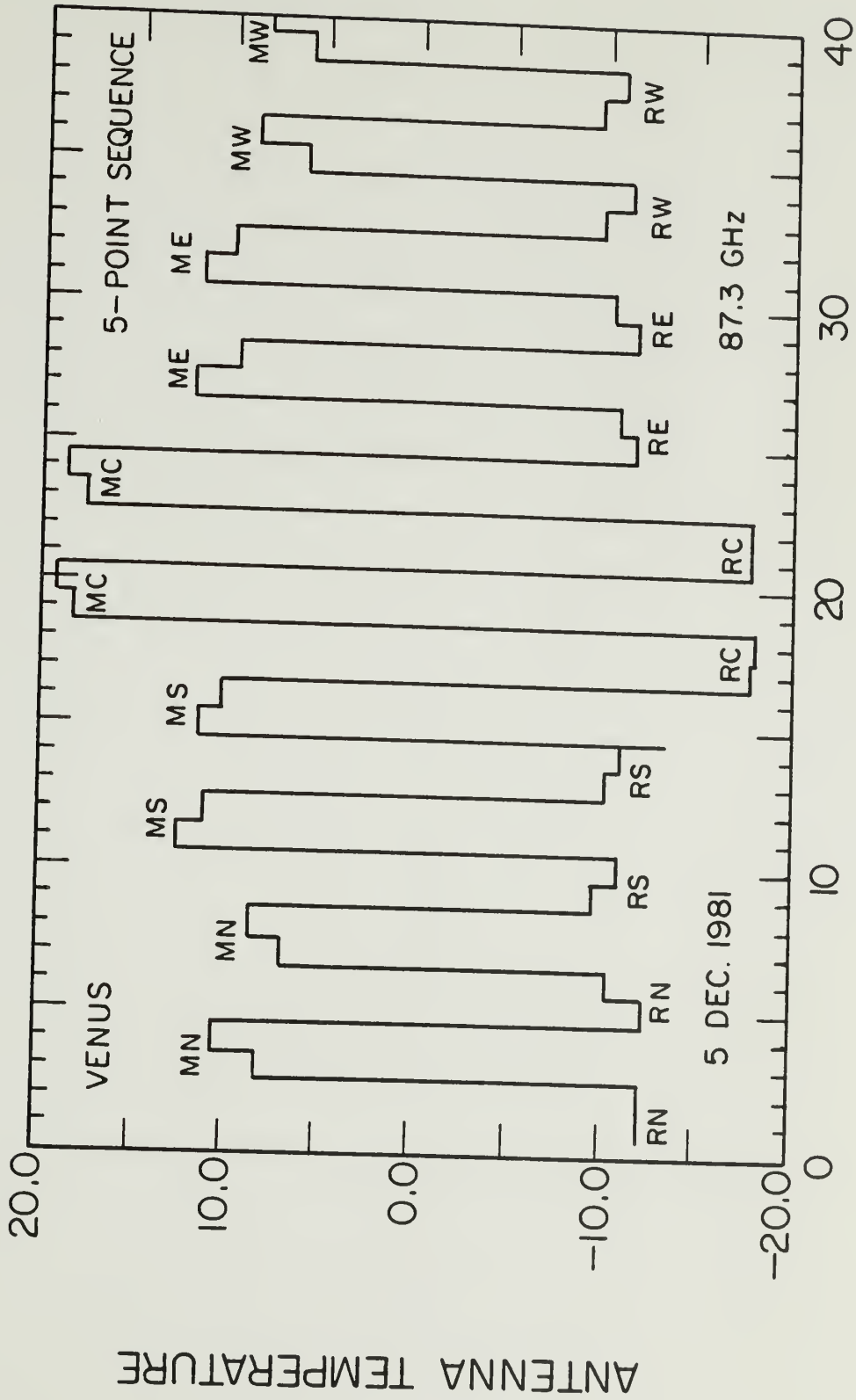
Corrections to the "standard" pointing model were determined during each observing session, if possible. The pointing corrections obtained during each observing session represent minor, residual corrections to the "standard" pointing model. The measured pointing corrections during most sessions cover a limited range in antenna azimuth and elevation due to the small sample of available strong sources. For weak sources, the assumed pointing correction was derived from measurements obtained from strong sources at nearby azimuths and elevations.

The pointing corrections differed between observing sessions, but typically the rms of the total pointing correction (azimuth plus elevation) within an observing session was less than 8" (0.0022°). The limited amount of pointing information available during a single observing session prevented detailed determination of positional pointing errors. Also, it was not possible to draw any conclusions as to whether the pointing characteristics of the telescope are strongly temperature dependent.

The offset of the reference beam from the main antenna beam is measured by performing separate "five-point" observations for the two beams and differencing the pointing results, or, alternately, using the reference beam as the "off" position during the five-point routine (figure 8b). For both the room temperature and cooled receivers, the reference beam has been offset between ~0.08 and 0.10° in azimuth and only a few milli-degrees in elevation from the main beam. The absence

of any significant elevation offset assures that the atmospheric (elevation dependent) temperature contribution is the same in both beams. The azimuth offset is large enough that the reference beam position is beyond the sidelobe pattern of the main beam, but small enough that the atmospheric conditions should be essentially the same in the two beams.

Source strength measurements consist of a series of "on-offs" in which the main beam of the antenna is alternately pointed at the source position ("on") and at a nearby ("off") position in the sky. For those observing sessions in which the reference beam position was well known, the "off" position corresponded to the offset such that the reference beam was pointed at the source position. Otherwise, the "off" position was located such that neither beam was directed at the source. Positioning the reference beam at the source position during the "off" observation doubles the observed source strength, thus effectively doubling the signal-to-noise ratio for the "on-off" sequence.

A typical "on-off" sequence consisted of 10-20 "on-off" measurements, with the "on" or "off" source integration time being 8 or 16 seconds for most sources, and 4 seconds for the stronger planets. The integration time used depended upon the atmospheric conditions - 8 seconds being used during cloudy or unstable conditions, and 16 seconds during clear, cold conditions. The time required for the antenna to move between the "on" and "off" positions (with a pointing accuracy of

0.001°) is ~8 seconds. This moving time thus constrains the useful integration times - short integrations are inefficient since a large fraction of the total time is spent moving the antenna. "On-off" sequences were repeated until the desired signal-to-noise ratio was obtained for the ensemble of "on-off" measurements. The error in the average of the "on-off" measurements was calculated by equation II-6. Typical "on-off" observations are shown in figure 9. Corrections to the observed source strength for antenna gain and atmospheric extinction were made independently to each sequence prior to averaging the ensemble. These corrections are described later.

Errors in the telescope pointing will result in the observed source strength being less than the actual source strength. If the same pointing corrections are used for all sources, and if there is no positional dependence of this error, then all sources will have the same percentage error in their flux density determination which will be removed by later calibration. If there are time or position dependent pointing errors, then the error in the flux density determination can be estimated from the rms pointing scatter during the observing session. For the FCRAO beam (HPBW ~50-65" at frequencies between 85 and 115 GHz), a 0.0022 (8") pointing error corresponds to a 5% error in flux density. Pointing errors will be reflected in scatter in the calculated source flux densities during later stages of calibration. For weak sources the error in the flux density determination due to pointing errors is less than the error due to random noise. For strong sources, the error due

Figure 9. Representative "on-off" observations at 87.3 GHz. Each integration is 8 seconds in duration. The "ticked" measurements correspond to the main beam pointed on the source position, "unticked" measurements corresponding to the reference beam.

(a) OJ287: The calculated average antenna temperature and standard deviation (equation II-6) of this single "on-off" sequence is 0.241° ± 0.007°, corresponding to a flux density of 6.8 Jy.

(b) CTA 102: The average of four individual "on-off" sequences for this weaker source. The average antenna temperature and standard deviation of the combined four scans is 0.061° ± 0.005°, corresponding to a flux density of 2.0 Jy.

SINGLE "ON–OFF" SEQUENCE

OJ 287

5 DEC. 1981

87.3 GHz

ANTENNA TEMPERATURE

INTEGRATION NUMBER

CTA 102

AVERAGE OF 4 "ON-OFF" SEQUENCES

5 DEC. 1981

87.3 GHz

ANTENNA TEMPERATURE

INTEGRATION NUMBER
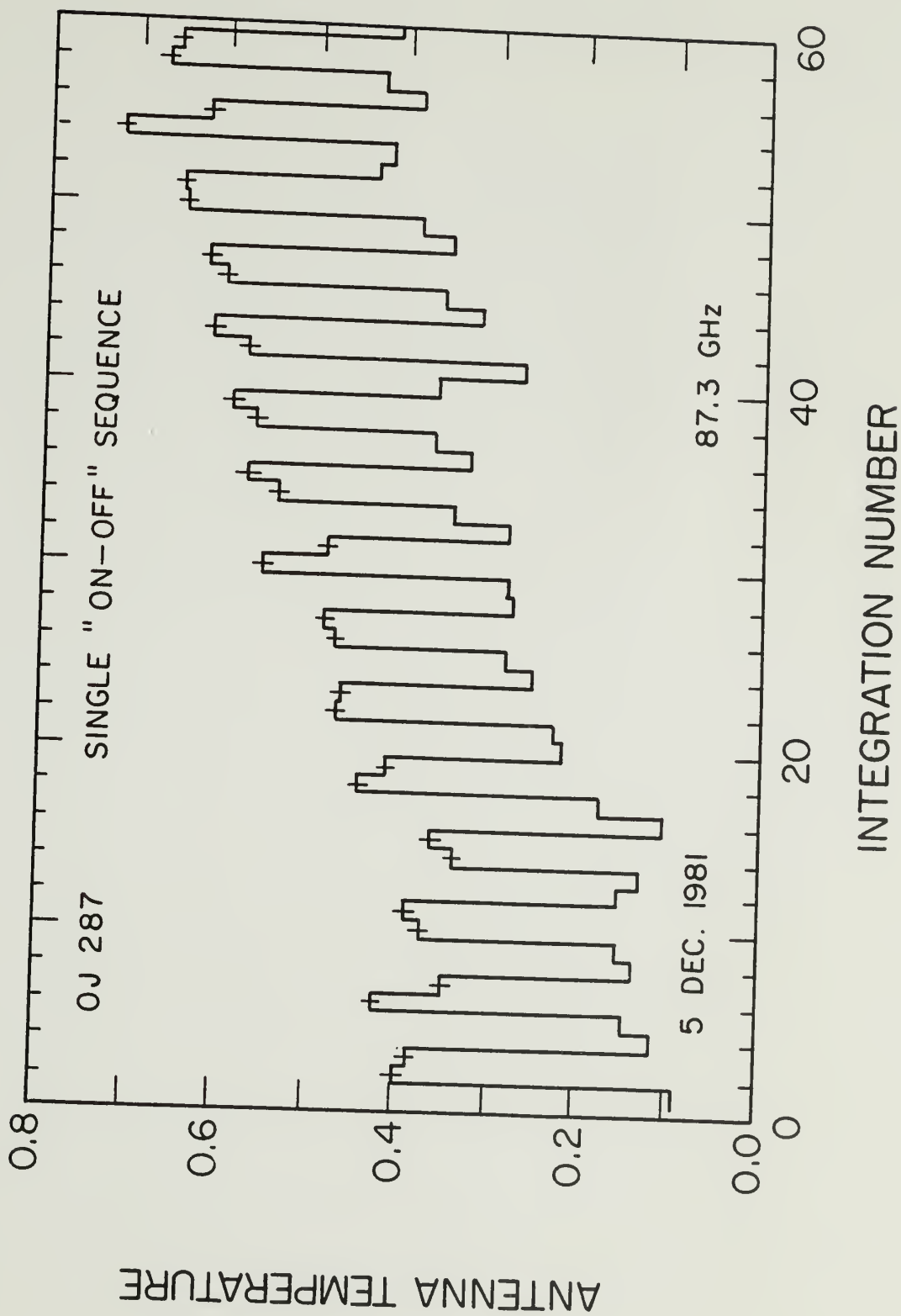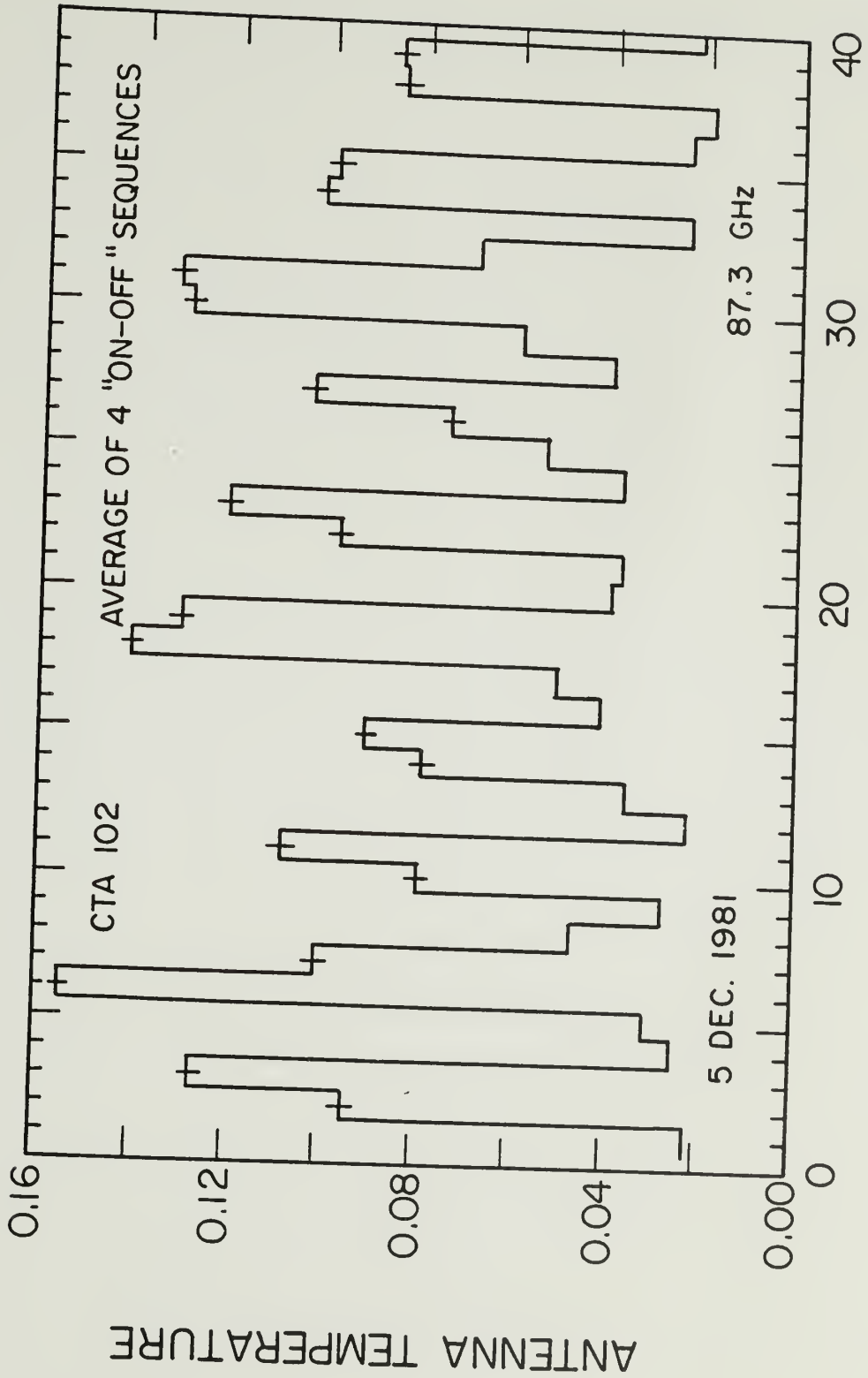
to pointing may be larger than the contribution from noise. However, scatter in the flux density scale calibration will partially reflect and compensate for these pointing errors.

For two beam continuum observations it is preferable to maximize the sum of the responses of both beams to a source, as well as having nearly equal total power in both beams. Equalizing the total power provides for better sky and receiver gain subtraction from the beam switching procedure. The path length difference between the main and reference beams makes it impossible for both beams to be simultaneously in focus. The focus (radial subreflector position) is determined by measuring the source strength (by the "on-off" procedure) at several radial positions of the subreflector, to determine the position which gives the maximum response to a small angular size source (typically Jupiter, which is the strongest small diameter continuum source at these wavelengths). During many of the observing sessions reported here, the focus was left at the value determined for the main beam, with the consequence that the source strength in the reference beam was less than (often 50-90%) that of the main beam. When this ratio was known, the observed source strength from a two beam "on-off" sequence was normalized to the corresponding single (main) beam strength.

The observed strength of Jupiter in the main and reference beams as a function of the radial subreflector position (focus) is shown in figure 10. The difference in the peak observed source strength in the

Figure 10. Focus curve for the main and reference beams at 88.0 GHz. Shown is the observed strength of the planet Jupiter as a function of the radial subreflector position (focus). The path length difference for the two beams results in the offset in "focus" of the peak response of the two beams. At the maximum signal strength for the average of the two beams (focus -1.5 mm), the signal strength in the reference beam is only 80% that in the main beam.

Focus Determination for Main and Reference Beams
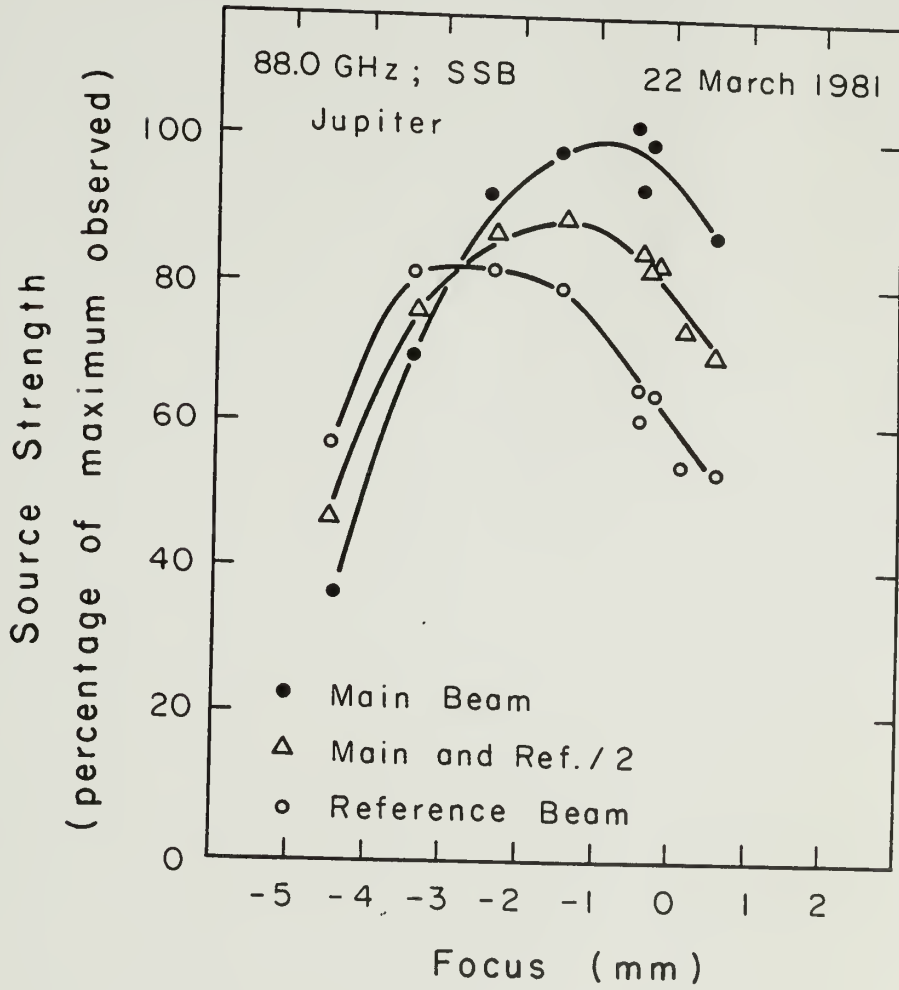
beams is due to the reference beam being located off the axis of the telescope and losses from two additional reflections for the reference beam. The path length difference for the two beams causes the offset in "focus" of the peak response in the two beams. The measurements presented in figure 10 indicate that equalizing the response to a point source in both beams (focus -2.75 mm) would result in a total system response five percent lower than the maximum value (at focus -1.5 mm). Tests conducted in fall 1981 (by Barvainis and Predmore) indicate that changing the tilt of the reference beam mirror alters the peak response of the reference beam, but the maximum repsonse is only 80% that of the main beam (similar to the results presented in figure 10). The peak responses could be equalized by tilting the subreflector such that the electrical axis pointed approximately midway between the reference beam mirror (reference beam) and the chopper blade (main beam). For any focus, the observed strength of the moon (diameter $1/2°$) is the same ($\pm 5\%$) in both the main and reference beams, indicating that the power lost from the beam peak response due to defocusing goes into broadening the primary beam and into the nearby sidelobe pattern.

Temperature scale calibration. The antenna temperature for a source is calculated by comparison with the receiver response to known temperature loads. Prior to fall 1980, this was accomplished by alternately observing ambient (T ~280K) and cold (T ~77K) loads placed in front of the beam chopper assembly (termed a "hot-cold" measurement). The loads were observed with the same backend and by the same observing procedure

as a celestial source. From the observed response (in volts or "counts") to the known temperature loads, both the receiver temperature and temperature scale conversion factor (termed "calset", in units of degrees K per volt or count), were obtained. Unfortunately, this calibration procedure could not be performed remotely from the telescope control room. The system calibration involved manually inserting the loads in front of the receiver. This procedure was cumbersome, boring, a slight bit dangerous (for sleepy astronomers), and required about ten minutes of observing time, so it was performed only a few times during each observing session. The observed source strengths from the "on-off" sequences were converted to antenna temperature by multiplication by the determined calset factor. If the calset factor changed during an observing session, a time dependent correction factor was calculated by linearly interpolating the measured values. Non-linear changes in the receiver gain were not observable by this procedure, but were reflected in temporal changes in the corrected antenna temperature (T_A) of strong sources.

Since fall 1980, calibration at FCRAO has been performed using the chopper wheel calibration method (Schloerb and Snell, 1980). The temperature scale is set by comparison with the noise power of the receiver when looking at an ambient load and when looking at the sky adjacent to the source position. This method has the advantage of correcting for the atmospheric absorption as well as for receiver gain changes. A second order correction to this method, which is a function of the

atmospheric opacity and the difference between the ambient and sky temperatures, must be applied to the calculated temperature scaling factor and system temperature.

During the 1980-81 observing season, this latter correction was applied during the post-observing stages in the data reduction. This correction is now calculated and applied directly to the raw data as it is being obtained. Errors in the assumed atmospheric opacity or in the sky temperature will result in an error in the calibrated antenna temperature for a source which increases at the lower elevations (higher air masses). Observations of strong sources (such as the planets) at low elevations ($< 20°$) can be compared to observations made at high elevations to determine the errors introduced by this calibration method. Results from 1980-81 indicate that even for elevations as low as $10°$ this method is accurate to a couple percent during good observing conditions. The advantage of this calibration method is that short term or localized changes in the atmospheric opacity are compensated for from the direct observation of the receiver response to the sky emission prior to each measurement.

§3. Reduction of the λ3 mm Observations

The 3 mm continuum data obtained at FCRAO since 1979 have been separated into four distinct periods in terms of antenna characteristics and subsequent data reduction procedures. Corrections to the observed

source antenna temperatures must be made for: source size extension, atmospheric opacity, antenna elevation dependent aperture efficiency, and miscellaneous (e.g. time dependent) system gain changes. Finally, the conversion factor (calibration constant) from corrected antenna temperature to flux density must be determined from observations of known flux density standards. Changes in the antenna panel setting and data taking techniques result in these reduction procedures being different between the four observing periods: spring 1979; fall 1979 - spring 1980; fall 1980 - spring 1981; and post fall 1981. Each of the antenna temperature correction factors will be discussed separately, with differences between the observing periods detailed for each factor.

Source size correction. When a radio source has an angular size comparable to the size of the antenna beamwidth, the observed peak antenna temperature must be corrected for partial resolution of the source. For the FCRAO telescope at ~3 mm, the ~55" beamwidth is comparable to the angular size of the planets, so the source size correction factor is very sensitive to the antenna beam size and can be as great as 25%. In addition, the calibration sources DR21 and 3C274 are not point sources. To assure accurate calibration of the flux density scale for the FCRAO antenna, the antenna beamwidth must be well determined at each observing frequency.

The source size correction factor for a Gaussian beam and a disk source is given by equation II-8 (Predmore, 1978; Ulich and Haas, 1976).

At frequencies for which the beamwidth was not measured or could not be interpolated from results at nearby frequencies, it was calculated from the equation

$$BW = 1.22 \ (206,265 \ \lambda \ / \ D)$$

$$= 55.1 \ / \ (100 \ / \ \nu_{GHz})$$

(III-1)

where BW is the beamwidth in arcseconds, λ is the observing wavelength, D is the antenna diameter (=1371 cm for the FCRAO antenna), and ν_{GHz} is the observing frequency in GHz.

Prior to fall 1980, the observed beamwidths were less than 5% larger than the calculated beamwidths. The quasi-optics installed in front of the cooled reciever (post fall 1980 observations) produces larger beamwidths (by ~10") than given by equation III-1 (Snell and Schloerb, 1981). For large angular size sources, such as Jupiter or Venus which can have angular diameters ~45", the difference in source size correction factors based upon the observed 1980-81 beamwidths and the calculated beamwidth can be as large as 5%, thus producing errors of up to 5% in the corrected antenna temperature for the planets. The effect is smaller for smaller angular size sources. Since the planets have been used as the primary calibration sources for the observations reported here, the possibility exists that the absolute flux density level may be in error. However, recent measurements of the beamwidth (61" at 91 GHz) using the point source 3C84 indicate that the antenna beam widths based upon the planet observations are accurate to ~2".

This implies that the source size correction factor (and thus the flux density scale) is accurate to within a couple percent.

Atmospheric opacity. The observed source temperature must be corrected for the attenuation due to atmospheric opacity. Ideally, this correction should be determined prior to each observation in order to remove time dependent changes in the opacity. Practically, this is not feasible since measuring the opacity is time consuming. In practice, the opacity is determined several times during an observing session - the scatter in the results providing an indication of changes in the opacity. Two different observing procedures have been used to determine the atmospheric opacity. A "sky dip" measures the atmospheric emission temperature at several elevations (air masses) in order to determine indirectly the atmospheric absorption. The zenith (one air mass) opacity is calculated by fitting the observed atmospheric emission temperature, $T_{em}(el)$, to the equation

$$T_{em}(el) = C_0 \, e^{\tau_0 / \sin(el)} + C_1 \qquad\qquad (III-2)$$

where C_0 is a function of the mean temperature of the atmosphere, el is the elevation, τ_0 is the zenith opacity, and C_1 is a constant which depends upon the receiver temperature and spillover losses. The measured opacity at FCRAO in the frequency interval 85-110 GHz has ranged from 0.10 to 0.25 during good observing conditions. The total atmospheric opacity at millimeter wavelengths is frequency dependent. It is a combination of the molecular oxygen opacity which is essentially

constant in time but a function of frequency, and the water opacity which is time variable. A discussion of the contribution and calibration of the oxygen and water opacities can be found in Kutner (1978) and Waters (1976).

The second method by which the atmospheric opacity has been determined at FCRAO is by doing a series of "on-off" measurements of large angular size sources, such as the moon or sun, at different elevations. The moon or sun will be weaker at the lower elevations due to the absorption by the atmosphere. The atmospheric opacity, τ_o, (for $\tau_o \ll 1$) is found from the slope of the best fit line to the equation

$$\ln(T(el)) = \{ \tau_o / \sin (el) \} + C_2 \ . \qquad \text{(III-3)}$$

This method measures the opacity by observing the absorption character of the atmosphere, while the sky dip method is based upon the emission character of the atmosphere. Large angular size sources must be used to unambigously determine the atmospheric opacity since the elevation antenna gain dependence (see next section) affects the observed strength of sources with angular extent smaller than the beam size. There is no noticeable elevation dependent gain for sources of angular extent $\sim 1/2°$. If the elevation gain curve is well known, then this procedure could effectively be used with small diameter sources.

The absorption method is unreliable if the atmospheric conditions are time dependent since a source must be observed over a several hour time span in order that it traverses several air masses. Also, this

method is not applicable if no strong sources are available during the observing session! This method is preferable in that it directly measures the atmospheric effect which is being calibrated and subsequently applied to the source measurements. During stable weather conditions, both methods were found to agree to within the errors inherent in each procedure.

During the 1979 and 1979-80 observing seasons, the atmospheric opacity was determined using both techniques. Each "on-off" source measurement was multiplied by the atmospheric correction factor

$$CA = e^{\tau_0} / \sin(el) \quad . \quad\quad (III-4)$$

The error that will be introduced to a flux density measurement as a result of an error in the assumed opacity can be readily estimated. Sources are observed at elevations between ~20 and 70°. An error in the determination of τ_0 of 0.03 will produce only a 6% scaling difference between observations at these extreme elevations.

Beginning in fall, 1980, the chopper calibration method has been used to correct for the atmospheric opacity. The zenith atmospheric opacity, τ_0 (which might vary in time during non-optimal conditions), must still be measured (by a sky dip) in order to determine the second order correction to the chopper calibration method. However this second order correction is ~1/10 as sensitive as the direct method to errors in τ_0. Observations at FCRAO during 1980-81 indicate that the chopper wheel calibration scheme is accurate to a few percent, even during marginal observing conditions.

<u>Antenna</u> <u>elevation</u> <u>dependent</u> <u>efficiency.</u> Gravitational deformation of the antenna backstructure and surface results in an elevation dependent antenna efficiency (gain) and beam shape changes. This elevation gain is calibrated by observing strong sources (such as the planets or 3C84) at a range of elevations, correcting the observed source antenna temperatures by the atmospheric correction factor, and least-squares fitting the results to the third-order polynomial

$$T_C = T_0 + T_1 \cos(el-el_o) + T_2 \cos^2(el-el_o) ,\qquad (III-5)$$

where el is the elevation, el_o is the elevation corresponding to the maximum observed efficiency, T_C is the observed antenna temperature corrected for opacity, and T_0, T_1, and T_2 are the fitted coefficients. The parameter el_o was determined from visual inspection of the data.

The antenna gain at elevations above 60° is not as well determined as for lower elevations since the planets, confined to the ecliptic, do not reach elevations above 60° as seen from FCRAO. The source 3C84 has been observed at high elevations in an attempt to better determine the high elevation gain, but the measurements are not as reliable as those of the planets due to the weakness of 3C84 and the pointing uncertainties at elevations above 70°. However, since few sources have been observed at elevations above 70°, the lack of knowledge about the high elevation gain does not have a major affect on the accuracy of the flux density measurements reported here.

The shape of the elevation dependent gain was different for each observing season due to resetting of the antenna surface panels during

the summers of 1979 and 1980. The antenna resettings were discussed in Section 2. During 1979, the peak observed antenna efficiency was at an elevation above 70°, consistent with the antenna surface having been set while directed at the zenith. During 1979-80, the peak efficiency was in the 40-45° elevation range, again consistent with the panel setting which had taken place the previous summer. The gain was less at elevations above and below this range, indicating that the antenna did not maintain a parabolic shape (also indicated by the high sidelobe levels). Since summer, 1980, there has been no evidence of gain changes greater than 5% within the elevation range 15-70°. The telescope panel setting is such that the structure maintains a parabolic shape throughout this elevation range. At elevations lower than 15° the atmospheric correction factor uncertainty is sufficiently large that it is not possible to distinguish between elevation gain and atmospheric effects. At higher (>70°) elevation the pointing characteristics of the telescope had not been adequately determined prior to most efficiency measurements. It is encouraging that the lack of significant observed antenna efficiency dependence since summer, 1980, reionforces the confidence which we felt in the accuracy of the surface panel setting.

Determining the atmospheric and elevation gain corrections. In practice, it was difficult to distinguish between the atmospheric opacity, elevation dependent efficiency, and time dependent contributions to the gain. Although unique solutions for each of these corrections could not be determined during an observing session, the results from several

sessions during an observing season are consistent in terms of the magnitudes and trends of the corrections. The elevation efficiency results are consistent with knowledge of the antenna panel settings. To demonstrate the calibration procedure, results from each of the four periods of receiver/telescope parameters are discussed. The results are discussed at length since this stage of calibration can be the major contributor of scaling errors to continuum observations.

Prior to the calculations of the atmospheric opacity and antenna elevation dependent efficiency, the previously discussed temperature scale calibration has been applied to the observed source strength. Time dependent receiver gain changes which have not been compensated for will be reflected in scatter of the final flux densities.

Figure 11a presents the opacity and efficiency results for an observing session during the spring, 1979, season. Observations of the moon (A) at a range of elevations covering a nine hour period (both rising and setting) are well fit by a zenith opacity (equation III-3) of $\tau_0 = 0.09$. Observations (over three hours) of the planet Jupiter (B) are least-squares fit by an "effective" opacity of 0.16 (note that all the measurements lie within 5% of the fitted line). The difference between this value and the opacity determined from the moon is due to elevation dependent efficiency. If the Jupiter measurements are corrected (equation III-4) for an opacity of 0.09, a fit can be made (equation III-5) for the antenna efficiency (C). Fits B and C to the Jupiter

observations are equally good. Observed source antenna temperatures can be corrected by sequential application of an opacity (A) and elevation gain (C) or, alternately, by an "effective" opacity (B).

The elevation gain (elgain) fits for the spring, 1979, data indicate a maximum efficiency at elevations above 70°. Insufficient observations exist above 70° to determine the exact elevation of maximum efficiency. The lower elevation observations also do not constrain the elevation of maximum efficiency. Elgain fits for different observing sessions do not produce identical results for the efficiency elevation dependence – due in part to the limited number of observations. The general elevation dependence to the antenna efficiency is consistent with the antenna panels having been set at and optimized for peak zenith efficiency.

Figures 11b and 11c present results obtained during the 1979-80 season. The antenna surface had been set to maximize the efficiency at ~45° elevation. The observations indicate a peak efficiency within the elevation range 40-45°, dropping at higher and lower elevations. However, it was difficult to solve for the antenna efficiency elevation dependence. At low elevations (high air mass) errors in the opacity correction can become large, especially during periods of changing opacity. Few measurements were made at high elevations. The planets transitted at ~55° elevation, and the receiver was not sufficiently sensitive to obtain high signal-to-noise measurements of other sources.
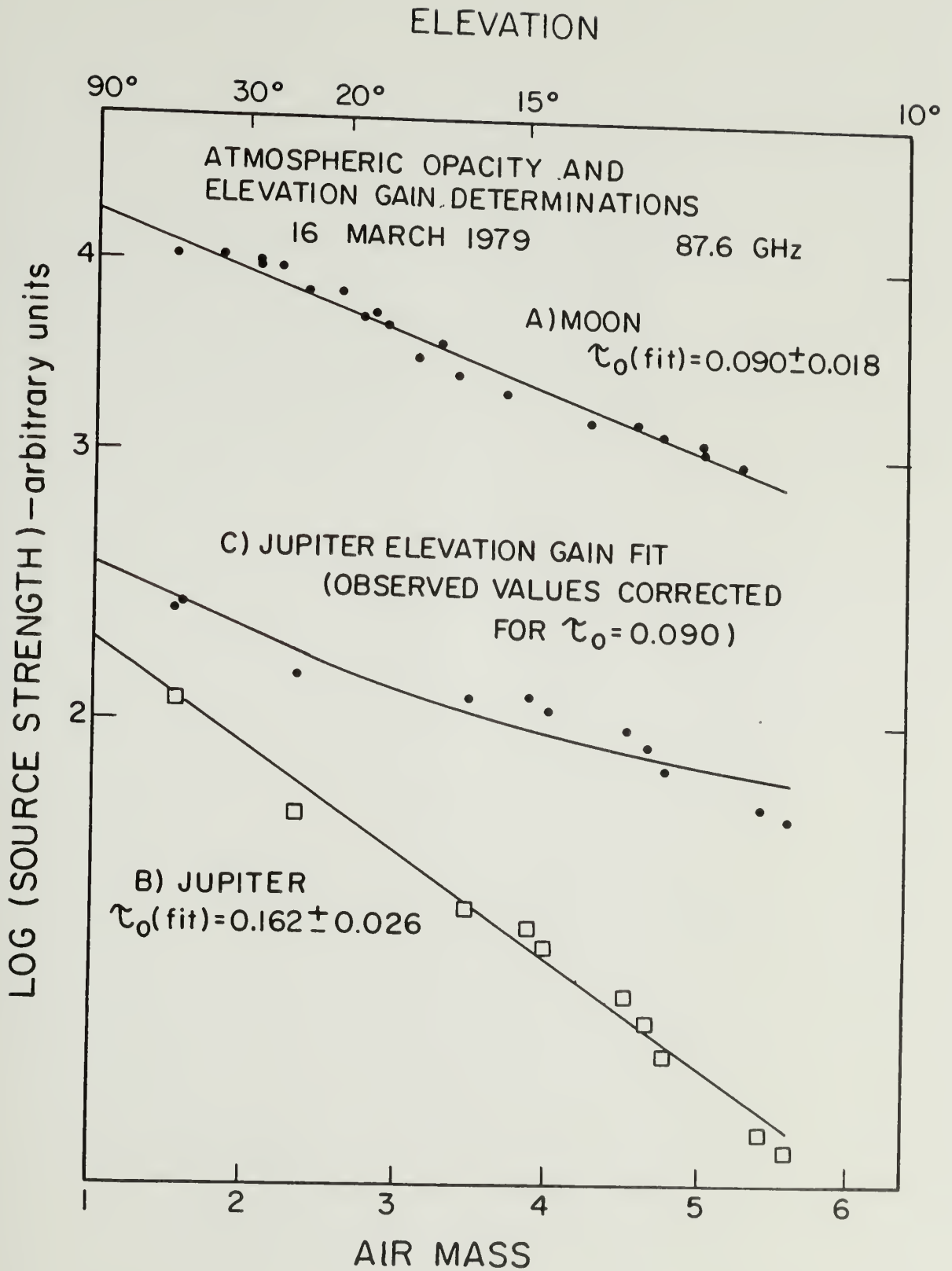
Figure 11. Atmospheric opacity and elevation dependent efficiency (gain) measurements. The figures show typical elevation efficiency dependence corresponding to the three different panel settings which have occurred for the FCRAO telescope (a: pre-summer, 1979; b and c: 1979-1980; d: post-summer, 1980).
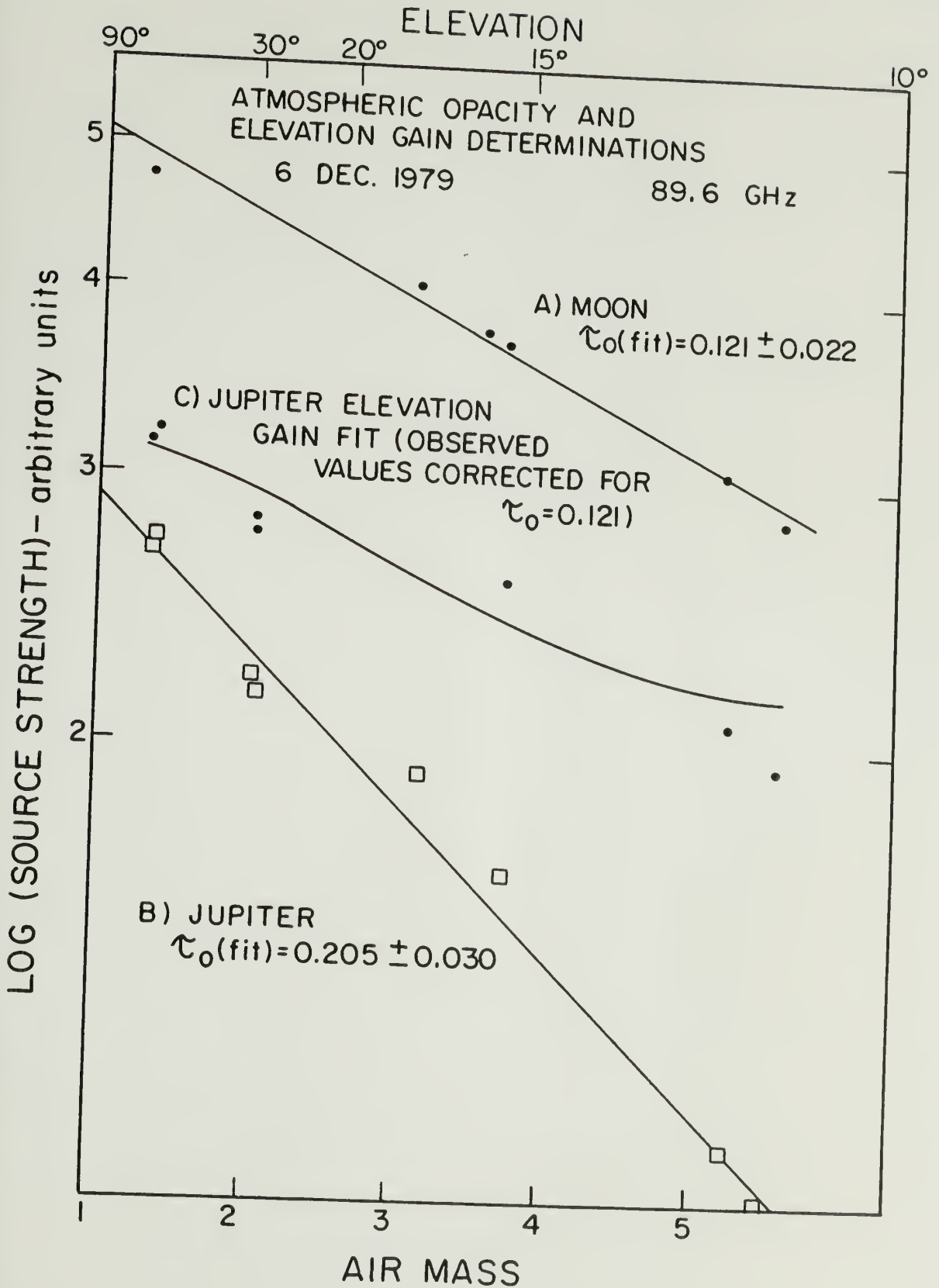
(a) 16 March 1979. Observations of the moon (A) fit by a zenith opacity of $\tau_o = 0.09$; Jupiter (B) fit by an "effective" opacity of 0.16, which is the combination of the antenna efficiency (C) and atmospheric opacity. The results indicate maximum efficiency at an elevation above 70°.

(b) 6 December 1979. Atmospheric opacity 0.12 fit to moon observations (A), consistent with a sky dip value of 0.125. Jupiter observations below 48° elevation (B) have been corrected for opacity to show the elevation dependent efficiency (C).
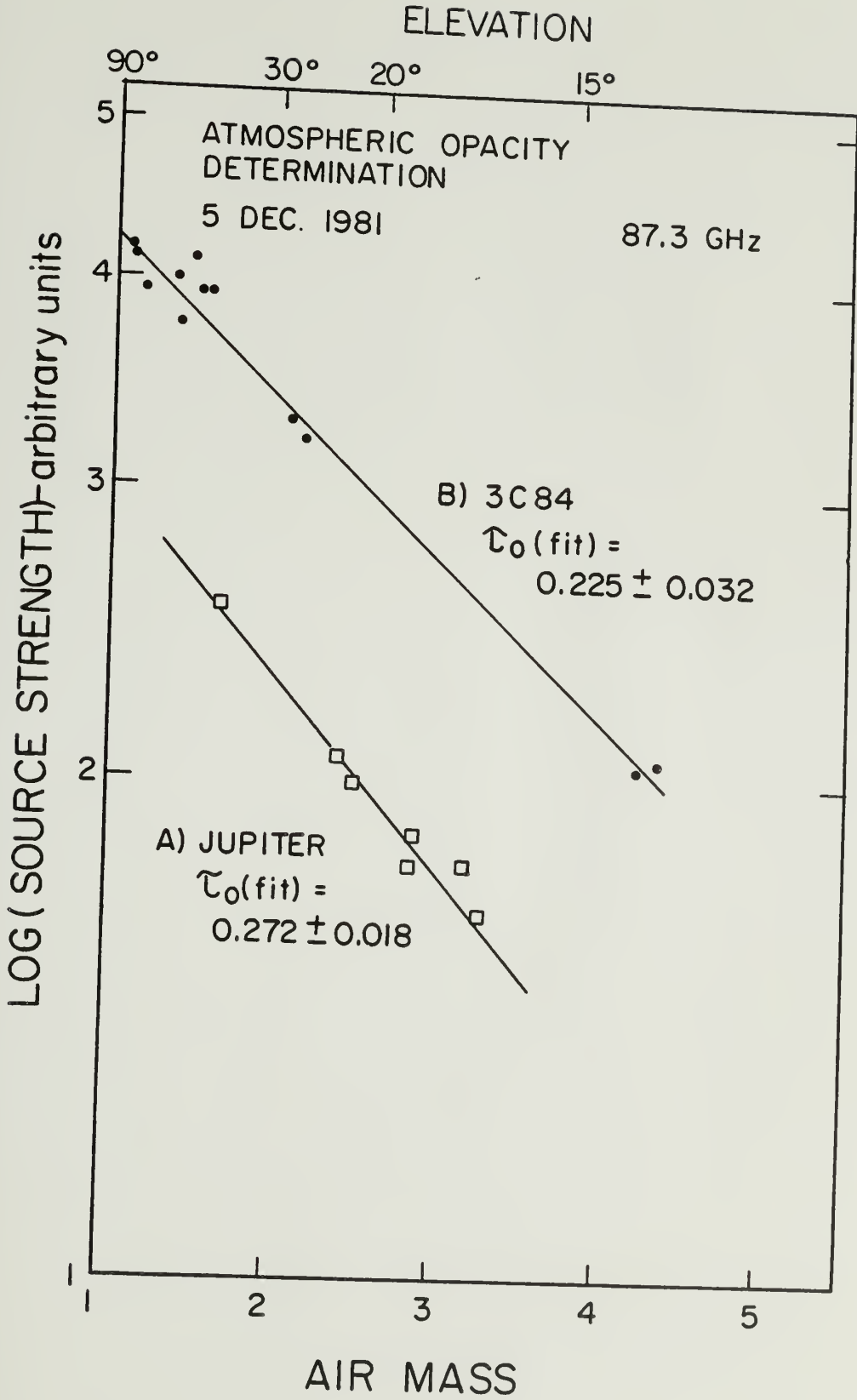
(c) 2 January 1980. These measurements of Jupiter cover a larger elevation range than in (b), showing the falloff in the efficiency at elevations above and below 40°. The lines in (A) are exponential fits to the observations("effective" opacities), while the curve in (B) is a polynomial fit for the elevation dependent efficiency. Note that the efficiency decrease at high elevations is not seen in figure 11b due to the limited elevation range of the observations.

(d) 5 December 1981. Opacity fits for Jupiter and 3C84. No evidence is seen for elevation efficiency changes at elevations below ~65°. The observed source strength change with elevation can be accounted for by an opacity $\tau_o = 0.25$.

ELEVATION

ATMOSPHERIC OPACITY AND
ELEVATION GAIN DETERMINATIONS
16 MARCH 1979   87.6 GHz

A) MOON
τ_0(fit)=0.090±0.018

C) JUPITER ELEVATION GAIN FIT
(OBSERVED VALUES CORRECTED
FOR τ_0=0.090)

B) JUPITER
τ_0(fit)=0.162±0.026

LOG (SOURCE STRENGTH) – arbitrary units

AIR MASS

ELEVATION

ATMOSPHERIC OPACITY AND
ELEVATION GAIN DETERMINATIONS
6 DEC. 1979   89.6 GHz

A) MOON
$\tau_0(fit)=0.121\pm0.022$

C) JUPITER ELEVATION
GAIN FIT (OBSERVED
VALUES CORRECTED FOR
$\tau_0=0.121$)

B) JUPITER
$\tau_0(fit)=0.205\pm0.030$

LOG (SOURCE STRENGTH) - arbitrary units

AIR MASS

ELEVATION

ATMOSPHERIC OPACITY AND
ELEVATION GAIN DETERMINATIONS
2 JAN. 1980   87.6 GHz

B) COSINE FIT
$T = T_0$
$+ T_1 \cos(\text{elevation} - 40°)$
$+ T_2 \cos^2(\text{elevation} - 40°)$

$\tau_0(\text{fit}) = 0.102 \pm 0.015$

$\tau_0(\text{fit}) = -0.450 \pm 0.024$

A) EXPONENTIAL FITS
$T = T_0 \, e^{\tau_0/\sin(\text{ELEVATION})}$

LOG(SOURCE STRENGTH) – arbitrary units

AIR MASS

ELEVATION

ATMOSPHERIC OPACITY
DETERMINATION
5 DEC. 1981   87.3 GHz

B) 3C 84
τ_0(fit) =
    0.225 ± 0.032

A) JUPITER
τ_0(fit) =
0.272 ± 0.018

LOG(SOURCE STRENGTH)—arbitrary units

AIR MASS

Some measurements were obtained of 3C84 at high elevations, but pointing uncertainties at high elevations limited the usefulness of these observations.

Results from 6 December 1979 are shown in figure 11b. The opacity determined from measurements of the moon (A) is 0.12, in agreement with a sky dip value of 0.125. Observations of Jupiter (B) at elevations below 48° have been corrected for the opacity (C). The elevation gain fit (C) is of comparable quality as the exponential atmospheric fit (B).

Observations of Jupiter on 2 January 1980 (figure 11c) cover a greater elevation range. The maximum efficiency occurs at an elevation ~40°. "Effective" opacities (exponential fits) are determined for observations above and below this elevation (A). The low elevation slope of 0.10 is the same as calculated from moon and sun measurements. If the Jupiter data was corrected for this opacity, there would be no elevation gain changes in the Jupiter data below 40°. This is inconsistent with results from other observing sessions. The cause of this discrepancy is unknown, although changing atmospheric opacity or receiver gain during the time span of the observations could be partially responsible. The elevation efficiency is determined from the uncorrected Jupiter observations (B) using equation III-5. Observations of Saturn and Mars, obtained over the same elevation range, are consistent with this efficiency function.

In conclusion, the 1979-80 observations are difficult to calibrate as a result of the limited elevation range of the observations, but

indicate a peak efficiency at ~40° elevation. To determine the errors that may be introduced by a poorly determined elevation efficiency, the several elevation gain curves obtained from the different observing sessions were applied to the data for each session. It was found that for elevations below ~60°, the final calculated flux density values from all tests had a scatter comparable to the quoted errors (less than ±10%). Thus, even though the efficiency was not well determined, we have confidence that the flux density errors are realistic.

The third period in the development of the FCRAO antenna, 1980-81, occurred after the most recent panel setting (in which the author participated). The aperture efficiency at 86 GHz is 33% (this includes losses due to radome transmission and blockage, as well as losses in the quasi-optical system). The observations indicate no efficiency changes (±5%) within the elevation range ~15-70°. Few observations were made beyond this elevation range. The chopper wheel calibration procedure was employed to remove the effects of atmospheric opacity. Second order opacity corrections (Schloerb and Snell, 1980) were applied to the chopper wheel calibrated antenna temperatures.

No additional elevation dependent correction was necessary. There is some evidence for decreasing source strength at elevations above 65°. However the decrease in source strength with elevation is too rapid to be due solely to efficiency changes. The limited pointing information at high elevations is consistent with the observed decrease being due to

pointing errors. Consequently, observations above ~65° elevation were deleted from further analysis.

The fourth period of continuum measurments commenced in fall, 1981. The chopper wheel calibration procedure had been improved, removing the need to apply second order opacity corrections subsequent to the observations. Tests by other observers (e.g. Barvainis, 1981) confirm the accuracy of this improved calibration procedure.

Observations were conducted on 5 December 1981. Mechanical problems precluded the use of the chopper calibration. The observations were thus conducted under conditions similar similar to 1979-80. This did have the advantage of permitting a test of the antenna efficiency by a procedure different from those performed in 1980-81. Jupiter and 3C84 (up to 66° elevation) were observed at a range of elevations to determine the atmospheric opacity (figure 11d). The determined opacity (~0.25) is similar to values obtained by sky dips prior to the observing session. There is no evidence for a gain falloff at elevations up to 66°, confirming the results from 1980-81.

It is clear from the above discussions that a major source of error in flux density measurements can occur during the atmospheric opacity and elevation efficiency corrections. The early continuum measurements at FCRAO are more prone to calibration errors than the recent measurements which have relied upon improved calibration procedures. However, any gross calibration error due to these procedures would be evident during the final stage of calibration.

Antenna temperature to flux density conversion. The final stage in the calibration of source flux density is the calculation of the conversion factor (calibration constant) from corrected antenna temperature to flux density. If all the prior corrections to the source antenna temperature have been applied correctly, the calibration constant (equations II-1 and II-2) is a measure of system efficiency.

To determine the calibration constant, the ratio of the flux density to corrected antenna temperature is calculated from sources of known flux density. The major difficulty encountered in this procedure is determining the absolute flux density scale at millimeter wavelengths. The criteria for selection of calibration sources include source compactness, strength, non-variability, and known radio spectrum.

The small beamwidths of large millimeter antennae result in significant resolution of the planets and the primary low frequency sources DR21 and 3C274 (Dent, 1972). If the antenna beam shape is well-known, correction factors for the planets can be readily calculated (equation II-8). However, the commonly used source sizes for DR21 and 3C274 have been determined from observations made with larger beamwidths at lower frequencies. The uncertainty in the size correction factor thus is larger for observations obtained with small beamwidths. In order to better determine the size correction for the galactic HII region DR21, the region surrounding DR21 should be carefully mapped with the small beam of the FCRAO antenna.

At millimeter wavelengths, the strongest calibration sources are the planets (Venus, Mars, Jupiter, and Saturn) - with flux densities of hundreds to thousands of Jy, dependent upon the earth-planet separation. Both DR21 and 3C274 are much weaker, but with the current FCRAO system it is feasible to obtain good signal-to-noise measurements of these objects. Prior to summer, 1980, the system sensitivity was not adequate to use these two as calibration sources.

The flux density and brightness temperature of calibration sources at millimeter wavelengths has been investigated in detail (Ulich, Cogdell, and Davis, 1973; Ulich, 1974; Ulich, 1981; Ulich, Davis, Rhodes, and Hollis, 1981; Schloerb and Good, 1982) and will not be discussed in depth here. The following brightness temperatures have been adopted for the planets at frequencies between 85 and 115 GHz: Venus 360 K, Mars 200 K, Jupiter 180 K, and Saturn 150 K. These values are consistent with recent measurements in this frequency range (Ulich, 1981). It has been assumed that the planets have the same brightness temperature within the 30 GHz frequency interval, an assumption which is consistent with the results of Ulich (1981).

The flux density of DR21 has been assumed to be 16.90 Jy throughout the frequency interval 85 to 105 GHz. At millimeter wavelengths, thermal emission from dust grains contributes to the total flux density of DR21 (Righini et al, 1976). The falling thermal bremsstrahlung spectrum (equation II-10; Dent, 1972) and the rising dust spectrum produce a near

constant flux density in the frequency range of the 3 mm observations. An assumed value of 16.90 Jy agrees with the results of Ulich (1981) and the assumed value used for calibration of observations with the NRAO 36' antenna (Hobbs and Dent, 1977). The source 3C274 (Virgo A) has not been used as a calibration source at FCRAO due to its weakness (~7 Jy) compared with the other calibrators. The measured flux densities for 3C274 thus provide an independent check on the system calibration.

Several authors have reported variations in some of the calibration sources. DR21, a large HII region, should not exhibit short term variations, and can thus be used as the primary variability reference. Dent (1982) reports the possible variation of Jupiter during the past decade at 90 GHz, ranging between ~160 K and 205 K. However, during the epochs of the FCRAO observations, Dent's observations with the NRAO 36' antenna indicate a more limited range of ~175 to 195 K (this is discussed further in §4). Jupiter has been the major calibration source for the FCRAO observations, so variability of Jupiter will be difficult to detect from these measurements. The emission from Saturn has been reported to be variable at 3 mm (Epstein et al, 1980; Ulich, 1981) and at 9 mm (Dent, 1982). The variations are a function of the inclination of Saturn's rings as viewed from Earth. The FCRAO observations were obtained during low ring inclinations (only 1 measurement, 5 December 1981 at 11.6°, was outside the range of inclinations 1.4 to 7.4°) where no major variations have been reported. Schloerb and Good (1982) report that Venus may be the best calibration standard at milli-

meter wavelengths, since its brightness temperature can be determined from atmospheric models.

In the observations reported here, Jupiter and Saturn are used most frequently as the main calibration sources. Venus, DR21, and Mars are used less frequently. Using Jupiter and Saturn as flux density calibrators as well as for the efficiency and opacity calibration may result in apparent low errors in the calibration constant calculation. Ideally, separate sources should be used in each stage of calibration. Usually, a sufficient number of observations of several calibration sources were obtained, such that a valid measure of the calibration constant error could be determined.

The final calibration constant was calculated as the average of the calibration constant from all individual observations of calibration sources above elevation 15°. The error was determined from either the standard deviation of the entire set of measurements (if more than 9 individual observations) or from the peak-to-peak range in the (<9) individual observations. The corrected antenna temperatures were multiplied by the calibration constant to derive the flux density. The flux density error is the quadratic sum of the errors in the antenna temperature and the calibration constant.

As mentioned earlier, the calibration constant is a measure of the antenna aperture efficiency. Efficiency measurements of the FCRAO antenna have been fully documented by Schloerb and Snell (1980).

§4. Measured λ3 mm Flux Densities and Brightness Temperatures

Observations of extragalactic variable sources have been obtained on 24 dates between March 1979 and December 1981 with the FCRAO antenna at frequencies between 87 and 113 GHz. Observations have not been made at regular time intervals, and individual sources were not observed uniformly during this time period. Many of the observing sessions were scheduled primarily as system performance and development tests, with flux density measurments of variable sources constituting a fraction of the total observing time. Fortunately, these extensive calibration periods have provided valuable information on the antenna and receiver characteristics, as well as providing ample calibration for the various steps in the data reduction process.

The sources were selected for observation based upon strength and previous variability. Strong sources were initially selected due to lower sensitivity of the FCRAO system. As the system improved, it was posssible to include weaker sources in the schedule. Sources exhibiting rapid variations were selected since the frequent observations at FCRAO would provide information on the variability timescales and outburst evolution in these sources. The efforts were rewarded by the fortuitous observation of short term (few month) events in several sources, which were not evident in monitoring programs with longer intervals between observations. A discussion of these sources occurs in Chapter IV.

The 3 mm observing sessions are listed in Table 8 at the end of this chapter. Given are the dates and frequencies of observations,

calibration sources, measured or assumed atmospheric opacity, sources used for elevation efficiency calculations, calculated error in the calibration constant, and weather conditions.

The derived 3 mm flux densities are tabulated at the end of this chapter in Table 9. If more than one measurement was obtained for a source, an average flux density was calculated — with each measurement weighted by the reciprocal of its error. The average (S_{AVE}) and error (ΔS) were calculated by the formulae

and

$$S_{AVE} = \frac{\Sigma (S_i / \Delta S_i)}{\Sigma (1 / \Delta S_i)} \quad , \qquad \text{(III-6a)}$$

$$\Delta S = \frac{\sqrt{N}}{\Sigma (1 / \Delta S_i)} \qquad \text{(III-6b)}$$

where S_i and ΔS_i are individual flux density (or brightness temperature) and error for N measurements. If the calibration constant was determined by a single source, the source is not listed in Table 9. Inspection of the entries in Table 9 shows the steady improvement of the FCRAO continuum system.

Most measurements have been obtained at frequencies between 87.3 and 105.0 GHz (with a few measurements at 113 GHz). In comparing observations at different frequencies, it is necessary to correct for the source spectral index. If observations are conducted at two frequencies ν_1 and ν_2, the ratio of the flux densities, S_1 and S_2, are given by

$$S_1 / S_2 = (\nu_1 / \nu_2)^\alpha$$

<div align="right">(III-7)</div>

where α is the spectral index. The spectral index at millimeter wavelengths is not always known, since little higher frequency data is available for construction of a spectrum. Typically, however, active sources exhibit flat spectra ($-0.5 < \alpha < +0.5$) at longer wavelengths. Even for such a low spectral index, an 8% difference would exist between flux densities at 87 and 105 GHz. For the early epochs, this would be comparable to the measurement error, but this is not the case for recent observations. In the discussions on individual sources (Chapter IV), no correction is made for spectral index unless indicated.

Calculation of the (unweighted) average brightness temperatures for Venus (359.6 ±1.8 K), Jupiter (182.1 ±0.9 K), and Saturn (148.5 ±0.9 K) indicates that the FCRAO planetary brightness temperatures are in agreement with values obtained at other observatories (Ulich, 1981). The ratio of Saturn to Jupiter brightness temperature is 0.82, in agreement with the low inclination measurements in Ulich. There is no evidence for variation in this ratio.

The FCRAO measurements for the planets and DR21 are presented in figure 12, along with the results obtained by Dent, Hobbs, and Balonek with the NRAO 36' antenna (Dent, 1982). It is important to note again the the FCRAO measurements have used the planets Jupiter, Saturn, and occasionally Venus, as primary (constant) calibration osurces, whereas the measurements by Dent et al use DR21 as the primary standard. The
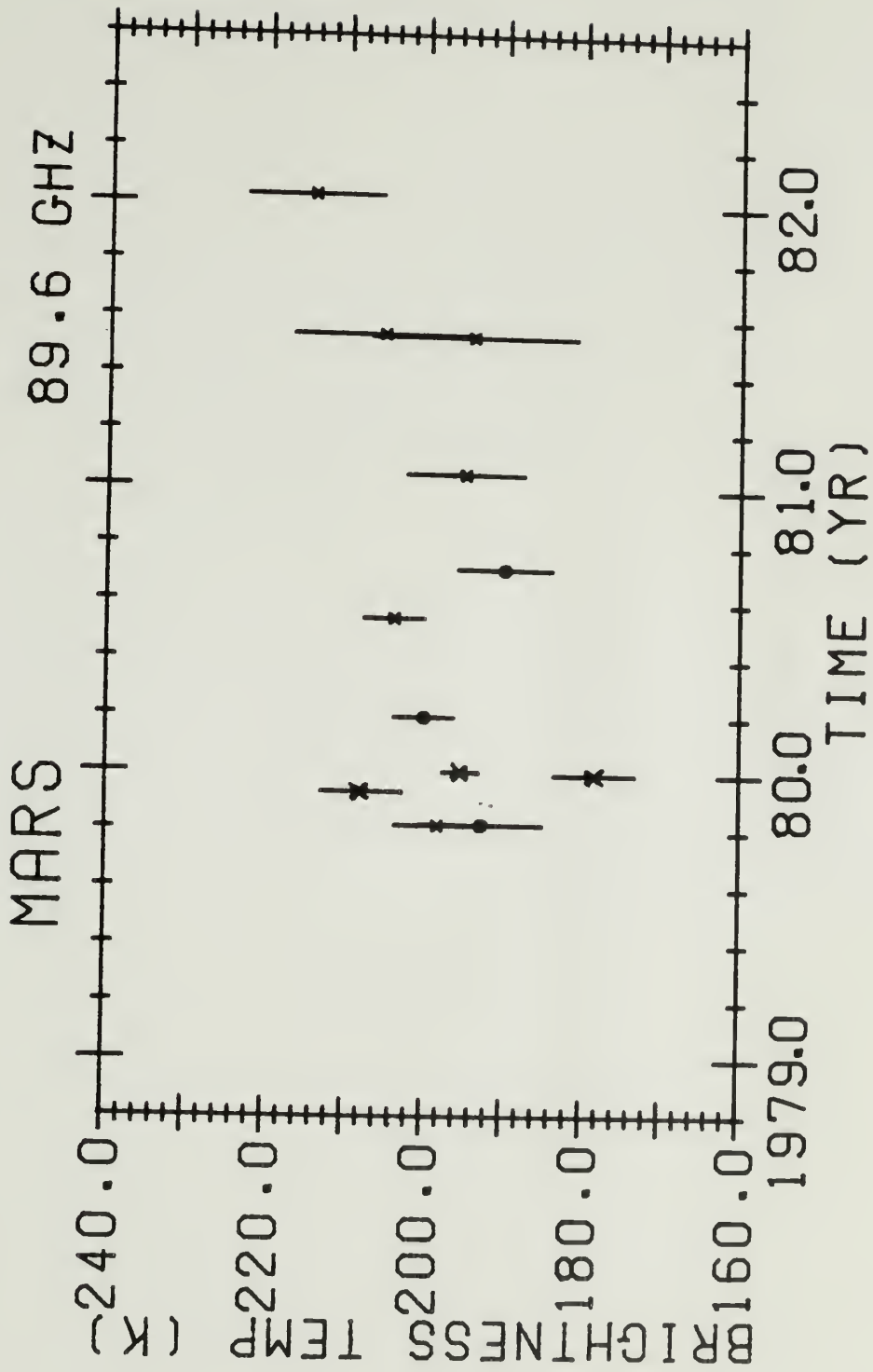
Figure 12. Brightness temperature measurements of the planets and flux density measurements for DR21. FCRAO measurements are indicated by large X's. NRAO measurements (Dent, 1982) by smaller symbols.
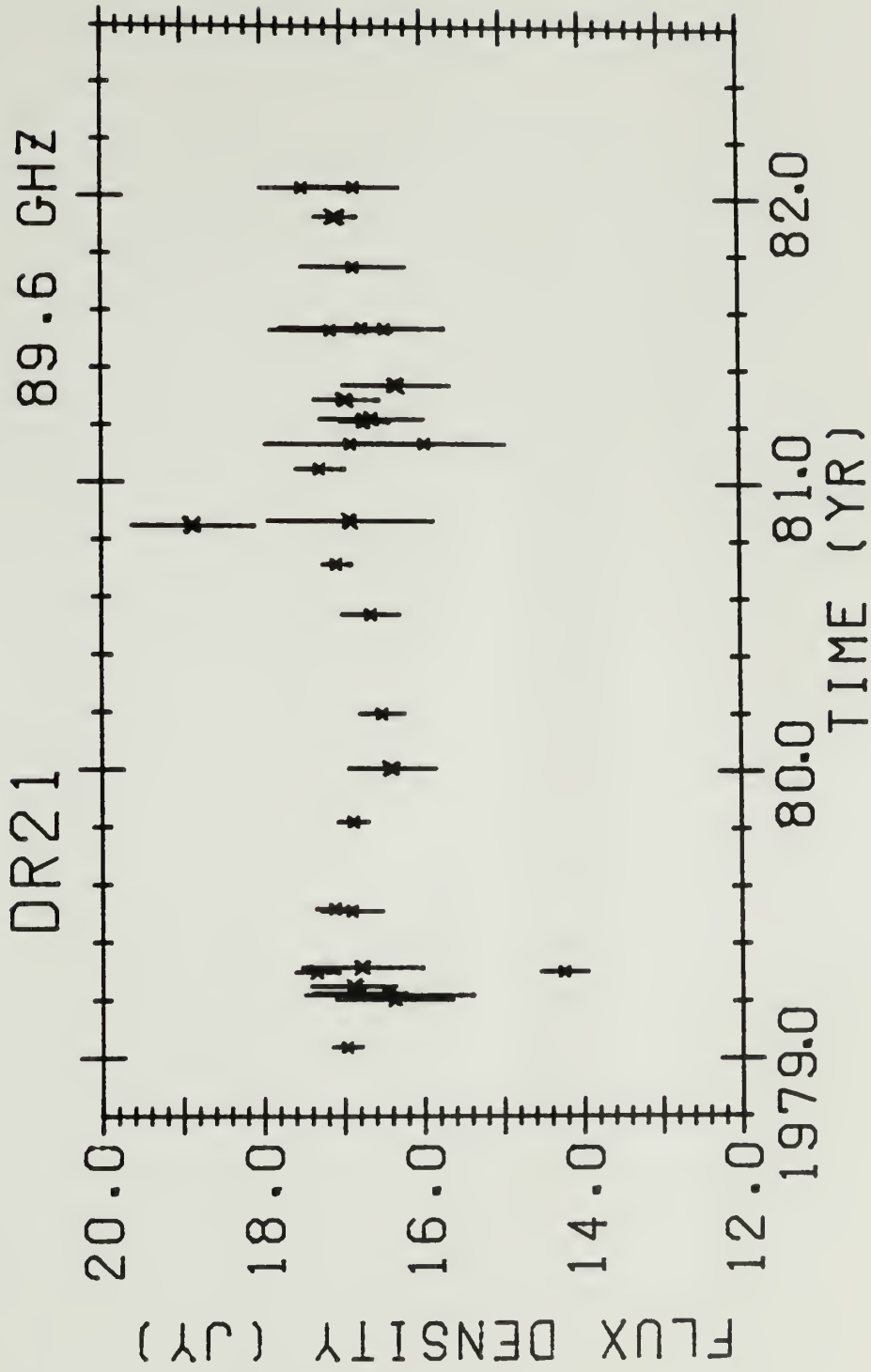
(a) Jupiter, (b) Saturn, (c) Venus, (d) Mars, and (e) DR21.

JUPITER   89.6 GHZ

MARS   89.6 GHZ
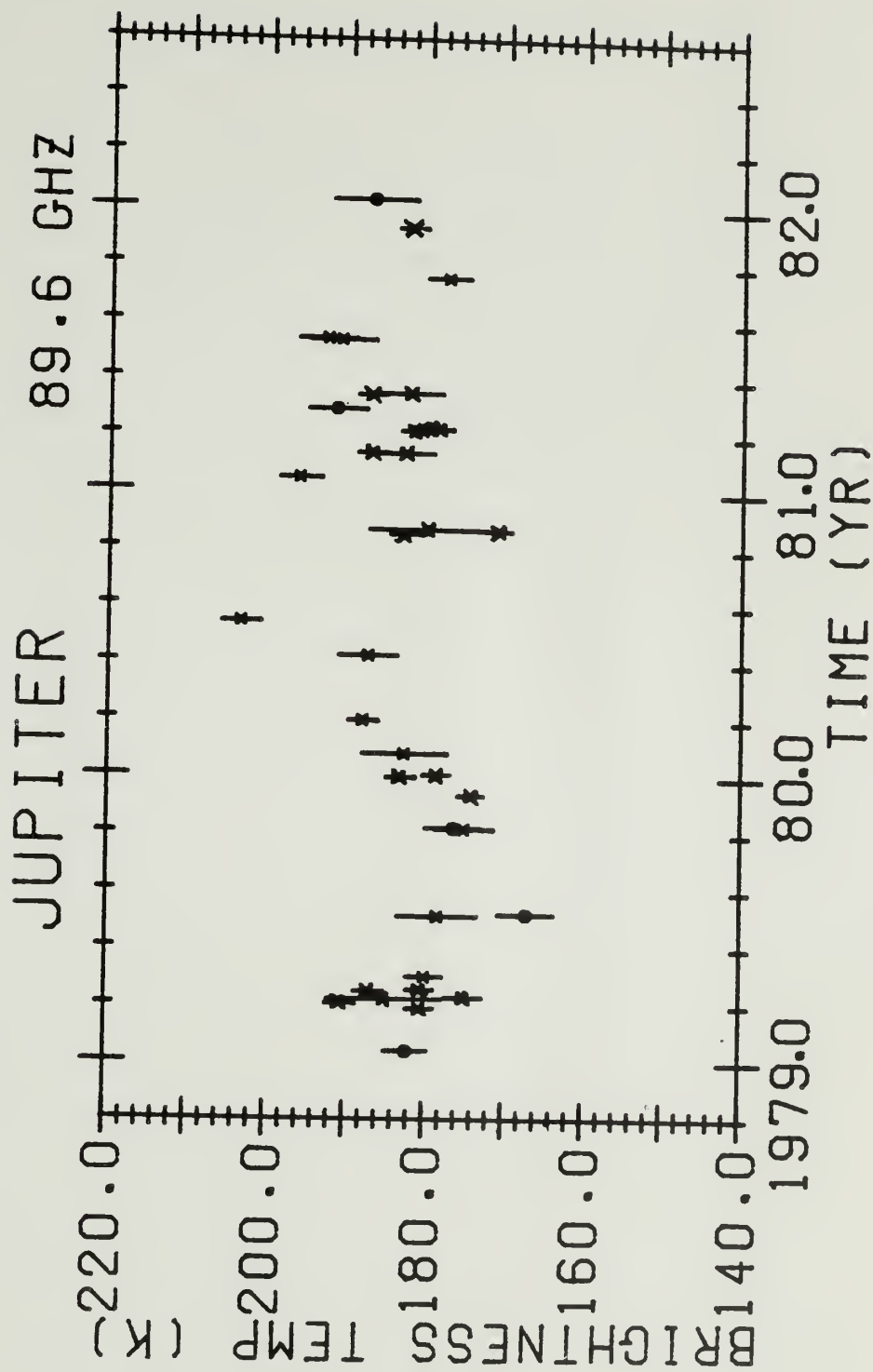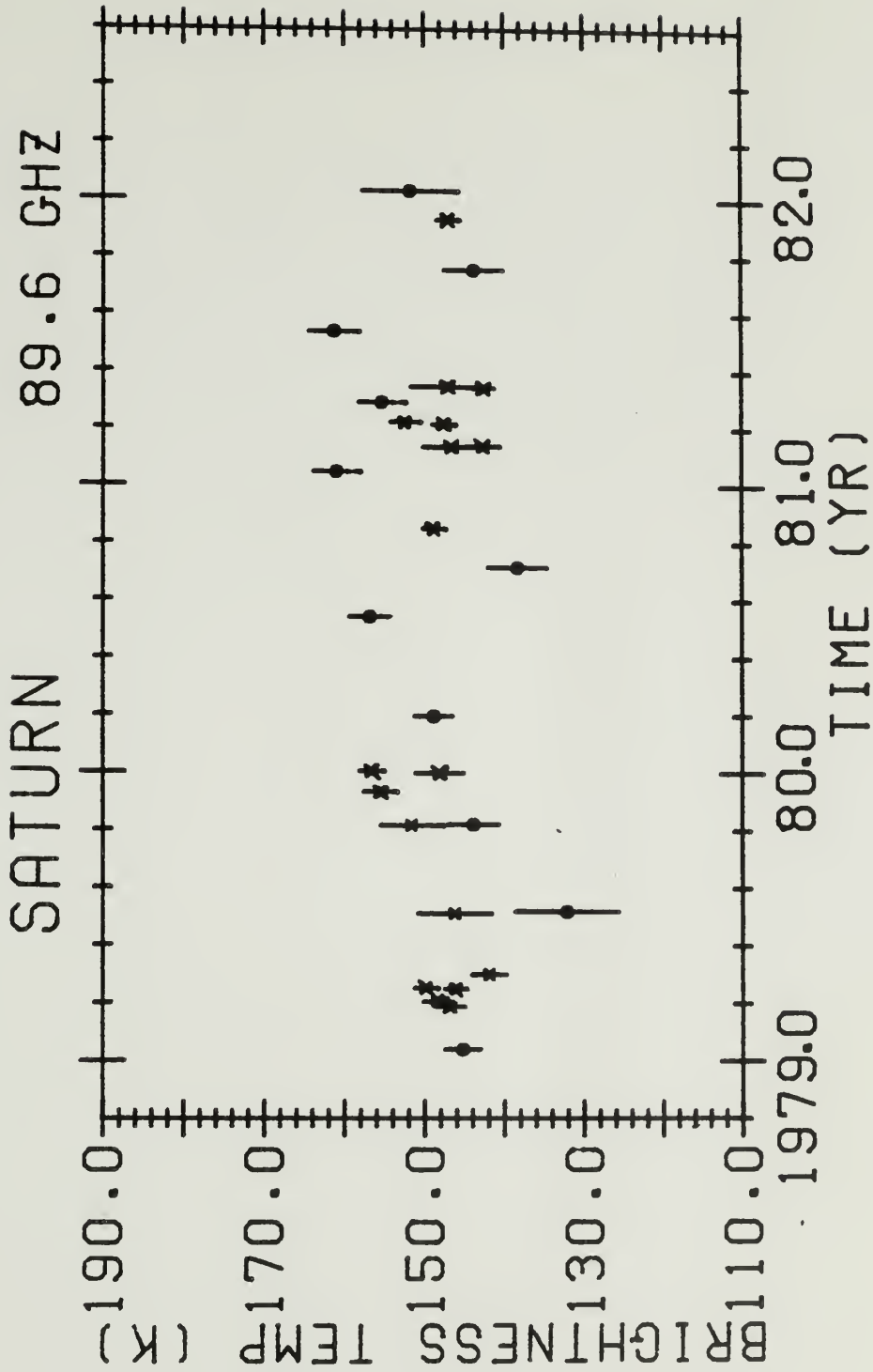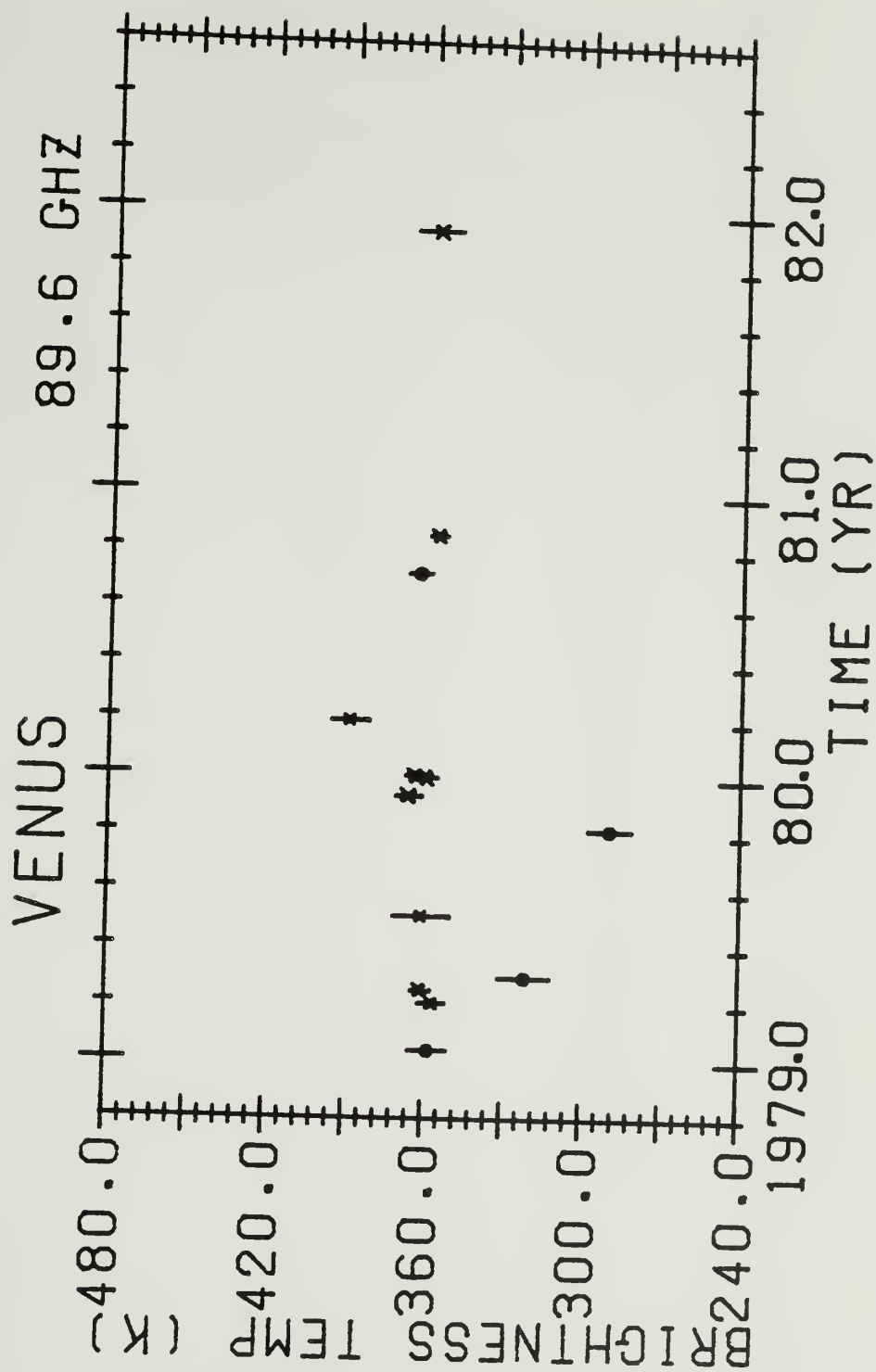
±~10% variation in Jupiter and Saturn since 1976 (and to a lesser extent Mars) seen in the NRAO data appear to follow the same trends in time. Two possible explanations can be invoked to explain the apparent correlated variations: (1) real variations in the planetary brightness temperatures are due to external causes (e.g. changing incident solar flux), or (2) errors exist in the flux density scale calibration for several observing sessions. This systematic variation must be investigated further in order to substantiate claims of planetary brightness temperature variations at 3mm.

The fluctuations in the FCRAO measurements reflect the slight difference between the observed and assumed planetary brightness temperature ratios, as well as calibration uncertainties within an observing session. Based upon the error in an individual epoch brightness temperature measurement (e.g. ~ 2.0 K for Saturn) and the observed scatter in the FCRAO measurements (e.g. RMS of 4.2 K for Saturn), there is no clear evidence for time variations in planetary brightness temperature ratios since 1979.

The results for DR21 (which was seldomly used as a calibration source) are presented in figure 12e. There is some suggestion from visual inspection of the figure that the FCRAO measurements are lower by ~2% compared with the NRAO measurements, though this difference is not statistically significant. The unweighted average flux density for DR21, 16.86 ±0.25 Jy, agrees with the assumed value at these frequen-

cies. This agreement confirms the accuracy of the FCRAO flux density scale (over a factor of 100 in intensity), which has been based upon the planets Jupiter, Saturn, and Venus.

§5. λ7 mm Observations – Flux Densities and Brightness Temperatures

Observations of extragalactic variable radio sources have been obtained on 11 dates between April 1979 and February 1980 with the FCRAO antenna at frequencies between 41.7 and 49.7 GHz (λ7 mm). The time coverage of the 7 mm observations was limited and the number of sources observed was small. However, even these limited observations provide valuable data on source millimeter spectra and reveal significant flux density changes in a few sources. In conjunction with the FCRAO results at 3 mm and NRAO 36' observations (Dent, Hobbs, and Balonek) at 3 and 9 mm, outburst activity can be seen in the 7 mm measurements. The 7 mm results are discussed in Chapter IV, along with the 3 mm FCRAO results.

The observing procedures at 7 mm are similar to those at 3 mm except for one major difference. The 7 mm receiver is not equiped with a beam chopper, so observations must be conducted in the total power mode. The lack of sky subtraction produces higher noise scans (about $3^{1/2}$ times theoretical) than beam switched observations. Despite the lack of a chopper, the relatively low receiver temperature of the uncooled mixer (~300 to 450 K, double side band) allowed for low signal-to-noise measurements in a reasonable amount of observing time. The sources were typically integrated until measurement errors of ~$^{1/2}$ to 1 Jy were obtained.

Since the observation and data reduction procedures are similar to those at 3 mm, they will not be discussed in detail. The temperature scale was set by comparison to the system response to cold and ambient loads. The IF signal was amplified and fed into a digital volt meter (DVM) which was sampled every 0.2 seconds. Five point and "on-off" observations were made, with the integration times being shorter (2 or 4 seconds) than at 3 mm due to the lack of a chopper. Sky fluctuations were readily visible in the raw data. As was seen at 3 mm, the pointing accuracy was less at high elevations (several observing sessions were in fact designated pointing performance tests). Atmospheric opacity was determined from sky dips or from observations of the moon or planets at multiple elevations. The sky dip and moon opacity measurements agree well. The observations took place during two panel setting periods (spring, 1979 and 1979-80). There is no unambiguous data showing elevation dependent efficiency at these frequencies (as expected due to the surface variations being $1/2$ the size in wavelengths as at 3 mm). Observations were not obtained at extreme elevations where efficiency effects would be clearly seen.

The flux density calibration sources were Jupiter (150 K), Saturn (135 K), Venus (420-437 K), and DR21 (17.3-17.7 Jy). Both Venus and DR21 have frequency dependent flux/brightness temperature, whereas Jupiter and Saturn are constant in this frequency ranges. The reduction program for the 7 mm data was the same as employed for the corresponding 3 mm data, but with little or no elevation efficiency applied to the observed temperatures.

The 7 mm observing sessions are listed in Table 10 (same format as Table 8), and the derived flux densities and brightness temperatures in Table 11. Individual sources are discussed in Chapter IV.

TABLE 8

FCRAO OBSERVING SESSIONS AT λ 3 mm

Date[1] m/ d/ y	Frequencies (GHz)[2] RF LO IF SB	Calibration Sources[3]	Comments[4]
03/09/79	113.9 113.9 1.4 DSB	Jupiter 180.0 K (9) Saturn 150.0 K (2)	τ_0=0.42 (moon); elgain (Jupiter); Calcon error 1.5%; overcast
03/15/79	87.6 87.6 1.4 DSB	Venus 360.0 K (1) DR 21 16.90 Jy(2)	τ_0=0.21 (Venus); Calcon error 4.9%; clear
03/16/79	87.6 87.6 1.4 DSB	Venus 360.0 K (2) Jupiter 180.0 K (3) Saturn 150.0 K (2)	τ_0=0.09 (moon); Elgain (Jupiter); Calcon error 2.0%; clear, some clouds
03/21/79	90.6 90.6 1.4 DSB	Jupiter 180.0 K (1) DR 21 16.90 Jy(1)	τ_0=0.20 (assumed); Calcon error 3.9%; overcast
03/23/79	90.6 90.6 1.4 DSB	Jupiter 180.0 K (1) DR 21 16.90 Jy(1)	τ_0=0.07 (assumed); Elgain Jupiter; Calcon error 1.5%; clear
03/31/79	96.6 96.6 1.4 DSB	Jupiter 180.0 K(15) Saturn 150.0 K (7)	τ_0=0.51 (Jupiter, Saturn); Calcon error 1.7%; Fog
04/01/79	96.6 96.6 1.4 DSB	Venus 360.0 K (4) Saturn 150.0 K (7)	τ_0=0.07 (assumed); Elgain Saturn; Calcon error 1.5%; clear
04/02/79	96.6 96.6 1.4 DSB	Jupiter 180.0 K (5) Saturn 150.0 K (7)	τ_0=0.49 (Jupiter, Saturn); Calcon error 2.4%; overcast

TABLE 8 (continued)

Date					Source	Flux		Notes
04/25/79	87.6	87.6	1.4	DSB	DR 21	16.90	Jy(2)	τ_0=0.49 (Saturn); Calcon error 4.7%; clear
12/06/79 part 1	89.6	89.6	1.4	DSB	Venus Jupiter Saturn	360.0 180.0 150.0	K (7) K (6) K (2)	τ_0=0.00 (assumed); Elgain 12/30/79; Calcon error 2.3%; high elev. not well calibrated; clear - overcast
12/06/79 part 2	89.6	89.6	1.4	DSB	Venus	360.0	K (6)	τ_0=0.00 (assumed); Elgain 12/30/79; Calcon error 4.9%; overcast - clear
12/07/79	90.0	90.0	1.4	DSB	Mars Jupiter Saturn	200.0 180.0 150.0	K (2) K (5) K (2)	τ_0=0.00 (assumed); Elgain 12/30/79; Calcon error 2.3%; after rain
12/30/79 part 1	87.6	87.6	1.4	DSB	Mars Jupiter Saturn	200.0 180.0 150.0	K (1) K (6) K (2)	τ_0=0.00 (assumed); Elgain Jupiter; Calcon error 2.5%; clear
12/30/79 part 2	87.6	87.6	1.4	DSB	Venus	360.0	K (4)	τ_0=0.00 (assumed); Elgain from part 1; Calcon error 2.9%; clear
01/02/80 part 1	87.6	87.6	1.4	DSB	Venus Mars Jupiter Saturn	360.0 200.0 180.0 150.0	K (3) K (5) K(17) K (9)	τ_0=0.00 (assumed); Elgain Jupiter; Calcon error 1.5%; High elevations not well calibrated; changing: clear - overcast - clear
01/02/80 part 2	87.6	87.6	1.4	DSB	Jupiter Saturn	180.0 150.0	K (3) K (2)	τ_0=0.00 (assumed); Elgain part 1; Calcon error 5.0%; overcast - clear

TABLE 8 (continued)

11/06/80 part 1	104.0 108.8 4.8 SSB	Venus 360.0 K(11) Jupiter 180.0 K(14) Saturn 150.0 K(11)	τ_o=0.18 (tip); Calcon error 1.5%; 1 beam; clear
11/06/80 part 2	113.5 108.8 4.8 SSB	Venus 360.0 K (4) Jupiter 180.0 K (4) Saturn 150.0 K (4)	τ_o=0.23 (assumed); Calcon error 1.5%; 1 beam; clear
11/06/80 part 3	104.0 108.8 4.8 SSB	Venus 360.0 K (3) Jupiter 180.0 K (4) Saturn 150.0 K (2)	τ_o=0.18 (tip); Calcon error 1.5%; 1 beam; clear
11/06/80 part 4	113.5 108.8 4.8 SSB	Venus 360.0 K (7) Jupiter 180.0 K (8) Saturn 150.0 K (7)	τ_o=0.23 (assumed); Calcon error 1.5%; 1 beam; clear
11/06/80 part 5	104.0 108.8 4.8 SSB	Jupiter 180.0 K (1) Saturn 150.0 K (1)	τ_o=0.19 (tip); Calcon error 3.4%; 1 beam; clear
11/06/80 part 6	104.0 108.8 4.8 SSB	DR 21 16.9 Jy (1) 3C 84 59.0 Jy (1)	τ_o=0.19 (tip); Calcon error 5.0%; 2 beams; clear
11/11/80	99.3 99.3 4.8 DSB	Jupiter 180.0 K (1)	τ_o=0.12 (tip); Calcon error 1.5%; snow flurries
11/12/80	99.3 99.3 4.8 DSB	DR 21 16.90 Jy(1)	τ_o=0.15 (assumed); Calcon error 4.4%; cloudy
11/12/80	91.0 91.0 4.8 DSB	Jupiter 180.0 K (1)	τ_o=0.15 (assumed); Calcon error 4.0%; cloudy-clear
02/18/81 part 1	86.3 91.0 4.8 SSB	Jupiter 180.0 K (2) Saturn 150.0 K (2)	τ_o=0.20 (assumed); Calcon error 3.5%; clear, dew
02/18/81 part 2	91.0 91.0 4.8 DSB	DR 21 16.90 Jy(1)	τ_o=0.18 (tip) Calcon error 4.5%; clear, warm
02/18/81 part 3	86.3 91.0 4.8 SSB	Jupiter 180.0 K (1)	τ_o=0.22 (tip); Calcon error 3.0%;

TABLE 8 (continued)

02/18/81 part 4	86.3	91.0	4.8	SSB	Jupiter	180.0 K (6)		τ_0=0.22 (assumed); Calcon error 2.0%; fog
					Saturn	150.0 K (6)		
03/19/81	104.2	104.2	4.8	DSB	Jupiter	180.0 K (9)		τ_0=0.12 (tip); Calcon error 1.5%; clear, cold
					Saturn	150.0 K (4)		
03/21/81	88.1	83.3	4.8	SSB	Jupiter	180.0 K (1)		τ_0=0.21 (assumed); Calcon error 1.5%; overcast; circular polariz.
03/22/81	88.1	83.3	4.8	SSB	Jupiter	180.0 K (4)		τ_0=0.17 (tip); Calcon error 2.0%; overcast; circular polariz.
					Saturn	150.0 K (3)		
05/04/81	105.0	105.0	4.8	DSB	Jupiter	180.0 K (7)		τ_0=0.15 (assumed); Calcon error 2.0%; clear
					Saturn	150.0 K (5)		
05/06/81	105.5	105.5	4.8	DSB	Jupiter	180.0 K (4)		τ_0=0.18 (assumed); Calcon error 4.5%; clear
					Saturn	150.0 K (2)		
05/07/81	105.5	105.5	4.8	DSB	Jupiter	180.0 K (1)		τ_0=0.00 (assumed); Calcon error 1.5%; clear
12/05/81 part 1	87.3	87.3	1.4	DSB	Jupiter	180.0 K (7)		τ_0=0.25 (Jupiter, 3C84); Calcon error 1.5%; orthogonal linear; cloudy
					Saturn	150.0 K (3)		
					DR 21	16.90 Jy(1)		
12/05/81 part 2	87.3	87.3	1.4	DSB	Venus	360.0 K (3)		τ_0=0.25 (assumed); Calcon error 4.3%; orthogonal linear; cloudy
					DR 21	16.90 Jy(2)		

Notes to Table 8

(1) Observing sessions which were separated into more than one part for calibration purposes are listed individually, although flux density measurements are averaged for a given date.

(2) DSB = Double sideband (RF = LO)
SSB = Single sideband (RF = LO + or - IF)

(3) Flux density scale calibration sources, assumed flux density or brightness temperature, and number of measurements used in calibration.

(4) Measured or assumed zenith atmospheric opacity (source of this determination); error in flux density scale calibration constant; polarization (linear polarization if not specified); sky conditions; general comments on quality of data.

TABLE 9

FCRAO Flux Density Measurements at λ 3 mm

Source	Date m/ d/ y	Flux (Jy or T_B)[1]	Error	N[2]	Frequency (GHz)	Comments[3]
0007+10	12/05/81	1.03	0.20	1	87.3	
0235+16	03/16/79	2.06	0.64	1	87.6	
	12/30/79	1.76	0.38	1	87.6	
	01/02/80	2.00	0.41	1	87.6	
	03/19/81	1.95	0.37	1	104.2	
	12/05/81	4.01	0.21	1	87.3	
3C 84	03/09/79	46.77	5.19	1	113.9	
	03/16/79	40.20	0.73	2	87.6	
	12/06/79	46.38	2.82	2	89.6	
	12/30/79	45.40	3.20	1	87.6	
	01/02/80	53.06	0.76	3	87.6	
	11/06/80	59.30	1.03	2	104.0	
	11/11/80	62.24	0.82	3	99.3	
	11/12/80	57.51	2.71	1	99.3	
	11/12/80	58.36	2.87	1	91.0	
	02/18/81	51.93	1.26	3	86.3	
	03/19/81	46.29	0.54	3	104.2	
	03/22/81	59.33	0.79	7	88.1	&03/21/81
	12/05/81	52.09	0.52	5	87.3	
NRAO 150	04/02/79	4.55	0.86	1	96.6	
	02/18/81	5.98	0.84	1	86.3	
	03/19/81	4.77	0.49	1	104.2	
	03/22/81	5.75	0.77	1	88.1	
	12/05/81	5.47	0.13	1	87.3	
0420−01	03/16/79	3.52	0.33	2	87.6	
	01/02/80	4.87	0.28	1	87.6	
	02/18/81	2.56	0.30	1	86.3	
	03/19/81	3.34	0.27	1	104.2	
	03/22/81	3.78	0.83	2	88.1	&03/21/81
	12/05/81	2.84	0.20	1	87.3	

TABLE 9 (continued)

3C 120	03/19/81	1.33	0.29	1	104.2	
	03/22/81	1.19	0.89	1	88.1	&03/21/81
	12/05/81	2.03	0.27	1	87.3	
0458−02	02/18/81	2.49	0.50	1	86.3	
	03/19/81	1.32	0.28	1	104.2	
	12/05/81	1.89	0.19	1	87.3	
0552+39	12/05/81	1.72	0.21	1	87.3	
0735+17	12/05/81	1.44	0.18	1	87.3	
0736+01	03/16/79	2.33	0.33	1	87.6	
	11/11/80	1.34	0.93	1	99.3	
	03/19/81	1.95	0.41	1	104.2	
	12/05/81	1.66	0.17	1	87.3	
OJ 287	03/16/79	2.22	0.36	1	87.6	
	12/06/79	2.96	0.53	1	89.6	
	01/02/80	4.34	0.41	1	87.6	
	03/19/81	3.79	0.27	1	104.2	
	05/04/81	5.16	0.56	1	105.0	
	12/05/81	6.82	0.17	1	87.3	
0953+25	12/05/81	1.17	0.18	1	87.3	
1055+01	12/05/81	1.67	0.19	1	87.3	
1127−14	12/05/81	0.65	0.15	1	87.3	
1156+295	12/05/81	2.91	0.27	1	87.3	
1219+28	12/05/81	1.57	0.21	1	87.3	

TABLE 9 (continued)

3C 273	03/09/79	11.32	1.21	1	113.9	
	03/16/79	15.18	0.36	2	87.6	
	03/23/79	14.69	0.50	1	90.6	
	03/31/79	15.21	1.07	1	96.6	
	04/01/79	14.27	0.97	1	96.6	
	04/02/79	14.56	0.72	1	96.6	
	12/06/79	18.10	0.86	2	89.6	
	12/07/79	16.31	0.72	1	90.0	
	12/30/79	20.13	0.87	1	87.6	
	01/02/80	20.39	0.42	4	87.6	
	02/18/81	26.83	0.71	4	86.3	
	03/19/81	24.53	0.44	2	104.2	
	03/22/81	26.78	0.36	6	88.1	&03/21/81
	05/04/81	27.20	0.64	2	105.0	
	05/06/81	26.23	0.76	2	105.5	&05/07/81
	12/05/81	19.57	0.35	1	87.3	
3C 274	03/09/79	6.89	2.32	1	113.9	
	03/16/79	9.66	0.49	1	87.6	
	12/07/79	7.40	0.88	1	90.0	
	01/02/80	9.15	0.69	1	87.6	
	03/19/81	6.88	0.40	1	104.2	
	03/21/81	8.93	1.10	1	88.1	
	05/04/81	8.02	0.52	1	105.0	
3C 279	03/16/79	6.75	0.53	1	87.6	
	12/07/79	6.03	0.75	1	90.0	
	01/02/80	5.14	0.37	2	87.6	
	03/19/81	6.64	0.42	1	104.2	
	03/21/81	7.57	0.54	2	88.1	&03/22/81
	05/04/81	6.24	0.60	1	105.0	
1335-12	03/16/79	4.75	0.46	1	87.6	
	03/21/79	5.73	0.82	1	90.6	
	03/31/79	4.34	1.49	1	96.6	
	04/02/79	6.66	1.07	1	96.6	
	12/06/79	5.87	0.40	1	89.6	
	12/07/79	5.97	0.80	1	90.0	
	12/30/79	4.17	0.72	1	87.6	
	01/02/80	6.24	0.43	1	87.6	
	03/19/81	2.69	0.36	1	104.2	
	03/22/81	5.16	0.80	1	88.1	

TABLE 9 (continued)

1413+13	03/19/81	4.49	0.30	1	104.2
	03/21/81	5.14	0.51	2	88.1
	05/04/81	2.69	0.50	1	105.0
	05/07/81	2.93	0.38	1	105.5
	12/05/81	2.22	0.22	1	87.3
1510-08	03/09/79	4.90	1.06	1	113.9
	03/16/79	3.04	0.31	1	87.6
	03/21/79	4.46	0.73	1	90.6
	03/23/79	3.23	0.46	1	90.6
	03/31/79	3.60	0.87	1	96.6
	04/01/79	5.08	1.23	1	96.6
	04/02/79	3.40	1.39	1	96.6
	04/25/79	2.44	0.36	1	87.6
	12/06/79	1.35	0.46	1	89.6
	01/02/80	2.89	0.36	2	87.6
	03/19/81	1.42	0.25	1	104.2
	12/05/81	1.39	0.16	1	87.3
3C 345	03/16/79	7.91	0.68	1	87.6
	04/01/79	6.13	0.44	1	96.6
	12/06/79	5.46	1.29	1	89.6
	01/02/80	6.90	0.34	1	87.6
	11/06/80	10.32	0.65	1	104.0
	02/18/81	11.41	1.17	1	91.0
	02/18/81	11.60	0.52	2	86.3
	03/22/81	11.55	0.49	2	88.1
	12/05/81	12.97	0.60	1	87.3
1642+69	12/05/81	0.72	0.14	1	87.3
1730-13	03/16/79	4.59	0.55	1	87.6
	03/23/79	4.85	0.62	1	90.6
	12/05/81	3.57	0.28	1	87.3
1749+09	12/05/81	1.93	0.24	1	87.3

TABLE 9 (continued)

1921−29	03/16/79	7.90	0.71	1	87.6
	03/23/79	5.12	0.81	1	90.6
	12/06/79	13.40	2.88	1	89.6
	12/30/79	12.90	1.00	1	87.6
	01/02/80	9.59	0.64	1	87.6
	11/06/80	4.67	1.57	1	104.0
	02/18/81	5.91	1.51	1	91.0
	02/18/81	3.35	0.82	1	86.3
	03/19/81	2.31	0.43	1	104.2
	12/05/81	5.25	0.34	1	87.3
2021+614	03/21/81	4.74	0.53	1	88.1
3C 418	03/15/79	1.65	0.40	1	87.6
	03/16/79	3.16	0.47	1	87.6
	03/23/79	2.91	0.34	1	90.6
	04/01/79	2.40	0.42	1	96.6
	04/25/79	2.29	0.29	1	87.6
DR 21	03/15/79	16.38	0.74	2	87.6
	03/21/79	16.45	1.05	1	90.6
	03/23/79	16.82	0.58	1	90.6
	03/31/79	17.39	1.65	1	96.6
	04/01/79	16.79	0.55	3	96.6
	01/02/80	16.39	0.55	3	87.6
	11/06/80	19.37	1.07	1	104.0
	02/18/81	15.97	1.02	1	86.3
	03/19/81	16.72	0.31	2	104.2
	03/22/81	16.63	0.66	1	88.1
	05/04/81	16.32	0.68	1	105.0
	12/05/81	17.08	0.26	4	87.3
2121+053	12/05/81	0.41	0.17	1	87.3
2131−021	12/05/81	1.72	0.22	1	87.3
BL Lac	11/12/80	5.28	0.71	1	99.3
	02/18/81	3.60	0.35	1	86.3
	03/19/81	3.91	0.34	2	104.2
	03/22/81	4.31	0.43	2	88.1
	12/05/81	3.22	0.18	1	87.3

TABLE 9 (continued)

3C 446	03/15/79	3.04	0.77	1	87.6
	03/16/79	3.57	0.52	1	87.6
	01/02/80	5.38	0.46	1	87.6
	12/05/81	5.12	0.24	1	87.3
CTA 102	03/15/79	3.12	0.36	1	87.6
	03/16/79	2.88	0.68	1	87.6
	04/01/79	2.49	0.76	1	96.6
	04/25/79	1.98	0.24	1	87.6
	12/05/81	2.00	0.16	1	87.3
3C 454.3	03/16/79	4.08	0.45	1	87.6
	11/12/80	6.80	0.70	1	99.3
	03/19/81	5.76	0.33	1	104.2
	03/22/81	8.41	1.47	1	88.1
	12/05/81	7.71	0.17	1	87.3
Venus	03/15/79	384.93	19.04	1	87.6
	03/16/79	351.17	5.22	2	87.6
	04/01/79	361.26	3.61	4	96.6
	12/06/79	366.93	4.90	14	89.6
	01/02/80	364.33	3.86	3	87.6
	11/06/80(1)	355.20	1.97	11	104.0
	11/06/80(2)	361.02	3.00	4	113.5
	11/06/80(3)	360.25	3.37	3	104.0
	11/06/80(4)	356.75	2.46	7	113.5
Mars	12/07/79	207.97	5.06	2	90.0
	12/30/79	178.43	5.20	1	87.6
	01/02/80	195.45	2.24	5	87.6

TABLE 9 (continued)

Jupiter	03/09/79	180.53	1.81	12	113.9
	03/16/79	190.58	1.91	11	87.6
	03/21/79	184.98	7.25	1	90.6
	03/23/79	175.01	2.48	2	90.6
	03/31/79	187.00	1.87	15	96.6
	04/02/79	180.50	1.80	8	96.6
	12/06/79	173.95	1.74	6	89.6
	12/07/79	174.79	1.86	5	90.0
	12/30/79	183.27	1.83	11	87.6
	01/02/80	178.70	1.79	27	87.6
	11/06/80(1)	183.20	0.76	14	104.0
	11/06/80(2)	181.75	1.46	4	113.5
	11/06/80(3)	181.34	1.49	4	104.0
	11/06/80(4)	183.72	1.07	8	113.5
	11/06/80(5)	184.41	6.54	1	104.0
	02/18/81(1)	182.86	3.67	3	86.3
	02/18/81(4)	187.16	1.87	8	86.3
	03/19/81	181.74	1.82	10	104.2
	03/22/81	178.72	1.79	5	88.1
	05/04/81	187.17	1.87	7	105.0
	05/06/81	182.31	4.17	4	105.5
	12/05/81	182.25	1.82	7	87.3
Saturn	03/09/79	146.29	2.05	2	113.9
	03/16/79	148.39	1.85	3	87.6
	03/31/79	140.82	1.46	7	96.6
	04/01/79	150.12	1.50	11	96.6
	04/02/79	149.85	1.50	7	96.6
	12/06/79	156.89	3.33	2	89.6
	12/07/79	154.48	2.77	2	90.0
	12/30/79	148.08	3.14	2	87.6
	01/02/80	156.67	1.57	16	87.6
	11/06/80(1)	149.13	0.93	11	104.0
	11/06/80(2)	148.18	1.47	4	113.5
	11/06/80(3)	147.60	2.27	2	104.0
	11/06/80(4)	149.32	1.34	7	113.5
	11/06/80(5)	146.51	5.91	1	104.0
	02/18/81(1)	146.53	3.68	2	86.3
	02/18/81(4)	142.57	2.23	6	86.3
	03/19/81	147.53	1.48	4	104.2
	03/22/81	152.37	1.91	3	88.1
	05/04/81	142.45	1.42	5	105.0
	05/06/81	146.92	4.80	2	105.5
	12/05/81	147.00	1.47	3	87.3

Notes to Table 9

(1) Flux density in Jy for extragalactic sources; Brightness temperature in K for planets (In observing sessions with calibration dependent upon only one planet, the measurement for that planet is not listed.)

(2) Number of flux density or brightness temperature measurements.

(3) For the sessions 03/21-22/81 and 05/06-07/81, the measurements have been averaged together.

TABLE 10

FCRAO OBSERVING SESSIONS AT λ 7 mm

Date[1] m/ d/ y	Frequencies (GHz)[2] RF	LO	IF	SB	Calibration Sources[3]			Comments[4]
04/04/79	44.5	44.5	1.4	DSB	Venus Jupiter DR 21	430.0 K 150.0 K 17.50 Jy	(2) (1) (1)	τ_0=0.13 (moon); Calcon error 1.7%; clear; good
04/06/79	49.7	49.7	1.4	DSB	Jupiter Saturn	150.0 K 135.0 K	(1) (2)	τ_0=0.30 (moon); Calcon error 5.0%; clear; scans noisy
04/11/79	47.6	47.6	1.4	DSB	Jupiter Saturn DR 21	150.0 K 135.0 K 17.34 Jy	(1) (2) (1)	τ_0=0.20 (moon); Calcon error 1.5%; clear; good
04/12/79	47.6	47.6	1.4	DSB	Jupiter Saturn DR 21	150.0 K 135.0 K 17.34 Jy	(2) (2) (1)	τ_0=0.22 (moon, Jupiter, Saturn); Calcon error 2.9%; haze-clouds; time-dependent Calcon?
09/28/79	41.7	41.7	1.4	DSB	Jupiter Saturn	150.0 K 135.0 K	(10) (1)	τ_0=0.12 or 0.06 with elev. gain (Jupiter, Saturn, 3C84); elevation gain fit to 3C84; Calcon error 1.5%; clear; good
10/31/79 part 1	47.6	47.6	1.4	DSB	Jupiter Saturn	150.0 K 135.0 K	(5) (3)	τ_0=0.33 (Jupiter); Calcon error 3.4%; clear; noisy
10/31/79 part 2	47.6	47.6	1.4	DSB	Jupiter Saturn DR 21	150.0 K 135.0 K 17.34 Jy	(1) (2) (1)	τ_0=0.22 (Jupiter); Calcon error 5.0%; clear; very noisy

TABLE 10 (continued)

Date					Source	Value	Notes
11/15/79	42.0	42.0	1.4	DSB	DR 21	17.64 Jy(1)	τ_0=0.13 (assumed);
					3C 84	48.50 Jy(2)	Calcon error 4.0%;
							overcast
11/22/79	41.7	41.7	1.4	DSB	Jupiter	150.0 K (9)	τ_0=0.17 or 0.06
					DR 21	17.66 Jy(1)	with elev. gain
							from 09/28/79
							(Jupiter);
							Calcon error 1.5%;
							Cloudy; total power
							fluctuations
12/07/79	47.6	47.6	1.4	DSB	Venus	420.0 K (5)	τ_0=0.14 (tip);
							Calcon error 5.0%;
							cloudy
12/15/79	42.0	42.0	1.4	DSB	Venus	437.0 K (5)	τ_0=0.14 (tips);
					DR 21	17.64 Jy(2)	Calcon error 4.1%;
							clear
02/13/80 part 1	41.7	41.7	1.4	DSB	Venus	437.0 K (4)	τ_0=0.11 (tips and
					Jupiter	150.0 K (12)	moon);
					Saturn	135.0 K (7)	Calcon error 1.5%;
							clear; good; high
							elevations low?
02/13/80 part 2	41.7	41.7	1.4	DSB	Venus	437.0 K (3)	τ_0=0.11 (assumed);
					DR 21	17.66 Jy(1)	Calcon error 1.5%;
							hazy; good

Notes to Table 10

(1) Observing sessions which were separated into more than one part for calibration purposes are listed individually, although flux density measurements are averaged for a given date.

(2) DSB = Double sideband.

(3) Flux density scale calibration sources, assumed flux density or brightness temperature, and number of measurements used in calibration.

(4) Measured or assumed zenith atmospheric opacity (source of this determination); error in flux density scale calibration constant; sky conditions; general comments on quality of data.

TABLE 11

FCRAO Flux Density Measurements at λ 7 mm

Source	Date m/ d/ y	Flux (Jy or T_B)[1]	Error	N[2]	Frequency (GHz)	Comments
0235+16	11/22/79	1.57	1.11	1	41.7	
	02/13/80	2.29	0.55	2	41.7	
3C 84	04/04/79	41.55	0.89	1	44.5	
	09/28/79	48.69	0.43	5	41.7	
	11/15/79	(48.64	1.67)	2	42.0	
	11/22/79	40.54	1.87	2	41.7	note 3
	12/15/79	47.46	1.45	3	42.0	
	02/13/80	47.08	0.85	3	41.7	
0420-01	09/28/79	5.24	1.46	1	41.7	
	02/13/80	5.29	0.68	2	41.7	
OJ 287	04/12/79	3.88	0.57	1	47.6	
	02/13/80	4.11	0.60	2	41.7	
3C 273	04/04/79	15.15	0.44	1	44.5	
	04/06/79	14.36	1.22	1	49.7	
	04/11/79	14.92	0.83	1	47.6	
	04/12/79	15.54	0.71	1	47.6	
	02/13/80	20.45	0.67	2	41.7	
3C 274	04/04/79	12.41	0.35	2	44.5	
	04/06/79	12.14	0.76	2	49.7	
	04/11/79	12.61	0.82	1	47.6	
	04/12/79	11.02	1.30	1	47.6	
	02/13/80	12.62	0.82	2	41.7	
3C 279	04/11/79	8.65	0.89	1	47.6	
	02/13/80	6.85	0.67	1	41.7	
1335-12	04/11/79	5.05	0.60	1	47.6	
	04/12/79	5.16	0.35	1	47.6	
	10/31/79	6.64	1.28	2	47.6	
	02/13/80	5.16	0.71	1	41.7	

TABLE 11 (continued)

1510-08	04/04/79	4.39	0.30	1	44.5
	04/11/79	3.90	0.53	1	47.6
	04/12/79	3.51	0.38	1	47.6
	09/28/79	2.51	0.28	1	41.7
	02/13/80	4.01	0.68	1	41.7
3C 345	04/12/79	8.21	0.43	1	47.6
	09/28/79	8.61	0.59	1	41.7
	11/15/79	12.51	1.83	1	42.0
	02/13/80	9.00	0.64	1	41.7
1921-29	11/15/79	22.14	2.02	1	42.0
	12/07/79	22.13	3.60	1	47.6
	12/15/79	20.50	1.60	1	42.0
	02/13/80	11.99	0.61	1	41.7
3C 418	04/04/79	4.55	0.41	1	44.5
	04/11/79	2.82	0.47	1	47.6
DR 21	04/04/79	17.58	0.62	1	44.5
	04/11/79	17.46	0.74	1	47.6
	04/12/79	16.31	0.72	1	47.6
	10/31/79	15.99	2.32	1	47.6
	11/22/79	17.80	0.84	1	41.7
	12/15/79	16.28	1.04	2	42.0
	02/13/80	17.99	0.90	1	41.7
2121+053	02/13/80	2.63	0.99	1	41.7
BL Lac	02/13/80	3.39	0.83	1	41.7
Venus	04/04/79	422.63	5.75	2	44.5
	02/13/80	423.20	7.46	4	41.7
Mars	02/13/80	168.73	7.17	3	41.7

TABLE 11 (continued)

Jupiter	04/04/79	152.33	1.91	2	44.5
	04/06/79	(139.14	5.06)	2	49.7
	04/11/79	150.50	3.47	1	47.6
	04/12/79	149.76	2.70	3	47.6
	09/28/79	151.89	0.82	12	41.7
	10/31/79	155.03	2.71	5	47.6
	"	157.70	5.00	3	47.6
	02/13/80	154.02	1.53	13	41.7
Saturn	04/06/79	(142.98	5.72)	2	49.7
	04/11/79	133.61	1.99	3	47.6
	04/12/79	135.93	3.52	3	47.6
	09/28/79	131.11	2.33	4	41.7
	10/31/79	130.48	4.68	3	47.6
	"	140.95	7.34	3	47.6
	02/13/80	133.21	2.91	7	41.7

Notes to Table 11

(1) Flux density in Jy for extragalactic sources; Brightness temperature in K for planets (In observing sessions with calibration dependent upon only one planet, the measurement for that planet is not listed.)

(2) Number of flux density or brightness temperature measurements.

(3) Observed at high elevation. Flux density may be low due to calibration scale errors at high elevations.

C H A P T E R   IV

VARIATIONS AT $\lambda 3$ mm and $\lambda 7$ mm: EVIDENCE FOR RAPID VARIABILITY

§1. Introduction

As discussed in Chapter III, millimeter observations of variable extragalactic radio sources are important in studying the evolution of outbursts which are affected at longer wavelengths by opacity effects and expansion processes. Variations at millimeter wavelengths permit us to probe the physical conditions in the energetic radio core – possibly the same region responsible for the optical and infrared emission.

The observations at 3 and 7 mm obtained with the FCRAO antenna, presented in Chapter III, indicate several instances of rapid variations not seen at longer wavelengths. Combined with the 3 mm results (Chapter II) of Dent, Hobbs, and Balonek obtained with the NRAO 36' antenna (and a few measurements by other investigators obtained with the same instrument), it is possible to follow the millimeter variations in several sources with unprecedented (~monthly) time resolution. This is the first high sensitivity study of short term millimeter variability (Epstein et al 1982 observed five sources over a nine year period, but with sensitivity too low to be of value for the study of short term variations). To study the spectral evolution of these events, the measurements obtained at lower frequencies (Chapter II) are used.

Selected sources whose evolution is defined by the FCRAO millimeter observations are discussed in §2. The discussions are limited to the

general variability characteristics of rapid outbursts. In many instances, the spectral evolution presented is the most extensive discussion to date. The discussions are limited to the time period of the FCRAO observations, with more detailed analyses of individual sources to appear in subsequent papers. Despite the limited time coverage and small source sample of the FCRAO observations, numerous instances of rapid variations were observed. Previous observations at millimeter wavelengths (obtained roughly quarterly) were insensitive to the short timescale (monthly) variations reported in §2.

Unless otherwise indicated, the term "millimeter wavelengths" in §2 is understood to refer to 31 and 90 GHz, while "centimeter wavelengths" refers to frequencies at or below 15 GHz.

§2. Variations in Nine Sources

3C84. FCRAO 3 mm measurements clearly delineate rapid variations during a two year period of activity in the Seyfert galaxy, NGC 1275. A large amplitude (~35 Jy) outburst (figure 13a) occurred at 3 mm in 1980 and was much weaker at lower frequencies (<10 Jy at 31.4 GHz). This outburst exhibited considerable structure at 3 mm during the two years following the maximum.

The variations prior to the 1980 outburst are discussed by O'Dea, Dent, and Balonek (1982). A small outburst (~10 Jy) beginning in 1978 followed four years of only minor flux variations around a level of 30

Figure 13. 3C84.

(a) Flux density variations in 3C84 at 90 GHz. Large X's are FCRAO measurements. NRAO measurements from Howard (1982); Puschell and Heeschen (1982); Epstein, Landau, and Rather (1980); Owen et al (1978); Owen, Spangler, and Cotton (1980); Owen and Puschell (1982); and Chapter II.

(b) Radio spectra of 3C84 during the large millimeter outburst of 1980-81. Data from Chapters II and III. 1978.0: end of period of millimeter inactivity; 1979.8: maximum of slow millimeter and centimeter outburst; 1980.2: maximum of large millimeter outburst; 1982.0: during decay of large millimeter outburst.
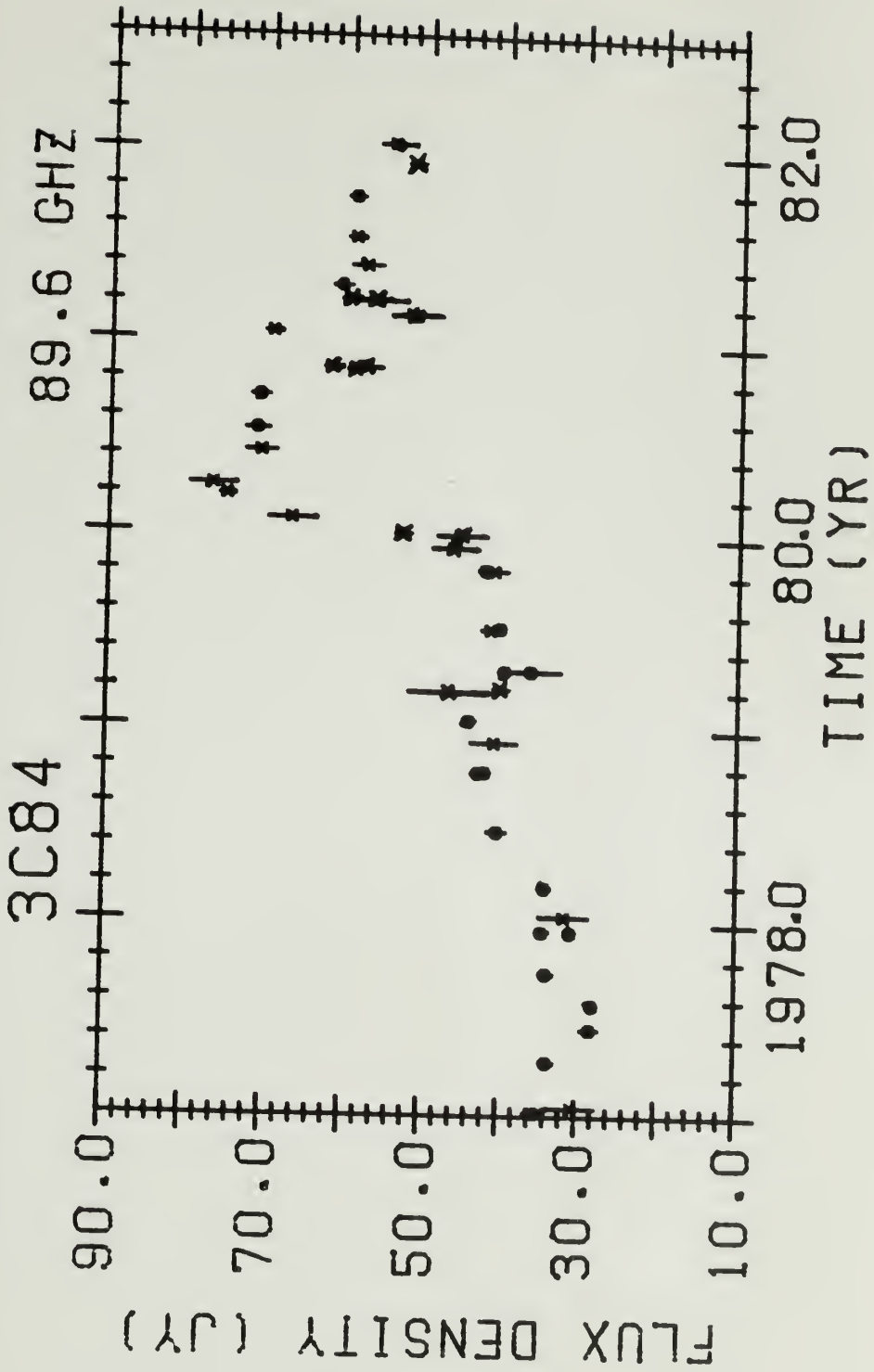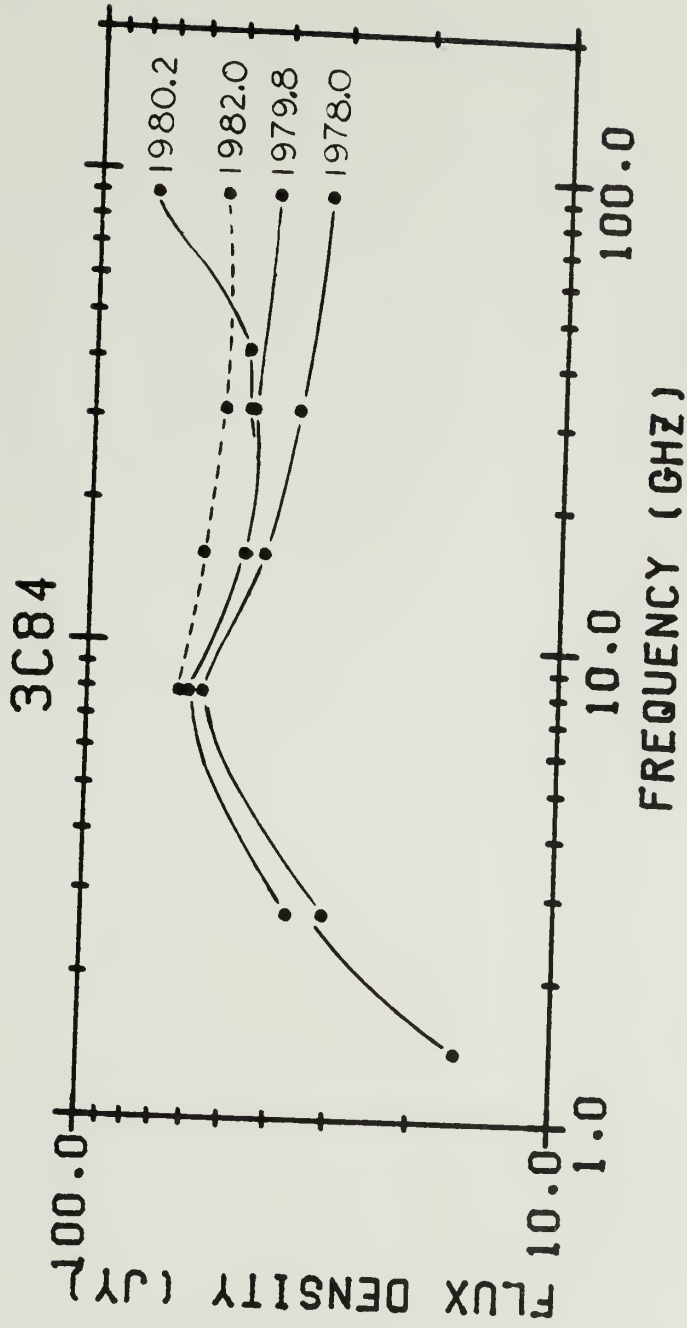
Jy. This outburst had leveled off at ~40 Jy by late 1979, when the flux density increased dramatically – rising from 42 Jy on 26 October 1979, to 46 (±3) Jy on 6 December, 52 Jy on 1 January 1980, and increasing dramatically to 67 Jy on 29 January (a rate of 1/2 Jy per day), peaking at 75 Jy in March.

In late 1980 and early 1981, the outburst showed considerable fluctuations which were undersampled. FCRAO measurements in November 1980 at three frequencies between 91 and 104 GHz reveal a drop of 10 Jy from 71 Jy in September 1980. Schloerb and Good (1982) measured a similar 3 mm flux density of ~60 Jy at Hat Creek in mid December 1980, using 3C273 and 3C345 NRAO flux densities from January 1981 as calibration standards. By mid January 1981 the flux density had returned to 70 Jy, followed by another drop (to 52 Jy) in mid February, then rising to only ~60 Jy by late March.

Between early 1980 and 1981.0, the flux density at 31.4 GHz slowly increased from 45 Jy to 53 Jy. The flux density remained constant during the subsequent year. The total flux density spectral evolution is shown in figure 13b. It is evident that the activity is limited to high frequencies and does not contribute significantly to the flux density at centimeter wavelengths. This is the only period (1980–81) in the last one and a half decades during which the radio spectrum has exhibited a millimeter excess. By 1982, the outburst had decayed at millimeter wavelengths, such that the millimeter spectrum had flattened,

approaching its pre-outburst index of $\alpha \sim -0.2$. Dent et al (1982) discuss the details of this outburst in more detail.

There might be concern that the drops in flux density in late 1980 and early 1981 are due to calibration errors in the FCRAO measurements. The FCRAO measurements which define these drops are separated by about one month from the NRAO measurements, so there is no blatant discrepancy. The ~20 to 30% errors required to account for the possible discrepancy with the NRAO measurements are not consistent with observations of other strong sources (e.g. 3C273, DR21). Additionally, a single measurement by Howard (1982) in March 1981 agrees with FCRAO measurements made a few day later, and the value of Schloerb and Good (1982) is consistent with the drop observed in late 1980.

Historically, 3C84 has exhibited other instances of rapid variations. Epstein et al (1982) observed a 10 Jy rise at 3 mm within a month in early 1973, followed by two months of constant flux density, and then an equally rapid drop to pre-outburst level. Similar behavior ($\Delta S \sim 4$ Jy) was seen at 15.5 GHz during this time.

It is not possible to distinguish whether the observed 3 mm variations in 1980-1 are the result of multiple separated outbursts or sharp temporary drops ("quenchings") within a single outburst. Epstein et al (1982) discuss quenchings observed in other sources, and the implications for source models. These drops are much sharper than predicted by existing models, and may be indications of source rotation or eclipsing/obscuration phenomena.

The 1980-81 outburst observed at 3 mm is the most dramatic event which has been observed at millimter wavelengths in 3C84. This recent activity also contrasts with the slower trends at centimeter wavelengths (O'Dea, Dent, and Balonek 1982). Millimeter VLBI observations during this time should have readily detected this component, since the timescale of variability implies a physical source size of order one light month. By 1982, however, this component had weakened and presumably expanded, decreasing the possibility of detection. No structural VLBI component from this event is expected at centimeter wavelengths due to the lack of appreciable centimeter emission associated with this outburst.

1413+13. This quasar, embedded in a galaxy, exhibits many characteristics typical of BL Lacertae type quasi-stellar objects (e.g. a steep optical-infrared continuum spectrum (Rieke, Leboksky, and Kinman 1981) and rapid variability). Its radio-infrared-optical characteristics have been discussed in detail by Beichman et al (1981a and b) and Bregman et al (1981). These studies found that the energy spectrum is that of a red BL Lacertae object, with 90% of its luminosity emitted in the range 0.35 μm to 1 mm. The spectrum steepens sharply at wavelengths shorter than 5 μm, suggesting a high energy cutoff in the electron distribution. The radio spectrum between 4.8 and 14.5 GHz was found to be inverted (stronger at higher frequencies), with simultaneous outbursts at 8 and 15 GHz having timescales of a few months. Based upon the 20 cm measurement (1.13 Jy) of Perley (1982) and 4.8 GHz value of

1.3 Jy (Bregman et al 1981) in mid February 1981, the spectrum clearly
flattens at low frequency.

The limited observations reported in Chapters II and III began in
early 1981. The 3 mm observations (figure 14a) from FCRAO and NRAO,
though undersampled, reveal rapid, large amplitude variations. The 2 Jy
drop between 20 March and 6 May 1981 occurs during a maximum at 4.8,
8.0, and 14.5 GHz (Bregman et al 1981) which exhibits only small
centimeter wavelength fluctuations ($\Delta S < 0.2$ Jy). Following a minimum in
July/August 1981 at centimeter wavelengths, a maximum was reaching in
October, at which time another rapid decay ($\Delta S = 2$ Jy in 3 months) com-
menced at millimeter wavelengths.

During the decay of <u>both</u> outbursts in 1981, the spectral peak moved
from 90 to 15 GHz (figures 14b and c), with α (15, 90) steepening from
+0.2 to −0.25 in the first outburst. The spectrum has always been
inverted between 8 and 15 GHz, even during decay stages in the evolution
of an outburst (Bregman et al 1981, and Chapter II). The radio spectra
are typical of millimeter excess outbursts, showing steepening milli-
meter spectra during the outburst decay, and a progression to lower fre-
quency (but never below ~10 GHz) of the flux density maximum. Clearly,
monthly (or more frequent) observations at centimeter and millimeter
wavelengths are necessary to understand the evolution of outbursts in
1413+13 and their relationship to the infrared and optical spectrum and
variability.

168

Figure 14.   1413+13.

(a) Flux density variation in 1413+13 at 90 GHz.   Large X's are FCRAO measurements.   NRAO measurements from Chapter II.

(b) Radio spectra of 1413+13 during the outburst in early 1981, showing the rapid decay at millimeter wavelengths during a period of constant centimeter emission.   15 November 1980 at centimeter flux density minimum; 20 March thru 6 April 1981 at maximum (constant) flux density at centimeter wavelengths but during the rapid decay at 3 mm.   Data from Perley (1982);   Bregman et al (1981);   Beichman et al (1981b);   and Chapter II.

(c) Radio spectra of 1413+13 during the outburst in late 1981. Data from Chapters II and III.
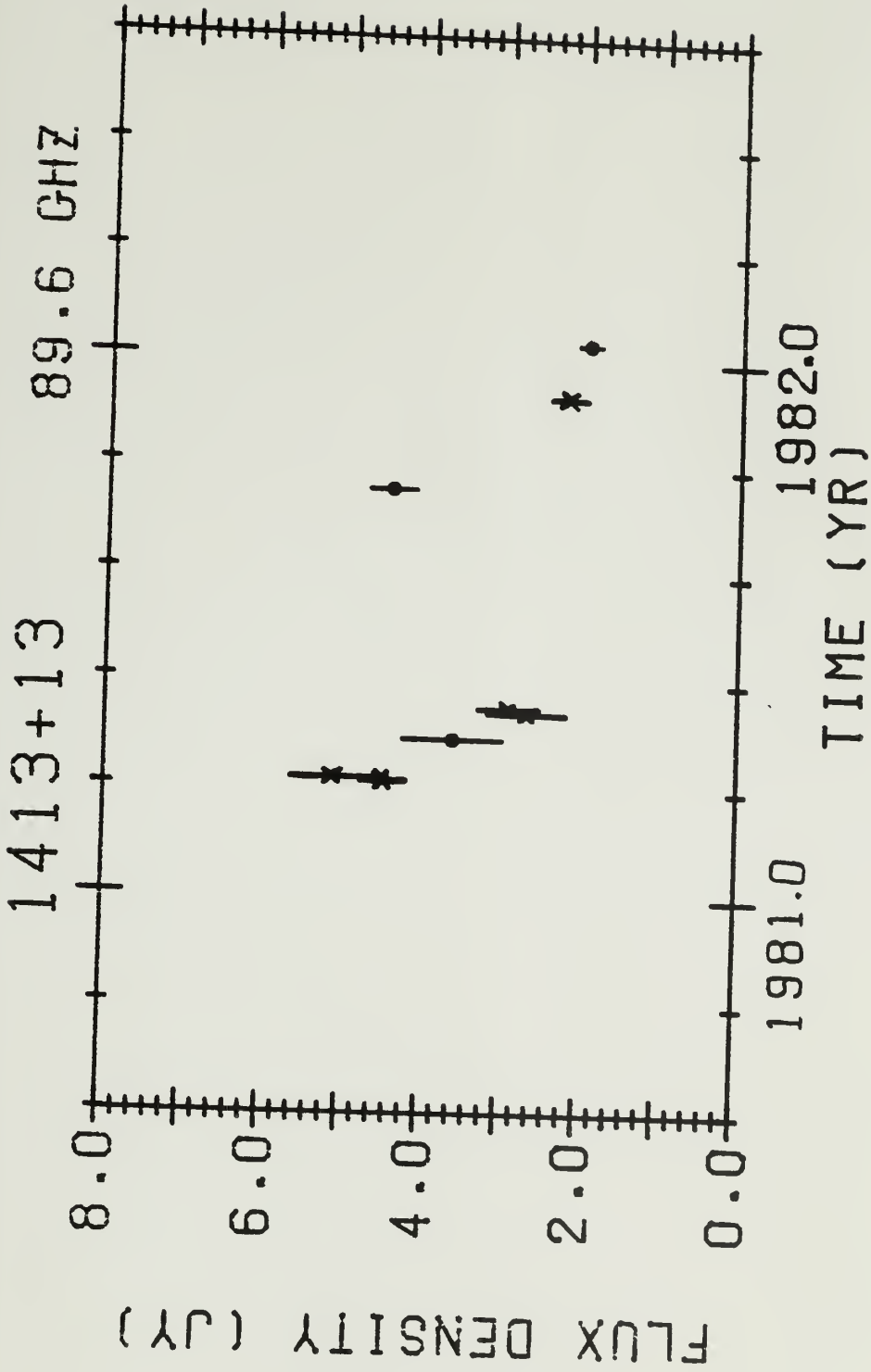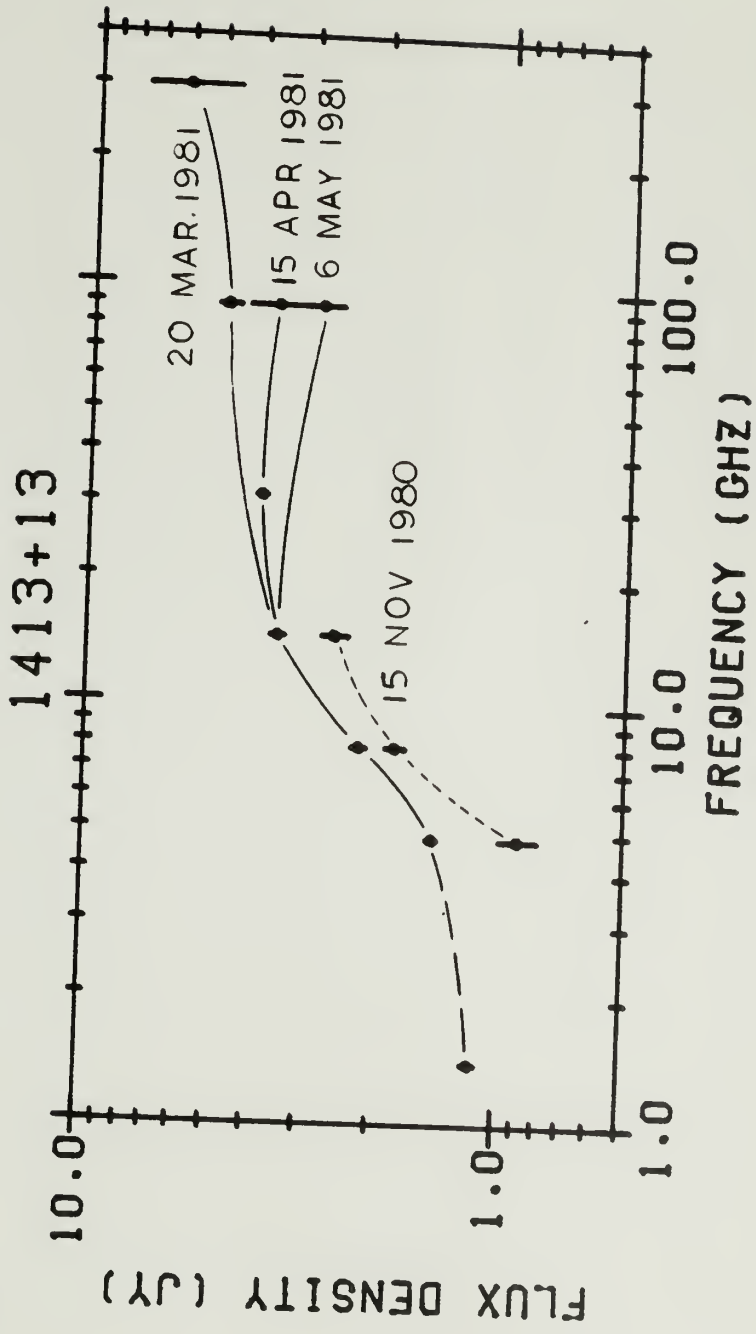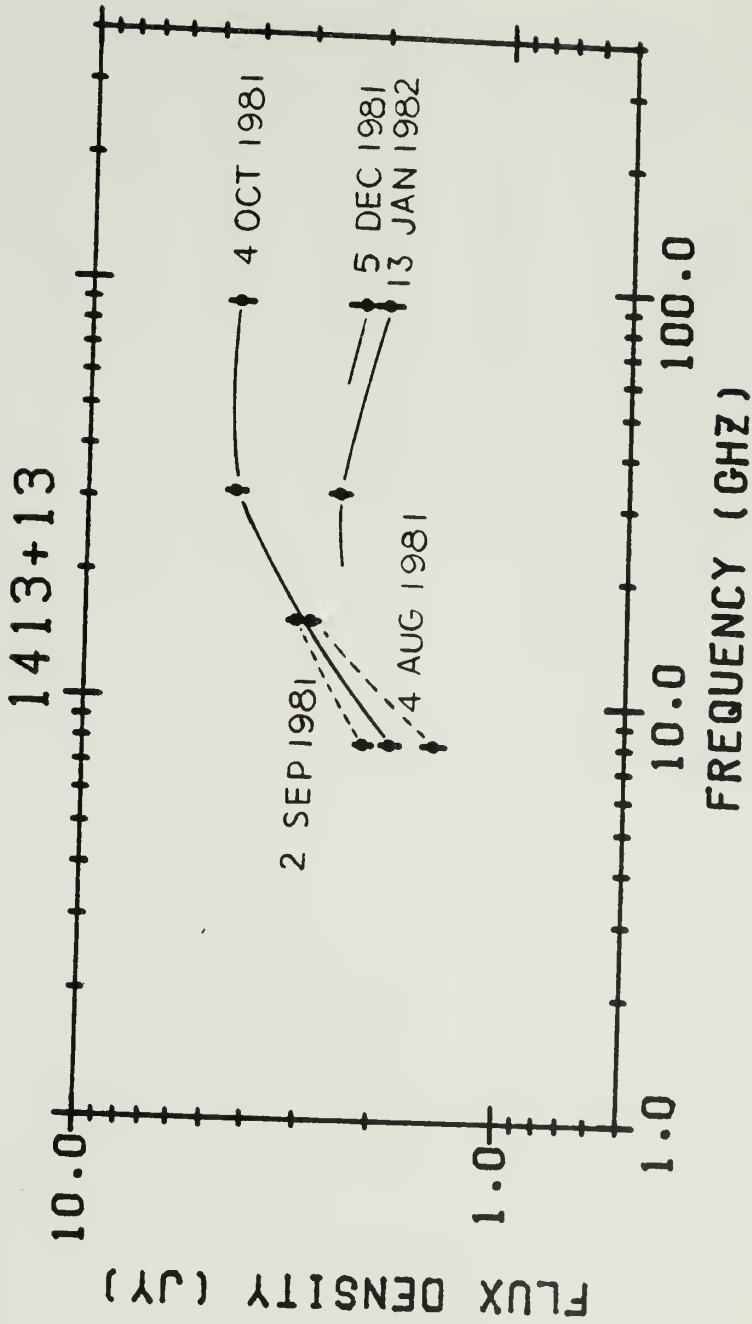
Figure 15. 1510-08.

(a) Flux density variation in 1510-08 at 90 GHz. Large X's are FCRAO measurements. The crucial 27 November 1978 measurement is from Jones et al (1981). Other NRAO measurements from Epstein, Landau, and Rather (1980), and Chapter II.

(b) Radio spectra of 1510-08 during the large outburst in 1979. Measurements from Aller, Aller, and Hodge (1982) at 4.8 GHz, and from Chapter II.

(c) Radio spectra of 1510-08 during the large outburst in 1979 with the spectra immediately preceding the outburst subtracted from the total flux density.

1510-08   89.6 GHZ

FLUX DENSITY (JY)

TIME (YR)
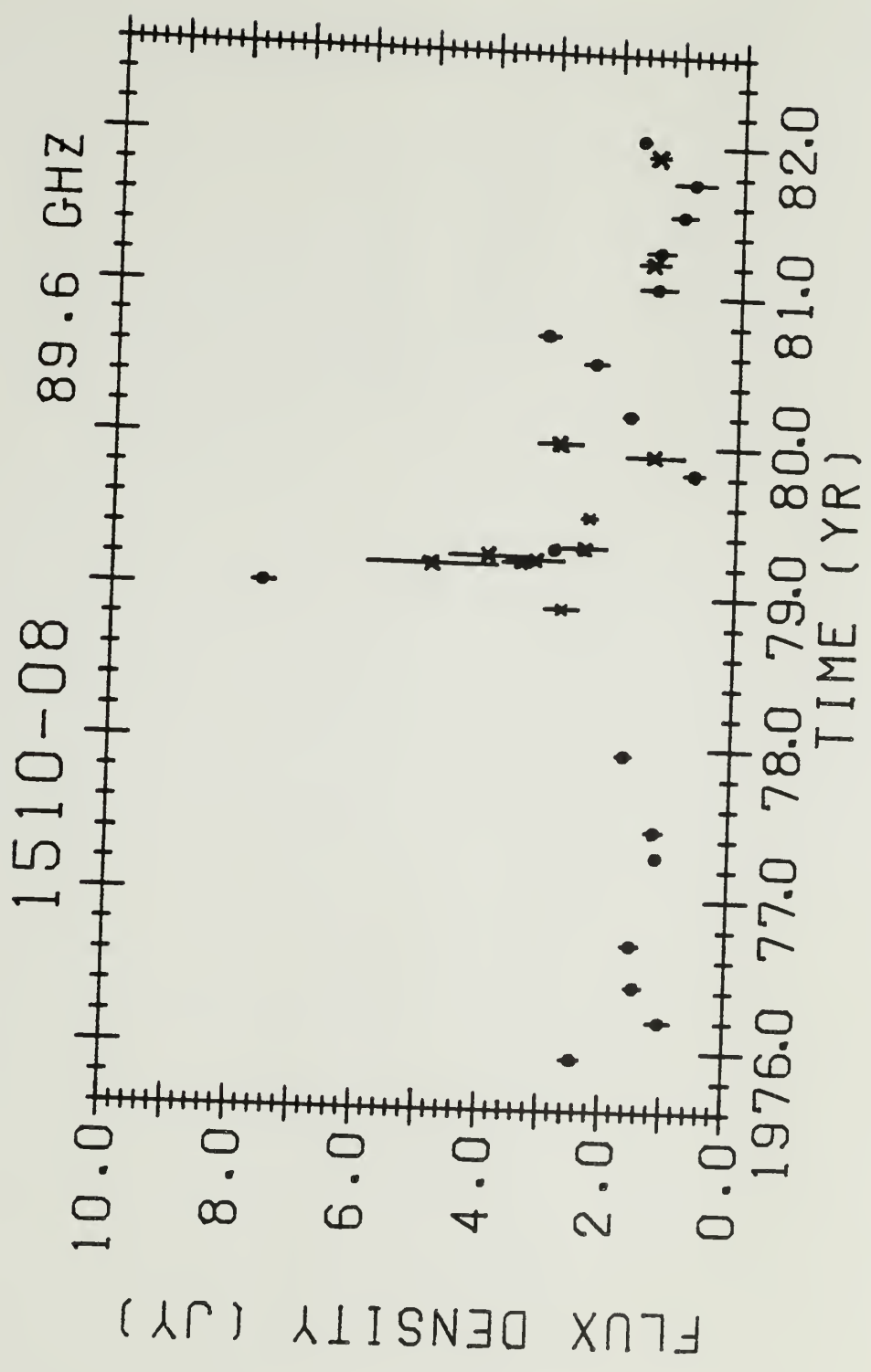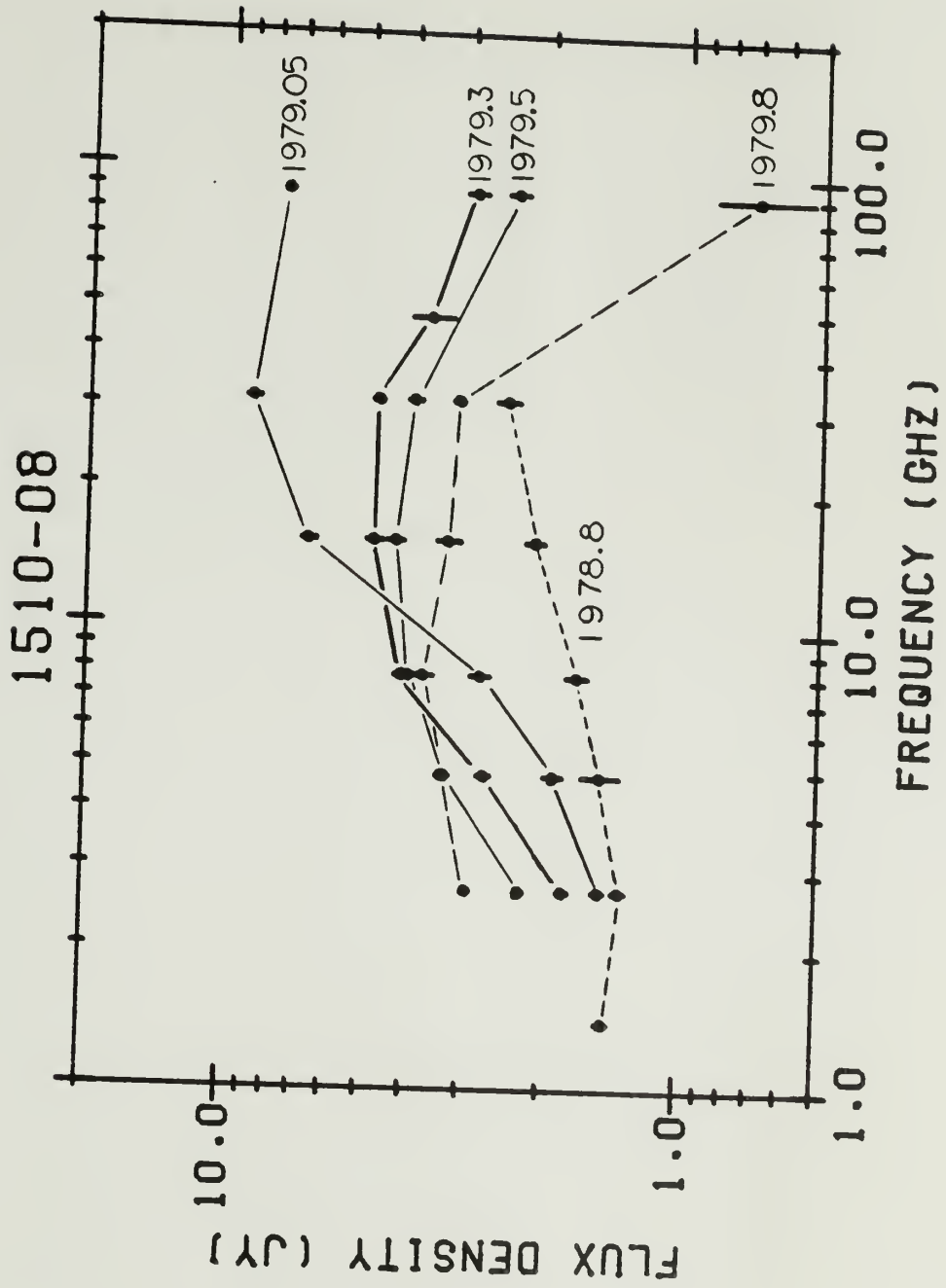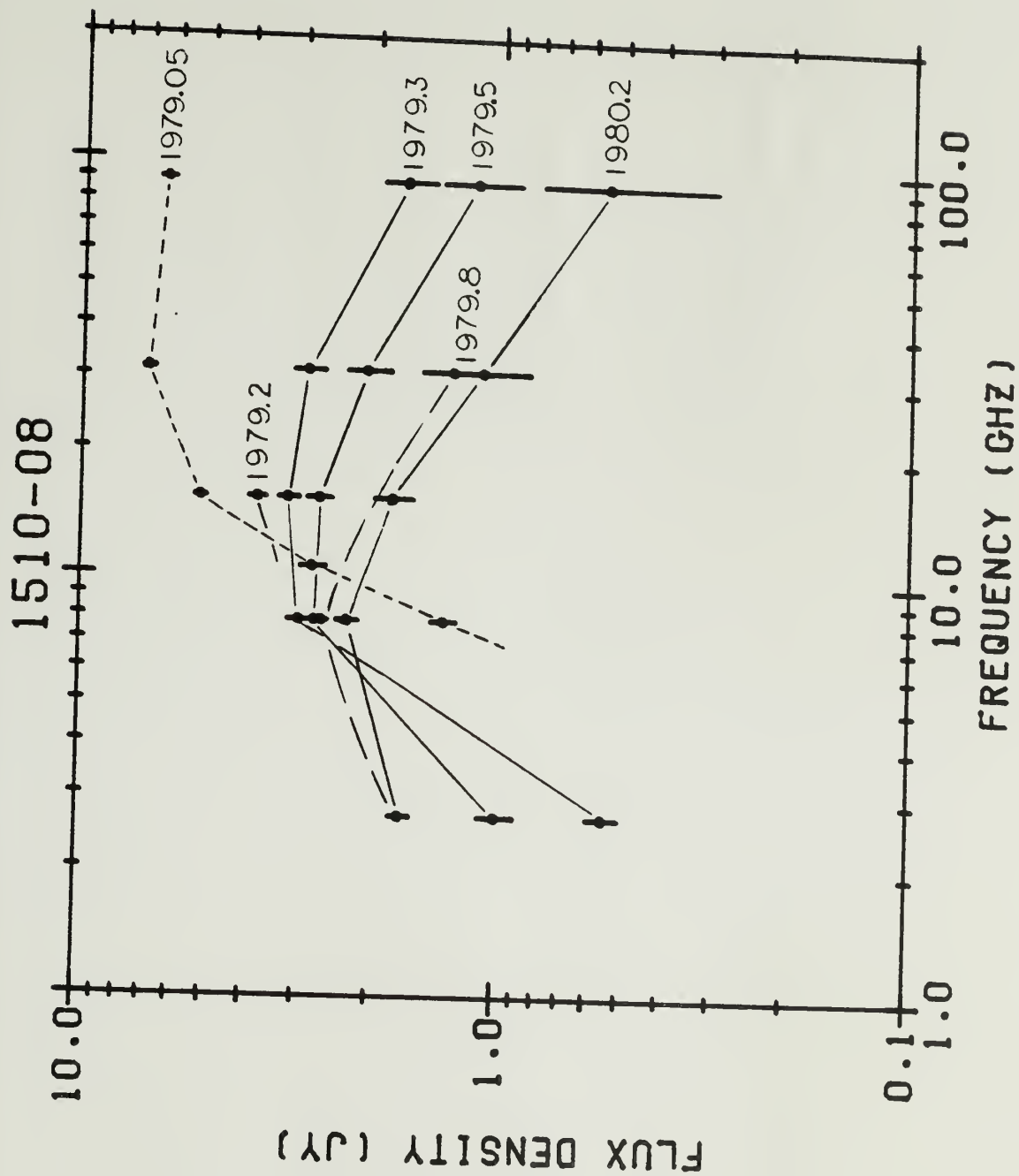
<u>1510-08.</u> This quasar has a history of rapid variations at millimeter and centimeter wavelengths (Balonek and Dent 1979). The largest amplitude and most rapid outburst occurred in early 1979, and was well observed at centimeter and millimeter wavelengths. Aller, Aller, and Hodge (1982) present linear polarization measurements for this outburst. The polarization position angle remained constant at centimeter wavelength during the outburst, and the polarized flux density at 8 GHz increased during the decay of the outburst.

The 3 mm variations (figure 15a) reveal the rapidity of the outburst rise and decay. After three years of relative inactivity, the flux density increased by 4.8 Jy in 48 days (from 2.8 to 7.6 Jy), then declined almost equally rapidly by 4 Jy during the next 65 days. The date and flux density of the maximum are not known, so the outburst could have been even more extreme than indicated by the data. Observations at 15.5 GHz indicate that the outburst had already begun to decay by 16 January, when the outburst was simultaneously noticed at millimeter and centimeter wavelengths. The decay rate decreased after 1979.2, with the flux density reaching its lowest level in four years by late 1979.

Another rapid outburst is indicated by the two FCRAO 3 mm measurements in late 1979, and the 7 mm measurement in early 1980. This event is also observed at centimeter wavelengths, superposed upon the more gradual longer wavelength decay of the earlier outburst. Data at 15.5

GHz indicates that the onset of the outburst was not delayed in time relative to millimeter wavelengths. This outburst was followed by a third outburst which peaked in late 1980, decaying to pre-outburst levels by early 1981.

The spectral evolution of the 1979 outburst is shown in figure 15b. During the maximum at millimeter wavelengths (1979.05) the spectral index on the low frequency side of the peak was ~+1.25. The frequency of maximum flux density rapidly propagated to lower frequencies (8 GHz by late 1979), while the high frequency spectral index steepened as the outburst decayed rapidly at millimeter wavelengths. The subsequent outburst in late 1979 prevents investigation of the evolution of the 1979 event after ~1979.8.

If the spectrum just prior to the 1979 outburst is due to a component not physically associated with the outburst, then its spectrum can be subtracted from the observed spectra. Figure 15c presents the resultant spectra. In this interpretation, the low frequency (opaque) spectrum of the outburst is +2.0, the high frequency spectral index steepens to a value of -0.75 as the source becomes transparent, as the frequency of maximum emission evolves to ~8 GHz. The outburst amplitudes are greater at centimeter wavelengths (figures 15b and 15c) than predicted by the canonical adiabatically expanding cloud of relativistic particles (van der Laan 1966), implying some combination of continuous injection of relativistic particles and an inhomogeneous magnetic field or particle distribution.

The variations in this source have not been resolved at millimeter and centimeter wavelengths. However, an upper limit to the size of the outburst component (assuming no relativistic motion) can be estimated from the full width half maximum time for the outburst ($1 \cong c \, \Delta t$). Assuming that the 3 mm flux density varied linearly between the pre-outburst level in November 1978, the January 1979 peak, and mid-March (when the source strength had fallen to half the peak flux density and the rate of decay began to decrease), a size of ~50 light days is calculated. Since the time of onset of the outburst and peak flux density are unknown, this value is an upper limit. From the observed decay rate, a lower limit of ~35 light days is implied. This is the smallest source size, for any source, which has been determined from a large amplitude ($\Delta S/S_{min} \gg 1$) outburst.

Weekly multi-frequency millimeter observations are clearly necessary to set accurate upper limits to variable source component dimensions. The observed millimeter variations are comparable to the optical variation timescales, indicating small volumes for the emission regions within both frequency bands.

1749+09. Although only one measurement has been obtained at FCRAO, this BL Lacertae type quasi stellar object is discussed due to its rapid variability during 1978 (figure 16). Within a seven day period, the flux density decreased from 10.60 ±1.06 Jy (27 November; Jones et al 1981) to 6.70 ±0.80 Jy (4 December; Epstein, Landau, and Rather 1980) -

Figure 16.   1749+09.

Flux density variations in 1749+09 at 90 GHz.   Large X is FCRAO measurement.   NRAO measurements from Jones et al (1981) on 27 November 1978 and 7 May 1979;   Epstein, Landau, and Rather (1980) on 4 December 1978 and 4 July 1979;   Geldzahler and Witzel (1981) on 22 November 1977; and Chapter II.
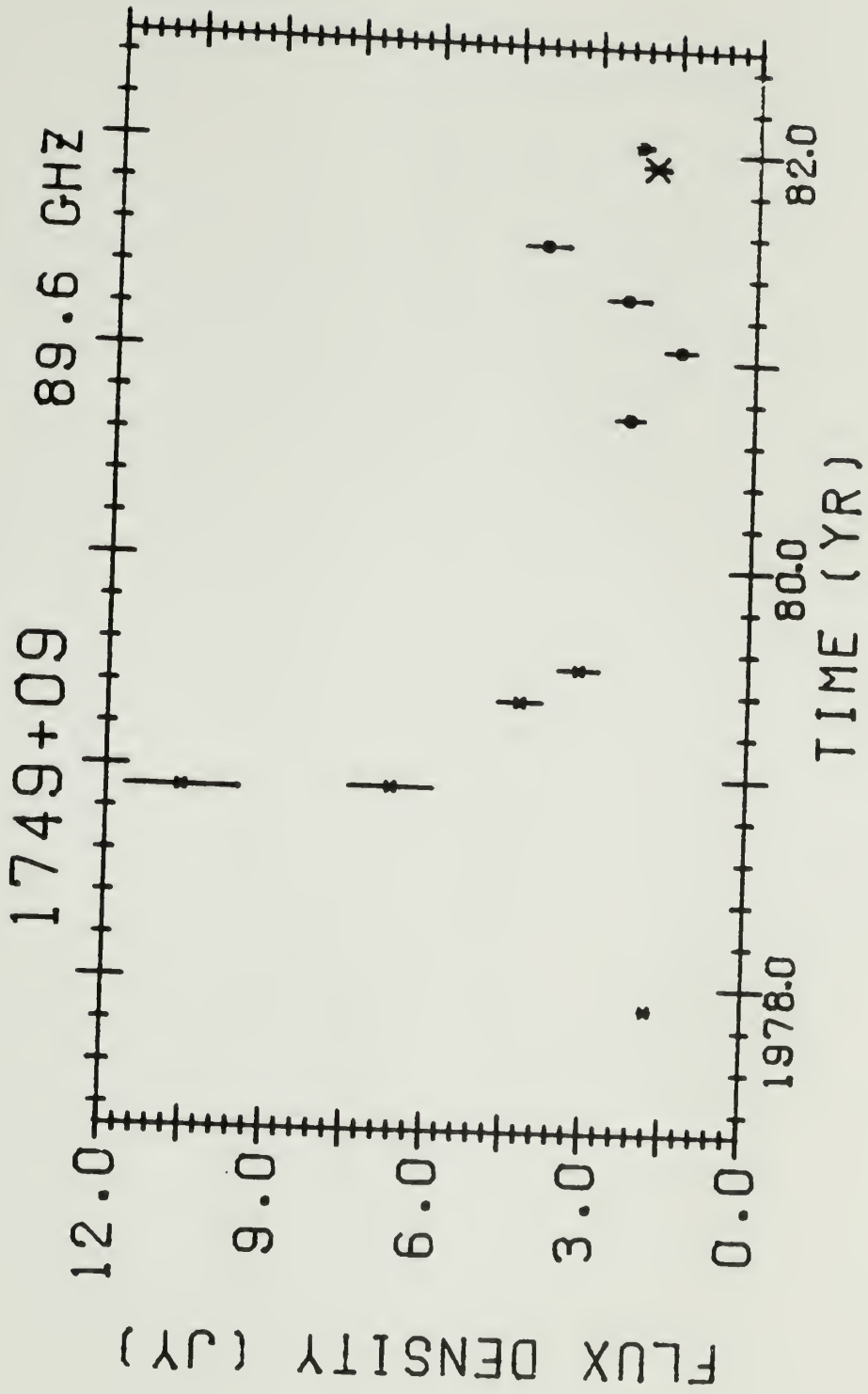
a rate of greater than $1/2$ Jy per day! The possibility exists that the value of Jones et al is in error, since Epstein, Landau, and Rather observed 1749+09 on 5 days between 1 and 8 December with no variation noted.

Variations are too rapid and the temporal coverage too limited to describe the spectral evolution. This source is of interest also due to its reported polarization variations. Altschuler (1980) reports linear polarization position angle changes of 6° per day at 8 GHz in 1974. This extreme rotation has not been observed during subsequent outbursts at centimeter wavelengths (Aller, Aller, and Hodge, 1981; Chapter II).

<u>1921-29.</u> This quasar underwent a large amplitude radio outburst in 1979-81. Dent and Balonek (1980) discuss the radio variations from 1972 to 1980.0. The flux density gradually increased in 1976-7, followed by a period of constant flux density until early 1979, when the large amplitude outburst began. Aller, Aller, and Hodge (1981) report centimeter linear polarization flux density changes in late 1978 to early 1979 (during a period of total flux density inactivity), and position angle changes during the onset of the outburst. Epstein, Landau, and Rather (1980) observed rapid variability in December 1978, in which the total flux density at 90 GHz within a five day interval dropped from ~6.5 Jy to ~2.4 Jy, and rose again to 6.5 Jy. It is of interest to note that this event occurred just prior to the onset of the large 1979 outburst.

Figure 17. 1921-29.

(a) Flux density variation in 1921-29 at 90 GHz. Large X's are FCRAO measurements. Measurement at 1978.93 is from Epstein, Landau, and Rather (1980), with the error bar indicating the total observed range in flux density within a nine day interval. Other measurements are from Dent and Balonek (1980) and Chapter II. The drop from 7.9 Jy on 16 March 1979 to 5.1 Jy seven days later (Table 9) is only marginally statistically significant.

(b) Radio spectra of 1921-29 during the decay of the large 1979 outburst. The 1.4 GHz measurement is from Perley (1982), 4.8 GHz measurements from Aller, Aller, and Hodge (1981). Other measurements from Chapter II.
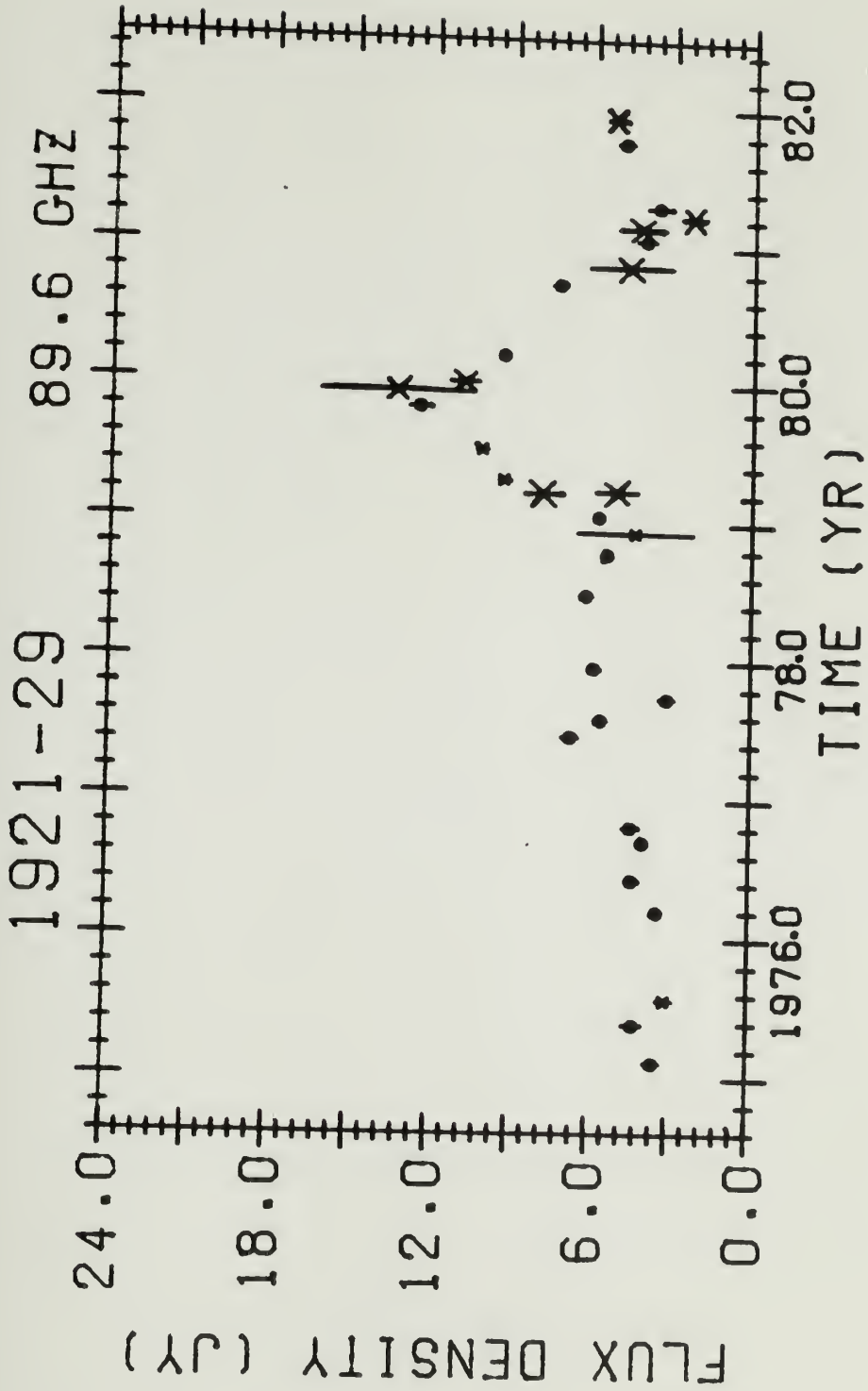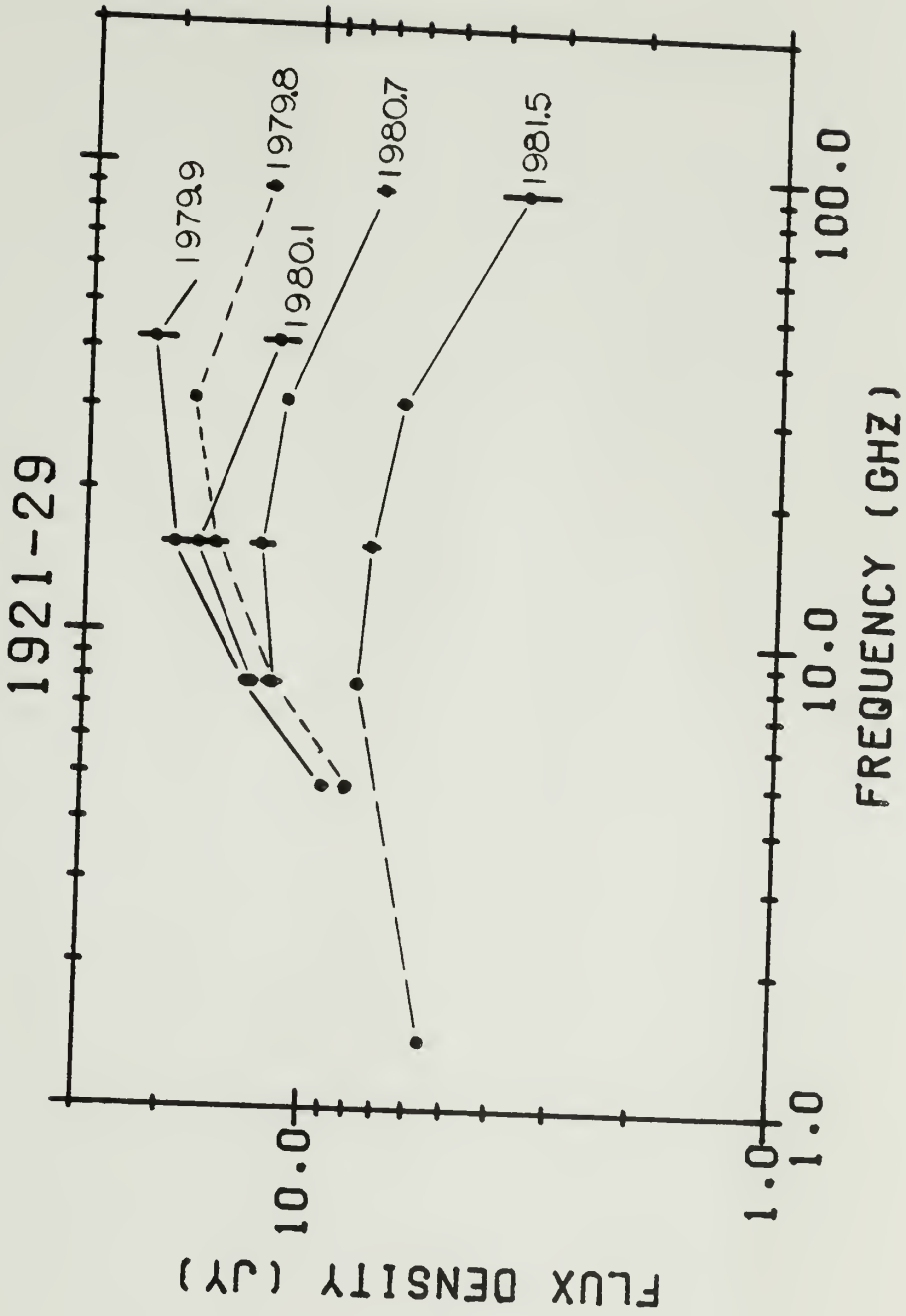
An additional two years of four frequency (Chapter II), and 7 and 3 mm FCRAO measurements (Chapter III) allow us to further define the evolution of the large outburst. Figure 17a presents all the available 3 mm observations. The FCRAO data helps define the variations since 1979. The total flux density spectrum during the decay of the 1979 outburst is shown in figure 17b.

Several comments beyond those presented by Dent and Balonek (1980) can be made based upon this expanded data set. The large outburst peaked in 1979.8 (±0.2), with the decay rate being slower than the rise. A small outburst in mid 1980, superposed upon the decay, is seen at four frequencies. The flux density reached a minimum in mid 1981 below the pre-outburst level, followed by a small outburst which began in late 1981.

The spectra presented by Dent and Balonek for the 1979 outburst (by subtracting the 1978 spectrum) must be updated, using a revised "base" (non-outburst) spectrum. Reanalyzing the outburst by subtracting either the 1981 minimum or a linearly interpolated minimum (fit to the late 1978 pre-outburst and mid 1981 post-outburst flux densities) from the observed flux densities does not alter the basic evolution described by Dent and Balonek. The spectral index below 15 GHz during the rise is $\alpha \sim$ +1.5 (compared to their value of +2), while the millimeter spectrum during the decay remains $\sim$ −0.3. Comparing the 7 mm with the 31 GHz data indicates that the peak flux density occurred above 31 GHz (which

would steepen the deduced high frequency spectrum), and the outburst decayed more rapidly at 7 mm than at 31 GHz.

One additional aspect of the millimeter variability not previously discussed is the evidence for multiple outbursts comprising the smooth centimeter variations in 1976-9. In particular, the 31 and 90 GHz data show a small outburst peaking ~1977.4, decaying within 3/10 years, followed by another rise (figure 17a). This suggests that the 1976-9 event seen at centimeter wavelengths is actually a superposition of two or more events. This interpretation is important when comparing the radio variations with the optical activity (Chapter VI).

BL Lacertae.   Following half a decade of only minor activity, BL Lacertae began a period of multiple large outbursts in 1980. The millimeter and centimeter flux density at maximum (12 to 16 Jy) was the highest observed strength since 1971. Aller, Hodge, and Aller (1981) observed a 12 degree per day (440° total) nonlinear rotation in linear polarization position angle during this period of activity.

The 3 mm variations are presented in figure 18. Simultaneous measurements on 17 July 1980 at 31.4 and 90 GHz indicate a spectral index near maximum of $\alpha(31.4, 90) = -0.25$. Using the Aller, Hodge, and Aller centimeter data from this epoch shows that the spectrum was flat between 15 and 31.4 GHz, falling off at lower frequencies. By mid September the spectral peak had progressed to between 8 and 15 GHz, the lower frequency (5 to 15 GHz) spectrum had flattened, and the millimeter

Figure 18. BL Lacertae.

Flux density variation in BL Lacertae at 90 GHz. Large X's are FCRAO measurements. NRAO measurements from Chapter II.

BL LAC   89.6 GHZ

FLUX DENSITY (JY)

TIME (YR)
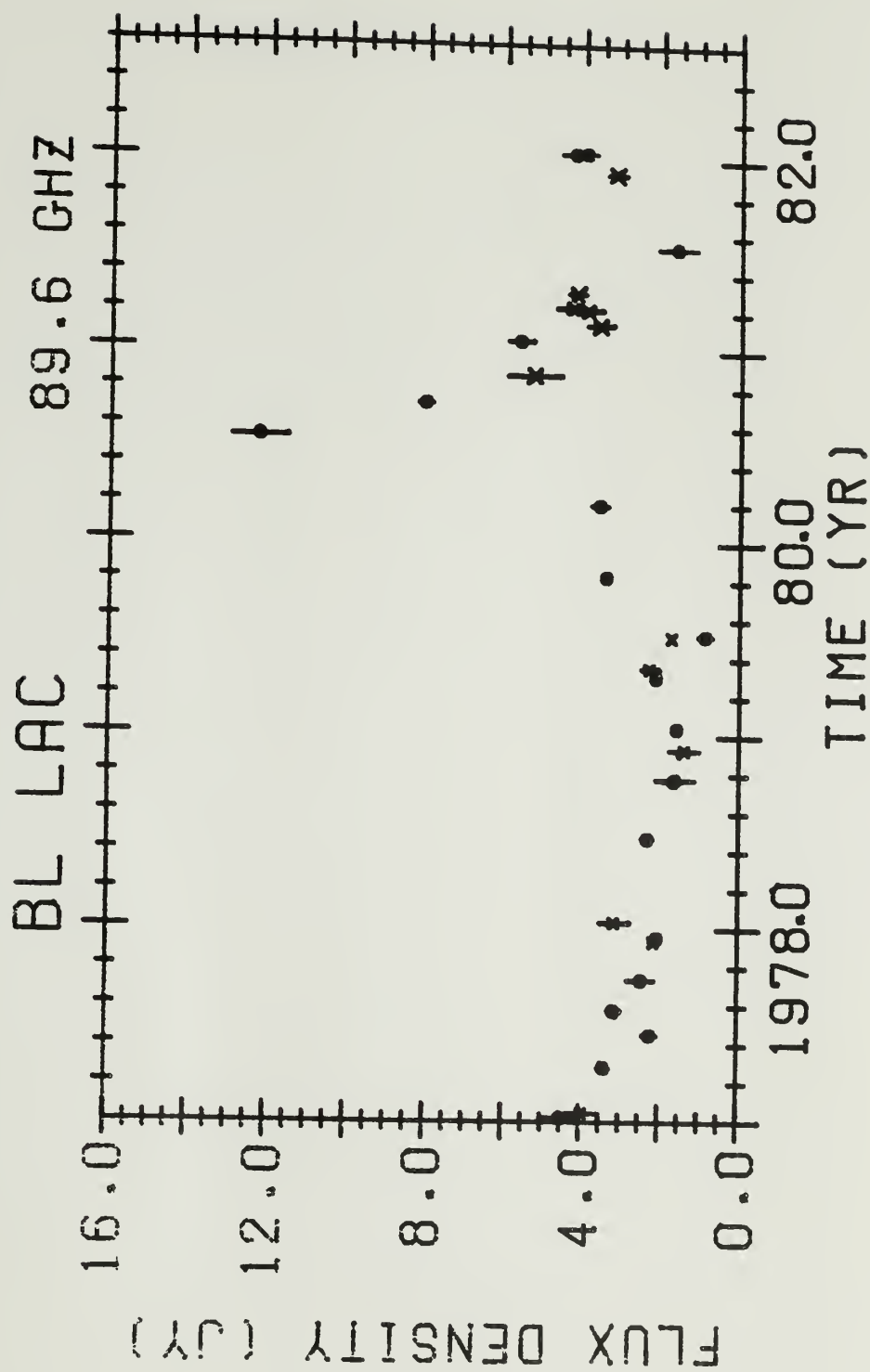
(15 to 90 GHz) spectrum remained at -0.25. The rapidity of the variations and the limited coverage at millimeter wavelengths prevents a more detailed analysis of the variations during this active period.

Although the centimeter spectrum rises at higher frequencies, there is no epoch during this active period during which the 3 mm flux density exceeds the 31.4 GHz value. The observed constant millimeter spectral index suggests that the spectral peak was around 30 GHz throughout the outbursts.

The variations at millimeter and centimeter wavelengths in BL Lac are among the most rapid observed, indicating the necessity of weekly (or more frequent) observations at millimeter wavelengths in order to understand the outburst evolution.

3C446. A distinguishing feature of the millimeter and centimeter variability in the quasar is its typical trapezoidal outburst profile (first noted by Dent, private communication) - a sharp rise, flat-topped maximum, and rapid decay. The 3 mm observations (figure 19a) reveal several instances of rapid variations. The most extreme example is the 2 Jy increase in 34 days in early 1979. The rate of variations is not as extreme at lower frequencies.

The spectral evolution of the 1979 outburst (figure 19b) shows the rapid rise at 90 GHz. For comparison, the flux density minimum in 1977 is included - showing the decimetric excess spectra shape. In 1979.04,

190
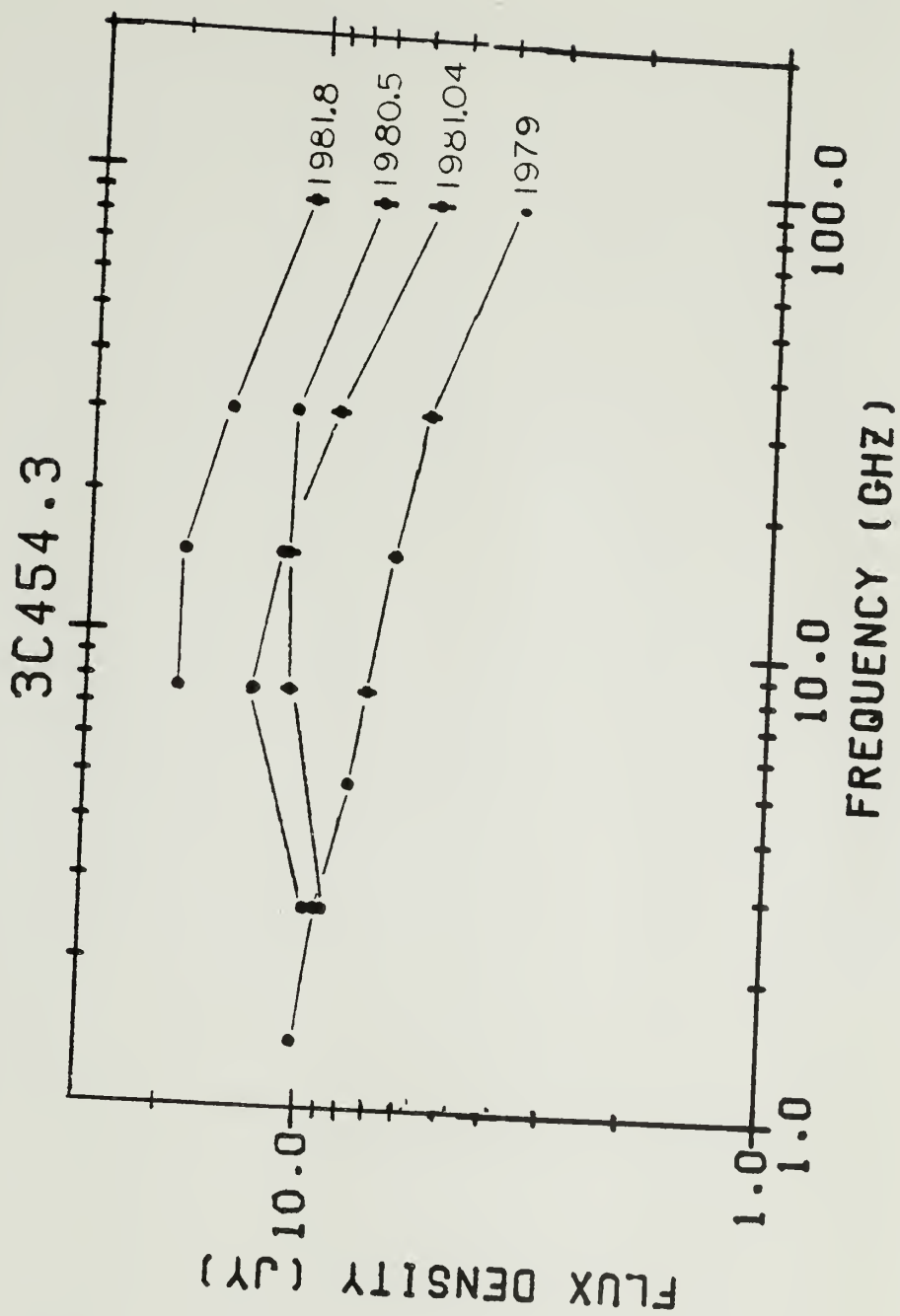
Figure 19.   3C446.
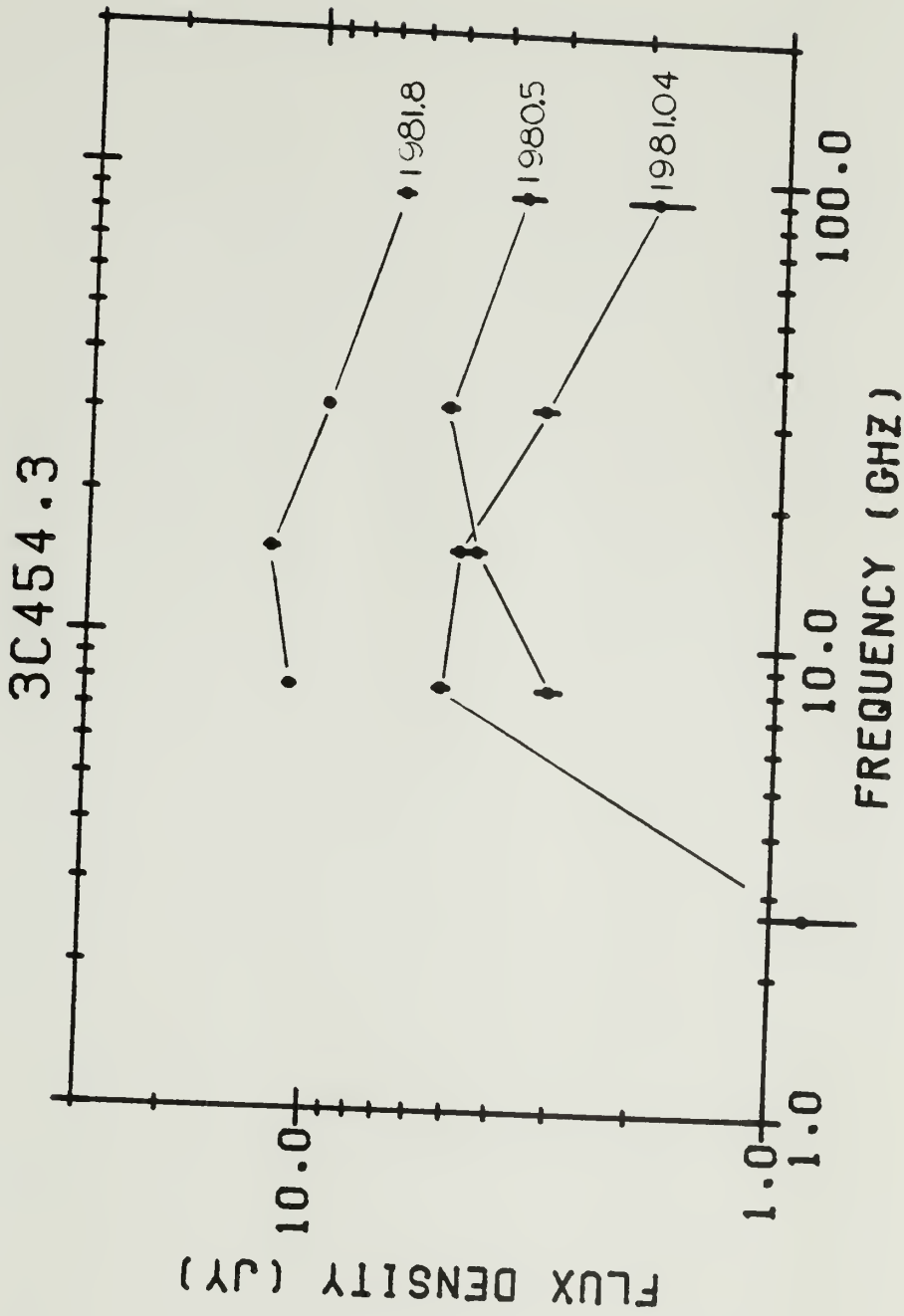
(a) Flux density variation in 3C446 at 90 GHz. Large X's are FCRAO measurements. NRAO measurements from Epstein, Landau, and Rather (1980) and Chapter II.

(b) Radio spectra of 3C446 during the large outburst in 1979. 1977: minimum, pre-1978 outburst;   1979.04: pre-1979 outburst with the small 1978 outburst still seen at 31.4 and 15.5 GHz;   1979.5: maximum at 31.4 GHz;   1980.5: maximum at 7.9 and 15.5 GHz, the outburst has decayed at 31.4 and 90 GHz.

3C446

FREQUENCY (GHZ)

FLUX DENSITY (JY)

10.0   1.0

10.0   100.0

1979.5
1979.3
1979.0
1980.5

MINIMUM-1977
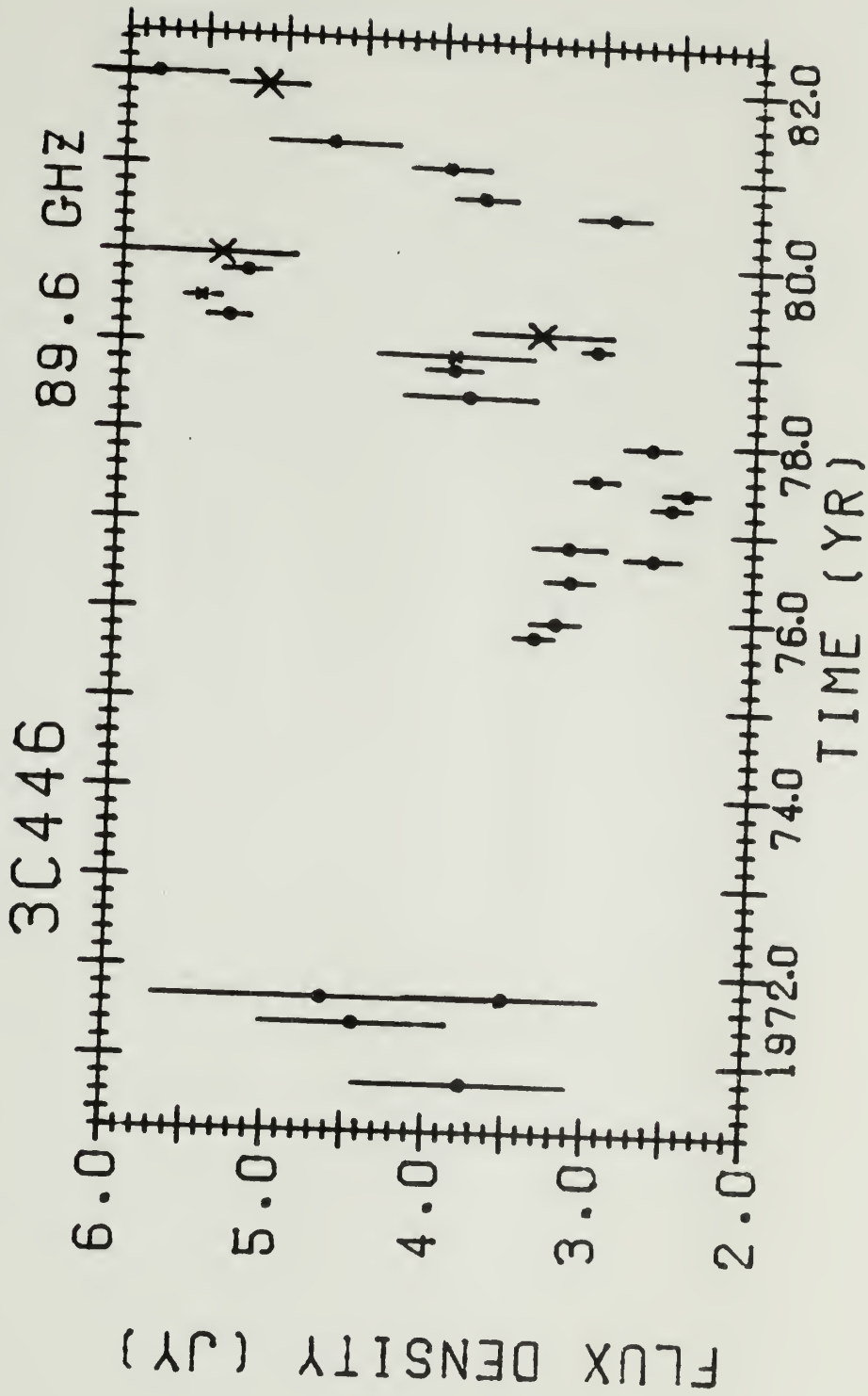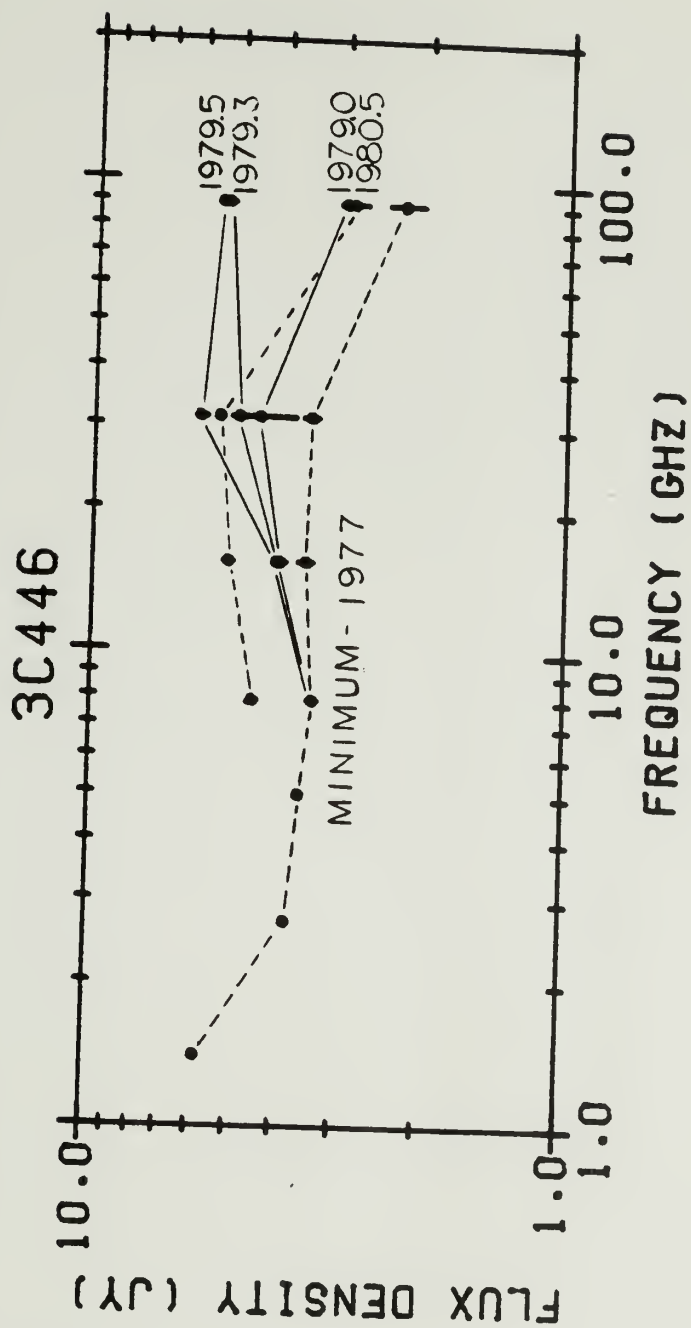
the 90 GHz flux density had decreased from the small 1978 outburst to near its pre-burst level, but the 31.4 and 15.5 GHz flux density had not yet decayed. By 1979.3, the rapid rise had occurred at 3 mm, with only small increases at longer wavelengths. The spectrum exhibits a milli-meter excess with spectral index $\alpha = -0.1$. By 1979.5, the outburst has peaked at 31.4 GHz, but is still only slowly increasing at 15.5 GHz. The outburst peaks a year later (1980.5) at 15.5 and 7.9 GHz, while it had already decayed at 3 mm and had begun to decay at 31.4 GHz (the millimeter spectral index had steepened to −0.6). The outburst sub-sequently decayed at centimeter wavelengths, concurrent with the onset of a new outburst at 3 mm (figure 19a). The magnitude and rapidity of the 1979 outburst is even more pronounced (and the evolution in fre-quency of maximum flux density more noticable) if the 1977 spectra is subtracted from the observed total flux density.

CTA102. Only limited data exists at 3 mm for this highly variable source (figure 20). The 31.4 and 90 GHz data are too undersampled to follow the outburst evolution. There have been at least three outbursts since 1978 which overlap at centimeter wavelengths. The radio spectrum consists of a decimeter excess component (of strength ~2 Jy at cen-timeter wavelengths) and the variable centimeter components.

The rise time for the 1979 3 mm maximum is not known, but the rise at 15.5 GHz and 31.4 GHz took 3/4 years. The decay time at 3 mm was only 1/2 year, but cannot be determined at lower frequencies due to

194

Figure 20.   CTA102.

Flux density variation in CTA102 at 90 GHz.   Large X's are
FCRAO measurements.   NRAO measurements from Chapter II.

overlap with the 1980 outburst. A third outburst occurs in early 1981, decaying at 3 mm by 1982.0 and more slowly at centimeter wavelengths.

A striking characteristic of the 3 mm variations is the rapid decay time, which is <u>not</u> observed at lower frequencies (even 31.4 GHz). CTA102 is among the most rapid variable sources at 3 mm. Any correlated optical activity would be best detected by comparison with the 3 mm observations, which do not exhibit long decay timescales.

<u>3C454.3.</u> This quasar is currently undergoing its most intense activity at millimeter and centimeter wavelngths since 1966 (figure 21a). The current activity began in late 1979 after ~3 years of minor fluctuations (ΔS <2Jy). The first outburst reached a maximum in mid 1980 at millimeter wavelengths and decayed until 1980. Maximum at 15.5 GHz occurred in 1981.0. A second, more intense outburst began in early 1981 at 3 mm, peaking in late 1981. The maximum occurred a few months later at 15.5 GHz. The outburst has been decaying at frequencies above 15 GHz since late 1981.

The total flux density evolution is shown in figure 21b. The flux density in 1979 prior to the activity shows the pronounced decimetric excess, with spectral index $\alpha = -0.3$. The spectrum preserved this index between 31.4 and 90 GHz during the rise of the initial outburst, subsequent decay, and second outburst rise. The flux density increase is minimal at 2.7 GHz. The spectral peak progresses from ~20 GHz in 1980.5 to ~8 GHz by 1981.0.

Figure 21.   3C454.3.

(a) Flux density variation in 3C454.3 at 90 GHz. Large X's are FCRAO measurements. NRAO measurements from Owen, Spangler, and Cotton (1980); Jones et al (1981); Epstein, Landau, and Rather (1980); and Chapter II.

(b) Radio spectra of 3C454.3 during the two outbursts in 1980 and 1981. The minimum flux density spectra (1979) is shown for comparison. The first outburst peaked at millimeter wavelengths in 1980.5, and decayed at these wavelengths thru 1981.04. The second outburst began at millimeter wavelengths at this time and peaked in 1981.8. Data from Chapter II.

(c) Radio spectra of 3C454.3 during the two outbursts in 1980 and 1981 with the pre-outburst spectrum (1979) subtracted.

3C454.3   89.6 GHZ

FLUX DENSITY (JY)

TIME (YR)

3C454.3

3C454.3

FLUX DENSITY (JY)

FREQUENCY (GHZ)

1981.8

1980.5

1981.04
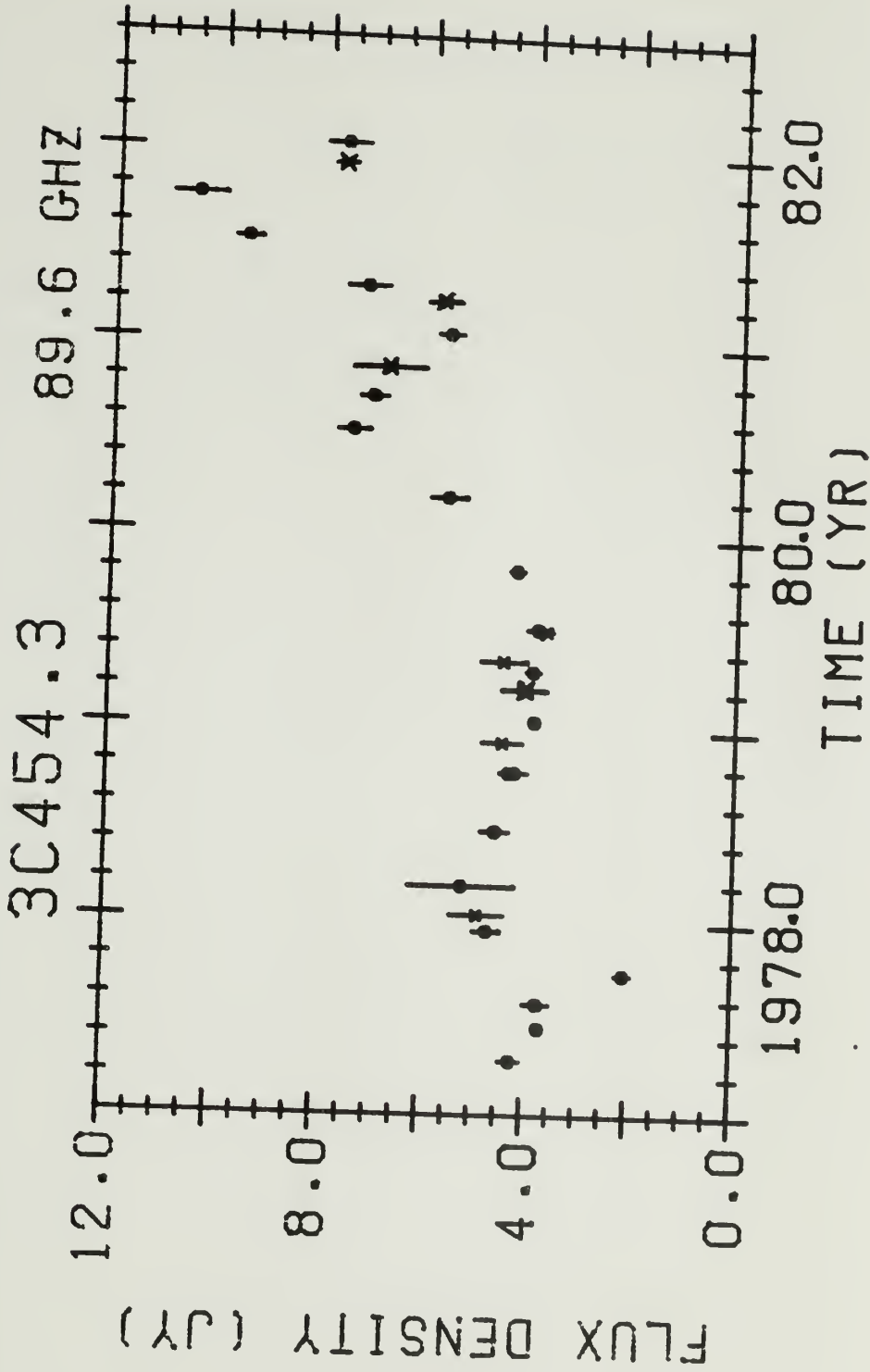
If the spectrum during the inactive period in 1979 is from a component physically distinct from the outburst, then this spectrum can be subtracted from the observed spectra to determine the outburst spectra (figure 21c). The 1980 outburst is clearly delayed at frequencies below 15 GHz, with the frequency of maximum progressing from 31 GHz in 1980.5 to 10 GHz in 1981.0. The evolution of this first outburst cannot be followed as the second event began at this time. The spectral index of the outbursts ($\alpha = -0.3$) is the same as for the underlying 1979 component spectrum. The low frequency outburst index is difficult to determine since it depends critically upon the assigned minimum flux density. However, reasonable estimates for this index between 2.7 and 7.9 GHz range from +1.5 to as steep as +2.5.

§3. Conclusion

The rapid 3 mm variations reported in §2 are summarized in Table 12. Listed are the epoch, flux density range, and timescale for the most rapid outbursts observed in each source since January 1979 (plus these parameters for OJ287 and 3C345, which were not discussed in §2). In several instances the timescale of variation is an upper limit (indicated by a "<" symbol) defined by the time interval between two measurements. Variations on timescales shorter than 1 month cannot be determined from existing observations, but can be inferred since several rapid variations were not resolved by monthly spaced observations.

Several important conclusions concerning radio source evolution can be drawn from the data presented in §2.

TABLE 12

RAPID VARIATIONS AT $\lambda 3$ mm

Source	Outburst Rises			Outburst Decays		
	Epoch	t_{rise} (days)	ΔS_{rise} (Jy)	Epoch	t_{decay} (days)	ΔS_{decay} (Jy)
3C84	6 Dec 79	54	46.			
	29 Jan 80		67.	17 Jan 81	<32	70.
				18 Feb 81		52.
OJ287	19 Mar 81	28	3.8			
	16 Apr 81		5.4	5 Dec 81	37	6.8
				11 Jan 82		1.4
1413+13		--		21 Mar 81	44	4.8
				4 May 81		2.8
1510-08	27 Nov 78	<48	2.8			
	14 Jan 79		7.6	14 Jan 79	65	7.6
				18 Mar 79		3.6
3C345	6 Nov 80	250	10.3			
	14 Jul 81		14.1	14 Jul 81	80	14.1
				2 Oct 81		11.9
1749+09	27 Nov 78	7	10.6			
	4 Dec 78		6.7		--	
1921-29	14 Jan 79	326	5.8			
	6 Dec 79		13.4	6 Dec 79	408	13.4
				17 Jan 81		4.1
BL Lac	12 Mar 80	<126	3.6			
	16 Jul 80		12.3	16 Jul 80	119	12.3
				12 Nov 80		5.3
3C446	16 Mar 79	<34	3.4			
	19 Apr 79		5.3	2 Jan 80	<196	5.4
				16 Jul 80		2.9
CTA102		--		14 Jan 79	<60	4.9
				15 Mar 79		3.0
				or		
				14 Jan 79	175	4.9
				8 Jul 79		1.6
3C454.3	19 Mar 81	198	5.8			
	2 Oct 81		10.5	2 Oct 81	64	10.5
				5 Dec 81		7.7

(1) Observations must be conducted <u>more</u> frequently than monthly at millimeter wavelengths in order to delineate the outburst profiles. The actual timescale of activity at millimeter wavelengths is unknown since no long term systemmatic programs have been conducted with sampling more frequent than once per month. Outburst rises and decays are more rapid at millimeter wavelengths than at centimeter wavelengths and have timescales nearly as short as fluctuations at optical frequencies.

(2) Strong outbursts at millimeter wavelengths may be undetectable at centimeter wavelengths (e.g. 3C84), due either to the intrinsic source spectrum or to opacity at longer wavelengths. In correlating radio activity with optical variability, it is thus clearly desirable to employ millimeter wavelength radio observations. However this is not possible at the present time (except for the few sources which have been observed regularly for the last decade) due to the lack of adequate coverage of a large sample of sources at millimeter wavelengths.

(3) The spectra during outbursts often exhibit a maximum at frequencies around 30 GHz. Outbursts do not always possess maxima at higher frequencies (e.g. 90 GHz) during any stage in an outburst. The outbursts in many sources are thus transparent at 3 mm during the entire outburst (including the rise). Outbursts have been observed which are transparent at frequencies above 10 GHz throughout the entire outburst (e.g. 0235+164, Balonek and Dent 1980). There <u>are</u> outbursts (though not as common as generally believed) which are opaque at 3 mm during the

early stages of the outburst (e.g. 3C84, 1921-29, 3C446). Outburst profiles are not necessarily consistent within a given source.

(4) The spectral index at millimeter wavelengths often remains constant (typically ~ -0.3 ±0.2) during the decay of the outburst. This spectral index implies a $\gamma = 1-2\alpha = 1.6$ for a relativistic electron distribution of the form $N(E) dE \alpha E^{-\gamma} DE$. This distribution is typical of most compact variable sources. The lack of change in this index during several stages in the outbursts (rise, maxima, and decay) reveals the constancy of the particle acceleration mechanism.

(5) The evolution of outbursts do not follow the simple expanding cloud model (van der Laan 1966), but require continuous injection of relativistic particles (Peterson and Dent 1973). In particular, the outburst strength at low frequencies is much greater than predicted by the single ejection model.

More extensive multi-frequency observations of a significant sample of sources must be conducted at millimeter wavelengths in order to understand more thoroughly the nature of the emission mechanisms and physical conditions in compact sources. The limited results obtained at millimeter wavelengths reveal variations which cannot be adequately understood from centimeter wavelength observations alone.

CHAPTER V

SINGLE EPOCH SPECTRA FOR 113 SOURCES

§1. The Single Epoch Spectra

In this chapter, single epoch radio spectra at seven frequencies for 113 sources are presented. The sources included in this study are listed in Tables 1 and 2. The observations have been discussed in Chapter II. The 2.7, 7.9, 15.5, 31.4, and 89.6 GHz measurements were obtained as part of an ongoing program to monitor the spectral evolution of compact extragalactic sources. The measurements at 1.4 and 5.0 GHz were obtained at two epochs, three months apart, with the intent of defining the lower frequency spectrum of this sample of sources. The spectra presented in this chapter are the first compilation of near-simultaneous multi-frequency observations of this sample of regularly monitored variable sources. A complete statistical analysis of the radio spectra is not undertaken here. Rather, the spectra of individual sources are discussed in Chapter IV (rapid radio variations) and Chapter VI (correlated radio-optical variability). In §2, the radio measurements are combined with near-simultaneous optical measurements to statistically search for correlation between the radio and optical emission.

The near simultaneous radio measurements are presented in Table 13, and the corresponding spectra presented in figures 22(a-1).

TABLE 13

ONE EPOCH SPECTRA OF VARIABILITY SAMPLE SOURCES

SOURCE	EPOCH[1]	DATES[2]	FLUX DENSITY (Jy)[3] Frequency (GHz)						
			1.4	2.7	5.0	7.9	15.5	31.4	89.6
0007+106	1978.8	aaaaaaa	0.13	0.24 .02	0.52	1.20±0.08	2.25±0.10	2.01±0.14	0.93±0.36
0048-097	1978.8	aaaaaaa	0.88	1.10 .04	1.29	1.51 0.06	1.41 0.10	1.57 0.18	0.69 0.24
0106+013	1978.8	aaaaaaa	2.86	3.29 .03	3.31	3.55 0.06	2.93 0.12	2.28 0.12	0.97 0.27
0133+476	1978.8	aaaaaaa	1.61	1.81 .01	1.85	2.14 0.08	2.56 0.11	3.25 0.14	2.41 0.11
0219+428	1980.2	---tvw-	-	-	-	0.77 0.06	0.57 0.09	0.46 0.12	-
0229+131	1979.3	bbbaac-	1.25	1.35 .03	1.94	2.42 0.10	2.40 0.11	2.33 0.07	-
0234+285	1980.2	---vvw-	-	-	-	2.62 0.08	2.48 0.08	2.07 0.09	-
0235+164	1978.8	aaaaaaa	1.71	1.70 .02	1.63	1.69 0.05	1.52 0.08	1.88 0.16	1.89 0.26
0237-027	1980.7	---wwy-	-	-	-	1.35 0.12	1.81 0.10	1.68 0.15	-
0238-084	1978.8	baaaaaa	0.67	1.12 .03	1.37	1.18 0.07	1.36 0.09	1.21 0.11	0.49 0.13
0240-002	1980.2	-a-vvw-	-	(2.98 .04)	-	1.23 0.07	0.71 0.09	0.25 0.05	-
0300+470	1979.8	aaaaaea	1.80	1.94 .03	2.26	2.28 0.08	2.35 0.17	2.45 0.09	1.14 0.19
0306+102	1981.3	---xyz-	-	-	-	1.27 0.09	1.05 0.07	0.77 0.14	-
0316+161	1980.2	baaagwb	7.53	5.08 .07	2.85	1.76 0.09	0.77 0.08	0.32 0.10	0.13 0.09
0316+413	1978.8	aaaacaa	16.07	33.11 .27	49.86	56.16 0.56	42.24 1.27	42.24 0.42	42.70 0.46
0333+321	1978.8	baaaaab	3.15	3.24 .04	2.48	2.07 0.09	1.91 0.12	1.70 0.21	1.10 0.14
0336-019	1978.8	aaaaaaa	2.39	2.46 .03	2.78	3.46 0.09	4.02 0.14	3.70 0.15	2.06 0.23
0355+508	1978.8	aaaaaaa	5.05	7.93 .07	9.65	11.84 0.12	10.94 0.24	9.15 0.17	4.64 0.17
0404+767	1979.3	--aadcb	-	-	2.95	2.05 0.22	0.90 0.07	0.61 0.16	0.42 0.15
0405-123	1978.8	aaabaab	3.17	2.31 .05	1.96	1.47 0.09	1.17 0.09	1.01 0.16	0.35 0.10

TABLE 13 (continued)

0415+379	1978.8	baabaaa	14.62	9.29	.08	4.99	4.39	0.14	2.54	0.11	2.75	0.14	1.40	0.18
0420-014	1978.8	aaaaaaa	0.89	1.46	.03	2.82	3.96	0.06	6.09	0.18	6.02	0.14	4.67	0.22
0430+052	1978.8	aaaaaaa	6.22	5.44	.02	4.82	4.94	0.07	4.34	0.13	2.90	0.12	1.63	0.13
0433+295	1977.7	--aaadb	-	-		16.17	10.70	0.14	5.12	0.17	2.49	0.20	0.77	0.13
0440-003	1978.8	aaaaaab	2.16	2.00	.03	1.61	1.12	0.07	0.87	0.08	0.86	0.12	0.53	0.13
0454-234	1978.8	---bdab	-	-		-	2.22	0.10	1.77	0.16	1.82	0.14	1.04	0.12
0458-020	1978.8	aaaaaaa	1.67	1.38	.04	1.79	2.04	0.06	2.24	0.10	2.00	0.35	0.73	0.32
0528-250	1980.2	---tvw-	-	-		-	0.97	0.09	0.63	0.11	0.28	0.09	-	
0528+134	1978.8	aaabdab	1.08	1.34	.02	1.91	3.02	0.15	3.20	0.08	2.78	0.17	2.20	0.12
0552+398	1978.8	baaaaaa	1.45	3.91	.02	4.61	4.69	0.09	3.43	0.15	1.64	0.15	0.82	0.21
0605-085	1978.8	baaaaaa	3.06	3.00	.06	2.82	2.33	0.07	2.43	0.14	2.55	0.16	1.72	0.15
0607-157	1978.8	baaaaaa	1.75	2.00	.07	2.53	2.49	0.06	3.24	0.16	3.30	0.15	1.87	0.09
0723-008	1978.8	baaaaaa	2.47	2.24	.01	2.18	1.98	0.07	1.77	0.11	1.44	0.13	1.66	0.34
0727-115	1978.8	baabaaa	2.17	2.93	.02	3.85	3.83	0.08	3.68	0.17	2.62	0.15	1.10	0.19
0735+178	1978.8	baaaaaa	1.79	1.96	.03	2.19	2.10	0.08	2.16	0.11	1.83	0.14	1.62	0.09
0736+017	1978.8	baaabaa	2.35	2.18	.03	2.01	1.82	0.06	2.30	0.12	2.64	0.11	2.07	0.16
0748+126	1978.8	baaafab	1.47	1.74	.02	1.94	1.88	0.08	1.63	0.09	1.69	0.15	1.23	0.09
0754+100	1979.0	bbbeh-b	0.63	0.61	.05	0.63	0.68	0.07	0.76	0.07	-		0.43	0.09
0814+425	1978.9	bbbcf-b	1.49	1.61	.04	1.59	1.62	0.08	1.37	0.09	-		0.52	0.10
0829+046	1981.3	---xyz-	-	-		-	1.29	0.07	1.29	0.08	1.67	0.13	-	
0831+557	1978.8	baabaab	7.97	7.71	.07	6.06	3.70	0.09	1.97	0.11	0.72	0.16	0.03	0.13
0834-201	1978.8	---adaa	-	-		-	1.53	0.12	1.01	0.11	0.82	0.15	0.41	0.18
0836+710	1978.8	bbbddab	4.12	3.19	.12	2.40	1.78	0.10	1.58	0.10	1.23	0.15	0.78	0.18
0851+202	1978.8	baaabaa	1.83	2.39	.01	2.71	3.77	0.07	4.55	0.25	4.57	0.22	3.85	0.17
0859-140	1978.8	baaadab	3.21	2.79	.03	2.45	1.80	0.06	1.30	0.11	1.33	0.13	0.37	0.10

TABLE 13 (continued)

0906+015	1981.3	-z-xyz-	—	0.97 .02	—	1.89 0.10	1.87 0.07	1.51 0.14	—
0923+392	1978.8	baaaaaa	2.48	5.15 .05	7.47	8.85 0.09	7.27 0.17	5.73 0.16	3.41 0.22
0951+699	1978.8	-aabeab	—	5.04 .16	3.64	2.58 0.08	1.58 0.13	1.10 0.16	0.48 0.08
0953+254	1978.8	baaaaab	0.84	1.32 .02	1.18	1.37 0.09	1.32 0.12	1.36 0.13	0.97 0.08
1055+018	1978.8	bbbabaa	2.90	2.68 .06	2.84	3.11 0.08	3.55 0.15	2.87 0.13	1.75 0.15
1101+384	1979.3	bbbcgcy	0.92	0.76 .02	0.69	0.62 0.07	0.66 0.26	0.41 0.12	(0.35 0.20)
1116+128	1981.3	bbbcgzb	2.09	1.59 .02	1.28	1.13 0.14	0.89 0.08	(0.57 0.15)	0.15 0.13
1127-145	1978.8	aaaabab	6.23	6.16 .06	4.87	3.84 0.12	3.06 0.16	1.88 0.16	0.82 0.08
1156+295	1981.3	-z-zyzz	—	1.89 .03	—	(1.60 0.13)	1.36 0.09	1.53 0.09	1.94 0.27
1215+303	1979.8	aaadcd-	0.59	0.60 .01	0.49	0.33 0.12	0.35 0.09	0.32 0.14	—
1219+285	1978.8	aaaabac	1.69	2.03 .01	1.87	2.11 0.10	1.90 0.10	1.53 0.15	1.01 0.07
1226+023	1978.8	baaacaa	44.79	45.36 .54	40.54	39.52 0.40	31.99 0.67	19.49 0.33	10.24 0.32
1228+126	1978.8	-b-ab--	—	115.10 2.65	—	49.08 0.49	28.51 0.41	16.90 0.35	6.77 0.28
1253-055	1979.0	bbbdhbb	10.77	10.74 .08	11.35	12.73 0.35	12.34 0.30	9.19 0.61	7.06 0.12
1308+326	1979.0	bbbdhbb	1.46	2.26 .05	2.57	2.87 0.19	2.87 0.09	2.20 0.20	1.90 0.08
1322-427	1978.8	---bdaa	—	—	—	30.69 1.72	14.28 1.73	14.84 0.77	8.89 0.75
1328+307	1978.8	-a-ab--	—	11.82 .17	—	5.87 0.08	3.38 0.16		
1334-127	1979.0	bbbdhbb	1.74	2.34 .07	2.82	4.80 0.15	5.62 0.18	5.85 0.34	4.93 0.15
1345+125	1979.8	aaacce-	5.01	3.86 .04	2.92	2.25 0.06	1.48 0.12	(1.01 0.08)	—
1354-152	1978.8	aaaaaab	1.30	1.39 .02	1.81	1.80 0.11	1.69 0.11	1.40 0.24	0.58 0.06
1404+286	1979.8	bbbbheb	0.68	1.99 .03	2.85	2.99 0.09	1.60 0.10	(0.58 0.08)	0.01 0.13
1413+135	1981.3	---xxzz	—	—	—	2.12 0.22	3.50 0.17	3.88 0.13	3.62 0.64
1418+546	1981.3	---xyzz	—	—	—	1.99 0.12	2.03 0.11	1.63 0.13	1.24 0.30
1458+718	1978.8	-aaccab	—	4.99 .08	3.36	2.53 0.07	1.48 0.09	1.08 0.16	0.37 0.23
1502+106	1978.8	aaaacab	1.53	1.73 .04	1.71	1.64 0.06	1.43 0.06	0.84 0.11	0.75 0.09

TABLE 13 (continued)

ID	Date	Code							
1510-089	1978.8	aaaaca-	1.44	1.30 .03	1.57	1.53 0.07	2.12 0.11	2.46 0.15	
1514-241	1978.8	---cbab	-	-	-	2.38 0.13	2.08 0.14	1.87 0.12	1.79 0.10
1548+056	1978.8	aaaacax	2.00	2.03 .02	1.89	2.10 0.09	1.82 0.09	1.30 0.23	(0.46 0.23)
1555+001	1978.8	aaaadab	1.53	1.58 .02	1.52	1.48 0.08	1.46 0.10	0.92 0.21	0.56 0.11
1607+268	1980.6	aaagcx-	4.43	3.11 .02	1.61	1.01 0.12	0.50 0.08	0.11 0.09	-
1611+343	1980.2	aaaadw-	2.61	2.51 .03	2.08	2.02 0.05	1.64 0.08	(1.22 0.11)	-
1622-253	1980.2	---vvww	-	-	-	3.13 0.10	2.65 0.16	1.94 0.10	0.82 0.08
1633+382	1978.8	aaaacaa	1.99	1.94 .02	1.59	1.91 0.07	1.72 0.06	1.45 0.15	0.96 0.31
1638+398	1978.8	aaabjab	0.44	0.44 .02	0.41	0.42 0.08	0.54 0.08	0.35 0.14	0.32 0.10
1641+399	1978.8	aaaabaa	6.91	8.09 .04	7.34	8.16 0.09	8.10 0.15	8.55 0.17	6.22 0.23
1642+690	1978.8	--abcaa	-	-	2.29	3.87 0.10	4.05 0.13	3.90 0.17	2.15 0.15
1652+398	1981.3	---xyz-	-	-	-	1.32 0.09	1.00 0.09	0.81 0.15	-
1656+053	1978.8	aaaacab	1.62	1.61 .01	1.82	2.06 0.06	1.55 0.09	0.53 0.19	0.43 0.08
1730-130	1978.8	aaaacab	5.13	5.58 .04	5.30	5.22 0.14	5.93 0.22	6.34 0.14	4.54 0.20
1739+522	1979.3	bbbf1cc	0.75	0.81 .05	1.08	1.97 0.11	2.09 0.06	1.72 0.10	1.26 0.09
1741-038	1978.8	aaaacaa	1.67	1.74 .02	2.26	2.81 0.08	2.96 0.11	2.65 0.13	2.25 0.39
1749+701	1979.1	bbbce--	1.52	1.34 .20	1.16	1.08 0.07	0.77 0.08	-	-
1749+096	1981.3	-aaxyzz	-	(1.09 .02)	(1.22)	1.73 0.10	2.60 0.12	2.78 0.12	2.43 0.40
1807+698	1978.8	aaabdaa	2.31	2.09 .03	1.77	2.23 0.11	1.90 0.10	1.55 0.16	1.16 0.12
1828+487	1978.8	baabcaa	13.55	9.02 .06	5.54	5.10 0.29	3.18 0.13	2.28 0.14	1.61 0.29
1845+797	1978.8	bbbbdad	10.14	6.20 .17	2.93	2.66 0.17	1.20 0.13	0.69 0.14	(0.44 0.18)
1909+048	1978.7	a-a----	0.73	-	0.40	-	-	-	-
1921-293	1978.8	---adaa	-	-	-	8.88 0.24	9.51 0.57	9.39 0.24	5.47 0.20
1958-179	1978.8	baaacaa	0.56	0.75 .02	0.79	1.10 0.06	1.11 0.09	1.38 0.11	1.31 0.25
2005+403	1978.8	aaaaaaa	3.11	5.04 .03	4.65	4.74 0.12	3.97 0.14	2.73 0.16	1.37 0.11

TABLE 13 (continued)

Source	Epoch	Code							
2021+614	1981.3	-z-yzz-	-	2.11 .05		2.54 0.07	1.78 0.11	1.49 0.08	-
2037+511	1978.8	aaaabaa	5.66	4.81 .04		4.60 0.07	5.03 0.12	4.71 0.19	3.06 0.31
2037+421	1978.8	-aabaa	-	15.42 .08		21.50 0.22	19.89 0.28	18.44 0.18	16.92 0.21
2048+312	1977.7	a-acdd-	0.71	-	18.21 0.43	0.32 0.07	0.55 0.09	(0.47 0.16)	-
2105+420	1979.8	-a-uveb	-	3.72 .01		6.25 0.11	6.18 0.12	5.78 0.07	4.80 0.16
2121+053	1978.8	aaaabaa	1.88	2.74 .03	3.01	2.97 0.05	2.75 0.11	2.31 0.17	1.23 0.10
2131-021	1978.8	aaaabaa	1.99	2.31 .04	2.30	2.37 0.08	2.01 0.11	1.44 0.15	0.99 0.15
2134+004	1978.8	aaaabaa	3.08	7.02 .04	9.78	10.53 0.17	7.32 0.16	4.74 0.21	2.01 0.16
2145+067	1978.8	aaaabaa	3.06	2.91 .02	2.54	2.82 0.09	3.84 0.12	3.51 0.12	2.77 0.13
2155-152	1978.8	--abdaa	-	-	1.59	1.51 0.13	1.41 0.10	1.08 0.16	0.75 0.23
2200+420	1978.8	aaaabaa	2.97	3.04 .07	2.68	2.70 0.06	2.56 0.10	2.39 0.15	1.66 0.27
2201+315	1978.8	baaaaaa	2.05	1.97 .03	1.82	2.37 0.11	2.18 0.11	2.55 0.13	2.63 0.10
2216-038	1978.8	aaaacaa	0.98	1.82 .01	3.44	4.70 0.18	4.62 0.18	3.65 0.15	2.42 0.26
2223-052	1978.8	aaaabaa	5.80	4.07 .02	3.54	3.48 0.11	3.88 0.16	4.33 0.21	3.91 0.18
2230+114	1978.8	aaabcaa	5.79	4.55 .02	3.09	2.27 0.09	2.06 0.10	2.63 0.15	3.78 0.42
2243-123	1978.8	aaaacaa	2.42	2.50 .02	2.63	3.05 0.09	3.03 0.14	2.90 0.11	2.05 0.15
2251+158	1978.8	aaaabaa	10.10	9.33 .04	8.02	7.81 0.11	6.04 0.15	4.92 0.22	4.32 0.15
2345-167	1978.8	aaabbaa	3.27	3.07 .02	2.52	2.24 0.10	1.52 0.12	1.14 0.14	1.12 0.08

211

Notes to Table 13

(1) Epoch of 31.4 measurement (or 15.5 GHz if no 31.4 GHz value), representing typical dates of observations.

(2) Dates of observations.

1.4 GHz
(a) 09/05/78
(b) 12/05/78

2.7 GHz
(a) 09/10/78
(b) 12/10/78
(z) 02/07/81

5.0 GHz
(a) 09/04/78
(b) 12/04/78

7.9 GHz
(g) 07/11/78
(a) 10/03/78
(b) 11/11/78
(c) 12/29/78
(d) 01/07/79
(e) 02/19/79
(f) 04/12/79
(t) 01/17/80
(u) 02/03/80
(v) 03/03/80
(w) 08/28/80
(x) 03/29/81
(y) 05/23/81
(z) 06/28/81

15.5 GHz
(j) 06/07/78
(a) 09/15/78
(b) 10/11/78
(c) 10/20/78
(d) 11/05/78
(e) 11/15/78
(f) 12/08/78
(g) 12/16/78
(h) 01/16/79
(i) 02/11/79
(v) 03/01/80
(w) 08/05/80
(x) 03/09/81
(y) 04/19/81
(z) 05/05/81

31.4 GHz
(d) 09/22/77
(a) 10/11/78
(b) 01/17/79
(c) 04/17/79
(e) 10/23/79
(w) 03/16/80
(x) 07/18/80
(y) 09/16/80
(z) 04/14/81

89.6 GHz
(d) 09/24/77
(a) 10/08/78
(b) 01/14/79
(c) 04/19/79
(w) 03/12/80
(x) 09/18/80
(y) 01/17/81
(z) 04/16/81

(3) Errors not listed for 1.4 and 5.0 GHz (see Tables 5 and 7). Flux densities in parentheses indicate measurement made at much different epoch than measurements at other frequencies.

Figures 22 (a to 1). One epoch radio flux density spectra (at 7 frequencies) for 103 sources. The epochs and flux density measurements are from Table 13.

Figure showing Flux Density (Jy) versus Frequency (GHz) for several radio sources: 0007+106 (III Zw2), 0048-097, 0106+013, 0133+476, 0219+428 (3C 66A), 0229+131, 0234+285 (CTD 20), 0235+164, 0237-027, 0238-084 (NGC 1052). Inset shows spectral index reference.

Flux Density (Jy) vs Frequency (GHz)

0528 + 134
0552 + 398
0605 - 085
0607 - 157
0723 - 008

0433 + 295 (3C 123)
0440 - 003
0454 - 234
0458 - 020
0528 - 250

Figure showing Flux Density (Jy) versus Frequency (GHz) for multiple radio sources: 0727−115, 0735+178, 0736+017, 0748+126, 0754+100, 0814+425, 0829+046, 0831+557, 0834−201, 0836+710.

218

Flux Density (Jy) vs Frequency (GHz) for sources 1514−241, 1548+056, 1555+001, 1607+268, 1418+546, 1458+718 (3C 309.1), 1502+106, 1510−089

Flux Density (Jy)

Frequency (GHz)

1611 + 343

1622 - 253

1633 + 382

1638 + 398
(NRAO 512)

1641 + 399
(3C 345)

1642 + 690

1652 + 398
(MKN 501)

1656 + 053

1730 - 130
(NRAO 530)

1739 + 522

1741 - 038

Figure showing Flux Density (Jy) versus Frequency (GHz) for multiple radio sources:
1921-293, 1958-179, 2005+403, 2021+614, 2037+511 (3C 418), 2037+421 (DR 21), 2048+312 (CL 4), 1749+701, 1749+096, 1807+698 (3C 371), 1828+487 (3C 380), 1845+797 (3C 390.3), 1909+048 (SS 433)

§2. Search for Single Epoch Optical-Radio Correlation

Simultaneous observations of the radio and infrared-optical emission in compact extragalactic sources indicates that the spectral-flux distribution can be explained as being due to synchrotron emission throughout the frequency interval. The spectra usually show flat radio spectra with steeper, power-law spectra at infrared and optical wavelengths. Several studies have been made of the broadband radio-infrared-optical spectra (e.g. O'Dell et al 1978) in order to investigate this proposed relationship between the radio and optical emission mechanisms. The shape of the spectra strongly indicate that the radio spectra can be smoothly extrapolated to connect with the infrared-optical spectra.

This result suggests that the optical and radio properties of a source may be correlated. One specific property that has been investigated (in lieu of multi-frequency quasi-simultaneous spectra) is the relationship between the flux density at radio and optical wavelengths. Owen and Mufson (1977) observed (at 90 GHz) a sample of flat spectrum radio sources which had originally been detected in a survey made at 5 GHz. Twenty two of the sources detected at 90 GHz were identified with optical sources on the Palomar Sky Survey plates. A linear regression analysis was performed finding a correlation coefficient r = 0.55. This result correponds to a 99% confidence that the optical and radio strengths were correlated. Surprisingly, the observed 3 millimeter flux

density and optical magnitude were found to be correlated, despite the observations having been obtained 20 years apart! A similar analysis between the 5 GHz and optical measurements, r = 0.31, indicated that the measurements were uncorrelated.

A more accurate test of correlated radio-optical emission requires simultaneous measurements at these frequencies. The radio measurements from Table 13 were used, along with the optical observation from Pica et al (1980) or Pollock et al (1979) (see Chapter II) closest in time to the radio observations. Only sources which had flat spectra ($\alpha > -0.5$) were used in the correlation analysis. Sources identified with galaxies were not included, since the optical magnitude would include the surrounding galaxy as well as the nucleus. Correlations were searched for between the single epoch measurements, the average source flux density, and the minimum observed flux density for the 2.7 GHz:optical, 31.4 GHz:optical, and 90 GHz:optical data sets.

No correlation was found between the single epoch radio and optical flux densities. The single epoch 90 GHz:optical flux densities are shown in figure 23. The calculated correlation coefficient for 24 sources was r = 0.22 (confidence <0.80). A similar coefficient was found between the 2.7 GHz and optical single epoch measurements (r = 0.23 for 25 sources, confidence <0.80).

In comparing this result to that of Owen and Mufson, it should be mentioned that weak optical and radio sources were selected against in

the study reported here (they would not be included in a variability study). Investigation of the results of Owen and Mufson indicate that deleting the weak sources (both optical and radio) would not destroy the correlation. Their correlation appears to be due to the stronger sources at both frequencies. The sources included in the study here were not selected from any complete statistical sample of sources, which may be the cause of the difference between the results of Owen and Mufson and this study.

It should be noted that the observed flux densities, rather than the intrinsic luminosities, have been used for the correlation search. A more meaningful analysis would have been based upon the luminosities, but the redshifts were not known for several of the quasars and BL Lacertae objects in the list of Owen and Mufson. Regardless, the correlation between radio and optical flux densities observed by Owen and Mufson has not been confirmed, at the epoch chosen, for the sample of sources included in this dissertation.

The next approach to take in the study of correlated radio-optical emission is to search for correlations in the time variability of sources. This study is undertaken in the next chapter.

Figure 23.   Comparison of one epoch flux densities at radio (90 GHz) and optical wavelengths.   Symbols: Quasar (o), BL Lac object (x), and galaxy (*).   Parentheses surrounding the point indicate sources which show a falling spectrum at millimeter wavelengths ($\alpha < -0.5$).   The lines indicate radio (90 GHz) - optical spectral indices of -1.0, -0.75, and -0.5.

1 EPOCH FLUX DENSITY

CHAPTER VI

SEARCH FOR CORRELATED VARIABILITY AT RADIO AND OPTICAL WAVELENGTHS

§1. Introduction

Variability of the radio and optical emission in compact extragalactic sources has been well documented. However, the relationship between variations at optical and radio wavelengths has been studied for only a small number of sources. Convincing evidence for correlated activity has been presented for a few objects, but no general relationships between radio and optical variability have been found.

The only extensive study of long-term variability in a large sample of sources was by Pomphrey et al (1976). Observations of 22 active sources, covering a decade of time, were investigated for correlated radio and optical events. Radio observations at 1.8 cm (Dent et al 1974) and 2.8 cm (Medd et al 1972) were compared with optical observations (predominantly from the Rosemary Hill Observatory of the University of Florida). Except for the BL Lacertae type quasi-stellar object OJ287, no significant correlations were found between the radio and optical variations. The correlation in OJ287 was not between individual outbursts but rather was due to similar radio and optical outburst envelopes during the time interval 1970-1974. Usher (1979) subsequently presented evidence for several synchronous individual radio-optical outbursts in OJ287 during this period.

Other studies have dealt with single objects, usually investigating short term variations over time spans of a few weeeks to at most a few years. Several programs of coordinated observations of the BL Lac objects OJ287 and BL Lacertae were conducted in the early 1970s during the period when both sources were active at both optical and radio wavelengths (Epstein et al 1972; Hackney et al 1972; Kinman et al 1974; Andrew et al 1974). The results of these studies were inconclusive, with no clear correlations found.

Correlated variations have recently been reported for three objects: two outbursts in the BL Lac object 0235+164 (Balonek and Dent 1980 and references therein), a single time-delayed outburst in the quasar 0420-01 (Dent et al 1979), and two events in the quasar 1921-29 (Dent and Balonek 1980; Gilmore 1980). In the case of 0235+164, the radio and optical outbursts peaked simultaneously. A detailed discussion of the results of these previous studies will be presented within the discussion of individual sources in §4.

Except for the outbursts in 0235+164 (Rieke et al 1976; Pica et al 1980) and a single outburst in 1308+326 (Puschell et al 1979) the optical-infrared continuum spectral evolution has not been observed during the periods of correlated rapid radio-optical activity. Thus the evolution of the radio-optical spectral flux distribution for the outbursts is not known. Observations of the broadband spectral evolution could provide unambiguous evidence for correlated activity.

Although the number of objects exhibiting correlated radio-optical activity is too small to determine characteristics common to this sample, there are several radio and optical variability characteristics which are common to many sources. These characteristics reflect the physical processes occurring in variable sources and should be considered when searching for correlated activity.

(1) The typical timescale of variation at optical wavelengths is shorter than at centimeter radio wavelengths. Significant optical variations can occur within days, whereas centimeter variations occur on timescales of months to years. Observations at millimeter wavelengths (Chapter IV; Epstein et al 1980) indicate that variations are more rapid at the shorter radio wavelengths, although it has not been conclusively shown that they are as rapid as the optical fluctuations. The search for correlated activity should be sensitive to this difference in timescale, and not be a priori biased against differing timescales. For example, 0235+164 shows optical "spikes" which are of much shorter duration than the radio events but also has underlying low level optical activity that has comparable timescales to the radio (Balonek and Dent 1980).

(2) The outburst amplitudes vary between outbursts and exhibit frequency dependence. This is clear from a casual inspection of the radio variations. Frequency dependent amplitude has not been as widely demonstrated for optical/infrared bursts due to the paucity of extensive

broadband coverage during the short events. However, infrared-optical spectral steepening has been observed during outburst decays in a few objects (O'Dell et al, 1977; O'Dell et al 1978; Puschell et al 1979). There is no compelling reason to expect outbursts to exhibit consistent radio/optical flux density ratios. Physical conditions within the source and particle energy or spatial distributions may be different for each outburst.

(3) The frequency dependent time-delay of the onset or peak of radio outbursts may vary between outbursts due to changing opacity or particle spatial distribution. Optical-radio correlation studies have typically employed centimeter observations, where opacity effects can result in time delays as large as months or years. Knowledge of the radio spectral evolution is necessary to deduce this delay. As discussed in Chapters IV and V, outbursts are usually initially opaque at frequencies below 15 GHz. Additionally, decay times are longer at the longer wavelengths, resulting in the superposition of outbursts. Thus correlations using longer wavelength radio observations would be more difficult to establish. Low correlation coefficients from numerical correlation analyses would result from different time delays in sequential outbursts.

(4) Since the physical conditions which may produce both radio and optical activity are unknown, one cannot exclude a priori those variations which seem unusual (e.g. radio variations preceding the optical activity). For example, it is widely accepted (Kellermann and

Pauliny-Toth 1981) that the two periods of activity discussed by Balonek and Dent (1980) in 0235+164 exhibit correlated optical-radio activity, even though the sharp optical "spikes" appear to follow the commencement of the radio outbursts.

(5) Long timescale (many year) correlated activity has not been adequately studied. Due to the short span of time during which both radio and optical observations have been conducted, studies have necessarily been limited to short-term activity. The observations reported here cover a decade in time, permitting investigation of long timescale correlations.

Previous studies of optical-radio activity in extragalactic sources have been limited by the lack of well-sampled, long-term radio and optical observations. The data sets described in Chapter II provide extensive frequency and temporal coverage of a large sample of sources, permitting a broader investigation of variability than previously possible. A complete review of the optical and radio observations for all the sources is beyond the scope of this dissertation. A thorough review of the optical and infrared variations of optically violent variables (OVVs) is presented in Pollock (1982).

The procedures employed in searching for correlated radio-optical activity are described in §2. Results for the entire sample of sources are discussed in §3, with individual sources detailed in §4. Plots of the time variability in the 45 sources included in this study appear in

Appendix A, and plots of the linear correlation coefficient for several sources appear in Appendix B. A summary of the results from the correlation search appears in §5.

§2. Correlation analysis procedures

In this chapter, 45 extragalactic sources (Table 1 in Chapter II) are investigated for correlated radio-optical activity. The variations at 15.5 GHz are compared with the University of Florida optical variations. The optical magnitudes have been converted to flux densities (see Chapter II). The 15.5 GHz radio data is used since this is the highest frequency for which well-sampled (~monthly) observations have been obtained. The lack of extensive coverage at higher frequencies, where variations are faster, precludes their being used for correlation searches in most sources. At frequencies below 15.5 GHz, the coverage is comparable, but opacity amd source evolution effects dominate the variations. For those sources in which correlated radio-optical activity is suspected, the radio observations at other frequencies are used to define the spectral evolution of the outbursts.

Plots of the 15.5 GHz and optical variations for all 45 sources in common to the University of Massachusetts and the University of Florida monitoring programs are presented in Appendix A. Some sources have limited coverage either at radio or optical frequencies, but are included for completeness.

The first step in the search for correlated activity was a careful visual inspection of the 15.5 GHz-optical variations. Emphasis was placed on long-term trends ("envelopes" of variations) as well as radio counterparts to the sharp optical features. This procedure is sensitive to certain variation features that would be missed in a numerical cross-correlation (e.g. varying timescales, variable flux ratios), but can also be strongly influenced by investigator biases.

In order to obtain a quantitative measure of possible correlations, numerical cross-correlations were performed. Since cross-correlation between two sets of unevenly spaced data is numerically difficult, it is desirable to generate evenly spaced interpolated values for at least one of the data arrays. Optical variations are so rapid and irregular that realistic interpolations cannot be made. The radio variations are not as rapid and the spacing between observations more uniform, so interpolated values can reliably be determined for all but the most rapid variables. Daily interpolated radio values were calculated by fitting a fourth order least-squares polynomial to the observations (Bevington, 1969; pp 140-142). To save computation time, the polynomials were fit at intervals of 1/6 the average time interval between observations (generally 5 to 10 days since observations were conducted monthly to bimonthly). The fit used the 7 observations nearest the interpolated date, weighting each measurement by the product of the reciprocal of the observed error and a gaussian (smoothing) weighting factor

$$G = e^{-0.5(\Delta t/1.5\Delta T)^2} \tag{VI-1}$$

where Δt is the time between the interpolated date and the date of observation, and ΔT is the average time interval between the seven observations.

The fit to the source 1921-29 is shown in figure 24. The discrete jumps in the fit occur at the dates when the interpolation time interval is changed. The interpolation routine had some difficulty fitting single extremum data points (about 10 instances in the entire sample). For times near the extremum measurements, the fit followed the trend in the variation but with a smaller amplitude than suggested by the single data point. Visual inspection of these poorer fits indicates that their effect on the numerical cross-correlation (§3) will be minor. The fit was unsatisfactory for long time intervals which contained only a few scattered measurements. If a good fit was not obtained, the time interval was deleted from the correlation analysis.

The linear-correlation coefficient (Bevington, 1969; pp 119-127) was calculated for a range of time shifts between the interpolated radio and the discrete optical arrays. The errors in the optical flux density are not considered in the calculation. The errors associated with the radio measurements are reflected in the polynomial fit. The linear cross-correlation coefficient, r (reflecting the probability that a linear correlation will be observed in a random sample of observations from uncorrelated populations), is given by (Bevington, equation 7-5)

$$r(\Delta t) \equiv \frac{N \sum x_i y_i(\Delta t) - \sum x_i \sum y_i(\Delta t)}{\left(N\sum x_i^2 - (\sum x_i)^2\right)^{1/2} \left(N\sum y_i^2(\Delta t) - (\sum y_i(\Delta t))^2\right)^{1/2}} \qquad \text{(VI-2)}$$

Figure 24. Polynomial interpolating fit to the 15.5 GHz radio observations of the quasar 1921-29. A fourth order polynomial was fit to the seven measurements closest in time to the date of interpolation.

1921-29 15.5 GHz

LEAST SQUARES 4TH ORDER
POLYNOMIAL FIT

239
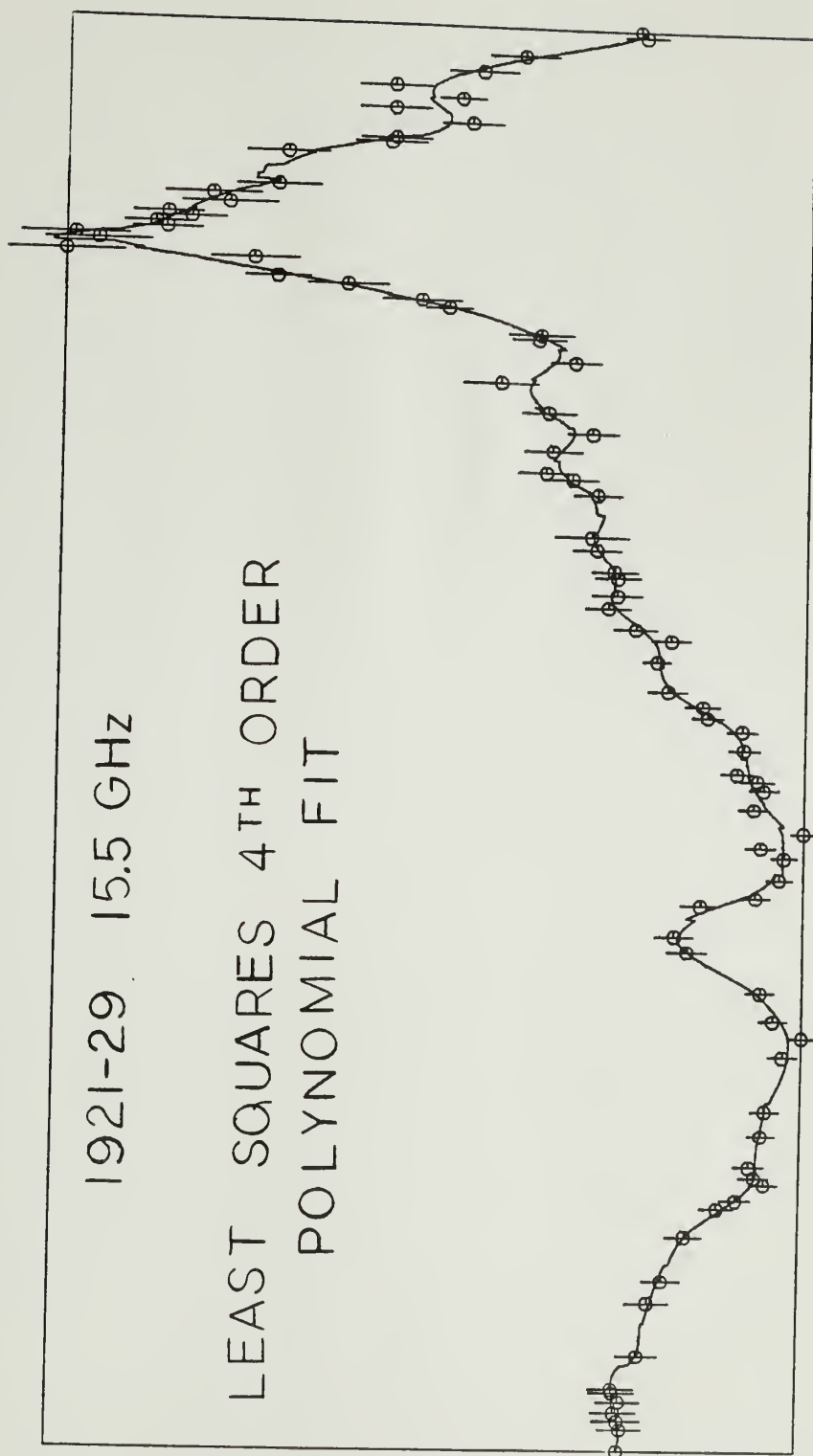
where x is the interpolated radio array, $y(\Delta t)$ is the array of optical observations offset by a time Δt, and N is the number of dates for which both radio and optical (with delay) values exist. Dates for which either no radio or optical data exist are ignored, and are not considered in the summations. A value of $r=\pm 1$ corresponds to a perfect correlation, and a value of 0 to no correlation. The confidence level for the correlation is determined from the linear correlation coefficient, r, and the number of points used in the correlation, N. As discussed by Usher (1979), the measurements are not randomly distributed since each observation is related (by physical processes) to the previous and following values. The confidence quoted for the linear correlation coefficient is thus only a relative measure of the correlation.

All sources which had more than 10 measurements at both optical and radio wavelengths were searched for correlations using the entire data set at both frequencies. Correlations were calculated at 15 day intervals for time delays from -900 days (optical events preceding radio) to +900 days. Fifteen days was chosen as the time increment since this is ~1/2 the typical interval between observations at 15.5 GHz (more frequent spacing would oversample the data, while less frequent would be insensitive to variation timescales comparable to the observation intervals).

Several sources were analyzed using a subset of the total data sets at either wavelength. These sources were selected based either on the results of the correlation with the entire data set or from the visual inspection of the variability curves.

§3. Cross-Correlation Results

Visual classification of the variability characteristics. The first step in the correlation search was to visually inspect the radio and optical variability records of Appendix A. Five variability characteristics were searched for: (1) short term activity (timescale less than ~3 to 5 years); (2) rapid short term activity (timescale <1/2 year); (3) "spike-like" behavior (timescale of months or less, with the variation greater than two σ above adjacent longer timescale measurements; (4) long timescale (>5 years) single, smooth outbursts; and (5) "envelopes" of emission (multiple, possibly overlapping, events superposed upon systemmatic changes occurring over a several year span).

The assignment of a particular characteristic to a source is a subjective process. These classes of variability are not well-defined, sources exhibit several of these characteristics, and gaps exist in the observational data (particularly the optical) which prevent the complete specification of outbursts. It was not always possible to distinguish between long timescale and envelope activity. The assignment was based upon the degree of fluctuations about the more gradual changes. It was difficult in some cases to distinguish between spike-like activity and rapid outbursts. The spike-like activity was not as clearly determined for some sources (e.g. 3C120, 1510-08) as it was in other more extreme examples (e.g. 1730-13).

The results of the visual search are given in Table 14. A source was judged as either exhibiting the characteristic (Y = Yes), possibly

TABLE 14

OPTICAL AND RADIO (15.5 GHz) VARIABILITY CHARACTERISTICS

Source	ID[1]	E_{opt}[2]	E_{rad}[3]	Variability Classification[4]											
				a	b	c	d	e	f	g	h	i	j	k	l
0007+10	G	3.9	5.8	Y	Y	N	N	Y	Y	Y	Y	N	N	3	3
0048−09	B	7.5	6.6	Y	Y	N	N	Y	Y	Y	Y	Y	Y	10	10
0133+47	Q	3.4	3.6	–	N	–	N	Y	Y	Y	Y	Y	Y	1	10
3C66A	B	3.2	2.2	N	N	N	N	Y	N	Y	N	–	N	7	7
0229+13	Q	2.0	2.5	N	–	N	P	N	N	N	N	N	N	11	4
0235+16	B	88.0	7.8	N	N	N	N	Y	Y	Y	Y	Y	Y	5	5
0306+10	B	8.8	1.5	N	–	N	–	Y	P	Y	–	Y	–	2	1
0333+32	Q	2.0	2.9	N	N	N	Y	Y	N	P	N	N	N	10	10
CTA26	Q	3.1	2.8	N	N	N	N	Y	Y	Y	Y	P	N	11	11
0420−01	Q	23.5	4.9	N	P	N	N	Y	Y	Y	Y	Y	N	11	11
3C120	G	4.7	9.4	Y	Y	N	N	Y	Y	Y	Y	Y	P	9	15
0440−00	Q	10.1	4.1	N	Y	N	N	Y	Y	Y	N	Y	N	11	11
0735+17	B	21.5	2.3	N	N	N	N	Y	Y	Y	N	Y	N	10	12
0736+01	Q	3.4	3.1	Y	P	N	N	Y	Y	Y	Y	Y	N	10	10
OJ287	B	41.1	6.0	Y	Y	N	N	Y	Y	Y	Y	Y	Y	11	10
0906+01	Q	5.2	1.4	N	–	N	–	Y	P	Y	–	Y	–	10	1
0953+25	Q	2.6	3.1	P	Y	N	N	Y	Y	Y	P	N	N	11	10
1101+38	B	2.5	2.5	–	N	N	N	Y	Y	Y	N	N	N	3	4
1116+128	Q	3.7	1.9	P	N	P	Y	Y	N	P	N	N	N	10	3
1127−14	Q	1.3	2.5	P	Y	N	N	N	N	N	N	N	N	7	12
1156+295	Q	30.7	–	–	–	–	–	Y	–	Y	–	Y	–	1	0
1219+28	B	6.9	5.5	P	P	N	N	Y	Y	Y	Y	Y	P	9	10
3C273	Q	2.3	2.9	N	Y	N	P	Y	Y	Y	N	N	N	7	16
3C279	Q	3.7	2.2	N	N	–	Y	Y	Y	P	N	N	N	5	16
1308+326	B	30.9	1.6	N	P	N	N	Y	Y	Y	N	Y	N	5	5
1510−08	Q	3.7	5.0	N	N	N	N	Y	Y	Y	Y	Y	Y	12	11
1514−24	B	10.0	2.6	N	Y	N	N	Y	Y	Y	N	Y	N	9	9
1638+39	Q	15.4	6.9	P	Y	N	N	Y	Y	Y	N	Y	N	11	11
3C345	Q	6.0	2.9	N	P	N	Y	Y	Y	Y	N	N	N	10	15
1652+39	B	2.3	1.7	–	–	–	–	Y	–	N	N	N	N	2	1

TABLE 14 (continued)

(1)		(2)	(3)	(a)	(b)	(c)	(d)	(e)	(f)	(g)	(h)	(i)	(j)	(k)	(l)
1730-13	Q	15.9	2.1	P	P	N	N	Y	Y	Y	N	Y	N	~4	13
1749+70	B	2.0	2.2	-	-	-	-	P	Y	N	N	N	N	2	3
1749+09	B	14.3	2.1	-	-	-	-	Y	Y	Y	P	Y	N	2	1
3C371	G	4.7	2.3	P	P	N	N	Y	Y	Y	N	Y	N	12	13
3C390.3	G	3.9	2.0	Y	N	N	N	Y	P	P	N	P	N	8	11
1921-29	Q	11.9	4.8	P	N-P	N	Y	Y	Y	Y	P	Y	N	5	10
2131-021	B	3.2	2.7	N	N	N	N	Y	Y	P	N	N	N	4	6
2134+00	Q	1.7	2.0	N	Y	N	Y	N	N	N	N	N	N	8	12
2145+06	Q	2.2	2.0	N	N	Y	Y	N	N	N	N	N	N	12	12
BL Lac	B	13.0	10.8	N	Y	N	N	Y	Y	Y	Y	Y	Y	10	12
2216-03	Q	1.9	2.1	N	N	N	Y	P	N	N	N	N	N	12	11
3C446	Q	22.1	2.0	P	N	N	N	Y	Y	Y	N	Y	N	9	13
CTA102	Q	2.8	2.9	N	P	N	N	Y	Y	Y	Y	N	Y	8	11
3C454.3	Q	3.8	4.9	N	P	N	Y	Y	Y	Y	P	P	N	9	11
2345-16	Q	10.3	3.6	N	Y	N	P	Y	Y	Y	Y	Y	N	12	11

Notes to Table 14

(1) Identification (see Table 1): Q= Quasar, B= BL Lacertae object, G= Galaxy.
(2) $E_{opt} \equiv S_{max}/S_{min}$ for optical data.
(3) $E_{rad} \equiv S_{max}/S_{min}$ for radio data.
(4) Characteristics of variability:
   Y= Yes, N= No, P= Possibly, -= not sufficient data to determine.
 (a) Long term trend over several outbursts (e.g. envelope) at optical?
 (b) Long term trend over several outbursts (e.g. envelope) at radio?
 (c) Long term single outbursts at optical?
 (d) Long term single outbursts at radio?
 (e) Short term (<3 to 5 years) activity at optical?
 (f) Short term (<4 to 5 years) activity at radio?
 (g) Rapid short term activity at optical?
 (h) Rapid short term activity at radio?
 (i) Spike-like activity at optical?
 (j) Spike-like activity at radio?
 (k) Number of years observed at optical wavelengths.
 (l) Number of year observed at radio wavelengths.

exhibiting (P), not exhibiting (N), or insufficent data to determine (-). Also given in the table is the fractional range in observed flux density, $E \equiv S_{max}/S_{min}$, and the number of years that the source has been observed.

The ratio of the extremum flux densities, E, at optical and radio wavelengths does not show a correlation (Figure 25). There is also no strong distinction between the distribution of $E_{opt}:E_{rad}$ for BL Lac objects and quasars. The BL Lac objects do show the more extreme E_{opt} values, and a greater fraction of them have $E_{opt} > 10$, but the difference is not pronounced. Of the sources which have been observed for more than three years, seven of the twenty three quasars, six of the twelve BL Lac objects, and none of four galaxies has $E_{opt} > 10$. All thirteen high E sources show optical spike-like behavior (Table 14). Of the twenty six sources with $E_{opt} < 10$, none lies beyond the range $1/2 < (E_{opt}/E_{rad}) < 2$. The large optical range is clearly associated with the rapid "spike" phenomena.

The small value of E at radio wavelengths may be due in part to the presence of a strong component (either constant or slowly variable) underlying the more rapid radio variations. This component could be the result of overlapping, long timescale decays from several outbursts or from a constant decimetric component. In Chapter IV, it was shown that outburst decays are rapid at millimeter wavelengths, so it may be expected that fractional variability would be larger at shorter wave-

Figure 25. Observed range of radio and optical flux densities, given as the ratio $E \equiv S_{max}/S_{min}$. Quasars are indicated by the symbol (o), BL Lac objects by (x), and galaxies by (*). Sources which exhibit spike-like optical flares are boxed. The lines indicate values of $E_{opt}/E_{rad} = 1/2$, 1, 2, 5, and 10. Note that all sources not exhibiting spike-like acivity fall in the range $1/2 < (E_{opt}/E_{rad}) < 2$.

OPTICAL-RADIO RANGES
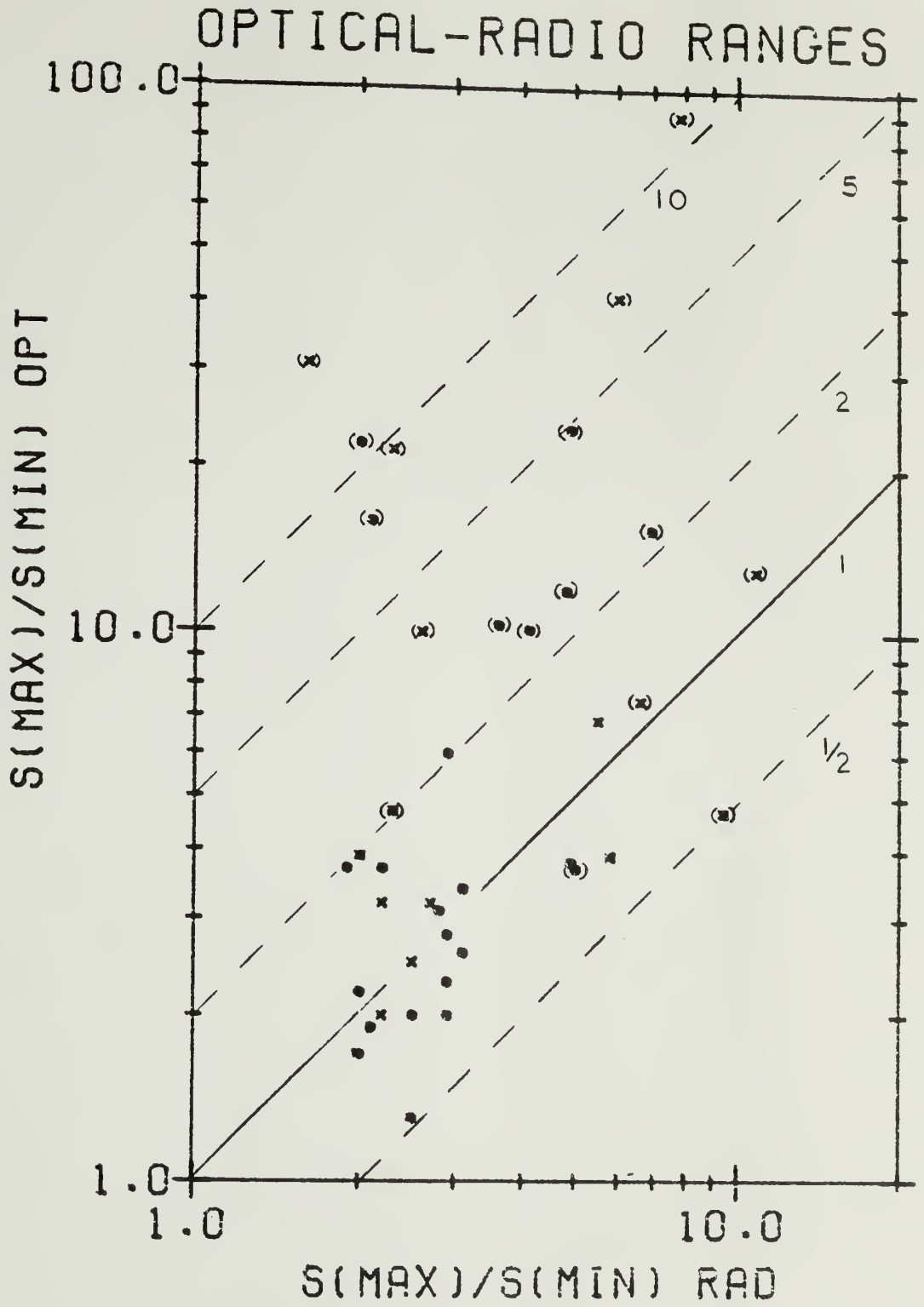
lengths. To test this hypothesis, an E value was calculated for sources at 90 GHz (from Chapter II). Although the data is more limited in time than the optical and 15.5 GHz records, several examples of large fractional variation (>10) were found. Specifically: 0007+10 (64.3), 0048-09 (19.7), OJ287 (10.7), 1510-08 (10.9), and BL Lac (11.9). The error in the E values increases for sources with high E since these sources have low S_{min}, with S_{min} of comparable strength to the measurement error.

It is not clear that the fractional variability is an important factor for discussing the physical processes in radio outbursts. However, it is relevant to the correlation search, since the sources exhibiting high fractional variability are the spike-like sources. These spikes are much shorter in duration than the radio events. A high numerical correlation coefficient cannot be expected in these sources due to the differing optical spike and radio outburst timescales and amplitudes. However, the linear correlation coefficient, r, for the spike-like sources is useful for determining the offset of the radio and optical maxima (the correlation is basically that of a delta function at optical wavelengths with the radio variations).

Sources which do not exhibit the spike-like phenomena have comparable fractional optical and radio flux density ranges. In these sources, which also show longer timescale variations, the numerical correlation procedure is more approporiate to searching for correlated activity.

<u>Visual</u> <u>search</u> <u>for</u> <u>radio</u> <u>events</u> <u>concurrent</u> <u>with</u> <u>optical</u> <u>spikes</u>. Since the spike-like activity appears to be a distinct phase of activity from the longer term variations, the correlation of these events with radio variations was separately studied. The variability records were visually searched by overlaying the optical record upon the radio record. Several optical events could be classified as either "spikes" or rapid outbursts. The radio activity at the time of the optical spikes are tabulated in Table 15. Those optical events which are not distinctively "spikes" (and may be rapid outbursts) are noted in parentheses. The higher radio frequency variations were also inspected for variations. If the identification of the activity at these frequencies differs from that at 15.5 GHz, it is noted. In radio events which show a time delay, the higher frequency activity will correspond more closely with the optical activity.

The results of this search are striking: there is a large fraction of radio peaks that occur simultaneous with the optical spikes. Of the 74 optical spikes with corresponding radio data, 51% occurred at radio peaks (p or b), with another 16% occurring just prior to or after the peak or within extended (year or longer) maxima. Only 11% occur at times not clearly associated with radio outbursts, with 11% occurring at the onset of outbursts.

To test whether the observed correlation of optical spikes with radio peaks was due to chance, the radio plots were reversed in time,

TABLE 15

VISUAL CORRELATION SEARCH FOR COUNTERPARTS TO OPTICAL SPIKES

Source	Number Optical Spikes[1]	Radio Activity During Optical Spikes[2]
0048−09	3 (4)	1972.9 p; 1974.9 p+,i; (1976.0 b); 1980.9 b
0235+16	2	1975.9 p; 1979.1 p
0306+10	1	1975.9 n
CTA26	3	1976.8 m (31.4 o); 1978.2 p; 1980.9 p− (31.4 p−; 89.6 p or p−)
0420−01	2 (3)	1975.2 m (31.4 b); 1978.0 o (31.4 o); 1979.8 p+
3C120	3 (8)	(1971.8 p); (1974.9 o);(1975.1 p− (31.4 p)); 1975.8 i,c; 1976.2 i or p; 1976.8 p; 1978.7 p; 1980.2 p
0440−00	3	1975.9 b; 1976.9 b−; 1978.0 i or c
0735+17	1 (6)	(1973.3 o); 1974.1 i (31.4 p); (1975.0 p); (1976.0−76.2 i); 1978.1−78.3 p to p+; 1980.8 b (31.4 b)
0736+01	0 (3)	(1975.1 b (31.4 m)); (1976.2 b); (1978.9 p)
0J287	3 (6)	1972.0 p; 1973.0 p; (1974.4 b); (1978.0 b+); 1978.8 p; (1981.2 i,o (31.4 p−))
0906+01	2	1971.1−71.3 n; 1974.3 n
1156+295	1	1981.2−81.6 n
1219+28	3 (4)	1975.5 p; 1976.4 b (31.4 b); 1977.2 m,o (31.4 o); (1979.3 o,r)
1308+326	4 (5)	(1977.2 b); 1978.2 r; 1978.4 p−; 1979.1 m,o; 1980.5 m or i (31.4 c or p); 1981.3 n (31.4 c)
1510−08	2	1972.4 i or p (31.4 p); 1975.4 r (31.4 p)

TABLE 15 (continued)

1514-24	1	1977.3 p+,c
1638+39	3 (5)	1970.3 n; 1971.6 r,b; 1972.2 b or i; (1972.8 p or p+ (31.4 p)); 1974.3 d or i
1730-13	1	1977.7 b (31.4 p+ or d; 89.6 m,o)
1749+09	1	1979.8 n
3C371	3	1975.4 d (31.4 b); 1977.6 b+ or d,i; 1978.6 c,m or c,i
1921-29	1 (2)	1977.5 p- (31.4 p or b; 89.6 p or b); 1979.5 o,p- (31.4 p-; 89.6 p-);
BL Lac	4 (7)	1971.7 m or i (31.4 m or i); (1972.3 i (31.4 b)); 1973.4 p (31.4 p); 1975.8 d or m; (1976.4 p); 1978.6 p or i; (1979.5 m)
3C446	4 (5)	1974.7 i (31.4 p); (1976.0 p+); 1977.8 i,m or o (31.4 o; 89.6 o); 1978.7-78.9 p+ (31.4 i; 89.6 p); 1980.0-80.4 p- or p (31.4 p; 89.6 p)
3C454.3	1 (2)	(1971.6 p- (31.4 i)); 1979.8 o (31.4 o; 89.6 o)
2345-16	1	1970.0 n

Notes to Table 15

(1) Number of optical spike-like outbursts (including less certain identifications).
(2) Radio activity at 15.5 GHz during the time of outburst (activity at other frequencies (in GHz) given in parenthesis).
   Symbols:
   b = small outburst
   c = constant or no change
   d = during decline of outburst
   i = inflection in rise or decline of outburst
   m = minimum
   n = no data
   o = onset of outburst
   p = outburst peak
   p- = prior to outburst peak or beginning of extended outburst
   p+ = after outburst peak or at end of extended outburst
   r = during rise of outburst

overlayed on the optical plot, and analyzed by the same procedure. Comparison indicates a higher percentage in the real data (51% versus 28%) of identifications at peaks of outbursts or small events ("blips").

The conclusion to be drawn from this visual correlation is that a significant fraction (>1/4)of optical "spikes" are associated with maxima or outbursts at radio wavelengths. There is no obvious relationship with the onset of radio outbursts, or with the time just prior to or following the radio maxima. There is no evidence that radio outbursts are generally time delayed reponses to spikes or rapid optical bursts. A significant fraction of the observed rapid optical events show no obvious corresponding centimeter radio activity.

Visual search for correlated long timescale activity. Several sources exhibit similar long term variations. This activity can be classified into two general categories - long-term, several year declines or rises in flux density upon which are superposed shorter timescale activity; and periods of intense activity ("envelopes" separated by periods of only minor activity. Unless there are several repetitions of these two types of activity within a source, chance correlation between the similar radio and optical profiles cannot be discounted.

Sources exhibiting long-term declines at both 15.5 GHz and optical wavelength include: 0007+10, 0048-09, 3C120, and 0953+25. Sources exhibiting of activity include 0420-01, OJ287, 1638+39, and 3C454.3. To establish a correlation between these radio and optical trends requires

a thorough analysis of the spectral evolution. Sources are discussed on an individual basis in §4.

Numerical correlation. The linear correlation coefficient, r (equation VI-3), was calculated for each source at time delays between -900 and +900 days using the entire optical and radio data sets. For sources which show visual correlation during some portion only of the entire data set, the linear correlation coefficient was calculated for this limited time interval. Plots of the results for some sources appear in Appendix B.

The source name, maximum linear correlation coefficient (r), corresponding time shift, half-width of the peak, and number of optical-radio data points which were used in the calculation of r are given in Table 16. Also included are the linear correlation coefficient for zero time delay (and the number of data values), and comments on the correlation. If the correlation coefficient showed no significant maximum, an "NC" appears in place of the correlation coefficient value. The results for individual sources are discussed in §4.

§4. Radio - Optical Variations in Individual Sources

In this section, the radio and optical variations in 45 sources are discussed, with the intent of identifying correlated activity. Plots of the radio (15.5 GHz) and optical (B or pg) measeurements are presented in Appendix A. The results of the numerical linear correlation analysis

TABLE 16

LINEAR CORRELATION COEFFICIENTS

Source	r^1	Δt^2 (days)	HW^3 (days)	N^4	$r\ (\Delta t=0)^5$	Comments[6]
0007+10	~0.4	−50	380	23	0.32 (23)	cagekl
0048−09	0.72*	−30	−	57	0.71 (57)	gbc
"	0.91*	+30	90	16		a opt. pre 1974.5
"	0.58*	−15	70	28		bc
3C66A	NC				−0.34 (36)	
0229+13	NC				−	k
0235+16	0.45*	0	65	81	0.45 (81)	b
"	0.80*	0	25	14		a opt. pre 1977.0
"	0.51*	0	~35	27		a opt. 1978.5−79.5
"	0.34*	−15	~30	32		b opt. post 1979.5
0333+32	NC				−0.19 (31)	
CTA26	0.52	~−300	440	46	0.08 (47)	bl
0420−01	0.61*	−260	~365	97	0.40 (103)	bde
or	0.75*	−720	~365	89		
"	0.73*	−645	215	37		be opt. post 1977.5
3C120	0.77*	−75	240	108	0.76 (108)	dbfg
"	0.77*	−145	150	35		b(d) both pre 1974.3
"	0.62*	−130	145	28		bd both 1974.3−77.3
0440−00	0.35	0	455	57	0.35 (57)	gfc
0735+17	0.18	+45	60	170	0.11 (170)	ie
"	0.71*	+15	75	55		a opt. 1976.5−78.5
"	0.64*	−5	50	39		b opt. post 1978.5
0736+01	NC				−0.33 (74)	
OJ287	0.81*	0	~255	162	0.81 (162)	bdg
"	0.40*	0	30	25		b opt. 1971.5−72.5
"	0.61*	−35	~160	103		b both post 1974.5
0953+25	NC				0.38 (54)	gcf
1101+38	NC				−	k
1116+128	NC				−	k
1219+28	NC				0.15 (90)	
or	0.66	+405	~210	89		e
3C273	NC				−0.29 (64)	
3C279	NC				0.17 (32)	k
1308+326	0.40	−45	210	53	0.40 (58)	beg

TABLE 16 (continued)

1510-08	0.36*	-90	75	46			
1514-24	NC				0.19 (46)	jea	
1638+39	0.50*	+30	180	128	0.25 (85)		
3C345	NC				0.49 (128)	db	
or	0.60	-720	200	148	-0.09 (168)		
	0.34	+45	90	85		a	
1730-13	NC					ac	opt. post 1974.0
or	0.65	-15	~95	28	0.63 (28)		
						j	
1749+70	NC						
3C371	NC				−	k	
3C390.3	0.65	+60	120	56	0.10 (104)		
1921-29	0.79*	-250	210	34	0.58 (56)	d	
"	0.87*	-190	220	23	0.11 (42)	bd	
2131-021	0.86*	0	255	7		d	opt. post 1978.0
					0.86 (7)	ka	
2134+00	NC				0.06 (24)		
2145+06	NC				0.13 (60)		
BL Lac	NC				-0.12 (224)		
"	0.76*	+30	55	24		ib	
						a	opt. post 1980.1
2216-03	NC				-0.09 (12)		
3C446	0.60	~-560	~340	68	0.05 (83)		
"	0.74	~-520	260	36		gejd	
						ejdg	opt. post 1977.0
CTA102	NC				0.15 (30)		
or	0.58	-345	~130	26			
3C454.3	0.66*	-310	230	59	0.12 (164)	a	
"	0.65*	-285	165	32		b	
"	0.72*	-180	225	32		bc	opt. pre 1977.0
2345-16	NC				0.46 (121)	ga	opt. post 1977.0
or	0.46	-15	175	120			
						gc	

Notes to Table 16

(1) Maximum linear correlation coefficient (for reasonable time delays). NC indicates no correlation. An asterisk indicates likely correlation.

(2) Delay of maximum linear correlation coefficient. Negative values indicate optical event precedes radio event.

(3) Half-width of the maximum linear correlation coefficient.

(4) Number of optical-radio data used to calculate r.

(5) Linear correlation correlation at zero delay (number of data points).

(6) Comments on the numerical correlation. Date range of data used in correlation if not entire data (opt. = optical).

  Symbols:

  a = correlation of 1 peak at each wavelength.
  b = correlation of several peaks at each wavelength.
  c = steady trend in both data sets correlates.
  d = envelope of emission correlates.
  e = possible effects of yearly gaps in optical data.
  f = effect of no flux density maximum or minimum in trends.
  g = plateau of several years length in correlation coefficient.
  h = peak at 1 wavelength only.
  i = correlation diminsihed by several outbursts at both wavelengths having different ratios of intensity.
  j = spike in optical.
  k = limited by small number of measurements.
  l = Δt is center of plateau.

(Table 16) are presented in graphical form in Appendix B (only those sources which are discussed in detail below are included). In the discussion below, and in Appendices A and B, the sources are presented in order of right ascension.

Unless otherwise indicated, the optical measurements discussed below are from Pollock et al (1979), Pica et al (1980), Pica (1981), and Pollock (1981). Further discussions of the optical variations can be found in the first two references. For brevity, reference to the work of Pomphrey et al (1976) is referred to as "Pomphrey". Unless specified, the term "radio variations" (or similar phrases) refers to the 15.5 GHz data from Appendix A.

In discussion of the of the numerical linear correlation analysis, the entire radio and optical data shown in Appendix A is used. For those correlations using a subset of the data, the frequency (optical or radio) and time interval of the data used is specified.

The descriptions of the variability are intended to describe the events relevant to the correlation search, and are not intended to be complete discussions of the source variability. It is worthwhile to note that, typically, $1/2$ year gaps exist in the optical coverage due to source proximity to the sun, during which time no information is available on the optical activity. Since the source will probably be as active during these intervals as during the interval containing observations, many events will be unobserved. This periodic lack of infor-

mation on source variability can affect the numerical correlation during active periods.

0007+10.   The 15.5 GHz and optical records show general declines during the 2 years after a small outburst ~1979.0.   The optical rise occurs 1/2 year before the 15.5 GHz rise, but nearly simultaneous with a rise at 90 GHz.   The positive value of r (~0.3) for ±1 year of time delays reflects the general decline at both wavelengths (figure B.1).   A local maximum in r at $\Delta t = -150$ days agrees with the observed difference between the events   at   the   two   wavelengths.   Other   maxima   occur   at   delays corresponding   to   the   single   major   optical   event   aligning   with   other radio events.   The correlation analysis suffers from a small number of measurements.

The time delays observed in the evolution of the millimeter excess spectrum (Schopper et al 1978; Chapter V) are consistent with the ~1979 radio and optical events being related.   Huchra, Geller, and Morton (1980) report an x-ray flare in late 1978, attributed to inverse Compton scattering of the radio photons.   This outburst thus appears over a wide frequency range (radio/optical/x-ray).   The short timescale, large frac-tional   amplitude   variations   at   radio   and   optical   wavelengths   makes 0007+10 an ideal source for continued study.

0048-09.   The optical and radio records show long term (10 year) decays, with rapid outbursts and optical spikes superposed.   The entire data

sets show a high linear correlation coefficient for all delays as a result of the long term decline (figure B.2a). The peak at zero delay indicates short timescale correlated activity which is also clearly seen by visual inspection of the variations. The pre 1974.5 optical variations show a strong correlation with the radio (figure B.2b; r=0.91, Δt=+30 days, N=16). This correlation is a one event correlation – the rapid 1972 radio and optical spike-like outbursts. The optical data prior to 1976.5 also shows a strong zero delay correlation (r=0.58, N=27, Δt=-20 days) over several events. However, the optical data since 1976.5 shows <u>no</u> correlation with the radio data. Although short intervals of data visually appear correlated (e.g. 1978 declines), the correlation is not maintained over an entire outburst. The large gaps in optical coverage hinder considerably the analysis of the rapid optical variations, and influence the interpretation of correlated activity.

Three characteristics of variablility are shown in the optical – radio data: the long timescale decline in the minimum ("envelope") emission is concomitant at radio and optical wavelengths; individual, very rapid spike-like variations show strong correlation with no time delay; and the yearly timescale variations do not exhibit clear correlations.

0133+47. The limited optical data reveals rapid variations. It is of interest that the strongest optical measurement (out of 7) corresponds to the time of radio peak, and the variations in late 1980 occur near

the maximum of another radio outburst. The single low point in 1975 occurs during the decay of an outburst.

3C66A. No significant radio variations are seen (the measurements are consistent with a constant flux density). The only notable optical variation is a small, short timescale event ~1980.0. Barbieri et al (1982) observed short timescale activity in 1972 thru 1981. No corresponding radio activity exists. The numerical correlation reveals no correlated activity.

0229+13. Only minor optical fluctuations have been seen over an 11 year period, with no short or long term activity. The radio flux density rose by a factor of two over a five year interval (but no radio data exists to define this rise). No similar rise is seen at optical wavelengths.

0235+16. The two large optical and correlated radio outbursts in 1975 and 1979 are discussed by Balonek and Dent (1980; and references therein). The two optical spikes occur simultaneous with the radio peaks. The linear correlation was calculated for the entire optical and radio data sets (figure B.3a). The maximum r occurs at zero time delay. Other maxima occur when either of the optical spikes are delayed to times of other radio outbursts. The value of maximum r is low since the optical events are considerably narrower than the radio outburst, effectively lessening the linear correlation.

The optical data was then broken into three segments, and correlated with the radio data. The optical data prior to 1977.0 (e.g. only the first outburst) showed a zero day offset with the radio (figure B.3b). The second large optical outburst (1978.5 - 1979.5) also gave a maximum (figure B.3c) at zero time delay (the secondary maximum at +90 days is due to the optical precursor aligning with the radio peak). The third interval (post 1979.5; figure B.3d) with maximum near zero time delay shows the correlation between the double peaked radio profile in 1980-81 and the 1980.8-80.9 optical activity. The single strong flux density in 1979.9 occurs near a radio peak. Both the spike like and smaller optical variations in 0235+16 correlate with the radio activity, with no time delay.

Impey, Brand, and Tapia (1982) observed a polarization and total flux density outburst at optical and infrared wavelengths in mid December 1979. These measurements reinforce the suggestion from the Florida data that an outburst occurred in late 1979, correlated with the radio outburst. The high degree of optical and infrared polarization (up to 40%) argue for a synchrotron origin for the emission.

There have been four well established periods of correlated radio and optical activity in 0235+164 (two events being optical spikes). During a new radio outburst in late 1981 (not shown in figure A.6), the flux density had reached its highest level since 1976 at millimeter and centimeter wavelengths. No optical data has been yet reported for this time interval.

<u>0306+10.</u> This source exhibits spike-like optical activity, and significant short timescale variations. The minimal radio data indicates short-term variability. Leacock et al (1976) discuss the radio and optical characteristics of this object.

<u>0333+32.</u> The radio variations show a long timescale decay thru 1974, followed by a steady rise during the next 6 years. The optical activity exhibits no long term trend, nor any short term activity. The numerical correlation shows no correlation.

<u>CTA26.</u> The linear correlation (figure B.4) shows a broad maximum peaking at $\Delta t \sim -1$ 1/3 $\pm 1/3$ years ($r=0.51$, $\Delta t=-440$ days, $N=45$), corresponding to alignment of the small 1970-72 and 1976-78 optical events with the large 1971-74 and 1977-79 radio outbursts. There is also possible correspondence between the small optical fluctuations in 1974-75 and the 1975-76 radio outburst. The optical data before 1975.5 shows a stronger correlation ($r=0.73$, $N=25$, $\Delta t=-360$ days), while the post 1975.5 optical data shows $r=0.54$ ($N=17$, $\Delta t=-620$ days). Pomphrey noted the correlation for the first set of events with $\Delta t=-1.1$ years. All three sets of outbursts exhibit similar $\Delta S_{opt}/\Delta S_{rad}$ ratios.

The onset and peaks of the radio outbursts are delayed between 31.4 and 15.5 GHz, indicating that the outbursts are initially opaque at centimeter wavelengths. The time delay between the optical and radio outbursts can thus be partly explained by opacity induced delays. There is no obvious consistent counterparts to the three optical spikes.

<u>0420-01</u> shows a period of intense optical and radio activity beginning in late 1974 and mid 1975, respectively, which followed a half decade of inactivity. Dent et al (1979) discuss the initial optical and radio outbursts, interpreting them as delayed, correlated events. Subsequent to their analysis, at least two additional outbursts occurred at each wavelength: a 1.5 year slow optical outburst in 1977-8, and a smaller amplitude outburst in 1979-80 which included an intense rapid spike (rise time 5 days). The optical activity fell to its pre-outburst level by 1981. A second radio outburst began in late 1977, peaking in mid-1978, with a third outburst peaking in mid-1979. The decay which began in 1980.0 was interrupted by a small rise in early 1981.

The optical-radio delay of 2.2 years seen for the first events is not seen for the subsequent outbursts. The second events show a delay of ~1 year in their maxima, while the third events peak simultaneously. <u>If</u> an optical event occurred in early 1976, but was unseen due to source proximity to the sun, then there would be a ~2 year delay between each sequential pair of optical and radio outbursts - with the 1980 optical event being associated with a mid 1981 peak seen at millimeter wavelengths. It is not clear which optical and radio events are associated.

Linear correlation of the entire data set shows a maximum at Δt ~1 3/4 years, slowly falling to zero at Δt ~+1 3/4 years (figure B.5a). This slow falloff is due to the long timescale of the radio activity (which is illuminated by the long term rise since 1976) and the several

year timescale of optical activity. Restricting the linear correlation to the optical 1975.5 to 1979.5 data shows strong maxima at $\Delta t = -300$ and -650 days, corresponding to the delays of the two large radio events from the 1977 optical event. Similar results are obtained for the post 1977.5 optical data (figure B.5b). The pre 1977.5 optical data shows minor peaks at $\Delta t = -30$ days ($r=0.37$, $N=65$) and -750 days ($r=0.30$, $N=65$), along with other smaller peaks, corresponding to delays of radio events with respect to the 1975 optical outburst.

Based upon only the observed optical variations, the time delays between optical and radio outbursts is not constant. Except for the increase in activity at both wavelengths in the late 1970s, there is not a clear correlation between the radio and optical activity.

3C120 exhibits a strong correlation in the long timescale variations as well as strong correlation in the short term activity. Following a broad maximum in the underlying envelope of emission in the early 1970s, the envelope has decayed with short timescale activity superposed. The linear correlation (figure B.6a) shows a maximum near zero delay, extending at this level for negative time delays. This broad maximum is a result of the similar long term decline and the periods of activity in 1972 and ~1974.0 at both wavelengths. The optical and radio data prior to 1974.3 (figure B.6b) exhibits a strong narrow maximum ($r=0.76$, $\Delta t = -5$ days, $N=46$). This shows the strong correlation of the 1972 radio and optical events (no optical data exists during the 1973.3 radio

outburst). The 1974.3-1977.3 radio and optical data show multiple maxima due to the many optical spikes which appear during this period. A broad maximum at $\Delta t=-130$ days, $r\sim 0.6$, $N=30$ (figure B.6c) is due to the time delayed 1975 optical and radio outbursts (the optical outburst occurs at the onset of the radio activity). Visually, the spike in 1976.8 coincides with the radio peak. The radio and optical data since 1977.3 show no statistical correlation, due in part to the lack of a radio counterpart to the long timescale 1980 optical outburst.

The slow optical and radio decays began in 1971 (see Pomphrey). This long term decay is also observed at infrared wavelengths (Rieke and Lebofsky 1979) where a factor of 2 steady decay occurred between 1971 and 1978, comparable to the rate of the optical decay.

0440-00 shows a long term radio decline with small outbursts superposed. The distinctive feature of the optical record is the series of spikes. Although the spikes do show a tendency to occur at small radio maxima or inflections, this visual correspondence is not strong. The limited number of optical measurements at low flux density give the visual impression of a long-term decline. This trend is not as evident for the median flux density level during each observing season. The linear correlation shows a low, broad maximum between $\Delta t=-1$ and $+1$ years, but is probably from coincidence of and optical envelopes of activity from 1976 to 1981 which do not show strong visual correlation.

<u>0735+17</u> has exhibited a series of very rapid, strong optical spike-like outbursts which are clearly undersampled. The optical activity visually correlates with the radio variations. The five periods of maximum optical strength correspond to peaks or inflections in the radio variations, although the radio/optical flux density ratios for these events are greatly different.

An inflection in the 15.5 GHz radio variations occurs as an outburst peaking ~1974.1 overlaps with the larger subsequent outburst which peaked in 1975.0. In support of this contention, the 31.4 GHz measurements show a decline from ~2.1 Jy in 1973.9–1974.1 to ~1.0 Jy in 1974.3, rising by 1974.7 to ~2.7 Jy. At 15.5 GHz, the inflection during the large outburst decay in 1976.0 suggests a third outburst peak at that epoch. A fourth radio outburst is clearly defined, rising rapidly and peaking in 1977.0. A subsequent outburst peaks ~1979.0, with the sixth outburst (since 1971) occurring in late 1980 (this outburst is more clearly defined at 31.4 GHz). Remarkably, five of these six radio outbursts peak at the same time as rapid optical outbursts (the exception being the 1979 radio outburst, which occurs during less intense optical activity). In analyzing the correlation of the optical spikes with radio events, it must be noted that $1/2$ year gaps exist in the optical coverage, with it being unlikely that no optical outbursts occur during this interval.

The lack of a constant radio and optical amplitude ratio for these events produces no clear numerical correlation (figure B.7a). The maxi-

mum at Δt=2 years corresponds to the offset between the large radio maximum in 1975 and the intense 1977 optical event. No numerical correlation is found for the pre 1976.5 optical data. The 1976.5-1978.5 optical data shows a strong numerical correlation with the radio (Δt=+15 days, r=0.71, N=55). Interestingly, the post 1978.5 optical data shows a clear correlation (figure B.7b) with the radio data, with zero time delay.

During the 1977 optical outburst (27 February 1977), the percent linear polarization was ~18-23% between 0.43 μm and 2.2 μm, with a frequency dependent position angle (Rieke et al 1977). This large polarization is consistent with the optical/infrared outburst emission being synchrotron in origin (see also Angel and Stockman 1980 for a discussion of polarization in active extragalactic objects).

0736+01 shows a sharp radio rise in mid 1976 which is followed by 5 years of rapid variations (flickering) at millimeter and centimeter wavelengths on timescales of months, making this one of the most active radio sources. This level of activity is not reflected in the optical variations, which show minor fluctuations superposed upon a decade long decline. The small optical events in 1975, 1976, and ~1979.0, occur near times of radio peaks, but more radio peaks have no corresponding optical events. The lack of any increase in optical activity after 1976 suggests that the three events are not associated with the radio activity. The linear correlation for the entire data sets and the pre 1976.5 period show no evidence of correlated activity.

OJ287 exhibits the highest correlation of the 45 sources studied. This correlation exists during several stages of activity in this rapidly varying source: the envelopes of radio and optical emission from 1970 to 1976 are correlated (first noted by Pomphrey); individual outbursts during this period are correlated (Usher 1979); and the lower level activity since the decay of the large envelope are correlated.

The linear correlation for the entire data set (figure B.8a) shows two strong maxima at $\Delta t=0$ days ($r=0.81$, $N=162$) and $\Delta t=-330$ days ($r=0.82$, $N=161$). The zero delay correlation is attributable to the large amplitude structure of and within the envelopes. The correlation coefficient is lower than found by Pomphrey due to the inclusion of data in the late 1970s which does not have the same radio/optical amplitude ratio as the 1970-5 interval. The correlation coefficient for $\Delta t=-1$ year is greater than that at zero delay, but this correlation is probably a chance coincidence. The radio outbursts are on the average separated by about 1 year, and the optical data used in the correlation begins 1 year prior to the radio data. By delaying the optical by 1 year, the 1971 optical outburst aligns with the 1972 radio outburst, and similarly for the other events. The optical envelope decay is more rapid than the radio, so the 1 year delay more closely aligns the radio and optical envelopes.

Pomphrey finds a delay of -0.875 years for the maximum correlation. Inspecting figure 1a of their paper shows that the 1972 radio otuburst

at 2.8 cm (10.6 GHz) reaches a peak of ~8 Jy, while the 1973.0 outburst reaches 9 Jy. The corresponding optical outbursts show the opposite amplitude relationship - the 1972 event being the stronger. Inspection of the 15.5 and 31.4 GHz variations shows that the 1972 peak is stronger than the 1973 event (12 versus 10 Jy at 15.5 GHz; 131/2 versus 10 Jy at 31.4 GHz). The spectrum of the 1972 outburst peaked between 15 and 30 GHz, and was opaque at 10.6 GHz, while the 1973 outburst had a flatter spectrum and lower opacity at 10.6 GHz. The ~year offset found by Pomphrey is thus influenced by outburst opacity.

The time delay was determined for various subsets of the data. The optical data from 1971.5-1972.5 was correlated with the entire radio data set, showing no offset (figure B.8b). Similarly, the pre 1974.5 optical data shows zero delay with the entire radio data set. The post 1974.5 radio and optical data (after the envelope decay; figure B.8b) show a peak at $\Delta t=-25$ days (r=0.61, N=102). This result is important since it occurs during lower level optical and radio activity than during the pre 1975 active period, demonstrating that individual events (and not just the envelope profile) are correlated with little or no delay. Limiting the optical and radio data to 1974.0-1978.0 produced a peak at $\Delta t=-35$ days (r=0.62, N=71).

Rieke and Kinman (1974) observed that the ratio of the flux densities at 0.44 μm (optical) and 10.5 μm (infrared) was constant during the envelope decay between late 1971 and early 1974 (short timescale, small amplitude fluctuations were seen on this general decay).

The radio and optical variations were visually searched for instances of correlated individual events (see the three enlargements of the radio variability, figures B.15b, c, and d). Usher (1979) has previously performed an exhaustive analysis of the pre 1977 activity, with more extensive data than used in the analysis here. Thus the activity prior to 1976 will not be discussed, except to point out again that the 1972 radio outburst was stronger, at frequencies above 15 GHz, than the 1973 event. The largest amplitude optical event thus was correlated with the major radio outburst, contrary to the discussion in Usher based upon the 10.6 GHz measurements. The radio data from Chapter II support the identifications of outbursts made by Usher.

Inspecting the post 1975 data reveals an optical rise in 1977.2, synchronous with the rise at 15.5 and 31.4 GHz. An optical spike in late 1978 coincides with a maximum at 15.5 GHz, followed by rapid decay at both wavelengths. The remaining optical record is too sparse to identify further correlations. The linear correlation results discussed above show that the correlated variations are nonetheless occurring.

The optical-infrared-radio correlated activity, rapid variations, and typically high linear polarization during the large outburst envelope strongly suggests that the emission mechanism is the same (synchrotron emission) throughout this frequency range and is produced by the same population of particles within a common volume.

<u>0906+01.</u>   This source exhibits spike-like optical activity.   The degree of optical activity appears to have decreased in recent years. The radio data are too limited in coverage for any correlation search.

<u>0953+25.</u>   The radio and optical records show a general decline since 1972, with small superposed outbursts.   The linear correlation (figure B.9) shows this common decline by the positive value of r for all time delays.   The optical timescales are shorter than the radio.

Except for the rise in 1970-71 and subsequent onset of decay in both the radio and optical flux density, there is no instance of strong visual correlation.   The linear cross coefficient for the pre 1975.5 optical data shows the peak at $\Delta t \sim -1\frac{1}{2}$ years mentioned by Pomphrey which is attributed to random trends.

Linear correlation of the pre and post 1975.5 optical data with the entire radio set show several extended periods of zero or negative correlation coefficient, r, with the maximum correlation coefficient being <u>lower</u> in the data subsets than for the entire set.   This is strong indication that the long term decays <u>may</u> be related, although chance coincidence cannot be ruled out due to the singular (declining) long term trend.

<u>1101+38</u> shows short term optical variations.   The radio data is of insufficient sensitivity (due to low flux density) to do a numerical

correlation search. There is some hint of radio variations, although they are at the level of the measurement errors.

<u>1116+128.</u> The radio observations (beginning in 1978) are not extensive enough for comparison with the larger time coverage optical data. The optical data suggests a long-term event from 1971 to 1978, although the gaps in the optical coverage prevent any detailed analysis.

<u>1127-14.</u> The radio record shows several outbursts superposed upon a long timescale decline. The optical measurements, obtained ~once yearly, indicate small variations, but unrelated to radio trends. Insufficient data exist for a numerical correlation.

<u>1156+295.</u> Insufficient radio data are available here to discuss correlated activity. Wills et al (1982) present additional radio and optical measurements, and discuss possible correlations.

<u>1219+28.</u> The only common variability characteristic is the rapid flickering at both radio and optical wavelengths, superposed upon longer timescale activity. This optical characteristic was also observed over the period 1931 to 1952 (Pollock et al 1974). The optical spikes do not consistently correlate with any specific phase of the radio variations (the 1975.4 does occur simultaneous with a centimeter maximum). The underlying variations do not visually show any correlation. Linear

correlation for the entire, pre 1975.5, and post 1977.5 radio and optical data sets reveal no consistent correlation between any of the three sets. The entire data set does show a peak in r at $\Delta t=+1.3$ years (radio preceding optical), due primarily to the simiar timescales of the 1974-77, 1977-81 radio and the 1975-78, 1978-82 optical "envelopes".

3C273. During the past decade, several radio outbursts have been superposed on a long timescale decline, while the optical variations show no long-term variations. The 1978 and 1979 optical events are not correlated with any radio activity. The linear correlation (figure B.10) shows an anti-correlation due to the optical rise since 1978 being opposite in trend to the radio decline.

3C279. The optical data is too limited to meaningfully search for correlations. The numerical analysis shows no correlation. The optical rise in 1981 corresponds in time with a radio outburst at millimeter wavelengths, but there is insufficient data to claim a correlation.

1308+326. This BL Lac object exhibits multiple spike-like optical variations but only minor centimeter radio variations throughout the 5 years of observations. The optical events in 1977 and 1978 occur near radio maxima, but the 1980 and 1981 events do not show corresponding radio activity. The linear correlation (figure B.11) shows a broad peak near zero time delay, reflecting the correlation of the near δ-function

optical variations with the ~yearly timescale radio variations. The maxima at $\Delta t=-1$, $+1$, and $+2$ years are caused by the yearly gaps in optical observations and the near periodic radio activity fluctuations.

A long timescale rise observed at 11 centimeters (O'Dea et al 1982) and the spectrum in Chapter V indicate that the variations observed at 15.5 GHz occur near the maximum of a long timescale outburst which appears to currently be decaying. Puschell et al (1979) conducted photometric and polarization observations during the 1978 optical outburst. The outbursts decayed more rapidly at visual than at infrared wavelengths and displayed rapid polarization variations (optical polarization typically ~15%). The rapid highly polarized optical outbursts, ~yearly radio variations , flat radio spectrum, and epochs of apparent correlated radio/optical activity in 1308+326 are similar to characteristics observed in the BL Lac object 0735+17.

1510-08 is active at both radio and optical wavelengths. In chapter IV it was shown that the radio outbursts in 1510-08 have timescales of a few months. The optical spike (single datum) in 1972.4 corresponds in time with a peak of 31.4 GHz. The spike in 1975.4 occurs just prior to a peak at 15.5 GHz, and during the peak at 31.4 GHz. Comparison of the variations at millimeter and centimeter wavelengths reveal that some of the outbursts show time delays as large as ~100 days. For every strong radio outburst observed without a corresponding optical event, there is either no optical observations simultaneous with the radio peak or at

times when optical outbursts could be expected from the observed radio delays.

The linear correlation (figure B.12) shows a maximum at a delay of -105 days, comparable to the observed millimeter-centimeter time delays. The long term underlying optical and radio variations show similar structure, especially since 1975, responsible in part for this correlation. The maxima at +1 to 2 years correspond to the delay between the double radio burst in 1973-74 and the 1975 optical event.

1514-24. This source shows one optical spike and several periods of rapid short term variations. The 1973 activity occurs at the onset of a long timescale 15.5 GHz rise; the 1976 activity after the initial radio peak; the 1977 spike during constant radio flux density; and the 1979-80 activity during a radio outburst. No consistent relation is seen between the radio and optical variations. The linear correlation oscillates about r~0.2 for times corresponding to radio events preceding the optical. Thus, the radio and optical variations show no correlated activity.

1638+39. Both the radio and optical records show periods of rapid variability in the early 1970's, followed by slower, lower amplitude activity during the next five years. The radio envelope is of longer duration than the optical. Pomphrey et al (1976) noted this feature and remarked that the degree of activity was similar, though not as

striking, as in OJ287. The linear correlation (figure B.13) of the entire data sets shows a maximum r=0.50 at $\Delta t \sim +20$ days (N=128). This correlation does not include the observed coincident decay at radio and optical wavelengths in 1970 reported by Pomphrey (which would strengthen the correlation).

The optical activity displays several spikes, the most rapid being a two day rise by 0.6 mJy in early 1970 (Folsom et al 1970). Radio maxima occur near times of several of the spikes, suggesting correlated short term activity. The optical envelope is of shorter duration than the radio envelope, but the lack of optical data in 1975-77 may partly be responsible for this visual appearance. Current optical observations are needed to see if renewed optical activity is related to the new phase of radio activity begun in 1979.

3C345. Historically, this quasar exhibited several large outbursts and lower amplitude activity between 1965 and 1973 (Barbieri et al 1977). In 1971-1973, a large, slow outburst occurred followed by lower level, more rapid variations superposed upon a long timescale rising "envelope" (see Pollock et al 1979).

The linear correlation analysis (figure B.14a) is dominated by the large 1971-3 optical outburst and the 1973 radio outburst. A maximum in r occurs at a delay of 2 years. This radio outburst peaks simultaneously between 15.5 and 90 GHz, indicating that the radio event is

transparent (also indicated by the flat radio spectrum). Thus, if the optical and radio events are related, the observed time delay cannot be attributed to opacity. As was proposed for the quasar 0420-01 (Dent et al 1979), the simplest explanation would attribute the delay as being due to time of flight, where the radio and optical emission regions are spatially separated. The single such event weakens the case for a correlation.

The optical "flickering" observed since 1976 does not correlate with any radio activity. To numerically search for correlation, the optical record since 1974.0 was analyzed with the entire radio record (figure B.14b). A small maximum (r=0.34, Δt=+45 days, N=87) occurs near zero delay, with a similar value of r for $\Delta t \sim$ -2 years (as the "envelope" begins to overlap with the recent large outburst). The absence of a large optical outburst associated with the intense radio outburst beginning in 1978 is disturbing if one interprets the 1971-3 activity at radio and optical wavelengths as being correlated.

1659+39. Limited radio observations prevent study of correlation. Quasi-simultaneous observations at frequencies ranging from radio to x-ray are presented in Kondo et al (1981).

1730-13 exhibits small amplitude short timescale structure superposed on larger amplitude, longer timescale outbursts at millimeter and cen-timeter wavelengths. The limited optical observations show an extremely

sharp spike, rising 2 magnitudes in 130 days, then dropping 0.85 magnitude in 1 day (see Pollock et al 1979 for further description). This spike occurs during a small 15.5 GHz burst and during the early decline of this burst at 31.4 GHz.

The lower level optical activity (with long gaps due to source inaccessibility), suggest a slow rise between 1975 and 1978 followed by a slower decay by 1980. This trend is similar to the underlying variations at 15.5 GHz. The optical data is too sparse to establish a clear correlation. Continued observations of long term trends at radio and optical wavelengths are necessary to confirm this suggested correlation.

If the 1978.5 and 1979.5 optical data correspond to distinct outbursts rather than longer term trends, then it is of interest to note that outbursts were observed at 31.4 GHz peaking in 1978.8 and 1979.5 (these outbursts are seen, although small, at 15.5 GHz).

The linear cross-correlation analysis (figure B.15) is dominated by the large spike. The observed correlation reflects the "delta function" nature of the optical variations correlating with small radio events and is presented to demonstrate the effect that a single event can have on the numerical correlation analysis. Note that there is no time delay between the optical spike and a small radio outburst. The plateau in the correlation coefficient between -2 and 0 years is due to the long term trends noted above.

<u>1749+70.</u> Slow small amplitude variations are seen at radio and optical wavelengths, although the time coverages do not overlap sufficiently to comment on correlated activity. This BL Lac object originally gained attention due to its proximity to the spiral galaxy NGC 6503 (Crane and Price 1976), with possible luminous filaments extending from the galaxy toward 1749+70 (Arp et al 1976).

<u>1749+09.</u> This source has not been well-observed. No correlated activity is suggested from the data presented here. Aller, Aller, and Hodge (1981) observed simultaneous maxima at 8.0 and 14.5 GHz in December 1979. The optical activity in late 1979-early 1980 occurs near the time of the radio outburst, but the limited optical coverage discourages any claim of correlation. This source does exhibit rapid variations at radio (chapter IV) and optical wavelengths.

<u>3C371.</u> Visual inspection of the radio and optical variations shows some hint of similar activity: a rise around 1972, slow decay in 1973-74, and rise by 1975. The subsequent five years do not show this similarity. Pomphrey noted this pre 1975 similarity. A linear correlation coefficient of the radio and optical data prior to 1975.0 shows the peak r~0.5 for Δt~+0.1 to +0.7 years (radio precedes optical) noted by Pomphrey (from slightly different data sets), as well as a peak in r~0.5 for Δt=-1$\frac{1}{2}$ years. Linear correlation of the post 1975.0 radio and optical data show <u>no</u> correlation. Similarly, the entire data set shows <u>no</u>

correlation indicating that the pre 1975 correlation is a one event correlation (as first proposed by Pomphrey).

There are also no distinctive radio events associated with the optical spikes.

3C390.3 shows a general optical decline from 1974 thru 1980. This decline is the continuation of the decline begun in 1970, after a large rise beginning in 1969 (Barr et al 1980). The radio flux density is relatively constant during the last decade, with a small rise over the two year period 1973-75. This is roughly coincident with a small rise seen in the Barr et al optical data, but the earlier and later optical trends do no correspond with the radio trends. The linear correlation shows a strong maximum near zero delay, but this is due to the limited optical coverage included in this analysis.

1921-29. The radio variations in this quasar are discussed by Dent and Balonek (1980) and in Chapter IV. Gilmore (1980) reports optical activity correlated with the 1977 millimeter maximum (Chapter IV) and a single high measurement in mid 1979 related to the rise during the intense radio outburst. The more extensive Florida optical measurements establish that the radio/optical emission are correlated during the past 5 years. The optical and radio flux densities rise between 1976 and 1977. with the sharp optical event ~1977.6 occurring during a milli- meter outburst (figure 17a) and at the time when the centimeter flux

density is leveling off. The Florida optical data in 1978 is sparse, but data presented by Gilmore (1980) indicates the source was slightly weaker than in 1979. The beginning of the strong optical outburst is not defined, but the flux density was rising quickly to a maximum between 1979.4 and 1979.5, followed by a rapid decay by late 1979. By mid 1980, the source had weakened to its lowest observed strength since 1976.

The optical outburst maximum occurs ~1/2 year prior to the 15.5 GHz peak. This offset is consistent with the radio evolution presented by Dent and Balonek (1980) and Chapter IV (figures 17a and b) in which the centimeter wavelength variations are delayed due to source opacity. The time of the millimeter maximum is not well-defined but occurs between 1979.5 and 1979.8, consistent with the optical results.

Overlaying the optical record upon the 15.5 GHz record (with the radio variations occurring 1/2 year after the optical) reveals a strikingly strong correlation. The optical timescale of decay in 1979-80 is shorter than the centimeter radio timescale, but is in agreement with the millimeter decay rates. The linear correlation for the entire data set (figure B.16a) shows a broad maximum (average r=0.76, N=43, half-width 410 days centered on Δt=-250 days). The rise at $-2^1/4$ years is due to the 1977 optical event correlating with the 1979 radio outburst. Excluding the 1977 event produces an even higher correlation coefficient (figure B.16b) centered on Δt=-240 days.

The small optical fluctuations in 1980.5 occur ~1/2 year before the inflection in the centimeter decay at 1981.0. The optical flux density reached a minimum in 1980.7 and rose again by mid 1981. A corresponding rise is seen at 3 mm (Chapter IV, figure 17b). Thus strong evidence exists for three (and weakly for a fourth) correlated optical/radio outbursts which are delayed by ~1/2 year at centimeter radio wavelengths.

2131-021. There is insufficient optical coverage to claim a firm correlation, but the radio and optical trends since mid 1975 are similar. The numerical correlation, using only the nine optical measurements, gives a correlation at zero time delay (r=0.86, N=7). The radio spectrum (chapter V) indicates that the source is transparent. Additionally, the outbursts peak simultaneously at 31.4 and 15.5 GHz in 1977.0 and late 1980, indicating that no radio/optical opacity time delay would be expected. The data are suggestive, but are too limited to allow us to propose correlated activity.

2134+00. This radio source was first noted by Shimmins et al (1968), who discussed the radio spectrum - which peaked at 6 GHz (one of only a few sources to peak at this frequency). The source has steadily decayed by ~45% at 15.5 GHz in the past 12 years, but the spectral frequency peak and shape (chapter V) have not changed from that in the 1960's! Historically, the source has exhibited rapid (possibly spike-like) variations (Gottlieb and Liller 1978).

The recent optical data is consistent with constant intensity, although an alternative interpretation would indicate a slow decline until 1979, followed by a small rise. The numerical correlation (figure B.17) gives a near zero value of r for no time delay. The peak in r at $-1\frac{1}{2}$ year delay (optical preceeding radio) occurs when the post 1980 optical data is beyond the range of the radio data. The rapid drop in r for even small increases in the delay indicates that the peak is not a result of long term trends in the two data sets. No correlation exists. It is interesting to note that the single high optical measurement in 1977.6 occurs during a small ($<\frac{1}{2}$ years) burst seen at 31.4 GHz (based upon three measurements).

<u>2145+06.</u> The centimeter and millimeter radio record shows a long term decline until 1975, followed by a long linear rise during the next 6 years. Observations at 31.4 GHz and 90 GHz show that this rise is comprised of two distinct outbursts, peaking in 1977 and 1980. The spectrum (Chapter V) shows that the sum of the outbursts is opaque at wavelengths below 15 GHz. The optical record does not show the pre 1975 decline. The optical variations can be interpreted as showing either a slow rise since 1970 upon which are superposed minor slow fluctuatuions; or a constant level from mid 1970 to 1974.0, then a $\frac{1}{2}$ year rise by 1974.5, after which no variations occurred until a slow rise in mid 1980. Neither scenerio is consistent with the millimeter or centimeter radio variations.

BL Lacertae. The prototype BL Lacertae type object exhibits the rapid (monthly) radio and optical outbursts often characteristic of this class of quasi-stellar objects. Visual inspection of the optical and radio variability indicates several instances of simultaneous activity, but also many periods with no apparent correlated variations. The most dramatic single event correlation is in 1973.4, when a sharp optical spike and rapid 5 Jy radio rise occur simultaneously. The optical event decays more rapidly than the radio. The radio and optical activity in 1980 possess similar timescales and structure. The radio (31.4 and 15.5 GHz) and optical activity from 1976.0 to 1977.5 also possess similar shapes and timescales.

Despite these instances of similar variations, linear correlation of the entire data set shows no correlation (figure B.18a). The 1974.0-1977.4 optical data does show a statistical correlation with the radio, $\Delta t=-140$ days, $r=0.73$, $N=55$ (figure B.18b). The 31.4-15.5 GHz variations do not indicate any time delay at radio wavelengths, so this correlation could be the result of chance coincidence of non-related events. The post 1980.1 optical variations show a correlation with the radio (figure B.18c; $\Delta t=+30$ days, $r=0.76$, $N=24$), with the radio event slightly leading the optical.

Other than these few instances of correlated events, the conclusion of Pomphrey et al (1976) is reinforced: there is "no obvious overall correlation except that both (frequencies) show numerous rapid events on a timescale of months."

284

2216-03. A long timescale outburst began in 1975 at millimeter and centimeter wavelengths, following half a decade of slow decay. The radio spectrum has peaked at ~10 GHz during the past decade, during all stages of activity. No variation is seen at optical data presented here, although Barbieri, Romaro, and Zambon (1978) report variations (possibly short-term) in 1968-1971. The numerical correlation reveals no correlation.

3C446. Several optical spikes have been seen in this source, with the optical activity increasing in 1978-80. The optical and 15.5 GHz data show little visual correlation. However, the radio variations are more rapid at millimeter wavelengths (Chapter V), with outbursts showing opacity induced delays at centimeter wavelengths. The 1974 optical spike occurs during a long maximum at 31.4 GHz (this outburst is delayed by over 1 year at centimeter wavelengths), while the envelope of optical activity begins in late 1977, coincident with the onset of the millimeter activity. Barbieri, Romano, and Zambon (1978) report an optical outburst in 1970, which is near the time of a radio outburst maximum. The yearly gaps in the optical record prevent comparison with the rapid millimeter variations. Interestingly, the optical activity decreased rapidly between 1980.4 and 1980.6, the same time interval in which the 3 mm rapid decay (figure 19) occurred (this decay is much slower in the 15.5 GHz record, and overlaps with the subsequent outburst rise). The presence of a rise in 1981-81 in the optical activity would lend further

support to correlated activity. The linear correlation (figure B.19) since 1977.0 shows a high correlation (r=0.70, Δt~-525 days, N=30) with a time delay just a little longer than suggested by the radio spectral evolution.

This source exhibits a correlation in the envelopes of activity, with weaker evidence for correlations in individual events.

CTA102 shows rapid variations at radio wavelengths (see also Chapter IV), but less extreme optical activity. The linear correlation (figure B.20) shows a peak at Δt=-1 year. The long timescale decay prior to 1978 and subsequent rise produce the broad bump between Δt=-1.5 and 0 years, with the peak at -1 year due to allignment of the 1978 optical event with the mid 1979 radio peak. The optical trends do not reflect the large amplitude radio outbursts, so the general trends at optical and radio wavelengths do not show a strong correlation. The single optical event (1978) occurs just prior to the large 1979.0 3 mm outburst (figure 20) which appears delayed by 1/2 year at 15.5 GHz. This time delay is consistent with these single optical events being related, but the data are too limited to claim a positive correlation.

3C454.3. The suggested correlation found by Pomphrey from variations prior to 1976 is seen also for the variations after that epoch. The entire optical-radio data shows a clear correlation (figure B.21a). The radio and optical records were split into two sections at epoch 1977.0,

with correlation searched for in the two subsets of the data. The pre 1977.0 data shows a pronounced correlation with r=0.65 (Δt=-290 days, N=32). The linear correlation (figure B.21b) shows the same shape as that of Pomphrey, even though their correlation analysis covers five more years including the large radio outburst in the late 1960's. Inspection of the variability plots show that optical outbursts clearly precede the 1972 and 1974.5 radio maxima by ~1 year. The optical activity occurs at the onset of both radio outbursts which begin simultaneously at 31.4 and 15.5 GHz.

The linear correlation after 1977.0 (figure B.21c) shows a much broader maximum centered at Δt~-300 days, (r=0.6, N~30). The drop at Δt=-1$\frac{1}{2}$ years is an edge effect, as the optical outburst is delayed beyond the radio data. The slow drop in r between Δt=-$\frac{1}{2}$ and +1 year is a result of the lack of a decline in either of the recent radio or optical outbursts (the correlation is thus between two rising functions). The 1980 optical activity occurs at the onset of the radio outburst at millimeter and centimeter wavelengths.

The three periods of activity which have thus been investigated reveal correlated activity with similar offsets (Δt~1 year), with the optical activity occuring at the onset of the radio events. As was shown in Chapter V, the radio outbursts are transparent at millimeter wavelengths during all stages of activity. The observed optical - radio time delay cannot be attributed to changing opacity. Since the optical

emission precedes the major period of radio activity, Compton scattering of radio photons cannot be producing the optical emission. The constancy of the millimeter spectral index during all stages of the outbursts indicates that the particle energy distribution producing the radio emission does not change, making it unlikely that evolution of the particle spectrum can produce the observed delays. A possible scenerio for the delay is a time-of-flight effect (as proposed by Dent et al 1979 for a similar delayed optical radio outburst in 0420-01) in which the radio and optical emitting regions are spatially separated, with the delay due to propagation time for the particles, photons, or shock wave responsible for the generation of the radio emission.

2345-16. A strong optical spike was observed ~1970 with no obvious radio outburst (Pomphrey). No radio measurements exist during the 1/2 year strong optical activity, so a short timescale radio event cannot be ruled out. A radio outburst was observed 1 year later, peaking in 1971.9 (Pomphrey and figure A.45). The decay of the radio outburst was followed by a long timescale sequence of radio events: the flux density rising sharply at 15.5 GHz in 1971-1972 (slower and delayed at longer wavelengths), decaying from 1973 until 1978, followed by an outburst peaking in 1979. This general trend is reflected also in the optical record since 1971.4 - a rapid rise, followed by a slow decay to a minimum level by 1978-79, and a slow rise in 1980-81. The trends at radio and optical are similar but visually not strongly correlated. Small

amplitude optical fluctuations are superposed upon this trend, with a small flare in late 1973 (at the time of an inflection in the radio decay).

The linear correlation for the entire data set as well as the post 1970.6 optical data (figure B.22) exhibit no significant maxima. The maxima at zero delay (seen in both correlation analyses) may reflect slight similarity between the long timescale structure.

§5. The Case for Correlated Radio-Optical Variability

In the preceding sections, the search for correlated variability has been conducted using visual inspection and numerical analysis of individual sources, and statistical analysis of variability characteristics in a sample of sources. Several sources have unambiguously been shown to possess correlated activity, and nearly a dozen other sources show strong evidence in favor of correlation. To firmly establish correlation in individual sources, continued monitoring must be conducted in order to detect repetitions of the suggested behavior. Other observational approaches to a correlation search are discussed.

Summary of the reported correlated radio-optical variations. It has become clear that there are several different types of variability which correlate at optical and radio wavelengths. Different physical mechanisms are undoubtedly responsible for these distinct classes of variability. The seven types of observed correlated variations are (from shortest to longest timescale):

(1) A radio outburst which reaches a maximum simultaneous with an optical spike. Spikes have timescales of weeks – a much shorter duration than the radio outburst. There may be lower level activity prior to and after the spike, with about the same duration as the radio outburst. Examples include 0048-09 in late 1972, 0235+16 in late 1975 and early 1979, 0735+17 in 1974-77, OJ287 in late 1978, and BL Lac in mid 1973. A spike in 1510-08 has a delayed radio maximum at 15.5 GHz, placing this event between classes 1 and 3.

(2) A radio outburst which is concomitant with an optical outburst (both having similar timescales of months to years). Examples are 3C120 in 1972, possibly 2131-021 in 1975-8, and BL Lac in 1980.

(3) A radio outburst which is delayed relative to an optical outburst, and also showing time delays within the radio spectrum. Examples include 0007+10 in 1979-80, CTA26 in 1971-3 and 1976-9, possibly 0420-01 in 1977-80, OJ287 in early 1972, and 1921-29 in 1978-82.

(4) A radio outburst which is delayed relative to an optical outburst, but with the radio spectrum showing little or no time delay, and being transparent at millimeter/centimeter wavelengths. These correlations are difficult to locate in the variability records since it is not always clear which of the radio and optical events are related. If only a single pair of events is observed, it cannot be proven from the variability alone that the events are related. The optimum conditions for detecting this class of correlation is in a source exhibiting

several radio and optical outbursts, separated in time by several outburst timescales. The most convincing evidence of this type of activity is 3C454.3, in which similar time delays have been observed in three time intervals during the last decade. 0420-01 possibly exhibits this behavior, though the overlapping of several outbursts makes the classification less certain. The radio spectrum of the total flux density in 0420-01 during outbursts shows a millimeter or centimeter excess, but the observed time delays are not sufficiently long to explain the optical/radio delay.

(5) Long timescale (~decade) decay(s) and/or rise(s) upon which are superposed generally minor fluctuations. Examples include 0048-09, possibly 0953+25, and 0007+10 (over only a three year interval).

(6) An envelope of activity, concurrent at radio and optical wavelengths, with multiple rapid outbursts (timescales < year) superposed upon a longer timescale (years) changing "minimum" flux density. The rapid outburst activity decreases after the envelope decay. It is not clear whether the envelope is a product of the outbursts, or vice-versa. Outstanding examples include 3C120 in 1971-78, OJ287 and 1638+39 in the early 1970s, and possibly 3C446 since 1977.

(7) Intervals of rapid (~monthly) fluctuations at radio and optical wavelengths, with little or no correlation between individual events. Sources exhibiting this characteristic are BL Lacertae and 1219+28.

There may be more classifications for correlated activity which have not been detected in this study (no classification has been found for a radio event preceding the onset of an optical outburst). In addition to the above seven classifications, there is another category which seems to contain the majority of variable sources, e.g. sources which exhibit variations at either or both wavelengths, but do not show obvious correlated activity. Any model for correlated activity must be able to explain the predominance of this behavior.

Interpretation of the correlated variations. Without multi-frequency data at optical-infrared wavelengths, it is difficult to construct and constrain models for the emission mechanisms which produce such divergent variability timescales, delays, and amplitudes. However, the single frequency optical and multi-frequency radio observations suggest that several different processes and physical conditions are responsible for the various characteristics.

The observed optical-infrared-radio spectral and polarization continuity (see discussion in Chapter I) suggest that the radiation is produced by a common emission mechanism (presumably synchrotron) within a common or adjacent volume. The different observed variability characteristics will be discussed in the context of this basic model.

Variations would be produced by an injection and subsequent expansion of a cloud of high energy (relativistic) particles from a core energy source. At frequencies where the source is transparent to the

radiation, the flux density will rise simultaneously. At lower frequencies, where the source is opaque, the onset and peak of the outburst will be delayed. The timescale of the variation will depend upon the length of time of the injection and the expansion rate. In this light, several of the observed types of charcteristic correlated variation can be understood.

The concomitant rapid radio-optical events (<u>type</u> <u>2</u>) would be produced in sources having low opacity at centimeter wavelengths (thus no time delay). The sources which show this variability behavior have falling (transparent) millimeter spectra during the outburst and non-outburst epochs. It has been shown in Table 14 (and from inspection of the variability plots in Appendix A) that the outburst amplitudes (S_{max}/S_{min}) for this type of outburst are comparable at radio and optical wavelengths. The particle energy distribution ($\gamma = -(2\alpha - 1)$, for $N(E) \, dE \propto E^{-\gamma} \, dE$) of the outburst is thus the same as that of the larger non-outburst component, and the optical and radio emission originate in the same volume. Observations of the polarization variations during these outbursts would offer a test of this interpretation. Since the emission originates in a common volume (and thus magnetic field) the polarization variations would show correlation.

The short timescale, time delayed (<u>type</u> <u>3</u>) events are similar to the non-time delayed events, except that opacity effects in the source produce an observable delay. The sources exhibiting this behavior have

centimeter/millimeter excess spectra (indicative of opacity at lower frequencies), and also have small E ratios for the outbursts. The exception is 0420-01, which may be a type 4 object. In 1921-29 (Dent and Balonek 1980; Chapter IV) the high frequency radio outburst spectrum has the same spectral index when transparent as the non-outburst spectrum, showing (as in type 2) that the particle energy distribution of the outburst is the same as the non-outburst component. Observations at millimeter wavelengths, where the optical-radio time delay would be less, are important to establish the correlation of these events.

It is feasible for a source to exhibit both types 2 and 3 characteristics, as a result of opacity changes (spatial or temporal) between outbursts. For type 2 and 3 events, it is not clear whether the outbursts are distinct physical components in the source, or whether changes in the rate of continuous injection of particles from a single region is responsible for the events. The constancy of the particle energy distribution argues for the latter. Again, polarization measurements, which probe the magnetic field structure of the outburst regions, would be a useful test.

Type 4 events require a different interpretation from the type 2 and 3 events. The lack of a radio delay rules out an opacity induced optical-radio delay. Dent et al (1979) propose a time-of-flight phenomena to explain the delays observed in 0420-01. In this scenerio, the radio and optical radiation is emitted from spatially separate regions.

The propagation time for the particles, photons, or shock wave to travel from the core (optical) region to a distant radio photon producing region gives rise to the time delay. There should be no polarization correlation in these events since the optical and radio emission regions are spatially distinct.

An alternative explanation could invoke a time dependent particle distribution: originally the distribution would produce more high frequency photons, with lower frequency (radio) photons produced later. The constancy of the 3C454.3 millimeter spectrum throughout the outburst stages contradicts this hypothesis.

It is not clear that 0420-01 is a member of this classification. There exists some frequency dependent time delay, but it is not sufficient to explain the optical-radio delay. Also, the radio spectrum shows a centimeter excess. It is possible that 0420-01 represents an additional class showing some opacity as well as non-opacity delay (in the same manner that types 2 and 3 differ).

Variability <u>type 5</u> sources can be interpreted as being similar to types 2 and 3, except the timescale of variation is longer - possibly a result of the emission originating in a larger volume. Except for timescale, there is no qualitative difference between this classification and types 2 or 3. Continued monitoring of this classification of sources is very important, to determine whether the correlation continues through several decays and rises.

Type 6 (envelope) activity is related to periods of rapid activity (type 2 or 3). Multiple rapid outbursts are superposed upon the longer timescale envelope. The E ratio for these sources is larger than for the previously discussed sources, with several of the superposed optical events being spike-like. The radio envelope typically has a millimeter or centimeter excess. The large E_{opt}/E_{rad} ratio indicates that the optical-radio spectral index should be flatter at envelope maximum than at pre/post-envelope epochs. The lack of an infrared-optical spectral change in the decay of the OJ287 envelope (Rieke and Kinman 1974) indicates that the spectral change occurred between infrared and millimeter wavelengths.

Aller and Ledden (1978) interpret the envelope rise in OJ287 as an increased rate (within a single region) of particle injection or acceleration, followed by a subsequent decay in these rates producing the envelope decline. The emitting region was initially opaque at centimeter wavelengths (accounting for the low 8 GHz peak for the 1972 outburst; discussed in §4), with the total spectrum becoming transparent in 1973. A linear polarization position angle change of 100° was observed at this time, consistent with the 90° jump expected as a synchrotron source becomes transparent (Aller, 1970). In this interpretation the ~monthly timescale outbursts are fluctuations in the injection rate. In this model the outbursts are "caused" by fluctuations in the envelope emission.

An alternative interpretation is that separate outbursts occur frequently enough to overlap in time, with the outburst decays producing the observed envelope of emission. In this model, the outbursts would produce the envelope of emission. Millimeter observations, where decay rates are more rapid, could distinguish between these models. In 3C446, the millimeter flux density during the alleged envelope of emission falls to near the pre-outburst level, suggesting that discrete events comprise the envelope.

Type 6 events are thus similar to the type 5 long timescale variations, except that type 6 sources exhibit higher E_{opt} values.

Type 7 activity (rapid flickering) can be interpreted by either of the two models discussed for type 6 events, except that the superposed events are of much shorter timescale. The lack of apparent correlation between the optical and radio flickering could be attributed to undersampling of the short timescale activity, or varying opacity-time delays between events. Although both sources which exhibit strong flickering show instances of spike-like behavior, the E_{opt} values are not extreme (<15) and E_{opt}/E_{rad} is of order unity. A related source, 0736+01, is among the most rapid radio variables, yet it does not exhibit large fractional optical flickering. In this instance, the presence of a strong optical component (which does not extend to radio wavelengths; see O'Dell et al 1978) reduces the E_{opt} ratio, making the alleged events difficult to detect.

In the six classifications discussed above, only the type 4 events require an interpretation different from the expanding cloud model. The other five types are manifestations of the same phenomena with differing timescales. The <u>type 1</u> classification (optical spikes) appears to be a distinct phenomena. The E_{opt}/E_{rad} ratio and the coincidence of the spike with the radio maximum distinguish these events from the other six.

0235+16 may hold the key to understanding this type of variability characteristic. It has the largest E_{opt} value of the sample, and has undergone several radio and optical events, sufficiently separated in time to permit distinguishing between outbursts. Additionally, the radio spectrum is transparent above ~10 GHz (Balonek and Dent 1980), so opacity induced time delays are not important. Two unambiguous type 1 correlations have been observed, each occurring during an interval of lesser (but significant E_{opt}) activity with timescale comparable to the radio. In two other instances, lower level optical activity has been correlated with radio events (it is possible that spikes existed but were not observed). Thus, though the optical spikes represent very energetic phenomena, they may be hiding the underlying optical activity which might be correlated with the radio. In several sources, there is no underlying optical actvity, as well as no major radio activity at that time. The presence of the optical spike forces the observer to search for corresponding radio activity.

Thus, although the optical spike phenomena is the most dramatic event observed in compact sources, its relationship to other variability mechanisms may be minor. Observations of the spectral evolution of the very narrow optical spikes (a difficult observational task) and polarization characteristics are necessary to determine the nature of this phenomena, and its relationship to other optical variations.

In the above discussions, no mention has been made concerning effects of beaming on the variability characteristics. If the radio radiation is emitted from a relativistic jet, the orientation of the jet relative to our line of sight can alter the observed timescale and amplitude of variation (Blandford and Konigl 1979). Differing alignments can be invoked to explain the different variability characteristics among compact sources. However, except for the type 1 variations, it is not clear that there is a profound difference in the variability characteristics between sources.

Where do we go from here? The study of compact source variations has been concentrated upon extreme variables, with the lack of counterparts to the optical spikes interpreted as a general lack of optical-radio correlated activity. As has been demonstrated in this chapter, a large number of sources exhibit correlated activity on widely different timescales. The low amplitude variations of non-spike events requires accurate optical and radio measurements to define the variations. Continued monitoring of a large number of sources still appears to be

the desirable method for studying the evolution of outbursts and the relation between the optical-infrared-radio emission mechanisms. The effort needs to be extended to systemmatic polarization measurements, and more frequent sampling. Observations must be made when the sources are near the sun (possibly a task for the space telescope) in order to follow the optical outburst evolution.

The results of the correlation search indicate that optical and radio emission mechanisms are related, and that the radiation is eminating from a common volume. Despite many instances of activity which appears correlated either from visual inspection or numerical analysis, there are few instances of unambiguous correlation. This leaves us with a final closing statement on the current knowledge of correlated radio-optical activity in compact radio sources:

"The data suggests, but we cannot yet propose..."

BIBLIOGRAPHY

Allen, R.J., Barrett, A.H., and Crowther, P.P. 1968, Ap.J., 151, 43.

Aller, H.D. 1970, Ap.J., 161, 19.

Aller, H.D., Aller, M.F., and Hodge, P.E. 1981, A.J., 86, 325.

Aller, H.D., Hodge, P.E., and Aller, M.F. 1981, Ap.J.(Letters), 248, L5.

Aller, H.D., and Ledden, J.E. 1978, p.53, Pittsburgh Conference on BL Lac Objects, ed. Wolfe, A.M., University of Pittsburg.

Altschuler, D.R. 1980, A.J., 85, 1559.

Altschuler, D.R., and Wardle, J.F.C. 1976, Mem.R.astr.Soc., 82, 1.

Altschuler, D.R., and Wardle, J.F.C. 1977, M.N.R.A.S., 179, 153.

Andrew, B.H., Harvey, G.A., Medd, W.J., Hackney, K.R., Hackney, R.L., Scott, R.L., Smith, A.G., Leacock, R.J., McGimsey, B.Q., Epstein, E.E., Montgomery, J.W., Mottmann, J., and Pomphrey, R.B. 1974, Ap.J., 191, 51.

Andrew, B.H., MacLeod, J.M., Harvey, G.A., and Medd, W.J. 1978, A.J., 83, 863.

Arp, H., Sulentic, J.W., Willis, A.G., and deRuiter, H.R. 1976, Ap.J. (Letters), 207, L13.

Barr, P., Pollard, G. Sanford, P.W., Ives, J.C., Ward, M., Hine, R.G., Longair, M.S., Penston, M.V., Boksenberg, A., and Lloyd, C. 1980, M.N.R.A.S., 193, 549.

Baars, J.W.M., Genzel, R., Pauliny-Toth, I.I.K., and Witzel, A. 1977, Astr. Ap., 61, 99.

Balonek, T.J., and Dent, W.A. 1979, B.A.A.S., 11, 458.

Balonek, T.J., and Dent, W.A. 1980, Ap.J.(Letters), 240, L3.

Barbieri, C., Cristiani, S., and Romano, G. 1982, A.J., 87, 616.

Barbieri, C., Romano, G., DiSerigo, A.S., and Sambon, M. 1977, Astron. Astrophy., 59, 419.

Barbieri, C., Romano, G., and Zambon, M. 1978, Astron.Astrophys.Suppl., 31, 401.

301

Barvainis, R. 1981, private communication.

Beichman, C.A., Pravado, S.H., Neugebauer, G., Soifer, B.T., Matthews, K., and Wooten, H.A. 1981a, Ap.J., 247 780.

Beichman, C.A., Neugebauer, G., Soifer, B.T., Wooten, H.A., Roellig, T., and Harvey, P.M. 1981b, Nature, 293, 711.

Bevington, P.R. 1969, Data Reduction and Error Analysis for the Physical Sciences, McGraw-Hill, Inc., New York.

Blandford, R.D., and Konigl, A. 1979, Ap.J., 232, 34.

Blandford, R.D., McKee, C.F., and Rees, M.J. 1977, Nature, 267, 211.

Bregman, J.N., Lebofsky, M.J., Aller, M.F., Rieke, G.H., Aller, H.D., Hodge, P.E., Glassgold, A.E., and Huggins, P.J. 1981, Nature, 293, 714.

Brosche, P., and Campbell, J. 1979, M.N.R.A.S., 187, 179.

Brosche, P., Wade, C.M., and Hjellming, R.M. 1973, Ap.J., 183, 805.

Burbidge, G., and Crowne, A.H. 1979, Ap.J.Suppl., 40, 583.

Cohen, M.H., Kellermann, K.I., Shaffer, D.B., Linfield, R.P., Moffet, A.T., Romney, J.D., Seielstad, G.A., Pauliny-Toth, I.I.K., Preuss, E., Witzel, A., Schilizzi, R.T., and Geldzahler, B.J. 1977, Nature, 268, 405.

Condon, J.J., Condon, M.A., Gisler, G., and Puschell, J.J. 1981, preprint.

Condon, J.J., and Dressel, L.L. 1978, Ap.J., 221, 456.

Condon, J.J., and Dressel, L.L. 1973, Ap. Letters, 15, 203.

Cook, D.B., and Spangler, S.R. 1980, Ap.J., 240, 751.

Crane, P. 1978, private communication.

Crane, P.C., and Price, R.M. 1976, Ap.J.(Letters), 207, L21.

de Bruyn, A.G. 1976, Astr. Ap., 52, 439.

Dent, W.A. 1972, Ap.J., 177, 93.

Dent, W.A. 1982, private communication.

Dent, W.A., et al 1982, in preparation.

Dent, W.A., and Balonek, T.J. 1980, Nature, 283, 747.

Dent, W.A., Balonek, T.J., Smith, A.G., and Leacock, R.J. 1979, Ap.J.(Letters), 227, L9.

Dent, W.A., and Hobbs, R.W. 1973, A.J., 78, 163.

Dent, W.A., and Kapitzky, J.E. 1976, A.J., 81, 1053.

Dent, W.A., Kapitzky, J.E., and Kojoian, G. 1974, A.J., 79, 1232.

Dent, W.A., and Kojoian, G. 1972, A.J., 77, 819.

Epstein, E.E., Fogarty, W.G., Hackney, K.R., Hackney, R.L., Leacock, R.J., Pomphrey, R.B., Scott, R.L., Smith, A.G., Hawkins, R.W., Roeder, R.C., Gary, B.L., Penston, M.V., Tritton, K.P., Bertaud, Ch., Veron, M.P., Wlerick, G., Bernard, A., Bigay, J.H., Merlin, P., Durand, A., Sause, G., Beklin, E.E., Neugebauer, G., and Wynn-Williams, C.G. 1972, Ap.J.(Letters), 178, L51.

Epstein, E.E., Fogarty, W.G., Mottmann, J., and Schneider, E. 1982, Ap.J., 87, 449.

Epstein, E.E., Janssen, M.A., Cuzzi, J.N., Fogarty, W.G., and Mottmann, J. 1980, Icarus, 41, 103.

Epstein, E.E., Landau, R., and Rather, J.D.G. 1980, A.J., 85, 1427.

Folsom, G.H., Smith, A.G., and Hackney, R.L. 1970, Ap.Letters, 7, 15.

Geldzahler, B.J., Pauls, T., and Salter, C.J. 1980, Astr. Ap., 84, 237.

Geldzahler, B.J., and Witzel, A. 1981, A.J., 86, 1306.

Gilmore, G. 1980, Nature, 287, 612.

Goldsmith, P.F. 1981, "Quasi-optical techniques at millimeter and sub-millimeter wavelengths", to appear in Infrared and Millimeter Waves, 6, K.S. Button (ed.).

Gottlieb, E.W., and Liller, W. 1978, Ap.J.(Letters), 222, L1.

Hackney, R.L., Hackney, K.R., Smith, A.G., Folsom, G.H., Leacock, R.J., Scott, R.L., and Epstein, E.E. 1972, Astrophys.L., 12, 147.

Haschick, A.D. 1981, private communication.

Hewitt, A., and Burbidge, G. 1980, Ap.J.Suppl., 43, 57.

Hobbs, R.W., and Dent, W.A. 1977, A.J., 82, 257.

Howard, R. 1982, private communication.

Huchra, J., Geller, M., and Morton, D. 1980, preprint (to appear in The Second Year of IUE.

Humason, M.L., Mayall, N.U., and Sandage, A.R. 1956, A.J., 61, 97.

Impey, C.D., Brand, P.W.J.L., and Tapia, S. 1982, M.N.R.A.S., 198, 1.

Jones, T.W., and Hardee, P.E. 1979, Ap.J., 228, 268.

Jones, T.W., Rudnick, L., Owen, F.N., Puschell, J.J., Ennis, D.J., and Werner, M.W. 1981, Ap.J., 243, 97.

Kapitzky, J.E. 1976, Ph.D. dissertation, University of Massachusetts.

Kellermann, K.I., and Pauliny-Toth, I.I.K. 1968, Ann.Rev.Astron. Astrophys., 6, 417.

Kellermann, K.I., and Pauliny-Toth, I.I.K. 1969, Ap.J.(Letters), 155, L71.

Kellermann, K.I., and Pauliny-Toth, I.I.K. 1981, Ann.Rev.Astron. Astrophys, 19, 373.

Kinman, T.D., Wardle, J.F.C., Conklin, E.K., Andrew, B.H., Harvey, G.A., Macleod, J.M., and Medd, W.J. 1974, A.J., 79, 349.

Kondo, Y., Worrall, D.M., Mushotzky, R.F., Hackney, R.L., Hackney, K.R.H., Oke, J.B., Yee, H.K.C., Neugebauer, G., Mathews, K., Feldman, P.A., and Brown, R.W. 1981, Ap.J., 243, 690.

Kristian, J. and Sandage, A. 1970, Ap.J., 162, 391.

Kutner, M.L. 1978, Astrophys.L, 19, 81.

Leacock, R.J., Smith, A.G., Edwrads, P.L., Pollock, J.T., Scott, R.L., Gearhart, M.R., Pacht, E., and Kraus, J.D. 1976, Ap.J.(Letters), 206, L87.

Marscher, A.P. 1977a, Ap.J., 216, 244.

Marscher, A.P. 1977b, A.J., 82, 781.

Marscher, A.P., and Broderick, J.J. 1981, preprint.

Medd,W.J., Andrew, B.H., Harvey, G.A., and Locke, J.L. 1972, Mem.R.astr.Soc., 77, 109.

Meeks, M.L., and Ruze, J. 1971, IEEE Trans. Antennas Propagat., AP-19, 723.

Miley, G.K. 1980, Ann.Rev.Astron.Astrophys., 18, 165.

Moffet, A.T. 1975, Stars and Stellar Systems, IX, 211, Univ. of Chicago Press.

O'Dea, C.P., Dent, W.A., and Balonek, T.J. 1982, in preparation.

O'Dea, C.P., Dent, W.A., Balonek, T.J., and Kapitzky, J.E. 1982, to appear in "Proceedings of Workshop on Low Frequency Variables", N.R.A.O.

O'Dell, S.L., Puschell, J.J., Stein, W.A., Owen, F., Porcas, R.W., Mufson, S., Moffett, T.J., and Ulrich, M.H. 1978, Ap.J., 224, 22.

O'Dell, S.L., Puschell, J.J., Stein, W.A., and Warner, J.W. 1977, Ap.J.(Letters), 214, L105.

O'Dell, S.L., Puschell, J.J., Stein, W.A., and Warner, J.W. 1978, Ap.J.Suppl., 38, 267.

Owen, F.N., and Mufson, S.L. 1977, A.J., 82, 776.

Owen, F.N., Porcas, R.W., Mufson, S.L., and Moffett, A.T. 1978, A.J., 83, 685.

Owen, F.N., and Puschell, J.J. 1982, private communication.

Owen, F.N., Spangler, S.R., and Cotton, W.D. 1980, A.J., 85, 351.

Peacock, J.A., Perryman, M.A.C., Longair, M.S., Gunn, J.E., and Westphal, J.A. 1981, M.N.R.A.S., 194, 601.

Penzias, A.A., and Burrus, C.A. 1973, Ann. Rev. Astr. and Ap., 11, 51.

Perley, R.A. 1982, subm,itted to A.J..

Peterson, F.W., and Dent, W.A. 1973, Ap.J., 186, 421.

Pica, A.J. 1981, private communication.

Pica, A.J., Pollock, J.T., Smith, A.G., Leacock, R.J., Edwards, P.L., and Scott, R.L. 1980, A.J., 85, 1442.

Pollock, J.T. 1981, private communication.

Pollock, J.T. 1982, Ph.D. dissertations, University of Florida.

Pollock, J.T., Hall, D.L., Ambruster, C., and Usher, P.D. 1974, Astron.Astrophys., 30, 41.

Pollock, J.T., Pica, A.J., Smith, A.G., Leacock, R.J., Edwards, P.L., and Scott, R.L. 1979, A.J. , 84, 1658.

Pomphrey, R.B., Smith, A.G., Leacock, R.J., Olsson, C.N., Scott, R.L., Pollock, J.T., Edwards, P., and Dent, W.A. 1976, A.J., 81, 489.

Predmore, R. 1978, "Antenna Efficiency Measurements", FCRAO internal report.

Preuss, E. 1981, "Proceedings of Second ESO/ESA Workshop", p.97.

Puschell, J.J., and Heeschen, D.S. 1982, private communication.

Puschell, J.J., Stein, W.A., Jones, T.W., Warner, J.W., Owen, F.N., Rudnick, L., Aller, H., and Hodge, P. 1979, Ap.J.(Letters), 227, L11.

Raisanen, A.V. 1980, Acta Polytechnica Scandinavica, Electrical Engineering Series No. 46.

Raisanen, A.V., Predmore, C.R., Parrish, P.T., Marrero, J.L., Goldsmith, P.F., Kot, R.A., and Scheider, M.V. 1980, Proc. 10th European Microwave Conference (Sept. 1980), Warsaw, Poland.

Rieke, G.H., Gradalen, G.L., Kinman, T.D., Hintzen, P., Wills, B.J., and Wills, D. 1976, Nature, 260, 754.

Rieke, G.H., and Kinman, T.D. 1974, Ap.J.(Letters), 192, L115.

Rieke, G.H., and Lebofsky, M.J. 1979, Ap.J., 227, 710.

Rieke, G.H., Lebofsky, M.J., Kemp, J.C., Coyne, G.V., and Tapia, S. 1977, Ap.J.(Letters), 218, L37.

Rieke, G.H., Lebofsky, M.J., and Kinman, T.D. 1979, Ap.J.(Letters), 232, L151.

Rieke, G.H., Lebofsky, M.J., and Wisniewski, W.Z. 1982, preprint.

Righini, G., Simon, M., and Joyce, R.R. 1976, Ap.J., 207, 119.

Rudnick, L., Owen, F.N., Jones, T.W., Puschell, J.J., and Stein, W.A. 1978, Ap.J.(Letters), 225, L5.

Schloerb, F.P. 1981, private communication.

Schloerb, F.P., and Good, J. 1982, private communication.

Schloerb, F.P., and Snell, R.L. 1980, "Calibration of the FCRAO 14m antenna: Evaluation of the chopper wheel calibration method and performance of the telescope", FCRAO report #150.

Schnopper, H.W., Delvaille, J.P., Epstein, A., Cash, W., Charles, P, Bowyer, S., Hjellming, R.M., Owen, F.N., and Cotton, W.D. 1978, Ap.J.(Letters), 222, L91.

Scott, R.L., Leacock, R.J., McGimsey, B.Q., Smith, A.G., Edwards, P.L., Hackney, K.R., and Hackney, R.L. 1976, A.J., 81, 7.

Shapiro,I.I., Wittels, J.J., Counselman, C.C. III, Robertson, D.S., Whitney, A.R., Hinteregger, H.F., Knight, C.A., Rogers, A.E.E., Clark, T.A., Hutton, L.K., and Niell, A.E. 1979, A.J., 84, 1459.

Shimmins, A.J., Searle, L., Andrew, B.H., and Brandie, G.W. 1968, Ap.Letters, 1, 167.

Snell, R.L., and Schloerb, F.P. 1981, "Calibration of data during the 1980-1981 observing season", FCRAO internal report.

Stein, W.A., O'Dell, S.L., and Strittmatter, P.A. 1976, Annual Review of Astronomy and Astrophysics, vol.14, 173.

Ulich, B.L. 1974, Icarus, 21, 254.

Ulich, B.L. 1981, A.J., 86, 1619.

Ulich, B.L., Cogdell, J.R., and Davis, J.H. 1973, Icarus, 19, 59.

Ulich, B.L., Davis, J.H., Rhodes, P.J., and Hollis, J.M. 1981, preprint.

Ulich, B.L., and Haas, R.W. 1976, Ap.J.Supple., 30, 247.

Ulvestead, J., Johnston, K., Perley, R., and Fomalont, E. 1981, A.J., 86, 1010.

Usher, P.D. 1979, A.J., 84, 1253.

van der Laan, H. 1966, Nature, 211, 1131.

von Hoerner, S. 1974, in Verschuur, G.I., and Kellermann, K.I., Galactic and Extragalactic Radio Astronomy, Springer-Verlag New York, Inc.

Wade, C.M. 1970, Ap.J., 162, 381.

Wade, C.M., and Johnston, K.J. 1977, A.J., 82, 791.

Walker, M.F. 1968, Ap.J., 151, 71.

Wardle, J.F.C. 1977, Nature, 269, 563.

Waters, J.W. 1976, chapter 2.3 of Meeks, M.L., Methods of Experimental Physics, vol. 12 - part B, Academic Press.

Webster, A.S., and Ryle, M. 1976, M.N.R.A.S., 175, 95.

Weiler, K.W., and Johnston, K.J. 1980, M.N.R.A.S., 190, 269.

Wills, B.J., et al 1982, in preparation.

Wills, D., and Wills, B.J. 1981, Nature, 289, 384.

Wright, A.E. 1980, private communication.

Wynn-Williams, C.G. 1971, M.N.R.A.S., 151, 397.

APPENDIX A

PLOTS OF RADIO (15.5 GHz) AND OPTICAL VARIABILITY

Radio data from Chapter II (observing program conducted by Dent, Balonek, Kapitzky, and Kojoian). Additional values from Allen, Barrett, and Crowther (1968); Ledden, Aller and Dent (1976); miscellaneous measurements obtained at Haystack Observatory and the University of Michigan Observatory (compiled by Dent, private communication).

Optical data from Pollock et al (1979), Pica et at (1980), Pica (1981), and Pollock (1981).

FIGURES:

0007+10

0048-09

0133+47

3C66A

0229+13

0235+16

15.5 GHZ

OPT (B)

0306+10

15.5 GHZ

OPT (B)

0333+32

CTA26

0420-01

3C120

3C120

15.5 GHZ

OPT (B)

0440-00

15.5 GHZ

OPT (PG)

0735+17

OJ287

OJ287

OJ287

OJ287

0906+01

0953+25

1101+38

1127-14

1156+295

1219+28

3C273

15.5 GHZ

OPT (B)

3C279

15.5 GHZ

OPT (PG)

3C279

1308+326

1510-08

1514-24

1638+39

15.5 GHZ

OPT (PG)

3C345

1749+70

3C371

1921-29

2131-021

2134+00

2145+06·

15.5 GHZ

OPT (PG)

BL LAC

BL LAC

BL LAC

2216-03

CTA102

3C454.3

15.5 GHZ

OPT (B)

2345-16

APPENDIX B

PLOTS OF (OPTICAL-RADIO) LINEAR CORRELATION COEFFICIENTS

Plots of the linear correlation coefficients, r, between the optical and radio variations. Data from Appendix A. If only a subset of the entire data is used for the analysis, the wavelength (optical or radio) and time interval is given.

<u>FIGURES:</u>

365

O235+16
OPT: PRE 1977.0

O235+16
OPT: 1978.5-79.5

OJ287
OPT: 1971.5-1972.5

OJ287
OPT: POST 1974.5
RAD: POST 1974.5

3C454.3
OPT: POST 1977.0

2345-16
OPT: POST 1970.6